



Universitat Autònoma de Barcelona

ADVERTIMENT. L'accés als continguts d'aquesta tesi queda condicionat a l'acceptació de les condicions d'ús establertes per la següent llicència Creative Commons:  http://cat.creativecommons.org/?page_id=184

ADVERTENCIA. El acceso a los contenidos de esta tesis queda condicionado a la aceptación de las condiciones de uso establecidas por la siguiente licencia Creative Commons:  <http://es.creativecommons.org/blog/licencias/>

WARNING. The access to the contents of this doctoral thesis it is limited to the acceptance of the use conditions set by the following Creative Commons license:  <https://creativecommons.org/licenses/?lang=en>



Prognostic and therapeutic significance of KIF11 in neuroblastoma

PhD thesis presented by

Marc Masanas Jimenez

To obtain the degree of

PhD in biochemistry, molecular biology and biomedicine

PhD thesis carried out in the group of translational research in child and adolescent cancer,
at Vall d'Hebron Research Institute (VHIR)

Thesis affiliated to the department of biochemistry and molecular biology from the UAB,
in the PhD program of biochemistry, molecular biology and biomedicine

Universitat Autònoma de Barcelona, 2021

Tutor: Dr. José Miguel Lizcano de Vega

Directors:

Dr. Miguel F. Segura Ginard

Dra. Anna Santamaria Margalef

Dra. Soledad Gallego Melcón

PhD Candidate: Marc Masanas Jimenez

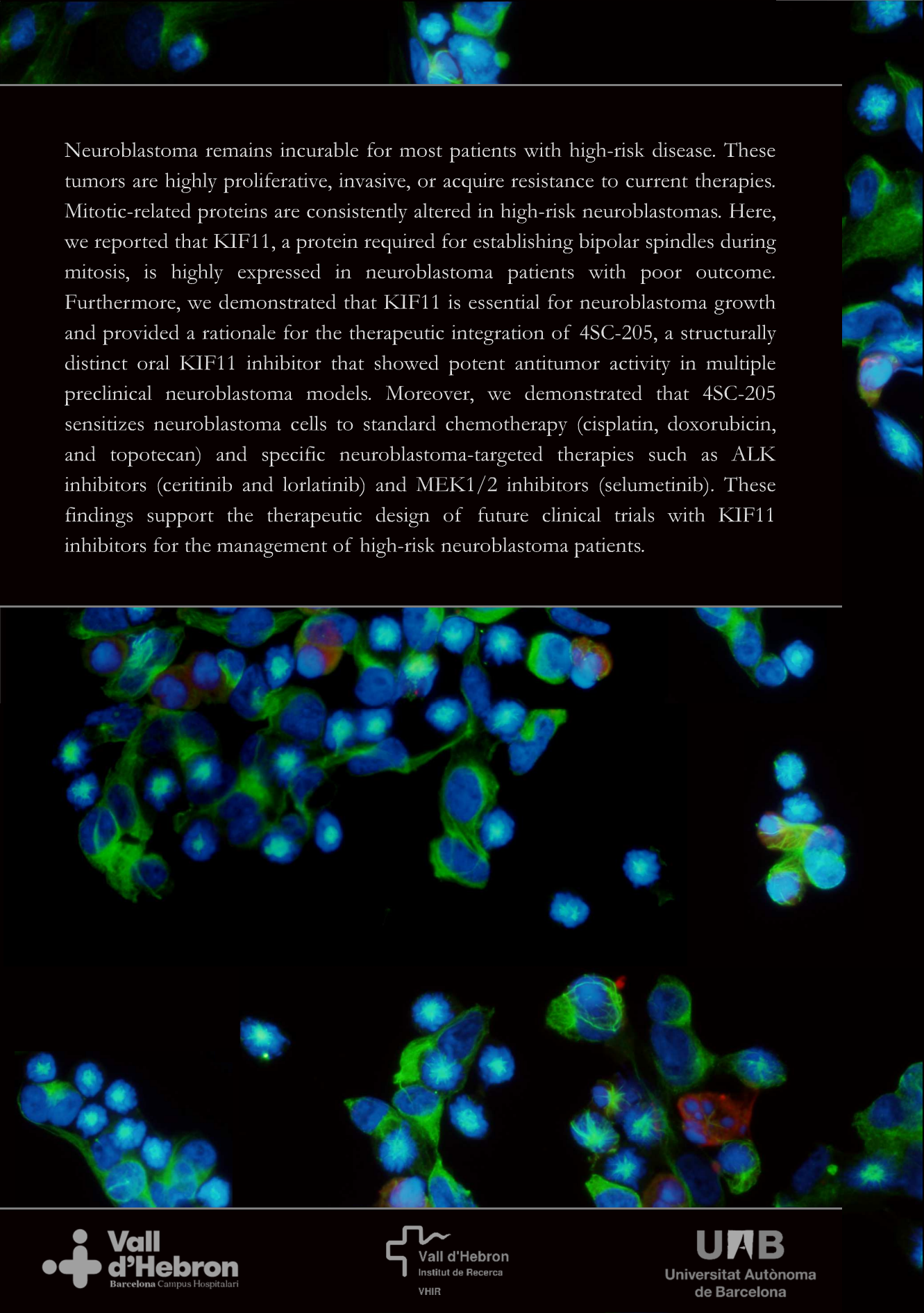
A fluorescence microscopy image of neuroblastoma cells. The nuclei are stained blue with DAPI. The cytoplasm and spindle apparatus are stained green, showing the localization of KIF11. A central cell shows a prominent spindle apparatus with KIF11 localization at the poles.

PROGNOSTIC AND THERAPEUTIC SIGNIFICANCE OF KIF11 IN NEUROBLASTOMA

PhD Thesis

Marc Masanas Jimenez

2021



Neuroblastoma remains incurable for most patients with high-risk disease. These tumors are highly proliferative, invasive, or acquire resistance to current therapies. Mitotic-related proteins are consistently altered in high-risk neuroblastomas. Here, we reported that KIF11, a protein required for establishing bipolar spindles during mitosis, is highly expressed in neuroblastoma patients with poor outcome. Furthermore, we demonstrated that KIF11 is essential for neuroblastoma growth and provided a rationale for the therapeutic integration of 4SC-205, a structurally distinct oral KIF11 inhibitor that showed potent antitumor activity in multiple preclinical neuroblastoma models. Moreover, we demonstrated that 4SC-205 sensitizes neuroblastoma cells to standard chemotherapy (cisplatin, doxorubicin, and topotecan) and specific neuroblastoma-targeted therapies such as ALK inhibitors (ceritinib and lorlatinib) and MEK1/2 inhibitors (selumetinib). These findings support the therapeutic design of future clinical trials with KIF11 inhibitors for the management of high-risk neuroblastoma patients.

ACKNOWLEDGMENTS



Acknowledgments

Primer de tot vull donar les gràcies als meus directors de tesis, el **Miquel**, l'**Anna** i la **Sole**, per tota la confiança que han tingut amb mi durant tots aquests anys. Se'm fa difícil de creure que ja fa més de 6 anys que vaig arribar al laboratori d'oncologia pediàtrica. Recordo que vaig començar les pràctiques de màster amb molta il·lusió i ganes d'aprendre. Després de tot un any de jornades molt llargues entre pràctiques i classes vam començar a parlar amb el Miquel de les opcions de poder fer el doctorat al grup. Finalment, al cap d'un any vam aconseguir la beca FPU, que em donava la oportunitat de quedar-me al grup durant 4 anys per fer la tesis. Miquel, et vull donar les gràcies per confiar amb mi, per guiar-me durant tots aquests anys, per donar-me la opció de poder dur a terme projectes de recerca molt ambiciosos i motivar-me quan era necessari. També vull donar les gràcies a l'Anna per tot el suport, tant personal com laboral que m'has donat durant tot aquest temps. Tenir-vos a vosaltres dos com a directors m'ha permès aprendre moltíssim. Gràcies a vosaltres he estat molt còmode i he gaudit molt fent la tesis doctoral. També vull donar les gràcies a la Sole per totes les seves aportacions. La feina que feu el personal del servei d'oncologia i hematologia pediàtrica és extraordinària. Cada any es curen molts nens amb càncer gràcies a la vostra feina i dedicació. Les teves aportacions i consells han permès realitzar un projecte molt encarat cap als pacients i tenir cobert el punt de vista clínic, que és imprescindible per realitzar aquests tipus de projectes d'investigació. Vull destacar també la confiança que diposita el servei d'oncologia i hematologia pediàtrica de la Vall d'Hebron en la investigació biomèdica. Gràcies a persones com la **Sole**, el **Pepe** i el **Lucas** es pot investigar per buscar noves teràpies per millorar els tractaments que hi ha actualment.

També vull mencionar la sort que he tingut de coincidir amb els meus companys de laboratori. **Ari**, vas ser la meva mentora quan vaig entrar al laboratori. He après molt de tu i de la teva manera de treballar. Ets una persona meravellosa i una treballadora incansable. Moltes gràcies per compartir tants bons moments amb mi. Encara em ric quan penso amb la pipeta "perduda", i mira que ja han passat 6 anys. **Roby**, eres una persona extraordinària que sempre està dispuesta a ayudar a tus compañeros. Te quiero dar las gracias por todos los momentos que hemos pasado juntos y toda la ayuda que me has dado durante estos años.

Acknowledgments

Como anécdota siempre podremos contar la historia del comercial que buscaba a Roberto, al final “no ta”. **Carlos**, vam començar les pràctiques de màster junts i acabarem la tesis doctoral al mateix moment. Ha estat un plaer poder compartir amb tu aquesta experiència. Ets una de les persones més treballadores i intel·ligents que he vist mai. Aconseguiràs tots els objectius que et proposis. **Aroa**, sempre t’has preocupat que estiguem tots bé i ens has donat suport quan ho hem necessitat. Ets una persona increïble i només puc donar gràcies per haver coincidit amb tu. També et vull agrair totes les contribucions científiques que has fet en aquest projecte. **Ainara**, eres una persona que se preocupa por todos nosotros. Siempre miras que estemos bien y nos ayudas cuando lo necesitamos. Quiero agradecerle todo el apoyo que me has dado a mí y al resto de compañeros desde que entraste al grupo. **Laia**, has estat molt bona companya. Ets una persona alegre i divertida. Hem passat molts bons moments junts i sempre em recordaré de les teves frases mítiques “primero tengo un ojo y luego otro”, “manos pequeñas, cerebro grande”, “almuerto”, entre altres. **Luz**, eres una persona muy extrovertida y divertida. Cuando empecé en el laboratorio me sorprendí del buen ambiente que había, gran parte era gracias a ti y tus anécdotas divertidas. Aun me río cuando me acuerdo de cuando nos contaste que Hikari había dejado un “regalo líquido” en el felpudo de la marquesa.

També vull donar les gràcies als companys d’OP. **Patri** i **Natalia**, igual que el Carlos, vam començar les pràctiques del màster junts i acabarem també la tesis doctoral al mateix moment. Ha estat un plaer compartir amb vosaltres aquest “viatge” i passar tants bons moments junts. Patri, eres una de las personas que conozco con más energía, siempre aportas buen ambiente y alegría. Natalia, ets la persona que aportes més tranquil·litat al grup i al mateix moment sempre fas que la resta ens sentim a gust. També saps animar els dies amb les teves anècdotes, com la del pimiento 0 o com rata com a femení de ratolí. **Irina**, ets optimista, divertida i molt bona persona. Tens un riure i una alegria que s’encomana als altres, i això és una qualitat que no la té massa gent. Moltes gràcies per regalar-me tantes bones estones. **Guillem, Gabriel, Isaac, Carla** i **Ana**, he estat molt afortunat de tenir-vos com a companys de grup. Heu estat molt importants fent que hi hagi sempre bon ambient al laboratori. També li vull agrair al **Pep** totes les aportacions que ha fet en aquest projecte que ens ha permès millorar la feina.

Vull mencionar també els integrants del grup de cicle cel·lular i càncer. Vull donar les gràcies a la **Núria** i la **Leti**, que han contribuït moltíssim en el desenvolupament d'aquest projecte. Núria, vam estar treballant junts durant molts mesos. Durant aquest temps ens vam ajudar moltíssim i vas amenitzar molt les jornades de 12 hores o més que fèiem al laboratori. Encara recordo un dels dies que vam entrar a les 7:00 i vam sortir a les 23:00 en el qual va coincidir el mateix vigilant de seguretat quan vam entrar i després al sortir, la seva cara al veure'ns sortir a les 23:00 va ser mítica. Leti, et vull donar les gràcies per tota la teva ajuda, sobretot en els *in vivos*. Anar els dos a l'estabulari va facilitar molt fer els experiments. Hem passat molts bons moments junts i ha estat un plaer compartir el projecte amb el teu. També m'agradaria agrair a la **Blanca** i la **Mireia** tota la seva ajuda en aquest projecte al llarg d'aquests anys. Al igual que la resta de dones que he mencionat, sou l'exemple clar del perquè les dones teniu un paper imprescindible en la societat i en el camp de la investigació. També vull donar les gràcies a l'**Alfonso**, a l'**Adrià** i a la **Marta** ja que sempre que he necessitat qualsevol material o parlar una estona amb algú han estat allà. **Ignasi**, tot i que només vas estar un any al nostre grup mentre feies el màster, ens vas ajudar molt en alguns experiments. Moltes gràcies per contribuir en aquest projecte i per estar sempre de bon humor i amb un somriure.

Em sento afortunat també per haver tingut la oportunitat d'haver fet un gran número de col·laboracions. **Cinthia**, ets un 10 de persona i molt treballadora. No tenia cap dubte que després d'acabar el doctorat aconseguiries una plaça per treballar a un hospital de genetista. T'ho has treballat moltíssim i tot el que tens és perquè t'ho mereixes.

También quiero agradecer a **Stefan**, **Oscar** y a **José** todas las aportaciones científicas que han realizado en las comisiones de seguimiento del doctorado. Sus comentarios nos han ayudado a mejorar la calidad científica del proyecto.

També vull donar les gràcies a la resta de persones que han col·laborat en aquest projecte i que no he mencionat anteriorment. **Laura Devis**, **Rebeca Burgos**, **Pau Rodriguez**, **Gabriela Guillén**, **Alexandra Navarro**, **David Llobet**, **Alberto Villanueva**, **Rosa Noguera**, **Rolf Krauss**, moltes gràcies per col·laborar amb nosaltres. Aquest projecte no hagués arribat fins a on ho ha fet sense els vostres coneixements i aportacions científiques.

Acknowledgments

Em sento afortunat d'haver pogut compartir espai amb altres persones que han fet el dia a dia molt agradable. **Eulàlia** i **Rosa** moltes gràcies per intentar solucionar els problemes que sorgeixen diàriament, tot i que l'edifici segueixi tenint molts defectes, com a mínim ja no estem a més de 30°C a cultius. **Nieves**, nuestras charlas en la sala de cultivos me amenizaban un poco la mañana cuando tenía que estar 4 horas o más allí, muchas gracias por compartir estos ratos conmigo. **Núria**, **Rashida** y **Paco**, muchas gracias por aportar un buen ambiente en el edificio. Tots vosaltres heu contribuït de forma indirecta en aquesta tesi doctoral.

Finalment, vull donar les gràcies a tota la meva família. Primer, vull donar les gràcies a la meva **mare** i al meu **pare**, sempre m'heu animat a continuar estudiant i això és el que ha fet que arribés fins aquí. També us vull agrair que haguessis estat sempre al meu costat i que m'haguessis cuidat tant. També li vull donar les gràcies al **Miquel**, després de viure separats durant 5 anys vaig pensar que seria estrany tornar a viure junts a Barcelona. La veritat és que vam estar molt bé els dos anys que vam estar vivint junts i em vas ajudar molt, sobretot els dies que arribava tard del laboratori. També li vull dedicar unes paraules als meus avis, **iaia Maria**, **iaia Remei** i **avi**, moltes gràcies per cuidar-me sempre. Sempre recordaré els estius de vacances a Saldes quan era petit o els dinars de restaurant d'estrella Michelin a casa la iaia Maria. Per acabar, et vull donar les gràcies **Sergi** per tot el teu suport al llarg d'aquests anys. No tinc paraules per descriure lo content que em fa tenir-te al meu costat.

Mil gràcies a tots!

Funding

La recerca portada terme en aquesta projecte no es podria haver dut a terme sense el finançament del **Ministeri d'Universitats** (FPU16/01099), l'**associació espanyola contra el càncer** (LABAE18009SEGU), l'**Institut Carlos III** (PI18/01017, PI20/00530), l'**associació NEN** (Nico contra el cancer infantil 2017–PVR00157), la iniciativa **todos con Mayka** i l'associació **Acunapatata**.



ABSTRACT



Abstract

High-risk neuroblastomas are highly proliferative embryonal tumors with extremely aggressive behavior. Despite multimodal therapies, more than 50% of patients relapse, and their 5-year overall survival is still below than 50%. Therefore, it is necessary to find more effective therapies to increase the survival chances of these patients. KIF11 is a motor protein that is essential for bipolar spindle formation and mitotic progression in human cells and is a therapeutic target in multiple tumor types. In this thesis, we investigated the effects of the oral KIF11 inhibitor, 4SC-205, in high-risk neuroblastoma using preclinical primary and metastatic models.

KIF11 prognostic value was analyzed by mining publicly available mRNA expression datasets and immunohistochemistry in neuroblastoma tissue microarrays. We found that high KIF11 expression correlated with poor overall survival and genetic variables associated with aggressive neuroblastomas, such as *MYCN* amplification, -1p36, and +17q23. We next investigated the genetic and pharmacological inhibition of KIF11 in neuroblastoma cell lines. We demonstrated that 4SC-205 recapitulated KIF11 silencing phenotypic effects *in vitro* and *in vivo*, inducing cell cycle arrest during mitosis and the subsequent induction of apoptosis. *In vivo*, 4SC-205 inhibited primary tumor growth in subcutaneous and orthotopic patient-derived xenografts and reduced the metastatic burden. Finally, 4SC-205 potentiated the therapeutic effect of standard chemotherapies (cisplatin, doxorubicin, and topotecan) and targeted therapies such as ALK and RAS/MAPK inhibitors.

These findings suggest that KIF11 inhibition using 4SC-205 alone or in combination with conventional and/or targeted therapeutics is a potential new therapeutic strategy to treat high-risk neuroblastomas.

Resum

Els neuroblastomes d'alt risc són tumors embrionaris molt agressius que proliferen molt ràpidament. Encara que actualment s'utilitzen teràpies multimodals per tractar els pacients, més del 50% recau, i la seva supervivència al cap de 5 anys és menor del 50%. Per tant, és necessari trobar noves teràpies més efectives que incrementin les probabilitats de supervivència d'aquests pacients. KIF11 és una proteïna motora que és indispensable per la formació del fus acromàtic i per la progressió de la cèl·lula a les diferents fases de la mitosis. KIF11 també ha estat descrita com a diana terapèutica en varis tipus de tumors. En aquesta tesis hem investigat els efectes de l'inhibidor oral de KIF11 4SC-205 en neuroblastoma d'alt risc utilitzant models preclínics de tumors primaris i de metastàsis.

El valor pronòstic de KIF11 es va investigar analitzant el nivell d'expressió de ARNm en bases de dades públiques i per immunohistoquímica en *microarrays* de teixits. A partir d'aquestes dades, vam observar que l'alta expressió de KIF11 està relacionada a pitjor supervivència i a alteracions genètiques associades a tumors agressius, com l'amplificació del gen *MCYN*, la pèrdua de heterozigositat del 1p36 o el guany del 17q23. A continuació vam investigar la inhibició gènica i farmacològica de KIF11 en línies cel·lulars de neuroblastoma. Vam veure que l'inhibidor 4SC-205 recapitula els efectes fenotípics del silenciament gènic, tant *in vitro* com *in vivo*, induint arrest en mitosis durant el cicle cel·lular i la subseqüent mort per apoptosis. *In vivo*, vam observar que el 4SC-205 inhibeix el creixement del tumor primari en models xenografts subcutanis de ratolí, en models PDOX (sigles de l'anglès Patient-Derived Orthotopic Xenograft) i models de metastàsis. Finalment, vam veure que el 4SC-205 potencia l'efecte de la quimioteràpia estàndard (cisplatí, doxorubicina i topotecan) i teràpies dirigides com la inhibició d'ALK i de la via de RAS/MAPK.

Aquests resultats suggereixen que la inhibició de KIF11 utilitzant el 4SC-205 tot sol o en combinació amb quimioteràpia convencional i/o teràpies dirigides podria ser una nova estratègia terapèutica per tractar els pacients amb neuroblastoma d'alt risc.

Resumen

Los neuroblastomas de alto riesgo son tumores embrionarios muy agresivos que proliferan muy rápidamente. A pesar del uso de terapias multimodales, aproximadamente un 50% de los pacientes presenta recaídas, y su supervivencia a los 5 años es inferior al 50%. Por lo tanto, es necesario encontrar nuevas terapias más eficaces que permitan aumentar la probabilidad de supervivencia de estos pacientes. KIF11 es una proteína motora que es indispensable para la formación del huso acromático y para la progresión de la célula a las distintas fases de la mitosis. KIF11 ha sido descrita como diana terapéutica en varios tipos de tumores del adulto. En esta tesis hemos investigado los efectos del inhibidor oral de KIF11 4SC-205 en neuroblastoma de alto riesgo usando modelos preclínicos de tumores primarios y de metástasis.

El valor pronóstico de KIF11 se investigó analizando los niveles de expresión de ARNm en bases de datos públicos y por inmunohistoquímica en *microarrays* de tejidos. Usando estos datos, observamos que la expresión de KIF11 correlaciona con una peor supervivencia y con alteraciones génicas asociadas a tumores agresivos, como la amplificación del gen *MYCN*, la pérdida de heterocigosidad del 1p36 o la ganancia del 17q23. A continuación investigamos la inhibición génica y farmacológica de KIF11 en líneas celulares de neuroblastoma. Vimos que el inhibidor 4SC-205 recapitula los efectos fenotípicos del silenciamiento génico, tanto *in vitro* como *in vivo*, induciendo arresto en mitosis durante el ciclo celular y la subsecuente muerte por apoptosis. *In vivo*, observamos que el 4SC-205 inhibe el crecimiento del tumor primario en modelos de xenotrasplantes subcutáneos de ratón, en modelos PDOX (siglas del inglés Patient-Derived Orthotopic Xenograft) y modelos de metástasis. Finalmente, vimos que el 4SC-205 potencia los efectos de la quimioterapia estándar (cisplatino, doxorubicina y topotecan) y terapias dirigidas como la inhibición de ALK y de la vía de RAS/MAPK.

Estos resultados sugieren que la inhibición de KIF11 utilizando el 4SC-205 sólo o en combinación con quimioterapia convencional y/o terapias dirigidas podría ser una nueva estrategia terapéutica para tratar pacientes con neuroblastoma de alto riesgo.

TABLE OF CONTENTS

| | |
|---|--------------|
| Acknowledgments | iii |
| Funding | vii |
| Abstract | xi |
| Resum | xiii |
| Resumen | xv |
| List of figures | xxi |
| List of tables | xxiii |
| Abbreviations | xxv |
| 1. Introduction | 3 |
| 1.1. Neuroblastoma | 3 |
| 1.1.1. Neuroblastoma epidemiology..... | 3 |
| 1.1.2. Origin of neuroblastoma | 5 |
| 1.1.3. Familial neuroblastoma..... | 9 |
| 1.1.4. Genetic alterations of neuroblastoma | 12 |
| 1.1.5. Neuroblastoma clinical presentation and diagnosis..... | 15 |
| 1.1.6. Neuroblastoma staging and risk assessment | 19 |
| 1.1.7. Risk stratification | 23 |
| 1.1.8. Neuroblastoma clinical management | 24 |
| 1.1.9. Late effects in children treated with intensive multimodal therapy | 34 |
| 1.2. Targeting cell cycle as a cancer therapy | 35 |
| 1.2.1. Cell cycle dysregulation in cancer..... | 35 |
| 1.2.2. Anti-cancer therapies targeting mitosis..... | 37 |
| 1.3. Kinesin family member 11..... | 43 |
| 1.3.1. KIF11 structure and function..... | 43 |
| 1.3.2. Regulation and subcellular localization of KIF11 | 45 |
| 1.3.3. KIF11 and cancer | 48 |
| 1.3.4. Pharmacological inhibition of KIF11 | 49 |
| 1.3.5. KIF11 and neuroblastoma | 50 |

| | |
|---|-----------|
| 2. Hypothesis and objectives..... | 53 |
| 3. Materials and methods | 57 |
| 3.1. Analysis of neuroblastoma gene expression datasets | 57 |
| 3.2. Immunohistochemistry | 57 |
| 3.3. Cell lines..... | 59 |
| 3.4. Western blot..... | 60 |
| 3.5. Depletion of MYCN in Tet21N cell line | 61 |
| 3.6. Quantitative real-time PCR | 61 |
| 3.7. Cell transfection | 62 |
| 3.8. Immunofluorescence..... | 63 |
| 3.9. Cell cycle analysis | 64 |
| 3.10. <i>In vitro</i> drug sensitivity assays | 64 |
| 3.11. Hoechst staining..... | 64 |
| 3.12. Differentiation of SH-SY5Y | 65 |
| 3.13. Three-dimensional spheroid culture | 65 |
| 3.14. Lentivirus production, transduction and isolation of clones | 65 |
| 3.15. <i>In vivo</i> experiments | 66 |
| 3.15.1. Subcutaneous xenografts..... | 66 |
| 3.15.2. Patient-derived orthotopic xenograft model..... | 66 |
| 3.15.3. Neuroblastoma liver metastases model | 67 |
| 3.16. Genomic analyses | 68 |
| 3.16.1. RNA sequencing..... | 68 |
| 3.16.2. Whole exome sequencing..... | 68 |
| 3.17. Drug combination studies | 69 |
| 3.18. Statistical analysis | 70 |
| 4. Results..... | 73 |
| 4.1. KIF11 is an independent factor of survival in neuroblastoma..... | 73 |
| 4.2. KIF11 expression correlates with MYCN mRNA levels | 76 |
| 4.3. 4SC-205 mirrors KIF11 depletion phenotype..... | 78 |
| 4.4. KIF11 inhibition reduces neuroblastoma proliferation..... | 81 |
| 4.5. KIF11 inhibition induces apoptosis in neuroblastoma cells..... | 83 |

| | |
|--|------------|
| 4.6. 4SC-205 is a reversible inhibitor of KIF11 | 85 |
| 4.7. KIF11 inhibition does not reduce cell viability of differentiated cells | 86 |
| 4.8. 4SC-205 reduces cell proliferation of tumor spheroids | 88 |
| 4.9. KIF11 silencing inhibits neuroblastoma growth <i>in vivo</i> | 89 |
| 4.10. 4SC-205 reduces tumor growth of subcutaneous xenografts..... | 92 |
| 4.11. KIF11 pharmacological inhibition is effective in neuroblastoma PDOX..... | 96 |
| 4.12. 4SC-205 improves overall survival in a metastases mouse model | 98 |
| 4.13. 4SC-205 has a manageable toxicity profile in mice | 100 |
| 4.14. 4SC-205 enhances standard chemotherapy efficacy..... | 101 |
| 4.15. 4SC-205 and ALK inhibitors cooperate to impair neuroblastoma growth..... | 107 |
| 4.16. 4SC-205 and selumetinib cooperate to reduce neuroblastoma growth | 109 |
| 5. Discussion..... | 113 |
| 5.1. Clinical challenges in the management of high-risk neuroblastomas | 113 |
| 5.2. KIF11 as a potential prognostic biomarker of survival | 114 |
| 5.3. Why is KIF11 more expressed in high-risk neuroblastoma? | 116 |
| 5.4. Targeting KIF11: exploring mitotic arrest and apoptotic cell death..... | 120 |
| 5.5. 4SC-205 is a candidate therapeutic agent for high-risk neuroblastoma | 123 |
| 5.6. Overcoming treatment resistance: combination therapies | 126 |
| 5.6.1. Results of clinical trials of KIF11 inhibitors | 126 |
| 5.6.2. Why excellent KIF11 inhibitors failed in clinical trials?..... | 129 |
| 5.6.3. Combination of KIF11 inhibitors with standard and targeted therapies..... | 132 |
| 5.7. Future directions: 4SC-205, from bench to bedside | 133 |
| 6. Conclusions | 137 |
| 7. References..... | 141 |
| 8. Annexes..... | 171 |
| 9. Publications | 177 |

List of figures

| | |
|--|----|
| Figure 1. Relative frequencies of childhood cancer (2009-2012) in children aged 0-14 years old..... | 3 |
| Figure 2. NC induction, delamination and differentiation | 6 |
| Figure 3. Model of neuroblastoma tumorigenesis | 8 |
| Figure 4. Genetic predisposition to neuroblastoma | 11 |
| Figure 5. Location of primary and metastatic neuroblastoma..... | 15 |
| Figure 6. Standard schedule for high-risk neuroblastoma therapy | 25 |
| Figure 7. COG and SIOPEN induction chemotherapy schedule | 26 |
| Figure 8. Cell cycle phases and checkpoints | 35 |
| Figure 9. Phases of mitosis and mitotic targets for cancer therapy | 38 |
| Figure 10. Microtubule structure and assembly | 39 |
| Figure 11. KIF11 structure and function | 43 |
| Figure 12. KIF11 inhibition suppresses bipolar spindle assembly..... | 44 |
| Figure 13. KIF11 mRNA expression correlates with poor outcome in neuroblastoma | 73 |
| Figure 14. KIF11 mRNA is more expressed in patients with common neuroblastoma genetic alteration..... | 74 |
| Figure 15. KIF11 protein expression is associated with worse overall survival in neuroblastoma | 75 |
| Figure 16. KIF11 mRNA expression correlates with MYCN in distinct neuroblastoma datasets | 76 |
| Figure 17. There is no correlation between KIF11 and MYCN protein expression in multiple neuroblastoma cell lines | 76 |
| Figure 18. MYCN silencing induces KIF11 downregulation in Tet21N but not in SK-N-BE(2)/CHLA-90 | 77 |
| Figure 19. Ectopic expression of MYCN does not increase KIF11 protein levels..... | 77 |
| Figure 20. 4SC-205 structure..... | 78 |
| Figure 21. KIF11 inhibition using 4SC-205 induces monopolar spindle phenotype in neuroblastoma cells | 78 |
| Figure 22. 4SC-205 blocks cell cycle progression in mitosis..... | 79 |
| Figure 23. Genetic and pharmacological inhibition of KIF11 induce histone H3 phosphorylation of Ser(10).. | 80 |
| Figure 24. Genetic and pharmacological inhibition of KIF11 reduce cell proliferation | 82 |
| Figure 25. KIF11 inhibition induces apoptosis in neuroblastoma cells | 83 |
| Figure 26. KIF11 inhibition increases the levels of active caspase-3..... | 84 |
| Figure 27. Effects of 4SC-205 on cell cycle are reversible | 85 |
| Figure 28. 4SC-205 does not affect cell viability of differentiated SH-SY5Y cells..... | 87 |

List of figures

| | |
|---|-----|
| Figure 29. 4SC-205 reduces the viability of 3D neuroblastoma spheroid cultures | 88 |
| Figure 30. Genetic silencing of KIF11 using inducible shRNA mirrors siKIF11 phenotype | 89 |
| Figure 31. Doxycycline does not reduce tumor growth of pTRIPZ-control xenografts | 90 |
| Figure 32. Genetic silencing of KIF11 reduces tumor growth in neuroblastoma xenografts | 91 |
| Figure 33. 4SC-205 impairs tumor growth in subcutaneous xenografts | 93 |
| Figure 34. Transcriptomic analysis confirms that 4SC-205 arrests xenograft tumors in mitosis | 94 |
| Figure 35. Tumor weight of subcutaneous xenografts correlates with tumor volume measurements | 95 |
| Figure 36. VH-NB PDOX model retains most of histological and molecular features of the original tumor | 97 |
| Figure 37. 4SC-205 impairs PDOX growth..... | 98 |
| Figure 38. KIF11 inhibition prolongs survival of mice bearing neuroblastoma metastases | 99 |
| Figure 39. 4S-205 is well tolerated in mice | 100 |
| Figure 40. Combination of 4SC-205 with chemotherapy leads to enhanced efficacy | 102 |
| Figure 41. Combination of 4SC-205 with standard chemotherapy exerts additive antitumor effects in neuroblastoma..... | 103 |
| Figure 42. Combination of 5 mg/kg of topotecan once weekly and 20 mg/kg of 4SC-205 three times per week is well-tolerated in mice..... | 104 |
| Figure 43. Combination of 4SC-205 and topotecan expands the lifespan of mice bearing SK-N-BE(2) metastases | 105 |
| Figure 44. Combination of 4SC-205 and topotecan efficiently remove liver and bone marrow metastases..... | 106 |
| Figure 45. 4SC-205 and ALK inhibitors combination impairs neuroblastoma proliferation | 108 |
| Figure 46. Combination of 4SC-205 and MEK1/2 inhibitors impairs neuroblastoma growth | 110 |
| Figure 47. High expression of KIF11 correlates with neuroblastoma patient recurrence..... | 116 |
| Figure 48. KIF11 inhibition results in Mcl-1 and NOXA degradation..... | 122 |
| Figure 49. KIF11 inhibition does not reduce BCL-2 and BCL-xL protein levels..... | 122 |

List of tables

| | |
|---|-----|
| Table 1. Neuroblastoma symptoms | 16 |
| Table 2. Tests and procedures used to diagnose neuroblastoma | 18 |
| Table 3. International Neuroblastoma Staging System | 19 |
| Table 4. International Neuroblastoma Risk Group Staging System..... | 20 |
| Table 5. International neuroblastoma pathology classification | 21 |
| Table 6. Modified INRG consensus pretreatment classification | 23 |
| Table 7. List of potential late effects of neuroblastoma patients | 34 |
| Table 8. KIF11 expression status in multiple malignancies | 48 |
| Table 9. KIF11-inhibiting compounds in clinical development | 49 |
| Table 10. Primary and secondary antibodies for immunohistochemistry | 58 |
| Table 11. Cell lines and medium | 59 |
| Table 12. Primary antibodies for western blot | 61 |
| Table 13. Secondary antibodies for western blot..... | 61 |
| Table 14. List of RT-qPCR primer sequences | 62 |
| Table 15. List of siRNA..... | 63 |
| Table 16. Primary and secondary antibodies for immunofluorescence | 64 |
| Table 17. List of pharmacological agents | 70 |
| Table 18. Univariate and multivariate regression analysis..... | 74 |
| Table 19. Relationships between KIF11 expression and clinico-biological characteristics | 75 |
| Table 20. List of neuroblastoma cell lines used in this study..... | 81 |
| Table 21. IC50 values for cisplatin, doxorubicin and topotecan in neuroblastoma cell lines..... | 101 |
| Table 22. Relationship between tumor response and treatment..... | 106 |
| Table 23. IC50 values for ceritinib and lorlatinib in <i>ALK</i> mutated neuroblastoma cell lines | 107 |
| Table 24. IC50 values for selumetinib in neuroblastoma cell lines..... | 109 |
| Table 25. <i>In silico</i> correlation analysis between the expression of KIF11 and the AP-1 complex subunits..... | 118 |
| Table 26. <i>In silico</i> correlation analysis between the expression of KIF11 and 720 transcription factors..... | 119 |
| Table 27. Fold change of the expression of mitotic kinesins in high-risk vs. low- and intermediate-risk neuroblastoma patients | 120 |
| Table 28. Pharmacokinetics properties and administration schedules of KIF11 inhibitors..... | 130 |

Abbreviations

| | | |
|----------|--------|--|
| A | AAG | α -1 acidic glycoprotein |
| | ALK | Anaplastic lymphoma kinase |
| | ASCT | Autologous stem cell transplant |
| | AURKA | Aurora kinase A |
| B | BDNF | Brain derived neurotrophic factor |
| | BMP | Bone morphogenetic proteins |
| | BSA | Bovine serum albumin |
| C | CDK | Cyclin-dependent kinase |
| | Cis-RA | Cis-retinoid acid |
| | COG | Children's Oncology Group |
| | CNA | Copy number alterations |
| | CT | Computed tomography |
| D | DMSO | Dimethyl sulfoxide |
| E | EFS | Event-free survival |
| | EMT | epithelial-to-mesenchymal |
| F | FBS | Fetal bovine serum |
| | FGF | Fibroblast growth factor |
| G | GBM | Ganglioneuroblastoma |
| | GCCR | German childhood cancer registry |
| | G-CSF | Granulocyte-colony stimulating factor |
| | GSEA | Gene set enrichment analysis |
| I | ICE | Ifosfamide, carboplatin and etoposide |
| | IDRF | Image-defined risk factors |
| | IMDM | Iscove's Modified Dulbecco's Medium |
| | Indel | Small insertions/deletions |
| | INPC | International Neuroblastoma Pathologic Classification |
| | INRG | International Neuroblastoma Risk Group |
| | INRGSS | International Neuroblastoma Risk Group's stratification system |
| | INSS | International Neuroblastoma Staging System |

Abbreviations

| | | |
|----------|--------|---|
| K | KIF11 | Kinesin Family Member 11 |
| L | LFS | Li-Fraumeni syndrome |
| | LOH | Loss of heterozygosity (LOH) |
| M | MAT | Myeloablative therapy |
| | Mcl-1 | Myeloid cell leukemia 1 |
| | mIBG | 123I-metaiodobenzylguanidine |
| | MiRNA | MicroRNA |
| | MKI | Mitosis karyorrhexis index |
| | MOMP | Mitochondrial outer membrane permeabilization |
| | MRI | Magnetic resonance imaging |
| | MTD | Maximum tolerated dose |
| N | NC | Neural crest |
| | NDDS | Neuroblastoma new drug development strategy |
| O | OS | Overall survival |
| P | PBS | Phosphate-buffered saline |
| | PDOX | Patient derived orthotopic xenograft |
| | PHOX2B | Paired-like homeobox 2B gene |
| | PLK | Polo-like kinases |
| S | SA | Sympathoadrenal |
| | SAC | spindle assembly checkpoint |
| | SCA | Segmental chromosomal aberrations |
| | SEM | Standard error of the mean |
| | SIOPEN | International Society of Paediatric Oncology European Neuroblastoma |
| | SiRNA | Small interfering RNA |
| T | SNV | Single nucleotide variants (SNV) |
| | TMB | Tumor mutational burden |
| | TVD | Topotecan-vincristine-doxorubicin |

INTRODUCTION



1. Introduction

1.1. Neuroblastoma

1.1.1. Neuroblastoma epidemiology

Childhood cancer is the leading cause of non-accidental deaths in children below age 15 in developed countries. The incidence rate of pediatric cancers has been increasing slightly since 1975 for unclear reasons. However, over the last decade, the annual incidence seems to have stabilized in Europe (1). There has been a marked increase in the probability of survival due to the improvement of diagnostic procedures and the introduction and advancement of multimodal treatment strategies. Nevertheless, treatment of pediatric cancer is still a challenge for the oncologists. The main categories of pediatric malignancies include leukemias, central nervous system tumors, lymphomas, neuroblastoma, soft tissue and bone sarcomas, renal tumors, germ cell tumors, retinoblastoma and hepatic tumors (Figure 1) (2,3).

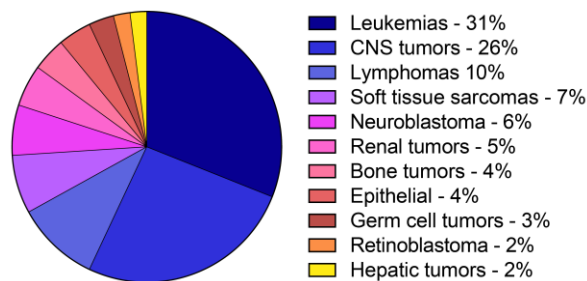


Figure 1. Relative frequencies of childhood cancer (2009-2012) in children aged 0-14 years old. Adapted from (3). Abbreviations: CNS, central nervous system.

Neuroblastoma is an embryonal tumor of the sympathetic nervous system which represents one of the most common solid tumors diagnosed in children being the most frequent neoplasm in the first year of life, with slight male predominance (1.2:1.0) (2,4). Neuroblastoma accounts for 6% to 10% of all childhood malignancies and 12% to 15% of childhood cancer-related deaths. The incidence rate of neuroblastoma is 10.9 cases per million children aged 0-14 years in Europe. The median age at diagnosis is 18 months. Specifically, 30% of neuroblastomas are diagnosed during the first year of life and 90% are

Introduction

Neuroblastoma epidemiology

diagnosed between birth and ten years of age. Neuroblastoma is very rare in adolescents and young adults (< 0.1 cases per 100,000 people); however, they frequently present indolent disease with very poor outcome (5-7). The phenotype of neuroblastoma is also associated with race. A higher proportion of patients with high-risk malignancy have been seen in patients with African ancestry than in children of European descent (8). There are no environmental factors clearly related to an increased risk of neuroblastoma. However, taking recreational drugs might still increase the odds (9). Neuroblastoma is considered an ultra-orphan condition, with less than 1,000 new cases per year in North America (10,11).

Neuroblastoma is a highly heterogeneous malignancy ranging from spontaneous regression without any need of therapy to resistant tumors with metastatic lesions and very poor outcome. The 5-year survival rate has improved over the last decades from below 50% to around 80%. However, survival of patients is still strongly dependent on the stage of the disease. Children with low-risk neuroblastoma present very good prognosis with survival rates above 85%, whereas 5-year survival rates for high-risk patients are below 50%, and less than 10% in children who relapse (4).

1.1.2. Origin of neuroblastoma

Neuroblastoma is an embryonal tumor, which means that it arises from cells that are in early stages of development. It is widely accepted that neuroblastoma is derived from neural crest (NC) specified to the sympathoadrenal (SA) lineage. NC cells are multipotent and transient cell population that arises during early embryogenesis and differentiate into a wide range of tissues, including peripheral neurons, enteric neurons and glia, Schwann cells, melanocytes, adrenal medulla, and much of craniofacial skeleton (12). NC induction, specification, delamination and differentiation are highly complex processes orchestrated by multiple gene regulatory networks (13).

NC induction, specification and delamination

NC induction starts during gastrulation with formation of tissues involved in neural tube development, precursor of the central nervous system. Neural crest gene expression pattern is coordinated by transcription factors activated by bone morphogenic protein (BMP), Wingless-Int, fibroblast growth factor (FGF), and Notch/Delta signalling pathways (14).

After neural crest induction, a second wave of transcription factors is expressed to promote cell proliferation, suppress neural differentiation, and maintain these cells in a multipotent state. The main factors involved in maintaining multipotency in this stage are c-Myc and ID3. A third wave of transcription factors is crucial to initiate the epithelial-to-mesenchymal (EMT) transition. EMT leaded by SOX9, SOX10, FOXD3, SNAIL2 and TWIST1, allows NC cells to reduce cell adhesion to neighboring neuroepithelial cells and acquire mesenchymal migratory characteristics to migrate to diverse locations in the embryo (12,13). Migrating NC cells can be divided in different subpopulations depending on their destination: cranial, vagal, trunk and sacral NC cells. These subgroups differ in their migratory pattern, gene expression profile and differentiation potential. MYCN expression during EMT is essential to induce ventral migration of trunk NC cells to reach the dorsal aorta, where they differentiate into SA progenitor cells, which ultimately originate peripheral nervous system, including the adrenal gland and sympathetic ganglia, which are the most common locations of primary neuroblastoma tumors.

SA specification

Neuroblastoma gene expression profiles and their anatomical sites at which they grow suggest that these tumors derive from SA precursors which arise from the neural crest cells that have migrated and settled in the dorsal aorta. Paired-like homeobox 2B gene (*PHOX2B*) expression and BMPs released from dorsal aorta are fundamental for SA specification (Figure 2). *PHOX2B* is a transcription factor that activates SA specifiers including *MASH-1*, *HAND2*, *GATA2*, *GATA-3* and noradrenergic markers such as tyrosine hydroxylase and dopamine beta-hydroxylase (13). *PHOX2B* is frequently expressed in neuroblastoma and has been identified as a sensitive and specific minimal residual disease marker (15).

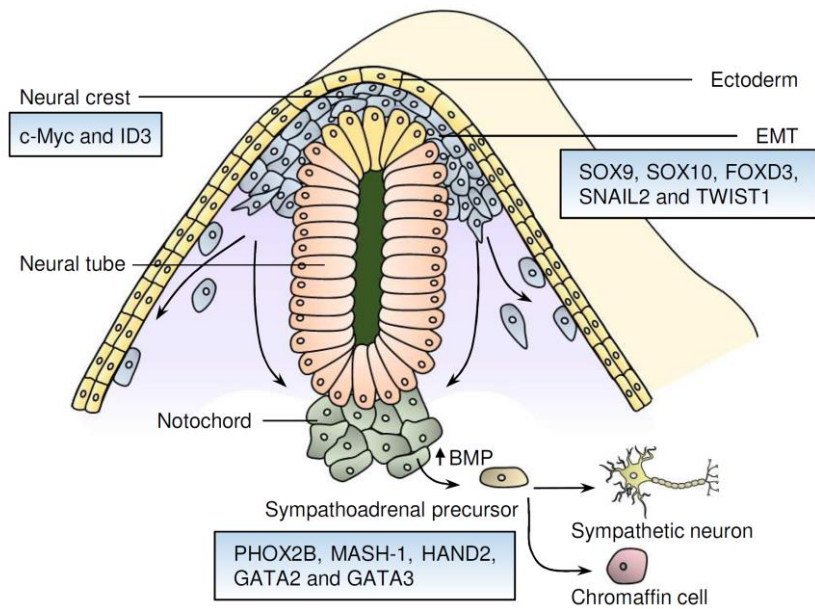


Figure 2. NC induction, delamination and differentiation. During embryogenesis, NC cells arise from dorsal neural tube and undergo EMT to migrate and differentiate to a wide range of cell types. NC delamination and differentiation are complex processes tightly regulated by epigenetic and transcriptional programs. *MYCN* expression during delamination is crucial for NC to reach the dorsal aorta and commit to SA precursors. Adapted from (12).

Role of MYCN in NC and neuroblastoma

As mentioned before, MYCN expression is crucial for the ventral migration of NC cells. However, low or absent MYCN expression is required to promote SA maturation; therefore, the levels of this protein progressively decrease during differentiation of sympathetic neurons. Multiple studies of MYCN expression during NC development indicate that neuroblastoma arises during early migration or SA specification and demands sustained MYCN expression to induce tumorigenesis (16,17). There is clear evidence to suggest that MYCN contributes to malignant neuroblastoma by promoting cell cycle progression and survival (18). In this line, *MYCN* amplification was found to correlate with poor outcome over 30 years ago and is a marker still used to stratify patient risk (19).

Model of neuroblastoma tumorigenesis

A singular characteristic of certain pediatric tumors, such as neuroblastoma, is that some patients with a specific pattern of primary tumor and metastasis have a high likelihood of undergoing spontaneous regression without therapy. That fact indicates that neuroblastoma arises in the embryo and ought to adapt in an adverse postnatal environment after birth to survive. Marshall G, et al (20) proposed a tumorigenesis model for embryonal malignancies with evidence of prenatal origin which includes three hits. The first hit is an excess of cell proliferation during organogenesis. For example, MYCN is the first hit from the tyrosine-hydroxylase (*Tb*)-*MYCN* transgenic mouse model. Other inherited genetic alterations, such as mutations in Anaplastic lymphoma kinase (*ALK*) or *PHOX2B*, are associated with familial neuroblastoma (21,22). A second hit would allow neuroblastoma cells to survive by avoiding cell death mechanisms that delete excess cells once organogenesis is completed. Nerve growth factor, secreted by local fibroblasts, is a powerful neural survival factor that regulates whether sympathetic ganglia matures into terminal ganglion or undergoes apoptosis. Premalignant cells must be resistant to trophic factor withdrawal. Finally, a third hit accelerates the genome instability to induce transformation (Figure 3). Genomic instability could be induced by the loss of function of one allele of a tumor suppressor gene, chromothripsis, feed-forward loops between MYCN and SIRT1, SIRT2 and Aurora kinase

Introduction

Origin of neuroblastoma

A (AURKA), or inherent properties of embryonal cells that enable their rapid proliferation (20).

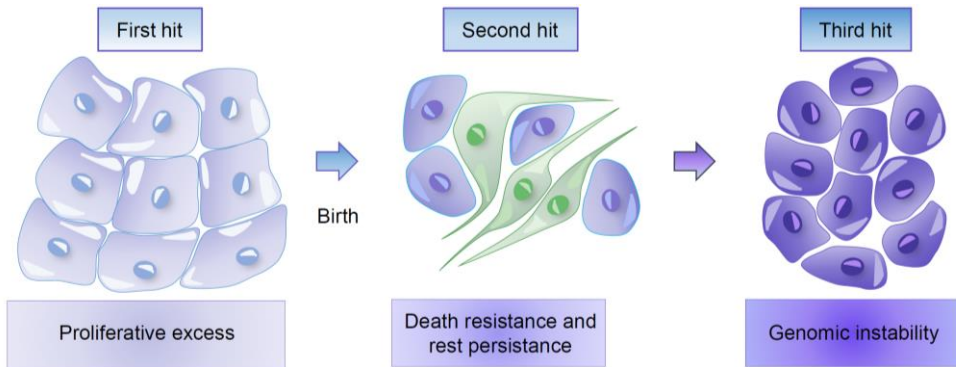


Figure 3. Model of neuroblastoma tumorigenesis. Marshall G, et al (20) propose that neuroblastoma need three hits to arise. First, a prenatal proliferative excess in the tissue of origin. Second, a cell intrinsic mechanism for surviving after birth. Third, accelerated pathway that promote genomic instability.

1.1.3. Familial neuroblastoma

Familial neuroblastoma has an autosomal dominant inheritance pattern, meaning that one copy of the altered gene increases the risk of developing the malignancy, but with incomplete penetrance because not all individuals who carry the altered gene develop the disease. In the 1970s, familial neuroblastoma was proposed to have a similar pattern than retinoblastoma, “two-hit” model. The first hit is the germline mutation which is followed by a second hit of an acquired somatic mutation. However, unlike retinoblastoma, nearly all patients with neuroblastoma are sporadic. Only about 1 to 2% of patients have familial neuroblastoma. Familial neuroblastoma tends to appear at younger age than sporadic neuroblastoma. It is associated with multiple primary tumors (10,23,24). Although familial neuroblastoma is rare, the identification of molecular events involved in familial neuroblastoma provided important information of neuroblastoma tumorigenesis and the identification of potential therapeutic targets.

PHOX2B

The first gene described to harbor germline mutations in neuroblastoma patients was *PHOX2B* (25,26), a crucial transcription factor involved in autonomic nervous system development (27). It was noted that patients with congenital central hypoventilation syndrome and Hirschsprung’s disease, which are related to a problem in NC development, had an increased probabilities of developing neuroblastic tumors compared to the general population (28). *PHOX2B* was first identified as a driver for these genetic disorders and eventually in patients with a family history of neuroblastic tumors (25).

ALK

ALK is a tyrosine kinase transmembrane receptor highly expressed during development of the nervous system (29). Mossé, Janoueix-Lerosey, and their respective colleagues reported that *ALK* germline mutations were the main cause of familial neuroblastoma. Most mutations were mapped to essential regions of the tyrosine kinase domain and predicted to be oncogenic drivers (21,30). Moreover, somatically acquired mutations and amplifications of

Introduction

Familial neuroblastoma

ALK were also identified in a significant number of sporadic neuroblastomas, which highlight the biological value of *ALK* for neuroblastoma tumorigenesis (21,30-32).

KIF1B

KIF1B is a motor protein member of the kinesin superfamily involved in the transport of mitochondria and synaptic vesicle precursors (33). Inherited loss-of-function of *KIF1B* by missense mutations was identified to be involved in neuroblastoma and pheochromocytoma development. Schlisio and colleagues proposed that loss of one allele of *KIF1B* would protect neuronal progenitor cells with malignant potential from apoptosis, and eventually constitute an aggressive malignancy (34). Interestingly, *KIF1B* is located in 1p36, a chromosomal region frequently deleted in neuroblastoma.

RASopathies

Patients with some germline activating mutations involving RAS pathway can be susceptible to developing certain types of malignancies, including neuroblastoma. Costello and Noonan syndromes are rare genetic conditions that involve genes of the canonical RAS pathway. RAS-MAPK pathway has a crucial role during NC differentiation (35). Mutations in this pathway may avoid the correct differentiation of NC cells and could explain the prevalence of neuroblastoma in people with these syndromes (36).

Cancer predisposition syndromes

Even though neuroblastoma is not a typical Li-Fraumeni syndrome (LFS) malignancy, multiple cases of neuroblastoma have been noted in LFS patients, especially the R337H *TP53* missense mutation (37,38). Beckwith-Wiedemann syndrome is a condition induced by the disruption of *CDKN1C* expression, which is a negative regulator of cell proliferation. Patients with this syndrome are predisposed to develop certain malignancies such as neuroblastoma (2 to 5%) (39,40).

Genetic variants

Genome-wide association studies have been performed with the aim of identifying genetic variants associated with human diseases. Twelve genetic variants associated with neuroblastoma onset were identified (Figure 4). Despite the modest individual effect of each variant, multiple polymorphisms could contribute to promote malignant transformation (41).

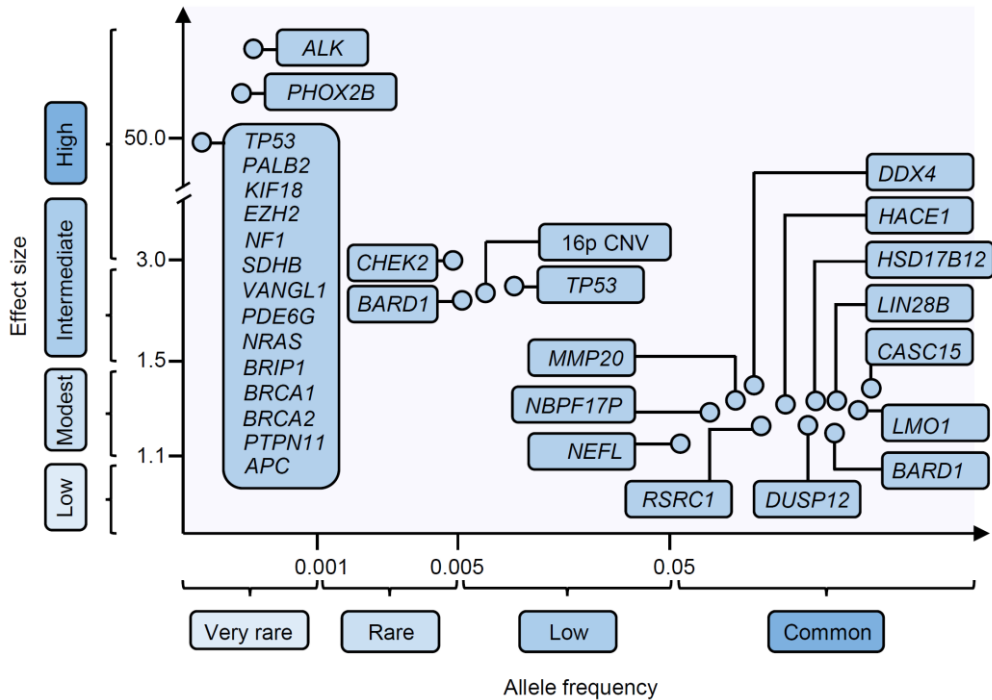


Figure 4. Genetic predisposition to neuroblastoma. *ALK* and *PHOX2B* mutations cause hereditary neuroblastoma with high penetrance. *ALK* and *PHOX2B* mutant alleles are uncommon in the population and are inherited in an autosomal dominant Mendelian manner. Other genes with rare mutations in the germline that may predispose to neuroblastoma have been reported (*TP53*, *BRAC2*, etc.), but the clinical relevance of these mutations has not yet been characterized. There are several common polymorphisms that individually have modest effect on neuroblastoma tumorigenesis but can cooperate to develop neuroblastoma. Adapted from (10).

1.1.4. Genetic alterations of neuroblastoma

Even though about 98-99% of all neuroblastoma cases are sporadic, there are no environmental factors described to raise the risk of developing neuroblastoma. Several somatic genetic alterations have been identified in neuroblastoma, the most common being chromosomal aberrations with gains or losses in genetic material.

Segmental chromosomal aberrations

Neuroblastoma aggressiveness is strongly associated with segmental chromosomal aberrations (SCA). Aggressive neuroblastoma is particularly characterized by a high number of SCA and low number of numerical changes (42). Gain of 17q has been detected in over 50% of neuroblastoma patients and loss of 1p36 has been reported in around 25% of cases. Both gain of 17q and loss of 1p36 correlate with *MYCN* amplification and poor outcome (43,44). Loss of heterozygosity (LOH) of 11q23 has been detected in one-third of neuroblastoma patients and unbalanced 11q LOH has been reported in 50% of those with 11q23 LOH. Both, unbalanced 11q LOH and 11q23 LOH are inversely correlated with *MYCN* amplification and are associated with poor outcome (43,45,46). The association of LOH of 1p36 and 11q with poor outcome suggests that some tumor suppressive genes are encoded in these chromosome regions. 1p36 region contains several potential tumor suppressor genes such as *CHD5*, *CAMPTA1*, *KIF1B*, *CASZ1* and *MIR34A* (47). 11q23 LOH region also contains multiple genes with tumor-suppressive functions such as *H2AFX*, *ATM* or *CADM1* (46,48). There are other common chromosomal alterations in neuroblastoma such as gains of 1q and 2p and loss of 3p, 4p and 14q, but their clinical relevance is still unclear (10).

***MYCN* amplification**

MYCN, located at chromosome 2p24, is a transcription factor, member of the MYC-oncogene family, involved in the control of essential processes during embryonal development (49). *MYCN* is situated downstream multiple pathways promoting cell growth and proliferation, and repressing genes involved in differentiation and apoptosis (18). The

amplification of *MYCN* (> 10 copies) is detected in about 20% of all neuroblastoma cases (4). *MYCN* amplification was one of the first alterations associated with poor outcome and remains one of the most important genetic markers associated with aggressive phenotype and poor survival (19,50). As mentioned before, *MYCN* overexpression in NC cells was found to be sufficient to develop neuroblastoma in transgenic mice model (16).

***ALK* mutations and amplifications**

ALK missense activating mutations not only were reported to be the main cause of familial neuroblastoma, but also were found to be present in 12% high-risk sporadic neuroblastoma cases (21). *ALK* activating mutations and high expression of the wild type form in sporadic neuroblastoma are associated with poor prognosis (51). Remarkably, transgenic mice expressing in the NC both *ALK^{F1174L}* and *MYCN* developed neuroblastoma with earlier onset, higher penetrance and enhanced lethality compared to *ALK^{F1174L}* and *MYCN* alone (52). George and colleagues reported that 15% of neuroblastoma with *MYCN* amplification presented concomitant *ALK* amplification. *ALK* amplification was present almost exclusively in those samples with *MYCN* amplification (21,32).

Other genetic alterations

Compared to adult malignancies, the number of somatic mutations in neuroblastoma patients is low. In fact, only a small subset of neuroblastomas have an identifiable oncogenic driver mutation (53). The use of whole-genome sequencing has identified genetic relevant alterations in multiple genes such as *ATRX* and *TERT*, both involved in telomeres lengthening. *ATRX* is a RNA helicase which belongs to the SWI/SNF family of chromatin remodelling proteins and its inactivation results in alternative lengthening of telomeres (54). About 10% of advanced stage neuroblastoma presented a loss-of-function alteration in *ATRX* (55). *ATRX* mutations were also found at very high frequencies in neuroblastomas from adolescent and young adults (56).

TERT encodes the telomerase reverse transcriptase of the telomerase complex. Valentijn, Peifer and their respective colleagues described that 23-31% of high-stage neuroblastoma presented *TERT* rearrangements associated with increased *TERT* expression. Interestingly,

Introduction

Genetic alterations of neuroblastoma

TERT rearrangements, *ATRX* inactivation and *MYCN* amplification were found to be almost mutually exclusive genetic alterations in neuroblastoma (55,57). As *MYCN* is known to activate *TERT* expression, these data suggest that lengthening of telomeres might be required for high-risk disease.

ARID1A and *ARID1B* genes, involved in the chromatin remodeling, are thought to have a role in neuroblastoma. Sausen and colleagues reported chromosomal deletions, LOH and point mutations of *ARID1A* and *ARID1B* in a significant number of high-risk neuroblastomas. *ARID1A* and *ARID1B* alterations were also associated with early treatment failure and decreased survival (58).

LIN28B

LIN28B is a RNA-binding protein that regulates mRNA translation and/or stability and microRNAs (miRNAs) maturation. *LIN28B* acts as an oncogene by binding to the precursors of certain miRNAs, including *let-7* family, thereby blocking their biogenesis (59).

LIN28B has been associated with neuroblastoma susceptibility. Diskin and colleagues performed a genome-wide association study and identified that the allele rs17065417 of *LIN28B* was associated with this particular malignancy. Interestingly, neuroblastoma cell lines homozygous for the rs17065417 risk allele were found to express higher levels of *LIN28B* mRNA and protein compared to heterozygous cell lines. Homozygous cell lines for rs17065417 also displayed absent or decreased expression of tumor suppressor *let-7* family miRNAs (60). Of note, *LIN28B* was also found to be associated with poor neuroblastoma outcome (60,61).

LIN28B expression was found to correlate with *MYCN* expression (61,62). Concordantly, overexpression of *LIN28B* in SA lineage induced neuroblastomas with high expression of *MYCN* in transgenic mice (61). These results have been recently supported by two vertebrate models, zebrafish and xenopus, with *LIN28B* overexpression (63,64). *LIN28B* was shown to regulate RAN, which promotes the phosphorylation and activation of AURKA. AURKA leads cell cycle progression by phosphorylating several cell cycle regulators and stabilizing *MYCN* protein afterwards (65). All these findings raises the opportunity to find new therapeutic approaches to inhibit neuroblastoma tumorigenesis (i.e. AURKA inhibitors).

1.1.5. Neuroblastoma clinical presentation and diagnosis

Clinical presentation

Neuroblastoma affects a wide range of ages, from birth through young adulthood. The median age at diagnosis of neuroblastoma is 18 months (5). Even though 90% of tumors arise in children younger than 10 years of age, neuroblastoma is likely to be much more indolent and lethal disease for adolescent and young adults (6). In fact, the phenotype of neuroblastoma is highly associated with the age of the children. For example, patients less than 18 months of age have much better prognosis than older patients. Interestingly, the attempt to detect neuroblastoma early using urine tests for catecholamine metabolites showed that 50% of all neuroblastoma that arise in the first year of life are never detected due to complete spontaneous remission (7).

The clinical presentation of neuroblastoma can be quite diverse, ranging from asymptomatic lesions to multiple metastases. Primary neuroblastomas can present anywhere along the sympathetic nervous system. The most common sites of neuroblastoma origin, in decreasing order, are the adrenal medulla (35%), extraadrenal retroperitoneum (30-35%), and posterior mediastinum (20%). The less common sites are the neck (1-5%) and pelvis (2-3%) (Figure 5).

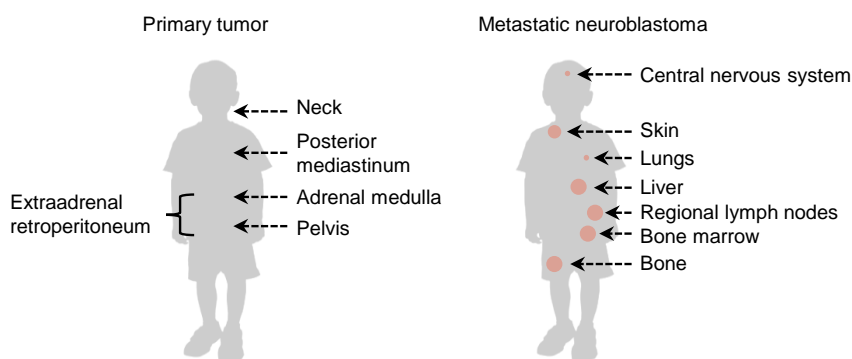


Figure 5. Location of primary and metastatic neuroblastoma. Primary neuroblastoma can arise anywhere in the sympathetic system, being the adrenal gland the most common site of origin. Neuroblastomas tend to spread to the bone marrow, bone, regional lymph nodes and liver. Metastases in the central nervous system, skin and lungs are less common.

Introduction

Neuroblastoma clinical presentation and diagnosis

Neuroblastomas arising in the adrenal gland are associated with lower survival compared to primary tumors of other locations (66). About 50% of patients present metastases at the time of diagnosis. The most common sites of metastases are bone marrow (56%), bone (46%), regional lymph nodes (24%) and liver (21%), whereas metastases in skin (4%), lung (3%) and in the central nervous system (1%) are rare (Figure 5) (67,68). Approximately 1% of patients debut with metastatic disease but the site of origin cannot be found at diagnosis (69). Clinical signs and symptoms are associated with the origin of the primary tumor and metastatic lesions (Table 1).

Table 1. Neuroblastoma symptoms (adapted from (70)).

| Location | Signs and symptoms |
|---|---|
| Abdomen/pelvis | Pain, constipation, distension, urinary retention, hypertension |
| Thorax | Respiratory distress, Horner syndrome |
| Presacral and paraspinal (includes abdominal and thoracic masses) | Symptoms of cord compression (urinary retention, paraplegia/paraparesis, clonus) |
| Neck | Mass/swelling |
| Metastases | Irritability, bone pain, cytopenias, periorbital ecchymoses, fever, weight loss, lymphadenopathy |
| 4S/4M metastases | Hepatomegaly, coagulopathy, hyperbilirubinemia, respiratory distress (from abdominal enlargement), skin nodules |
| Paraneoplastic syndromes | - Oposoclus myoclonus ataxia syndrome - VIP secreting tumors: intractable secretory diarrhea |

VIP, vasoactive intestinal peptide

Diagnosis

Diagnosis of neuroblastoma requires multiple laboratory tests, radiographic imaging and histological assessment of the tumor (Table 2). If neuroblastoma is suspected, a complete blood test, prothrombin time and partial thromboplastin time, electrolytes, creatinine, uric acid, liver function, ferritin and lactate dehydrogenase should be tested; the last two tests indicate a poorer outcome when increased (50). Altered levels of catecholamines or catecholamine metabolites (dopamine, homovanillic acid and vanillylmandelic acid) can be detected in the urine of nearly all neuroblastoma patients. The relative amounts and ratios of catecholamine metabolites correlate with the degree of cellular differentiation and are associated with biologically unfavorable malignancies (71).

Radiographic imaging and metastatic evaluation is essential for neuroblastoma staging, characterization and surgery. Ultrasonography, which is widely available and non-invasive, is usually the first imaging modality used to detect the presence of tumor mass. However, computed tomography (CT) or magnetic resonance imaging (MRI) are required for accurate localization and the identification of image-defined risk factors (IDRF). IDRF are imaging features determined at the time of diagnosis that predict surgical risk factors. CT and MRI show high resolution images critical to evaluate the size and localization of the primary tumor, arterial encasement, infiltration of adjacent organs, and/or structures or the spinal canal (72). Metastatic lesions are assessed by a ^{123}I -metaiodobenzylguanidine (mIBG) scan. MIBG is a radiolabeled norepinephrine analog which can be uptaken into tumor cells by the norepinephrine transporter in 90% of neuroblastomas. MIBG enables the detection of both primary tumors and metastases in soft tissues and bone marrow (73). Combination of mIBG with other imaging techniques, such as single-photon emission CT, provide the contrast of MRI and the anatomical precision of CT (74). Neuroblastomas that poorly accumulate mIBG can be assessed using other techniques such as ^{18}F -fluorodeoxyglucose positron emission tomography (75) (Table 2).

Tumor biopsy confirms the diagnosis and provides essential information on prognosis. Neuroblastoma, ganglioneuroblastoma and ganglioneuroma present different grades of maturation. Neuroblastomas are immature tumors composed of small round cells, whereas ganglioneuroma is composed of mature cells that have differentiated into ganglion cells. Ganglioneuroblastoma presents features of both of these tumors. Molecular examination of neuroblastoma is necessary to determine overall outcome. *MYCN* amplification, diploidy and SCA correlate with poorer survival. *MYCN* amplification is mainly evaluated by *in situ* hybridization (50,76). Cell ploidy and SCA are measured by flow cytometry and array comparative genomic hybridization, respectively.

Introduction

Neuroblastoma clinical presentation and diagnosis

Table 2. Tests and procedures used to diagnose neuroblastoma (adapted from (10)).

| Laboratory |
|--|
| <ul style="list-style-type: none">– Complete blood count and platelet count– Prothrombin time and partial thromboplastin time– Electrolyte, creatinine and uric acid levels and liver function– Levels of serum markers ferritin and lactate dehydrogenase– Catecholamines or catecholamine metabolites levels (increased in 90% of patients with neuroblastoma) |
| Imaging |
| <ul style="list-style-type: none">– CT or MRI of the primary site, chest, abdomen and pelvis– CT or MRI of the head and neck if clinically involved– mIBG scan and then 18F-fluorodeoxyglucose-positron emission tomography scan if the tumor is not mIBG-avid |
| Pathology |
| <ul style="list-style-type: none">– Tumor biopsy with immunohistochemistry and International Neuroblastoma Pathology Committee classification– Fluorescence <i>in situ</i> hybridization for <i>MYCN</i>– Array comparative genomic hybridization or other study for segmental chromosomal alterations– DNA index (ploidy)– Bilateral bone marrow aspirate and biopsy with immunohistochemistry to detect metastatic disease– Optional: genomic analysis for <i>ALK</i> alterations |

1.1.6. Neuroblastoma staging and risk assessment

Neuroblastoma is a complex and heterogeneous malignancy with prognosis ranging from spontaneous regression to highly aggressive disease that often becomes refractory to all current treatments. There are different prognostic factors that are used for risk assessment: age at the time of diagnosis, disease stage, *MYCN* amplification, tumor cell ploidy, grade of differentiation, 11q aberration and tumor histopathology according to the International Neuroblastoma Pathologic Classification (INPC) system (70).

Neuroblastoma staging

International Neuroblastoma Staging System (INSS) classified neuroblastoma in different stages depending on the local invasion, the amount of resection, node involvement and presence of distant metastases. INSS was developed in 1986 and revised in 1993 and has the objective of establish international consensus for a common staging system and therapy (77,78). INSS system is for post-operative patients and mainly for prognosis. INSS Stage 1 to 3 are localized tumors; in contrast, Stage 4 and 4S present distant metastases. Stage 4S (4Special) is defined by children younger than 365 days with primary tumor located as in stage 1, 2A or 2B and metastases in liver, skin, and/or bone marrow (Table 3).

Table 3. International Neuroblastoma Staging System (adapted from (78)).

| Stage | Description |
|----------|---|
| Stage 1 | Localized tumor that can be removed completely during surgery. Lymph nodes attached to and removed with the primary tumor may be positive for tumor microscopically, representative ipsilateral lymph nodes are negative. |
| Stage 2A | Localized tumor that cannot be entirely removed by surgery. Representative ipsilateral nonadherent lymph nodes are microscopically negative for the tumor. |
| Stage 2B | Localized tumor that can or cannot be totally removed during surgery, ipsilateral nonadherent lymph nodes are positive for tumor microscopically but contralateral lymph nodes must be negative. |
| Stage 3 | The tumor cannot be removed with surgery and has disseminated across the midline, with or without regional lymph node metastasis; or localized unilateral tumor with contralateral regional lymph node involvement; or midline tumor with bilateral extension by infiltration or by lymph node involvement. |
| Stage 4 | The primary tumor has spread to distant lymph nodes, bones, bone marrow, liver, skin, and/or other organs (except as defined for stage 4S). |
| Stage 4S | The primary tumor is located (as in stage 1, 2A or 2B) with dissemination only to skin, liver, and/or bone marrow, limited to infants younger than 365 days. |

Introduction

Neuroblastoma staging and risk assessment

In 2009, representatives from a major consortium in North America (COG, Children's Oncology Group), Europe (SIOPEN, International Society of Paediatric Oncology European Neuroblastoma), and other societies from Germany, Japan, and Australia developed the International Neuroblastoma Risk Group's stratification system (INRGSS). The objective of INRGSS is to create a consensus approach to stratify patients at the time of diagnosis (before surgery). The INRGSS is based on clinical criteria and IDRF (72). INRGSS can distinguish between loco-regional tumors that not involve vital structures (L1), locally invasive tumors (L2), tumors with distant metastases (M) or distant metastases in children younger than 547 days (18 months) to specific tissues (MS) (50,72) (Table 4).

Table 4. International Neuroblastoma Risk Group Staging System (adapted from (72)).

| Stage | Description |
|-------|--|
| L1 | Localized tumor not involving vital structures |
| L2 | Loco-regional tumor with presence of one or more IDRF |
| M | Distant metastatic disease (except stage MS) |
| MS | Metastatic disease in patients younger than 18 months with metastases confined to skin, liver and/or bone marrow |

Age at diagnosis

The age at diagnosis was one of the earliest prognostic markers defined for neuroblastoma (79). Patients older than 1 to 2 years at diagnosis have worse outcome than infants. Even though the 365 days cut-off had been historically used as a prognostic marker for clinical behavior of the tumor, several retrospective studies showed evidence that 18 months was a more clinically relevant cut-off and was selected for the INRGSS (5,50,80,81). Neuroblastoma is rarely diagnosed in adolescents and young adults. Despite these patients present an indolent disease and infrequent *MYCN* amplification, they display worse outcome than younger patients. However, no additional prognostic age cut-off greater than 18 months have been defined (6).

Histologic classification

Histopathological examination is essential for neuroblastoma staging. The INPC adopted with some changes the age-linked classification method proposed by Shimada et al. in 1984

(82). In the INPC, neuroblastic tumors are classified into four groups based on morphologic criteria: neuroblastoma (Schwannian stroma-poor); ganglioneuroblastoma intermixed (Schwannian stroma-rich); ganglioneuroma (Schwannian stroma-dominant) and nodular ganglioneuroblastoma (composite Schwannian stroma-rich/stroma-dominant and stroma-poor). The INPC also uses grade of neuroblastic differentiation and mitosis-karyorrhexis index (MKI) as prognostic indicators for neuroblastoma. Specifically, neuroblastomas are divided in 3 different subtypes depending on the grade of neuroblastic differentiation: undifferentiated, poorly differentiated and differentiating (83,84). Shimada et al. also demonstrated that three MKI classes (low, intermediate and high) presented distinctive prognostic values (85). Of note, these morphologic prognostic indicators are linked to the age of the patients (any age, < 1.5, 1.5 to 5.0 and ≥ 5.0 years) (Table 5).

Table 5. International neuroblastoma pathology classification (85).

| Category and subtype | Stroma development | MKI | Age (years) | Prognostic |
|-----------------------|--------------------|-------|-------------|------------|
| Neuroblastoma | | | | |
| Undifferentiated | Poor (0 < 50%) | Any | Any | UH |
| | | H | Any | UH |
| Poorly differentiated | Poor (0 < 50%) | Any | > 1.5 | UH |
| | | L / I | < 1.5 | FH |
| | | H | Any | UH |
| | | Any | ≥ 5 | UH |
| Differentiating | Poor (0 < 50%) | I | > 1.5 | UH |
| | | I | < 1.5 | FH |
| | | L | < 5 | FH |
| GNB nodular | Rich/dominant/poor | | | FH, UH |
| GNB intermixed | Rich | | | FH |
| Ganglioneuroma | Dominant | | | FH |

Abbreviations: GNB, ganglioneuroblastoma; H, high; I, intermediate; L, low; UH, unfavourable histology; FH, favourable histology.

Genetic alterations

MYCN amplification, 11q aberration and DNA ploidy are genetic alterations clinically relevant for prognosis used by the INRGSS. *MYCN* amplification is found in ~20% of cases and it was one the first alterations described to be strongly associated with neuroblastoma

Introduction

Neuroblastoma staging and risk assessment

outcome (19,86,87). Neuroblastoma with amplification of *MYCN* is particularly associated with advanced disease, high-risk category and poor prognosis (50). 11q deletion is a frequent genetic alteration in neuroblastoma which accounts for 35 – 40% of cases approximately. Interestingly, 11q aberration is almost mutually exclusive with *MYCN* amplification and its prognosis significance is similar to *MYCN* amplification (45,46,88). DNA ploidy was also identified as a prognostic value for neuroblastoma. Diploidy is associated with a poorer survival than triploidy (50).

1.1.7. Risk stratification

According to the previous described clinical and biological factors (i.e. INRG stage, IDRF, presence of metastases, age at diagnosis, histologic category, grade of differentiation, *MYCN* status, genomic profile and ploidy), neuroblastoma patients are classified into four risk groups: very low, low, intermediate or high risk (Table 6).

While patients classified as very low, low or intermediate risk have good prognosis, high-risk patients have a 5-year survival of less than 50%. These patients are subjected to intensive treatment; however, most children with high-risk neuroblastoma will not achieve long-term cure, and some of the survivors will suffer severe long-term side effects, such as second malignant neoplasm, and life-long disabilities induced by neuroblastoma treatment (89,90).

Table 6. Modified INRG consensus pretreatment classification (adapted from (10)).

| Risk group | INRG stage | IDRF | Distant met | Age months | Histologic category | Grade diff | MYCN | Genomic profile | Ploidy |
|--------------|------------|---------|-------------|------------|---------------------|------------|------|------------------|--------|
| Very low | L1 | Absent | Absent | Any | GNBn/NB | Any | - | Any | Any |
| | L1/ L2 | Any | Absent | Any | GN/GNBi | Any | - | Any | Any |
| Low | L2 | Present | Absent | <18 | GNBn/NB | Any | - | F | Any |
| | L2 | Present | Absent | ≥18 | GNBn/NB | D | - | F | Any |
| | MS | Any | Present | <12 | Any | Any | - | F | Any |
| Intermediate | L2 | Present | Absent | <18 | GNBn/NB | Any | - | U | Any |
| | L2 | Present | Absent | ≥18 | GNBn/NB | D | - | U | Any |
| | L2 | Present | Absent | ≥18 | GNBn/NB | PD/UD | - | Any | Any |
| | M | Any | Present | <18 | Any | Any | - | Any | HD |
| | M | Any | Present | <12 | Any | Any | - | U and/or diploid | |
| | MS | Any | Present | 12-18 | Any | Any | - | F | Any |
| | MS | Any | Present | <12 | Any | Any | - | U | Any |
| High | L1 | Absent | Absent | Any | GNBn/NB | Any | + | Any | Any |
| | L2 | Present | Absent | ≥18 | GNBn/NB | PD/UD | + | Any | Any |
| | M | Any | Present | 12-18 | Any | Any | - | U and/or diploid | |
| | M | Any | Present | <18 | Any | Any | + | Any | Any |
| | M | Any | Present | ≥18 | Any | Any | Any | Any | Any |
| | MS | Any | Present | 12-18 | Any | Any | - | U | Any |
| | MS | Any | Present | <18 | Any | Any | + | Any | Any |

12 months = 365 days; 18 months = 547 days. Met, metastases; diff, differentiation; GN, ganglioneuroma; GNBn, ganglioneuroblastoma nodular; GNBi, ganglioneuroblastoma intermixed; NB, neuroblastoma; D, differentiating; PD, poorly differentiated; UD, undifferentiated; U, unfavourable; F, favourable; HD, hyperdiploid.

1.1.8. Neuroblastoma clinical management

As mentioned before, stratification of neuroblastoma patients into different risk groups is necessary to decide the best treatment for each patient (91).

Very low- and low-risk neuroblastomas

Very low- and low-risk neuroblastoma accounts for nearly 50% of newly-diagnosed neuroblastoma. 5-year survival rates for these patients are higher than 95% with minimal therapy. Generally, most patients do not need treatment with chemotherapy since the tumor can be removed with surgery alone, or even revert spontaneously. COG P9641 and SIPOEN LNESG1 clinical studies showed excellent outcome for patients with surgical resection alone with OS rate of 99% for stage 1 and > 93% for stage 2 (92,93). Therefore, chemotherapy in very low- and low-risk patients is given only to patients who present life or organ-threatening symptoms, or in case of recurrence or tumor progression (94,95). Infants with localized adrenal masses showed very good outcome with observation alone. In a COG clinical trial, 81 % of infants younger than 6-months old were managed with observation and the remaining 19% underwent resection. None of the patients required chemotherapy and the 3-year OS rate was 100 % (96). Ongoing COG ANBL1232 clinical study (NCT02176967) has increased the age of observation (< 12 months) for non-high-risk neuroblastoma patients with localized tumors to determine whether observation alone is also convenient for these patients.

Intermediate-risk neuroblastomas

Intermediate-risk neuroblastoma includes a wide group of patients with INRG L2, M and MS without *MYCN* amplification. Their survival rates are higher than 90 %, and therapy is composed of moderate doses of multi-agent chemotherapy and surgical resection. Intermediate-risk chemotherapy consists of two to eight cycles of chemotherapy using multiple agents such as carboplatin or cisplatin, doxorubicin, etoposide, and cyclophosphamide (97). Recent studies have successfully reduced chemotherapy for these patients while preserving excellent survival rates (98,99). Surgical resection of the remaining

primary tumor is performed when possible but some trials suggest that complete resection is not essential (99,100). However, patients older than 18 months of age with unresectable neuroblastoma and either unfavorable genomic profile or histology present lower survival rates than the other patients, indicating that more intensive therapy including local radiotherapy could be necessary (99,101). The European study, LINES 2009 (NCT01728155) is currently studying to reduce the amount of chemotherapy for differentiating histology L2 neuroblastoma and nodular ganglioneuroblastoma patients and increase the amount of treatment, including radiotherapy and 13-cis-RA, for poorly differentiated or undifferentiated stage L2 neuroblastoma or nodular ganglioneuroblastoma patients.

High-risk neuroblastomas

The 5-year OS for high-risk neuroblastoma was 29%, 47% and 50% for patients diagnosed between 1990 and 1994, 2000 and 2004, and 2005 and 2010, respectively (102). The improvement in the OS was associated with the establishment of myeloablative therapy and immunotherapy in the regimen for high-risk neuroblastoma. Although the OS for high-risk neuroblastoma patients has improved since 1990s, further advances in the treatment are necessary as limited improvements have been achieved in the last two decades. Standard therapy for high-risk neuroblastoma patients involves three components: induction, consolidation and a post-consolidation phase (Figure 6).

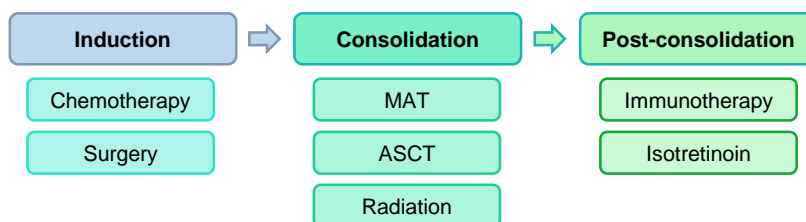


Figure 6. Standard schedule for high-risk neuroblastoma therapy. MAT, myeloablative therapy; ASCT, autologous stem cell transplant.

Induction phase

In the induction phase, patients are treated with a combination of chemotherapeutic agents. The aim of this pre-operative chemotherapy is to improve surgical resectability of the primary

Introduction

Neuroblastoma clinical management

tumor and reduce metastases. High-risk neuroblastoma treatment are distinct between cooperative groups (Figure 7). COG schedules, which include 6 cycles of combined administration of vincristine, doxorubicin, cyclophosphamide, cisplatin and etoposide, are used in North America. In addition, COG trials have integrated topotecan during the first two cycles of induction phase (103). On the other hand, in Europe, SIOPEN has established rapid COJEC regimen which consists of multiple chemotherapy cycles delivered every 10 days. Rapid COJEC gives 8 cycles using combination of cyclophosphamide (C), vincristine (O), carboplatin (J), etoposide (E) and cisplatin (C). Specifically, COJEC include two cycles of vincristine, carboplatin and etoposide; four cycles of cisplatin and vincristine; and two cycles of vincristine, etoposide and cyclophosphamide (104).

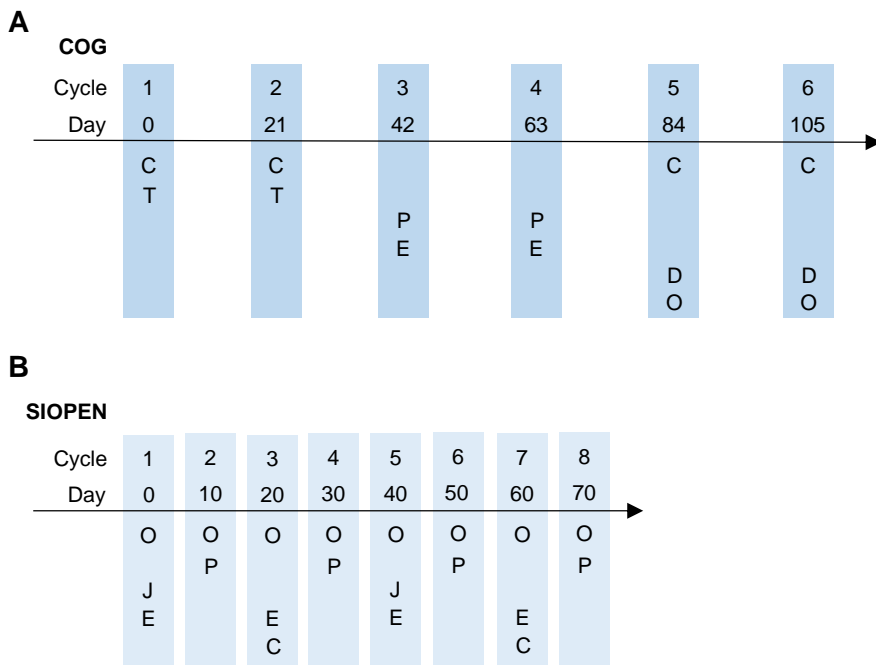


Figure 7. COG and SIOPEN induction chemotherapy schedule. (A) COG schedule in NCT00567567. **(B)** Rapid COJEC. C, cyclophosphamide; T, topotecan; P, cisplatin; E, etoposide; D, doxorubicin; O, vincristine; J, carboplatin. (Adapted from (104)).

Induction chemotherapy is a critical phase for the outcome of high-risk neuroblastoma patients. For example, response to chemotherapy measured by semi-quantitative mIBG scoring (Curie score) system is an independent prognostic factor for patients with high-risk

disease after induction (105). Even though a majority of patients with high-risk disease have favorable responses and achieve remission after induction therapy, up to 20% of patients experience disease progression or have unfavorable response to induction chemotherapy (6,94,106).

Surgical resection is essential for high-risk neuroblastoma treatment and it is usually performed at the end of the induction therapy. The timing of surgery is programmed to maximize tumor reduction before surgical resection. It is controversial whether a gross total resection of primary tumor is critical for the survival of high-risk neuroblastoma patients. Some trials show that the final outcome is determined more by metastatic relapse than by the degree of surgical resection (107). In addition, Simon and colleagues showed that complete resection of the primary tumor had no impact on outcome of stage 4 neuroblastoma older than 18 months of age (108). On the contrary, Du and colleagues reported that patients who underwent surgical intervention presented higher 3-year OS than patients who underwent biopsy only. However, no significant changes were accomplished in 3-year EFS (109).

Consolidation phase

The aim of consolidation phase is to eliminate remaining minimal disease. This phase is divided into two parts which include high dose of chemotherapy followed by autologous stem cell transplant (ASCT) and radiation therapy. The myeloablative regimen has been studied in multiple trials. Melphalan, carboplatin and etoposide are employed in several protocols, although clinical studies suggest that patients treated with busulfan and melphalan after rapid COJEC regimen present superior outcome with no increased toxicity (110,111).

Post-consolidation phase

Maintenance or post-consolidation phase is performed to reduce the number of patients that relapse. In post-consolidation phase, the differentiating agent cis-retinoid acid (cis-RA) is often given for 6 months after other treatments are completed (112,113). Multiple clinical trials using antibodies directed to GD2 ganglioside (expressed on neuroblastoma cell membrane) have been performed. Anti-GD2 monoclonal antibodies combined with cytokines (GM-CSF and interleukin-2) have been incorporated into the post-consolidation

treatment due to its capability to improve EFS of patients (56,114). Specifically, anti-GD2 induce antitumor activity by binding to GD2 and attracting immune cells (i.e. NK cells and granulocytes), which promote antibody-dependent cellular cytotoxicity and complement-dependent cytotoxicity (115). Interleukin-2 enhances tumor cytotoxicity by activating multiple immune cells (including NK cells, monocytes, and effector T cells, among others) and GM-CSF promotes clonal expansion and maturation of precursor cells to distinct immune cells (e.g. granulocytes and monocytes) (116,117).

Despite the intensive therapy for high-risk neuroblastoma patients described above, a majority of patients relapse. Patients who relapse have a 5-year OS of 8% due to the development of resistance to therapy (70).

Relapsed and refractory neuroblastoma

Despite advances in multimodal therapy, a majority of patients with high-risk neuroblastoma will either relapse or will respond poorly to standard treatment. Currently, there are no curative therapies for these patients. A retrospective study from Italy reported that 10-year OS rate was 6.8% after tumor progression and 14.4% after relapse in a subset of 424 and 357 patients, respectively. Tumor progression was registered at a median of 6.5 months and relapse was documented at a median of 16.2 months from diagnosis. Moreover, the majority of progressions and relapses were disseminated (> 75%) (118). In an effort to determine which biologic and clinical risk factors were associated with progression and relapse, a collaborative study among cooperative pediatric oncology groups from Europe, North America, Germany, Australia, New Zealand and Japan with a large cohort of patients was performed. In this study, time to first relapse, age, stage and *MYCN* amplification were identified as significant prognostic factors for relapsed and recurrent neuroblastoma (76). A more recent published meta-analysis of phase II studies of children with refractory or relapsed neuroblastoma performed in Europe reported that median OS rates were 27.9 months for patients with refractory disease and 11.0 for patients with relapsed neuroblastoma (119). Since patients with relapsed or refractory neuroblastoma have extremely poor

prognosis, many efforts are being made to find new therapies, which include combinations of additional chemotherapy or targeted therapies combined with chemotherapy.

Additional chemotherapy

Patients with relapsed/refractory neuroblastoma are often treated with additional chemotherapy regimens with different mechanism of action from those previously administered. Different combination strategies using topotecan, irinotecan, temozolomide and cyclophosphamide are currently being tested with the aim of improving OS rates.

Irinotecan and topotecan are camptothecin derivatives that inhibit topoisomerase I activity. Topotecan has shown efficacy and low toxicity in multiple clinical studies in combination with other chemotherapeutic agents such as temozolomide (TOTEM) (120), cyclophosphamide (121), cyclophosphamide and etoposide (TCE) (122), vincristine and cyclophosphamide (123) and vincristine and doxorubicin (TVD) (124). TVD combination has been recently evaluated in patients who failed to achieve the SIPOEN criteria for high-dose myeloablative therapy with the aim of improving the metastatic response. Amoroso and colleagues reported that TVD was significantly effective in improving the response rate of refractory neuroblastoma when following COJEC regimen and thereby in increasing the number of neuroblastoma patients eligible for high-dose myeloablative therapy (125). TVD regimen has been integrated as salvage treatment for neuroblastoma patients who do not have enough responses during induction phase (NCT01704716). On the other hand, irinotecan has shown efficacy and acceptable tolerability in combination with temozolomide and is regularly used in second line for recurrent neuroblastoma (126,127).

An additional chemotherapy regimen used for refractory neuroblastoma is the combination of ifosfamide, carboplatin and etoposide (ICE). A retrospective analysis of ICE performed by Kushner and colleagues showed great tolerability and satisfying disease regression rates: 14 out of 17 neuroblastoma patients with new relapse, 13 of out 26 patients with refractory disease and 12 of out 34 patients with progressive neuroblastoma (128). Moreover, ICE regimen has been tested during induction phase for high-risk neuroblastoma. Patients treated with intensive induction with ICE presented fast responses with high response rate (129).

Introduction

Neuroblastoma clinical management

Owing to its anti-neuroblastoma activity, there are multiple phase III clinical trials for high-risk neuroblastoma which are including ifosfamide in the induction regimen such as NCT04221035 in Europe and NCT02771743 in South Korea.

¹³¹I-MIBG therapy

¹³¹I-MIBG is a norepinephrine analogue which is selectively concentrated in the adrenergic tissues and tumors with similar histogenetic origin, such as neuroblastoma. Initial clinical studies using ¹³¹I-MIBG for recurrent and relapsed neuroblastoma showed acceptable tolerability and evidence of activity (130,131). More recent studies using higher doses of ¹³¹I-MIBG with a subsequent ASCT reported that 36% of patients presented objective responses and 34% of patients had disease stabilization for a median of 6.2 months after treatment (132). These results suggest that ¹³¹I-MIBG therapy could be used for high-risk patients during initial multimodal therapy. Some trials are testing ¹³¹I-MIBG during induction (NCT01175356, NCT03126916) and consolidation phase (NCT00798148, NCT03061656) (133).

Targeted therapies

Even though salvage chemotherapy and ¹³¹I-MIBG have shown antitumor activity against relapsed and refractory neuroblastoma, there are no curative therapies for these patients. Over the last decades, an intense investigation effort has been made to identify molecular aberrations in neuroblastoma, and as a result, a number of promising targets have been identified.

The Innovative Therapies for Children with Cancer, in partnership with the European Network for Cancer Research in Children and Adolescents and the SIOPEN, established the Neuroblastoma new drug development strategy (NDDS) project in 2012. The aim of NDDS is to accelerate the development of new inhibitors for neuroblastoma patients to increase survival rates. NDDS is a dynamic process that prioritizes targets and compounds according to tumor biology and new published data. Prioritized targets in 2017 were ALK, MEK, CDK4/6, MDM2, MYCN (druggable by BET bromodomain, AURKA and mTORC1/2 inhibition), BIRC5 and CHK1 (134,135).

ALK inhibitors

ALK activating mutations or amplifications are found in a significant number of neuroblastoma patients. The majority of familial neuroblastoma, which accounts for 2% of all cases, have *ALK* activating mutations in the tyrosine kinase domain, and 15% of high-risk sporadic neuroblastoma have *ALK* activating mutations or gene amplifications (21,136). Moreover, *ALK* wild type expression is increased in advanced and metastatic neuroblastoma (137). A phase I trial of the *ALK* inhibitor crizotinib showed good tolerability in pediatric patients and antitumor activity in patients harboring *ALK* translocations (NCT00939770) (138). Multiple *ALK* inhibitors such as crizotinib (NCT01606878, NCT02034981), ceritinib (NCT02780128), lorlatinib (NCT03107988) and entrectinib (NCT02650401) are currently being tested in clinics in patients with *ALK* activating mutations or translocations.

Inhibition of MYCN using BET bromodomain, AURKA and mTORC1/2 inhibitors

Even though *MYCN* is a promising therapeutic target for neuroblastoma, no compounds that directly inhibit *MYCN* have reached the clinics. However, promising approaches to target *MYCN* indirectly have been developed. BET bromodomain inhibitors have shown promising results in neuroblastoma preclinical studies in *MYCN* amplified tumors. BET inhibitors downregulated *MYCN* protein levels and conferred a significant survival advantage (139). A phase I study is currently testing BMS-986158 in pediatric solid tumors, brain tumors and lymphoma (NCT03936465). *AURKA* controls *MYCN* stabilization and the G2-M transition by promoting centrosome maturation and bipolar spindle assembly (140,141). Phase I clinical trials using alisertib, an oral small-molecule inhibitor of *AURKA*, alone and in combination with irinotecan and temozolomide showed good tolerability and evidence of efficacy with encouraging response and progression-free survival rates (142-144). Interestingly, combination of BET bromodomain and *AURKA* inhibitors have been reported to act synergistically to reduce viability of multiple neuroblastoma preclinical models (145). *mTOR* pathway is fundamental for oncogenesis and cancer progression of many tumors. Inhibition of *mTOR* signaling has been reported to destabilize *MYCN* protein (146). Multiple inhibitors are being tested as a single agent in phase I/II studies for pediatric

Introduction

Neuroblastoma clinical management

malignancies (NCT03213678, NCT01582191) or in combination with chemotherapy and radiotherapy (NCT01217177).

Cell cycle inhibitors

Several clinical trials are testing inhibitors that target proteins involved in cell cycle (i.e. CDK4/6, AURKA, CHK1). CDK4/6 are important kinases for G1-S transition during cell cycle. A phase I study of the CDK4/6 inhibitor ribociclib demonstrated an acceptable safety profile in pediatric patients (147). Further studies using ribociclib in combination with other compounds are ongoing in patients with neuroblastoma (NCT02780128). CHK1 is an indispensable kinase that regulates DNA damage response and cell cycle checkpoints during the S, G2 and M phases. Even though CHK1 inhibition has reported promising preclinical results in multiple tumors, few inhibitors have reached early phase clinical trials in adults, and only prexasertib (LY2606368) is currently being tested in pediatric tumors (NCT02808650) (148,149).

MEK1/2 inhibitors

MAPK pathway is crucial in complex cellular programs such as cell proliferation, differentiation, and apoptosis and it is often deregulated in human cancers. MAPK overactivation frequently occurs through amplifications or mutations in upstream receptor tyrosine kinases (*ALK*, *EGFR*, *ERBB2*), mutations in regulatory genes (*NF1*, *PTPN11*) and alterations in signal transduction proteins (*NRAS*, *KRAS*). Only 3-5% of newly diagnosed neuroblastoma present mutations in the canonical MAPK pathway (53). However, around 80% of relapsed neuroblastoma harbor genetic alterations predicted to activate RAS signaling (150). Selumetinib is a MEK1/2 inhibitor that has shown good tolerability and efficacy in children with recurrent low-grade gliomas (151) (NCT01089101). Selumetinib is currently in phase II studies for children with solid tumors harboring mutations in MAPK pathway, including neuroblastoma (NCT03155620, NCT03213691).

MDM2 inhibitors

MDM2 is the main negative regulator of p53. P53 is rarely mutated in newly diagnosed neuroblastomas (< 2%) and relapsed tumors (~15%). However, around 1/3 of relapsed neuroblastoma inactivate p53 via amplification of *MDM2* or impairment of *p14^{ARF}*, a negative regulator of MDM2 (152,153). In these tumors, reactivation of wild type p53 via inhibiting MDM2 is a promising therapeutic strategy. The MDM2 and MDMX inhibitor ALRN-6924 is currently being tested in a phase I study in refractory solid tumors, brain tumors, lymphoma or leukemia with wild type *TP53* (NCT03654716).

Other targeted therapies

BIRC5 is a negative regulator of apoptosis and is also implicated in cell cycle progression. It is located on the chromosome 17q, a region often gained in neuroblastoma. The BIRC5 inhibitor EZN-3042 was tested in pediatric patients in combination with chemotherapy. Even though some biological activity was observed, EZN-3042 was not well tolerated at the dose that reduced BIRC5 expression. Other examples of targeted therapies that are being explored in clinical trials in neuroblastoma include the ornithine decarboxylase inhibitor DFMO (NCT01586260, NCT02395666), HDAC inhibitors (NCT02035137, NCT01019850), and the anti-VEGF antibody bevacizumab (NCT02308527), among others.

Immunotherapy

There are multiple ongoing trials for patients with relapsed or refractory neuroblastoma that include immunotherapy. For example, of 17 patients treated with irinotecan-temozolomide-dinutuximab (GD2 antibody), nine had objective responses (53%), including four partial responses (23.5%) and five complete responses (29.4%) (NCT01767194) (154). Even though anti-GD2 antibody immunotherapy exerts antitumor effects, it has significant side effects such as pain, fever, vomiting, hypertension, hypotension, urticaria, and diarrhea (155). Other immunotherapeutic approaches are being studied for neuroblastoma treatment, which include antitumor vaccines (156,157), immunotherapy using donor NK cells transplants combined with chemotherapy (158), combined with anti-GD2 (NCT03242603) or both (NCT03242603), immune checkpoint inhibitors (159) or engineered cytolytic CD8+ T lymphocytes (NCT01460901, NCT03721068, NCT03373097).

1.1.9. Late effects in children treated with intensive multimodal therapy

The outcome of high-risk neuroblastoma patients has improved over the last decades. However, survivors can suffer a wide variety of treatment-related complications, also known as late effects, which may contribute to increased morbidity and premature mortality in this group of patients. For example, a retrospective analysis of 63 neuroblastoma survivors revealed that 95% of them presented late serious side effects, such as hearing loss (62%), ovarian failure (41% of females), primary hypothyroidism (24%), or musculoskeletal (19%), and pulmonary (19%) abnormalities (160). Late effects are frequently related to chemotherapy and radiotherapy (89,161-163) (Table 7).

Table 7. List of potential late effects of neuroblastoma patients (adapted from (164)).

| Potential late effect | Therapeutic Exposure |
|---------------------------|---|
| Thyroid dysfunction | Radiation to neck or scatter Total body irradiation 131I-MIBG therapy |
| Growth hormone deficiency | High-dose alkylating agents prior of transplant Radiation to hypothalamic-pituitary axis Total body irradiation |
| Gonadal dysfunction | Alkylating agents Cisplatin Radiation to the gonads |
| Skeletal dysplasia | Radiation to the spine or long bones Cis-retinoic-acid |
| Diabetes Mellitus | Abdominal radiation Total body irradiation |
| Hearing loss | Cisplatin Myeloblastic doses of carboplatin Ototoxic antibiotic exposures |
| Pulmonary dysfunction | Busulfan Radiation to the chest or upper abdomen |
| Cardiac dysfunction | Anthracyclines Radiation to the chest or upper abdomen |
| Renal dysfunction | Nephrectomy Platinum-based chemotherapy Radiation therapy involving the kidney |
| Secondary malignancies | Epipodophyllotoxins Alkylating agents Anthracyclines Radiation therapy |

1.2. Targeting cell cycle as a cancer therapy

1.2.1. Cell cycle dysregulation in cancer

Since ~50% of high-risk neuroblastoma patients relapse and survivors suffer severe adverse effects, it is imperative to find new approaches for improving drug efficacy and safety.

The cell cycle is a complex evolutionary conserved process necessary for cell growth tightly regulated by the sequential activation and deactivation of proteins that control progression through the distinct cell cycle phases: G1, S, G2 and M (mitosis). Some cells may enter in G0, where they remain quiescent, in a resting state that can be maintained for their entire lifespan. Some external growth factors stimulate cells to enter G1 phase, where cells grow in size and synthesize mRNA and proteins that are necessary for DNA replication in S phase. G2 phase is a stage of rapid cell growth and protein synthesis during which cells prepare to undergo M phase. In mitosis, the genetic material and cytoplasm are equally distributed between the two daughter cells (Figure 8).

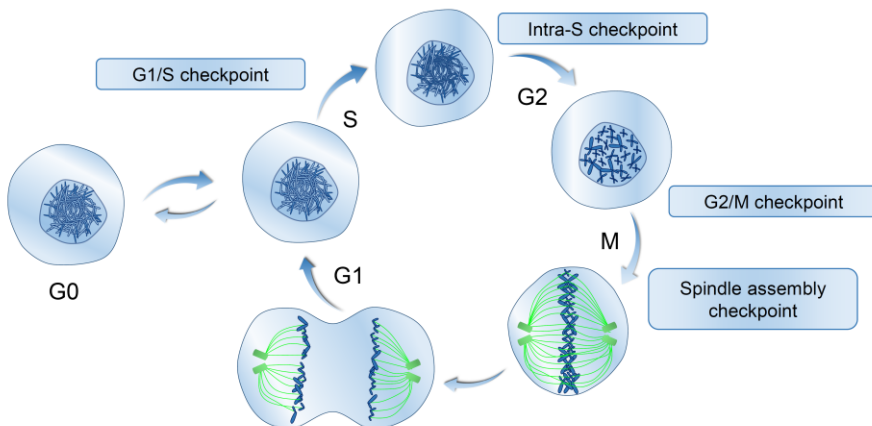


Figure 8. Cell cycle phases and checkpoints. Cell cycle is divided into two growth phases (G1 and G2) that separate the DNA synthesis (S phase) and mitosis (M phase). Non-dividing cells remain in a quiescent state (G0) until conditions are suitable for cell division. Cell cycle is controlled by G1/S, intra-S, G2/M and spindle assembly checkpoints to ensure its proper progression.

To ensure proper cell proliferation, multiple checkpoints control cell cycle progression. In case of detecting any defect during DNA replication or other steps leading to cell division,

Introduction

Cell cycle dysregulation in cancer

cells are arrested in the cell cycle and, if the problem is not solved, processes such as apoptosis, senescence or mitotic catastrophe are triggered to prevent the propagation of damaged cells (165). The mechanism of action of the cell cycle checkpoints is currently well established. G₁/S checkpoint is an essential regulator of genomic stability, impairing the cell cycle progression of cells with DNA damage. Intra-S checkpoint is activated during S phase to minimize replication errors protecting genomic integrity and ensuring replication fidelity. G₂/M checkpoint ensures that cells do not enter prematurely into mitosis and therefore, it avoids chromosome mis-segregation. The spindle assembly checkpoint (SAC) ensures the fidelity of chromosome segregation. All these checkpoints minimize genomic instability during cell-cycle progression.

Deregulation of cell cycle is a hallmark of human cancer (166). Tumors accumulate genetic alterations that induce sustained proliferation. Genomic instability and aneuploidy distinguish between malignant cells and non-malignant cells, and these features make malignant cells particularly sensitive to anti-mitotic compounds. For that reason, mitotic proteins are considered attractive targets in cancer therapy.

1.2.2. Anti-cancer therapies targeting mitosis

Mitosis consists of five phases, based on morphology of chromosomes and spindle. These mitotic phases are prophase, prometaphase, metaphase, anaphase, and telophase and cytokinesis. In prophase, chromosomes start condensing and the spindle begins to form. In prometaphase, the nuclear envelope is fragmented into small vesicles and microtubules attach at chromosome kinetochores. In metaphase, chromosomes are aligned along the equator of the cell. Once all chromosomes are properly aligned and the kinetochores attached, the cells enter to anaphase, when sister chromatids are separated. In telophase, the chromosomes reach the poles and the nuclear membrane reforms. Finally, the cytoplasm is divided into two daughter cells in a process known as cytokinesis (167).

Mitosis is tightly regulated by several proteins, including kinases, phosphatases and motor proteins. More than 32,000 phosphorylation and dephosphorylation events carried out by kinases and counterbalancing phosphatases occur during M phase to regulate the function and the correct localization of proteins involved in mitosis (168). The Cyclin-dependent kinase I (CDK1)-CCNB1 complex is the central driver of mitosis and orchestrates phosphorylation of mitotic proteins to regulate their activity (169,170). However, not only is CDK1 fundamental during mitosis, there are other relevant mitotic protein kinases such as polo-like kinases (PLKs), Aurora-A and -B, as well as the NEK family of kinases (171). On the contrary, mitotic phosphatases, such as Wee1 and Cdc25c, counteract mitotic kinases and regulate mitotic entry and exit (172,173). Ubiquitination and the subsequent degradation of proteins such as CCNB and securin, is necessary for anaphase onset. The E3 ubiquitin ligase APC/C-CDC20, activated after the SAC is satisfied, results in the destruction of many mitotic proteins, leading to cell division (174). Additionally, the rearrangement of microtubules is crucial for the organization of the mitotic spindle. Kinesins are motor proteins that regulate spindle formation, maintenance and chromosome segregation. 45 different kinesins have been described in humans, and at least 16 of them are involved in mitosis and cytokinesis (175).

Introduction

Anti-cancer therapies targeting mitosis

Pharmacological agents targeting fundamental mitotic components, such as tubulin, are well-established treatments for some hematologic and solid malignancies (176). Moreover, several compounds designed to target distinct mitotic proteins have been developed in the last decades. Specific inhibitory agents targeting mitotic CDKs (i.e. CDK1), non-CDK kinases (e.g. PLK1, AURKA, AURKB, MPS1), and mitotic spindle motor proteins (i.e. kinesins) are currently being tested in clinical studies (Figure 9) (177).

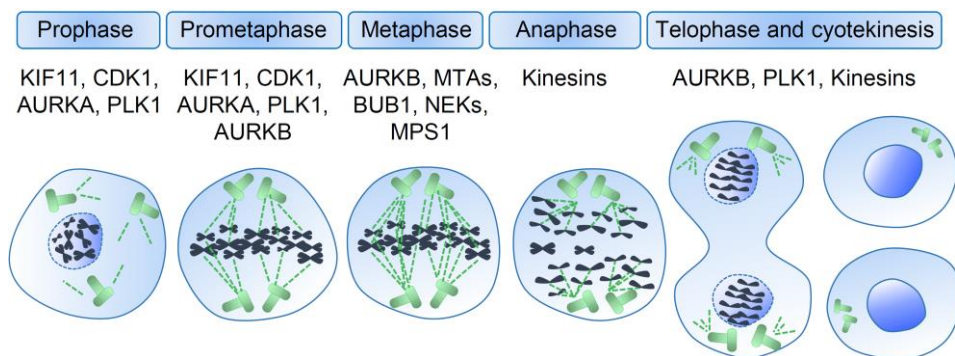


Figure 9. Phases of mitosis and mitotic targets for cancer therapy. Microtubules, CDK1, non-CDK-mitotic kinases, and kinesins are promising therapeutic targets involved in distinct phases of mitosis. Many compounds targeting these proteins have been developed in the last decades and several of them have reached clinical studies. Adapted from (177).

Targeting tubulin

Microtubules are highly dynamic structures that play a fundamental role during mitosis. Microtubules are heterodimers of α and β -tubulin that assemble head-to-tail to generate protofilaments which will further polymerize to form the microtubule cylinder (Figure 10). Microtubules are polar structures. The α -tubulin subunits are at one end (the minus end) whereas β -tubulin is at the other end (plus end). Microtubule stability is dictated by the GTP binding and hydrolysis of β -tubulin (178).

Microtubule dynamics is crucial during mitosis. When cells undergo mitosis, the microtubule network is reorganized to form the mitotic spindle. The process of depolymerizing and assembly to form the mitotic spindle requires highly coordinated microtubule dynamics (179). Therefore, drugs that block microtubule dynamics have a great impact on mitosis.

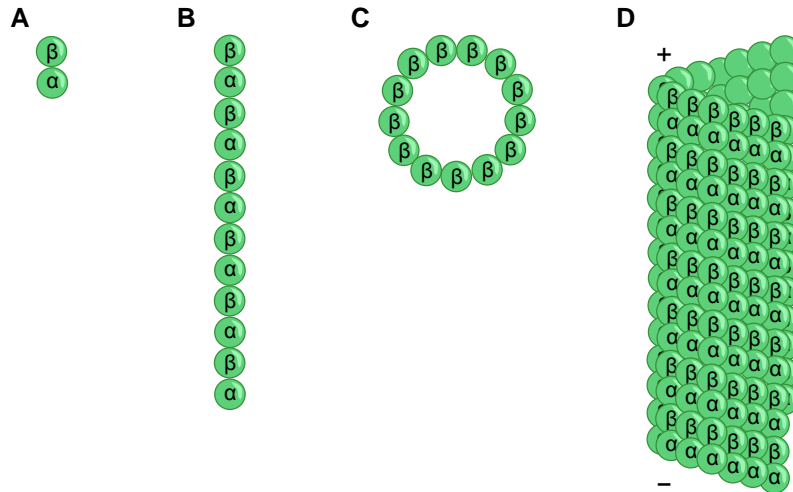


Figure 10. Microtubule structure and assembly. (A) α and β -tubulin heterodimer. (B) Protofilament build from head-to-tail interaction of α and β -tubulin heterodimers. (C) β -tubulin plus end. (D) Microtubule structure. Adapted from (178).

Anti-proliferative drugs that target microtubule dynamics have been used to treat certain hematologic and solid malignancies for decades (176). Microtubule poisons bind to tubulin causing microtubule stabilization (i.e. taxanes) or destabilization (i.e. vinca alkaloids) which, in both cases, result in suppression of microtubule dynamics that eventually lead to mitotic arrest and apoptosis (180). However, microtubule poisons have limitations, such as innate or acquired resistance and dose-limiting neurotoxicity derived from interfering with the axonal integrity and transport (181). Specific inhibition of microtubule-interacting-mitotic proteins, such as kinesins, could improve specificity for malignant cells. Targeting spindle proteins that mainly function in mitosis is believed to selectively eliminate dividing cells and leave unaffected the majority of non-proliferating tissues (177).

Targeting kinesins

Kinesins are a family of motor proteins that move unidirectionally along microtubules to fulfil their main roles, including cell division and intracellular transport of vesicles and organelles (182,183). Human genome contains about 45 kinesins, and at least 16 of them play

Introduction

Anti-cancer therapies targeting mitosis

important roles in spindle assembly, maintenance and chromosome segregation. Over the past decades, kinesins involved in mitosis have emerged as promising targets for cancer therapy. Several compounds that inhibit distinct kinesins have entered in clinical studies as monotherapy or combined with other drugs (175).

Kinesin member family 11 (KIF11) is a kinesin crucial for spindle assembly during prophase and prometaphase. More than 43 clinical trials involving different KIF11 inhibitors as a monotherapy or combined with chemotherapy have been completed (184). Even though the majority of KIF11-inhibiting agents have shown clear antitumor activity in several preclinical models, only filanesib (ARRY-520) has recently demonstrated to be effective in patients with multiple myeloma (185). Further studies testing different schedules of administration might determine whether a more sustained KIF11 inhibition could improve these results. CENP-E is a kinesin necessary for chromosome alignment. Its inhibition activates SAC and leads to mitotic arrest and apoptosis (186,187). A phase I study using the CENP-E inhibitor GSK923295 in refractory solid tumors showed encouraging results, as one patient presented a durable partial response and one third of patients displayed stable disease for a minimum of 8 weeks (188). Additional kinesins involved in mitosis, such as KIF15 and KIF18A, are currently being evaluated as drug targets in preclinical models with promising results (189,190).

CDK1

CDK-cyclin are key complexes that play fundamental roles during cell cycle and their activity is frequently deregulated in cancer (191). CDK1 is required for cell division and its deficiency results in early embryonic lethality (192). Aberrant CDK1 expression has been found in some malignancies and high levels of this protein are associated with poor outcome (193-195). Due to its potential role in restoring cell cycle, CDKs have been considered attractive targets for cancer therapy. Multiple inhibitors targeting CDKs have reached clinical trials. However, CDK inhibitors targeting CDK1 have shown only modest effects in the clinic with high toxicities (196). Experiments in mice suggest that CDK1 might be necessary for maintaining tissue homeostasis and its inhibition could produce general toxicities similar to those induced by cytotoxic drugs (191,192). On the contrary, inhibition of other CDKs (i.e. CDK2, CDK4

and CDK6) could cause manageable toxicities acceptable for cancer patients. Ongoing clinical trials are testing CDK4/6 inhibitors in pediatric and adult malignancies. As previously mentioned, ribociclib is currently being tested in multiple pediatric tumors, including neuroblastoma (NCT02780128). Moreover, palbociclib has shown encouraging results in the clinic and has recently been approved by FDA for treatment of patients with HR+/HER2-advanced breast cancer (197).

Targeting mitotic non-CDK kinases

There are several non-CDK kinases that play relevant roles during mitosis and the SAC. Aurora kinases are a family of serine/threonine kinases consisting of three members: AURKA, AURKB and AURKC. AURKA is necessary for spindle assembly and the formation of bipolar spindle (141). AURKB is a member of the chromosome passenger complex that mediates DNA condensation, and it is also involved in regulating the SAC, modulating the correct chromosome alignment (198,199). Aurora kinases are often overexpressed or amplified in tumors and their expression is associated with poor prognosis in multiple malignancies. In addition, AURKA and AURKB have been described to confer resistance to chemotherapy and tamoxifen, respectively (200,201). Thus, Aurora kinases are expected to be promising therapeutic targets for cancer treatment and several specific inhibitors have been developed in the last two decades (202). The AURKA inhibitor alisertib and the AURKB inhibitor AZD1152 have been tested in clinical trials with modest results in adult patients as monotherapy (203,204). Remarkably, alisertib combined with irinotecan and temozolamide has shown antitumor activity in neuroblastoma patients, suggesting that additional studies including combinations with chemotherapy could improve the current results for adult malignancies (144).

PLK1 is a key serine/threonine kinase activated by AURKA that plays several roles during cell division, including mitotic entry, centrosome maturation, spindle assembly, APC/C regulation and cytokinesis (177). PLK1 is commonly overexpressed in cancer and frequently correlates with poor outcome (205). Even though that PLK1 inhibition exhibited excellent preclinical results in several malignancies, most of PLK1 inhibitors have shown toxicity and limited efficacy in clinical trials for solid tumors (206,207). However, PLK1 inhibition using

Introduction

Anti-cancer therapies targeting mitosis

volasertib (BI 6727) showed encouraging results in patient with relapsed or refractory acute myeloid leukemia. 12% (5/43) of patients treated with volasertib alone achieved complete remission and, volasertib combined with low doses of cytarabine presented better results with 31% of patients achieving complete remission compared to cytarabine alone (13%) (208). On the other hand, in a clinical trial carried out in children with refractory or relapsed leukemia, patients only achieved limited responses when treated with volasertib (209). Considering the results of clinical trials, it is possible that PLK1 inhibition could be effective in a subset of patients with tumors that contain particular genetic mutations. For example, cells harboring Ras mutations have been described to be more sensitive to PLK1 inhibition than tumor cells with Ras wild type (210). For that reason, additional studies have to be performed in order to clarify whether PLK1 inhibitors could be effective in a particular subset of patients harboring tumors with certain genetic profiles.

Other mitotic kinases that are emerging as potential therapeutic targets are the NEK family of protein kinases, BUB1, MPS1, BUBR1, and MASTL. Multiple inhibitors for these proteins are currently being evaluated in preclinical and clinical studies with successful results. For example, MPS1 inhibition combined with low doses of taxanes have shown promising antitumor activity in multiple preclinical models (211,212). The MPS1 inhibitor empesertib (BAY 1161909) has been recently evaluated in a phase I clinical trial with patients with solid malignancies. The combination of empesertib with paclitaxel demonstrated good tolerability with manageable side effects and preliminary sign of efficacy (213) (NCT02138812). Additional preclinical studies are being carried out with BUB1-inhibiting compounds. Similarly to MPS1 inhibitors, the BUB1 inhibition using BAY 1816032 exhibited great efficacy in breast cancer when combined with taxanes and PARP inhibitors in xenograft models (214). Pharmaceutical agents targeting NEKs and MASTL are currently under investigation (215,216).

1.3. Kinesin family member 11

1.3.1. KIF11 structure and function

Kinesin family member 11 (KIF11) is a member of the kinesin superfamily. Kinesins belong to a class of motor proteins that contribute to cell division and intracellular transport of organelles and vesicles along microtubule cytoskeleton (183). Human genome codes for 45 kinesins, classified in 14 subfamilies. KIF11 belongs to the kinesin 5 subfamily (175). *KIF11* gene is located on the chromosome 10q23.33 and codes for a single isoform composed of 1,056 amino-acids with a molecular weight of 119 kDa. The amino-acid sequence and the structure of KIF11 are conserved across species (217,218). KIF11 protein contains a motor domain in the N-terminal, an internal stalk domain, and a tail domain. KIF11 monomers form homodimers via interaction between the stalk domains. The binding of two antiparallel dimers arrange the final homotetramer, resulting in two motor domains at both ends (Figure 11A). This structure enables KIF11 to cross-link antiparallel spindle microtubules and simultaneously move towards the plus end (Figure 11B) (217,219,220).

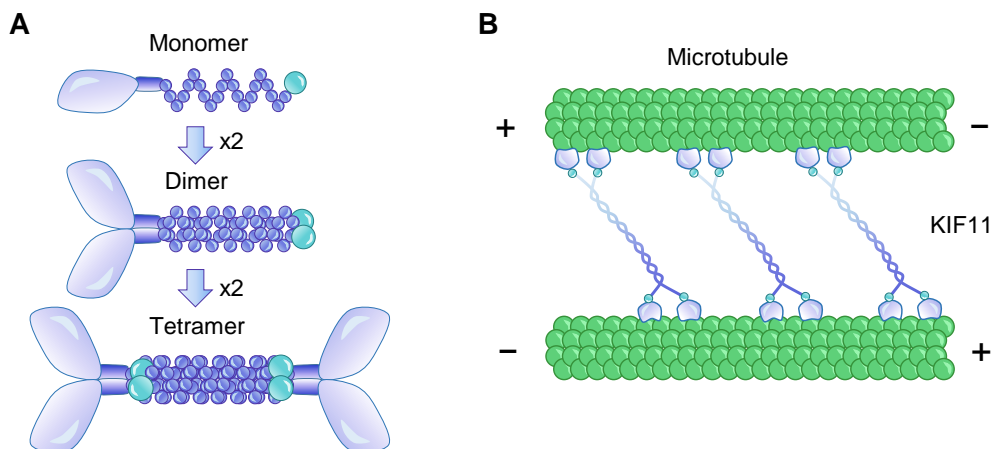


Figure 11. KIF11 structure and function. (A) The KIF11 protein contains a motor domain in the N-terminal, a stalk domain, and a C-terminal tail domain. KIF11 forms homotetramers via interactions between stalk domains. (B) KIF11 cross-links antiparallel microtubules for bipolar spindle formation during mitosis.

Introduction

KIF11 structure and function

ATP hydrolysis in the motor domain is fundamental for KIF11 binding to the microtubules. When ATP is hydrolyzed to ADP, the affinity for the microtubule decreases and the motor domain releases. When the ATP is restored, there is a conformational change that triggers a movement towards the next binding site on the microtubule, where it will reattach tightly thus pushing the antiparallel microtubules in opposite directions (220,221). Even though both ATPase activity and the microtubule-binding property are in the motor domain, the stalk and tail domains have essential roles. Stalk domain enables KIF11 to crosslink and move antiparallel microtubules. On the other hand, the tail domain is fundamental for KIF11 localization during mitosis and promotes its binding to microtubules (222)

The main function of KIF11 is to promote spindle assembly during mitosis. KIF11 dimers have been described to induce microtubule polymerization *in vitro* (223). In addition, KIF11 expression has been found to be fundamental during mitosis in multiple species (220). Genetic depletion or pharmacological inhibition of KIF11 results in cells with a monopolar spindle arrested in mitosis (224,225) (Figure 12). The formation of monopolar spindles support that the main function of KIF11 is to crosslink and move antiparallel microtubules during mitosis.

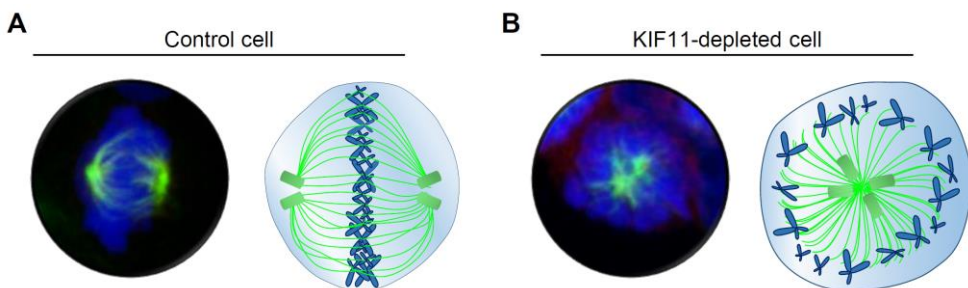


Figure 12. KIF11 inhibition suppresses bipolar spindle assembly. Immunofluorescence and schematic illustrations of the normal metaphase (A) and monopolar spindles in the KIF11-inhibited cells (B). Immunofluorescence images show α -tubulin (green), KIF11 (red), and chromosomes (blue) in SK-N-BE(2) cells.

1.3.2. Regulation and subcellular localization of KIF11

Regulation of KIF11 throughout cell cycle

As previously mentioned, phosphorylation and dephosphorylation events play a key role during mitosis. KIF11 function is tightly regulated during mitosis and its phosphorylation/dephosphorylation is carefully monitored by multiple kinases and phosphatases at specific time points. KIF11 has been found to be phosphorylated by CDK1 and NEK6 at Thr926 and Ser1033, respectively, leading to its activation and binding to microtubules (224,226-228). Nearly all KIF11 is phosphorylated by CDK1 at Thr926 during early mitosis whereas only ~3% is phosphorylated at Ser1033 at this stage. Interestingly, both phosphorylation sites are critical for proper mitosis. KIF11 depletion phenotype (monoastal spindles) can be totally rescued by wild type KIF11 but not by KIF11(Thr926Ala) and KIF11(Ser1033Ala) (228). After metaphase, KIF11 is dephosphorylated by the PP2A/B55 complex, one of the major regulators of mitotic exit. The complex binds to the C-terminal tail of KIF11 and dephosphorylates the Thr926. Liu and colleagues showed that lack of PP2A results in abnormal KIF11 activation, delaying mitotic exit (229). Interestingly, He and colleagues reported that PTEN phosphatase co-localizes and interacts with KIF11 during mitosis to balance KIF11 phosphorylation. The authors suggested that PTEN inhibits KIF11 phosphorylation to prevent its hyper-phosphorylation, which results in a reduced affinity of KIF11 to spindle microtubules (230).

Synthesis and degradation of certain proteins in specific time points throughout the cell cycle is crucial for cells to divide properly. KIF11 stability fluctuates during the cell cycle increasing its activity during mitosis. The APC/C is a fundamental complex that regulates mitotic progression, and selectively degrades distinct substrates. There are two subunits that can interact with the APC/C; CDC20 and CDH1. Both of them gather different substrates to the APC/C and are crucial for its enzymatic activity (231). In early mitosis, CDC20 and CDH1 are both phosphorylated by CDK1-CCNB1. While phosphorylation of CDC20 promotes its binding to APC/C, CDH1 phosphorylation prevents its association with APC/C. Once the SAC is satisfied, APC/C-CDC20 is activated and allowed to target its

Introduction

Regulation and subcellular localization of KIF11

substrates, including securin and CCNB1. When CCNB1 is degraded, CDK1 is inactivated and CDH1 is allowed to bind to the APC/C and control its activity until late G1 phase (232). It has been found that the APC/C-CDH1 complex regulates KIF11 protein levels throughout the cell cycle phases via inducing its proteasome degradation. In fact, the inhibition of the complex results in KIF11 stabilization that leads to unbalanced forces on the spindle (233,234).

Protein-protein interactions are necessary to promote their proper function and subcellular localization. KIF11 dynamic organization relies on its interaction with TPX2, a crucial spindle assembly factor that plays important roles during mitosis, including microtubules assembly. KIF11-TPX2 interaction has been found to be required for proper organization and stability of spindle microtubules. It also guides KIF11 localization into the mitotic spindle and the transition from the spindle pole to midzone (235,236). Blangy and colleagues described that KIF11 also interacts with dynein through the p150Glued subunit of the dynactin complex (237). This interaction, regulated by Thr926 phosphorylation, is important for KIF11 localization in the microtubules (236).

Subcellular localization of KIF11

KIF11 subcellular localization differs between species. For example, in *Sus scrofa*, KIF11 localization into the microtubules is highly dynamic throughout mitosis. In metaphase, it localizes along the mitotic spindle with an accumulation into the spindle poles. In late anaphase, KIF11 relocates to the midzone (236). In *Caenorhabditis elegans*, KIF11 localization also changes during cell cycle. In prophase, KIF11 begins to interact with mitotic spindle microtubules. In metaphase, KIF11 is enriched in the inner part of the centrosomes and kinetochore microtubules. In early anaphase, KIF11 remains associated with kinetochore microtubules and starts to populate the central spindle and, in late anaphase, KIF11 is localized mainly in the central spindle. Finally, in telophase, KIF11 is localized to the spindle midbody (238). On the other hand, in *Drosophila melanogaster* and *Xenopus laevis* cells, the protein is more concentrated near the spindle poles (227,239,240).

KIF11 subcellular localization is considerably different in plants. In *Nicotiana tabacum*, KIF11 expression was found to be cell cycle-dependent. Cells in the G1 phase do not express KIF11. During the S phase, KIF11 begins to appear and distributes along cortical microtubules. In premitotic cells, KIF11 is present in perinuclear microtubules and in the nucleus. During mitosis, KIF11 is localized along spindle microtubules and accumulated at the spindle midzone as the spindle lengthens (241). In, *Arabidopsis thaliana* KIF11 decorates abundantly microtubules in both interphase and mitosis, without end-plus accumulation (242). Surprisingly, KIF11 is not localized in the midzone spindle in *Physcomitrella patens*, suggesting that it may be not necessary for spindle bipolarization in this particular cell type (243).

1.3.3. KIF11 and cancer

Some findings suggest that KIF11 could play an important role in some malignancies. Castillo and colleagues reported that overexpression of KIF11 in transgenic mice resulted in spindle alterations and defects in chromosomal segregation. Aberrant KIF11 expression generated a broad spectrum of tumors that showed genetic instability and aneuploidy, typical hallmarks of solid malignancies (244). In consonance with the transgenic mice model, KIF11 was described to be overexpressed in several human tumors types compared to healthy/adjacent tissues, and its high expression was often associated with poor survival (Table 8).

Table 8. KIF11 expression status in multiple malignancies.

| Malignancy | KIF11 status | Reference |
|-----------------------------------|--|-----------|
| Breast cancer | Overexpressed vs. normal tissue High KIF11 expression is associated with poor outcome | (245,246) |
| Hepatocellular carcinoma | Overexpressed vs. normal tissue High KIF11 expression is associated with poor outcome | (247) |
| Oral cancer | Overexpressed vs. normal tissue High KIF11 expression is associated with poor outcome | (248) |
| Malignant pleural mesothelioma | Overexpressed vs. normal tissue | (249) |
| Meningioma | High KIF11 expression is associated with poor outcome | (250) |
| Bladder cancer | Overexpressed vs. adjacent tissue High KIF11 expression is associated with poor outcome | (251) |
| Neuroblastoma | High KIF11 expression is associated with poor outcome | (252) |
| Glioma | Overexpressed vs. normal tissue High KIF11 expression is associated with poor outcome | (253) |
| Glioblastoma | Overexpressed vs. normal tissue | (254) |
| Renal cell carcinoma | Overexpressed vs. adjacent tissue High KIF11 expression is associated with poor outcome | (255,256) |
| Gallbladder cancer | Overexpressed vs. adjacent tissue | (257) |
| Non-small cell lung cancer | High KIF11 expression is associated with poor outcome | (258) |
| Laryngeal squamous cell carcinoma | Overexpressed vs. adjacent tissue High KIF11 expression is associated with poor outcome | (259) |
| Chronic myelogenous leukaemia | Highly expressed in blast crisis chronic myelogenous leukaemia | (260) |
| Pancreatic cancer | Overexpressed vs. normal tissue | (261) |

Moreover, KIF11 inhibition leads to mitotic arrest and a subsequent cell death *in vitro* and tumor growth impairment *in vivo* in several adult (248,254) and pediatric malignancies (252), suggesting that KIF11 could be a good therapeutic target for cancer therapy.

1.3.4. Pharmacological inhibition of KIF11

As mentioned before, KIF11 is essential for bipolar spindle assembly, and its inhibition results in monoastral microtubule array surrounded by a ring of chromosomes. The first data supporting that KIF11 is important for spindle bipolarity came from temperature-sensitive KIF11 mutants. Cells with mutant KIF11 did not establish bipolar spindles at restrictive temperatures (262,263). Concordantly, KIF11-specific inhibition using antibodies also induced defects on mitotic spindle bipolarity (239).

The first pharmacological compound targeting KIF11, named monastrol, was discovered in 1999 by Mayer and colleagues (264). Since then, numerous KIF11-inhibiting agents have been developed (265,266). Co-crystallization of monastrol and KIF11 revealed that monastrol binds to an allosteric pocket between loop 5, $\alpha 2$ and $\alpha 3$ helices of the motor domain of KIF11, located 12 Å away from its active site (267). L5/ $\alpha 2/\alpha 3$ is clearly a hot spot to inhibit KIF11, as nearly all compounds bind to this pocket, including all of those that have reached clinical trials (Table 9).

Table 9. KIF11-inhibiting compounds in clinical development. Source: ClinicalTrials.gov.

| Agent | Company | Regimen | Phase | Number of trials |
|-----------|-----------------|---------------------------------|-------|------------------|
| Ispinesib | Cytokinetics | Single agent and in combination | II | 16 |
| Filanesib | Array BioPharma | Single agent and in combination | II | 8 |
| LY2523355 | Eli Lilly & Co. | Single agent | II | 7 |
| AZD4877 | AstraZeneca | Single agent | II | 6 |
| SB-743921 | Cytokinetics | Single agent | I/II | 2 |
| 4SC-205 | 4SC AG | Single agent | I | 1 |
| ARQ 621 | Merck & Co. | Single agent | I | 1 |
| MK-0731 | Merck & Co. | Single agent | I | 1 |
| EMD534085 | Merck & Co. | Single agent | I | 1 |

New KIF11 inhibitors that bind to distinct parts of the motor domain have been developed. For example, FCPT acts as an ATP-competitive inhibitor by binding to the nucleotide binding site (268). Moreover, Ulaganathan and colleagues described the molecule BI8 that binds to KIF11 in a distinct allosteric pocket formed by helices $\alpha 4$ and $\alpha 6$ (269). However, the efficacy of these inhibitors have not been evaluated in clinical trials.

Introduction

Pharmacological inhibition of KIF11/KIF11 and neuroblastoma

Even though KIF11 inhibitors showed promising preclinical results with low nanomolar biochemical potency and total tumor regression, clinical efficacy was insufficient for most agents (270,271). However, some compounds showed activity in clinical trials. For example, filanesib demonstrated to be effective in patients with relapsed or refractory multiple myeloma (185), and daily administration of 20 mg 4SC-205 showed signs of efficacy in patients with advanced solid malignancies and malignant lymphomas (272). These results suggested that KIF11 inhibitors could be more effective in certain types of malignancies (i.e. multiple myeloma), and constant drug exposure could increase the ratio of cells that respond to therapy.

1.3.5. KIF11 and neuroblastoma

Hansson and colleagues recently published promising results regarding KIF11 and neuroblastoma (252). They reported that neuroblastoma displayed the highest *KIF11* gene dependency among 22 different tumor types. Moreover, neuroblastoma was one of the most sensitive malignancies to KIF11 inhibition across 27 tumor types. They also demonstrated that KIF11 inhibition using filanesib resulted in tumor regression and increased survival time in mice with patient-derived xenograft tumors. All these results suggested that KIF11 inhibition could be effective for patients with high-risk disease.

HYPOTHESIS AND OBJECTIVES



2. Hypothesis and objectives

Despite significant advances in recent decades that improved the survival of children and adolescents with cancer, the 5-year overall survival of patients with high-risk neuroblastoma is less than 50%, and patients who relapse or present tumor progression display a 10-year survival rate below 15%. Moreover, survivors suffer a wide variety of treatment-related complications. Therefore, new therapeutic approaches to improve the efficacy and safety of standard of care are necessary for high-risk neuroblastoma patients.

Perturbation of transcription factors, kinases, and regulators of cell cycle checkpoints, among other factors, grant neuroblastoma cells with a high proliferative capacity, which, in turn, is closely associated with poor patient outcomes. Indeed, anti-proliferative agents that target microtubule dynamics are currently being used to treat these patients. However, microtubule poisons have limitations, such as innate or acquired resistance and dose-limiting toxicity. Strategies to circumvent these issues include targeting alternative mitotic proteins to improve the specificity towards tumor cells. One of these mitotic specific proteins is KIF11, which is essential for bipolar spindle formation and mitotic progression in human cells. KIF11 has been reported to be overexpressed in multiple malignancies and is often associated with poor outcome. Furthermore, there are several KIF11 inhibitors that have entered clinical trials. Among them, 4SC-205 has demonstrated efficacy in refractory tumors from adult patients, and it is the only KIF11 inhibitor that can be administered orally tested in clinical studies.

Hypothesis: High-risk neuroblastomas are highly proliferative tumors that need a robust expression of the cell cycle machinery. Our hypothesis is that elements of this machinery (i.e. KIF11) have functional roles in neuroblastoma and its specific inhibition could be effective to impair neuroblastoma proliferation and reduce the side effects associated with the classical microtubule poisons. We will evaluate our hypothesis through the following objectives:

Objective 1: To evaluate KIF11 prognostic potential in neuroblastoma.

Objective 2: To study genetic and pharmacological inhibition of KIF11 in multiple preclinical *in vitro* and *in vivo* models.

Objective 3: Provide a rationale for further development of 4SC-205 in clinical trials through the combination with other neuroblastoma therapies.

MATERIALS AND METHODS



3. Materials and methods

3.1. Analysis of neuroblastoma gene expression datasets

R2: Genomic Analysis and Visualization Platform (<http://r2.amc.nl>) was used to analyze the mRNA expression of KIF11 in neuroblastoma patients. Kaplan-Meier overall survival curves were generated to estimate the diagnostic power of KIF11 mRNA expression (SEQC498; GSE62564; (273)). Optimal cutoff value was defined according to the Youden index. Patients were divided into two groups that expressed high or low KIF11 levels (above or below the median). The log-rank test was used for comparing the survival outcome. Univariate and multivariate Cox-proportional hazard regression analysis were used to determine the prognostic significance of KIF11. Maris dataset (GSE3960; (274)) was used to evaluate KIF11 mRNA levels in patients with *MYCN* amplification, gain of 17q23, LOH of 1p36 and 11q genomic alterations. Correlation coefficient of KIF11 and *MYCN* mRNA levels was assessed using both SEQC498 and Kocak (GSE45547; (275)) datasets. All statistical analysis were performed with IBM SPSS 21. All *P* values are based on two-sided tests with *p* values < 0.05 considered statistically significant.

3.2. Immunohistochemistry

KIF11 immunohistochemistry in neuroblastoma patients was carried out in collaboration with Dr. Rosa Noguera (Group of Translational Research in Pediatric Solid Tumors, University of Valencia-INCLIVA Biomedical Health Research Institute). Twenty-five primary non-*MYCN* amplified neuroblastoma samples (at least two representative cylinders of 1 mm² from each tumor) classified according to INRG pre-treatment stratification criteria (50) were included in 5 tissue microarrays (Table 4). Patient samples were referred to the Spanish Reference Centre for Neuroblastoma Biological and Pathological studies (Department of Pathology, University of Valencia-INCLIVA) between 2008 and 2010. All patients, their relatives or their legal guardians signed the appropriate written informed consent. The present study was approved by INCLIVA's Clinical Research Ethics Committee (ref. B.0000339).

Materials and methods

For immunostaining, tissue sections were deparaffinized overnight at 60°C and re-hydrated with graded alcohols. Heat-induced antigen retrieval was performed using citrate buffer (pH 6, 4 minutes, 115°C) with a pressurized heating chamber. Primary antibodies (Table 10) were incubated at 4°C overnight after blocking endogenous peroxidase. Tissue sections were incubated with secondary antibody 30 minutes at room temperature, developed using diaminobenzidine (Dako, K3468) and counterstained with hematoxylin (Sigma-Aldrich; #H9627). The assessment of immunostained sections was carried out by two independent researches according to intensity and percentage of KIF11-positive tumor cells. The intensity of positive cells was scored as: 1 (weak), 2 (moderate), 3 (strong); and the percentage of cells: 1 (1%-25%), 2 (>25%-50%), 3 (>50%-75%), 4 (>75%-100%) in accordance with previous studies (255). The sum of these parameters allowed us to categorize the samples as follows: a staining scored less than 3 was considered as low expression, and a score of 4 or more was considered as high expression. The association between KIF11 protein expression and INRG features was analyzed using the χ^2 test. Survival analysis was performed using Kaplan-Meier curves and log-rank tests. Statistical significance was set at $P < 0.05$. All data were analyzed using SPSS 26.0 statistical analysis software (SPSS, Inc., Chicago, IL, USA).

Table 10. Primary and secondary antibodies for immunohistochemistry.

| Antibody | Dilution | Supplier | Reference |
|--|----------|---------------------------|-----------|
| Primary antibodies for immunohistochemistry | | | |
| KIF11 | 1:2,000 | Sigma-Aldrich | HPA006916 |
| p-Histone H3 (Ser10) | 1:100 | Cell Signaling Technology | #9701 |
| Chromogranin A | 1:20 | Roche | 760-2519 |
| Synaptophysin | 1:20 | Roche | 790-4407 |
| Secondary antibodies for immunohistochemistry | | | |
| Anti-Rabbit HRP | – | Dako | K4003 |
| Anti-Mouse HRP | – | Dako | K4001 |

3.3. Cell lines

Cell lines used in this thesis and their corresponding culture conditions are listed in Table 11. All cell lines were amplified and stored in liquid nitrogen. Upon resuscitation, cells were maintained in culture for no more than 2 months. Cells were cultured at 37°C in a saturated atmosphere of 95% air and 5% CO₂ and frequently tested for mycoplasma contamination.

Table 11. Cell lines and medium.

| Cell line | Supplier | Medium |
|--------------|--|--|
| SK-N-BE(2) | PHECC | IMDM + 10% FBS (v/v) + 1% ITS (v/v) + 100 U/mL penicillin + 100 µg/mL streptomycin + 5 µg/mL plasmocin |
| LA1-5s | PHECC | |
| SH-SY5Y | ATTC | |
| SK-N-AS | ATTC | |
| IMR-32 | ATTC | |
| SK-N-F1 | ATTC | |
| BE(2)-C | ATTC | |
| NBL-S | DSMZ | |
| NGP | DSMZ | |
| CHLA-90 | COG | |
| KELLY | PHECC | RPMI1640 + 10% FBS + 2 mM glutamine + 100 U/mL penicillin + 100 µg/mL streptomycin + 5 µg/mL plasmocin |
| Tet21N | Dr. Manfred Schwab | RPMI1640 + 10% FBS (v/v) + 25 mM HEPES + 4 mM glutamine + 200 µg/mL G418 + 0.5 µg/mL amphotericin B + 10 µg/mL hygromycin B + 100 U/mL penicillin + 100 µg/mL streptomycin + 5 µg/mL plasmocin |
| HEK293T | ATCC | DMEM + 10% FBS (v/v) + 100 U/mL penicillin + 100 µg/mL streptomycin + 5 µg/mL plasmocin |
| Reagent | Description | Supplier |
| IMDM | Iscove's Modified Dulbecco's Medium | Thermo Fisher Scientific |
| DMEM | Dulbecco's Modified Eagle's Medium | Thermo Fisher Scientific |
| RPMI-1640 | Roswell Park Memorial Institute (RPMI) 1640 | Thermo Fisher Scientific |
| FBS | Fetal bovine serum | South America Premium, Biowest |
| ITS | Insuline-transferrin-selenium supplement | Fisher scientific |
| Pen-Strep | Penicillin and streptomycin | Fisher scientific |
| Plasmocin | | InvivoGen |
| HEPES | 4-(2-hydroxyethyl)-1-piperazineethanesulfonic acid | Fisher scientific |
| Glutamine | | Fisher scientific |
| Amphotericin | | Fisher scientific |
| Hygromycin B | | Fisher scientific |

Abbreviations: PHECC, Public Health England Culture; ATTC, American Type Culture Collection; COG, Children's Oncology Group Cell Culture and Xenograft Repository.

3.4. Western blot

Proteins were extracted using RIPA buffer 1X (Fisher Scientific; #10017003) supplemented with 1X EDTA-free complete protease inhibitor cocktail (Roche; #04693159001) and phosphatase inhibitor cocktail 2 and 3 (Sigma-Aldrich; P5726 and P0044). Tumor lysates were generated by mechanical dissociation, homogenized (ten seconds; three times; Bead Ruptor 12 (Omni, Inc)) and sonicated (five seconds; three times; LABSONIC® M (Sartorius Stedim Biotech)) in lysis buffer. Cell lysis was done on ice for twenty minutes prior centrifugation at 16,200g for fifteen minutes at 4°C. Protein concentration was determined using Lowry DC protein assay (Bio-Rad) following manufacturer's instructions.

Samples containing between 20-40 µg of protein were mixed with loading buffer 1X (Invitrogen; NP0007), reduced with dithiothreitol (Fisher Scientific; #13296499), and heated for ten minutes at 70°C to ascertain complete protein denaturation. Samples were run in precast polyacrylamide gels (Fisher Scientific; #12020166) in MES-running buffer 1X (Fisher Scientific; #11509166), supplemented with NuPAGE™ Antioxidant (Fisher Scientific; #11529166) for 1 hour at 150 V at room temperature. Proteins were transferred to PVDF membranes (Fisher Scientific; #10617354), previously activated by methanol, by wet transfer method at 110 V for 1.5-2 hours.

Membranes were blocked with Tris-buffered saline with Tween-20 0.1% (v/v) containing 5% bovine serum albumin (BSA) (NZYT; MB04602) or 5% nonfat dry milk (VWR; #A0830.0500) for 1 hour at room temperature and incubated overnight at 4°C with the proper primary antibody (Table 12). Membranes were incubated with the corresponding secondary antibody for 1 hour at room temperature (Table 13). Actin was used as loading control. Membranes were developed with EZ-ECL Chemiluminescence detection kit (Fisher Scientific; #10340125). Protein expression was quantified using ImageJ software (276).

Table 12. Primary antibodies for western blot.

| Antibody | Molecular weight | Specie | Dilution | Supplier | Reference |
|----------------------|------------------|--------|---------------------------|---------------|------------|
| KIF11 | 119 kDa | Rabbit | 1:3,000 in TBS-T 5% milk | – | (224) |
| MYCN | 67 kDa | Mouse | 1:1,000 in TBS-T 5% BSA | SCBT | sc-53993 |
| CCNB1 | 58 kDa | Mouse | 1:2,000 in TBS-T 5% BSA | Millipore | #05-373 |
| p-Histone H3 (Ser10) | 17 kDa | Rabbit | 1:1,000 in TBS-T 5% BSA | CST | #9701 |
| Mcl-1 | 40 and 32 kDa | Mouse | 1:500 in TBS-T 5% BSA | SCBT | sc-12756 |
| Caspase-3 | 35 kDa | Rabbit | 1:3,000 in TBS-T 5% BSA | CST | #9662 |
| Caspase-3 cleaved | 19 and 17 kDa | Rabbit | 1:1,000 in TBS-T 5% BSA | CST | #9664 |
| PARP | 116 and 89 kDa | Rabbit | 1:2,500 in TBS-T 5% BSA | CST | #9542 |
| mCherry | 26 kDa | Goat | 1:1,000 in TBS-T 5% BSA | OriGene | AB0081-200 |
| BCL-XL | 26 kDa | Rabbit | 1:10,000 in TBS-T 5% BSA | BD Bioscience | #610211 |
| BCL-2 | 26 kDa | Mouse | 1:10,000 in TBS-T 5% milk | Dako | #M0887 |
| NOXA | 8 kDa | Mouse | 1:500 in TBS-T 5% BSA | Sigma-Aldrich | OP180 |
| Actin HRP | 43 kDa | Goat | 1:40,000 in TBS-T 5% BSA | SCBT | sc-1616 |

Abbreviations: SCBT, Santa Cruz Biotechnology; CST, Cell Signaling Technology; HRP, horseradish peroxidase.

Table 13. Secondary antibodies for western blot.

| Antibody | Specie | Dilution | Supplier | Reference |
|----------------------------|--------|----------|---------------|-----------|
| Anti-Rabbit IgG-Peroxidase | Goat | 1:10,000 | Sigma-Aldrich | #A0545 |
| Anti-Mouse IgG-Peroxidase | Rabbit | 1:10,000 | Sigma-Aldrich | #A9044 |
| Anti-Goat IgG-Perodixase | Rabbit | 1:5,000 | Dako | #P0449 |

3.5. Depletion of MYCN in Tet21N cell line

Tet21N cells are derived from the SHEP neuroblastoma cell line. Tet21N contain a tet-off system that repress MYCN expression in the presence of doxycycline in the culture medium. For MYCN depletion experiments, Tet21N (3×10^5 cells) were seeded in 100-mm dishes. After 24 hours, MYCN silencing was triggered by the addition of 100 ng/mL doxycycline (Fisher Scientific; #15510554) in the cell medium. Cells were harvested at the indicated time points for further analyses.

3.6. Quantitative real-time PCR

Total RNA was isolated using the miRNeasy Mini Kit (Qiagen; #217084) following manufacturer's instructions. MRNA (1 μ g) was reverse transcribed using high-capacity cDNA reverse transcription kit (Fisher Scientific; #10117254) following manufacturer's recommendations. Real-time PCR of KIF11 and MYCN was performed using 12.5 ng/ μ L,

Materials and methods

Power SYBR Green master mix (Fisher Scientific; #10658255) and 0.5 μ M of primers listed in Table 14. The PCR reaction was run in 96-well plates in duplicate in ABI700 sequence detection system equipment (Thermo Fisher Scientific) using standard settings (40 cycles, 15 seconds at 95°C followed by 1 minute at 60°C). mRNA expression was normalized against the *GAPDH* housekeeping gene. Relative quantification of gene expression was performed with a comparative $2^{(-\Delta\Delta CT)}$ method (277).

Table 14. List of RT-qPCR primer sequences.

| Gene | Primer sequence (5' to 3') | Amplicon (bp) |
|--------------|-------------------------------|---------------|
| <i>KIF11</i> | Fw: AAAACAACAAAGAAGAGACAATTCC | 93 |
| | Rv: CAGATGGCTCTTGACTTAGAGGT | |
| <i>MYCN</i> | Fw: AGAGGAGACCCGCCCTAATC | 123 |
| | Rv: TCCAACACGGCTCTCCGA | |
| <i>GAPDH</i> | Fw: CGCTCTCTGCTCCTCCTGTT | 100 |
| | Rv: CCAATGGTGTCTGAGCGATGT | |

3.7. Cell transfection

Cellular membranes and nucleic acid molecules are both negatively charged, which blocks the spontaneous internalization of DNA or RNA by electrostatic repulsion. Transfection reagents, such as Lipofectamine 2000 (Fisher Scientific; #10696153), are necessary to overcome this inconvenient. Lipofectamine 2000 is a cationic liposoluble reagent that form positively charged liposomes that entraps nucleic acid inside and enables their internalization into the cell by endocytosis. In this thesis, Lipotectamine 2000 was used for transfecting Small interfering RNA (siRNA) and DNA vectors. The protocol used was adapted following manufacturer's recommendations. Briefly, Lipofectamine 2000 and the indicated siRNA (Table 15) or DNA vector were mixed with Opti-MEM (Fisher Scientific; #11058021) and incubated for 5-10 minutes. After incubation time, the mix was added into cellular medium without antibiotics. After 14 hours, cell medium was changed to avoid toxicity.

Table 15. List of siRNA.

| Gene | siRNA | Sequence (5'-3') | Reference | Supplier | |
|--------------|-----------|------------------|----------------------|-------------------|------------------------|
| – | siControl | BLOCK-iT | – | Fisher Scientific | |
| <i>KIF11</i> | siKIF11-1 | KIF11 | CUAGAUGGCUUUCUCAGUA | – | Sigma-Aldrich |
| | | KIF11_as | UACUGAGAAAAGCCAUCUAG | | |
| | siKIF11-2 | KIF11 | – | L-003317-00 | GE health Dharmacon |
| | | KIF11_as | – | | |
| <i>MYCN</i> | siMYCN-1 | MYCN | GAAGAAAUCGACGUGGUCA | – | Sigma-Aldrich |
| | | MYCN_as | UGACCAGGUCGAUUUCUUC | | |
| | siMYCN-2 | MYCN | GAGAGGACACCCUGAGCGA | – | Sigma-Aldrich |
| | | MYCN_as | UCGCUCAGGGUGUCCUCUC | | |

For MYCN overexpression 2.5×10^3 SK-N-AS or SH-SY5Y were seeded in 35-mm dishes and reverse transfected using Lipofectamine 2000 (3 μ L/plate) with increasing concentrations of pCDNA3-HA-human MYCN or empty vector (0, 1, 2 or 4 μ g/p35). Forty-eight hours later, cells were harvested and protein was extracted for western blot analysis. pCDNA3-HA-human MYCN was a gift from Martine Roussel (Addgene plasmid # 74163 ; <http://n2t.net/addgene:74163> ; RRID:Addgene_74163) (278).

3.8. Immunofluorescence

2×10^5 cells/well SK-N-BE(2) and SH-SY5Y were seeded in 6-well plates on 15 mm coverslips and left 24 hours prior to drug treatment. For genetic silencing, 7.5×10^5 cells/well were seeded in 6-well plates and reverse transfected with control or KIF11 siRNA oligonucleotides (25 nM) using Lipofectamine 2000 (5 μ L/well). At the indicated times, cells were fixed using PTEMF buffer (50 mM Pipes, 0.2% Triton X-100, 10 mM EGTA, 1 mM MgCl₂, 4% formaldehyde) for 10 minutes and washed twice with phosphate-buffered saline (PBS). Samples were then blocked with 3% of BSA in PBS for 30 minutes at room temperature. Primary antibodies, diluted in 3% of BSA in PBS, were incubated for 1 hour at room temperature. Secondary antibody, DAPI (Thermo Fisher Scientific; #62248) and α -Tubulin were incubated protected from light for 1 hour at room temperature (Table 16). Coverslips were mounted with mounting medium (Thermo Fisher Scientific; P36965).

Table 16. Primary and secondary antibodies for immunofluorescence.

| Antibody | Dilution | Supplier | Reference |
|--|----------|---------------------------|-----------|
| Primary antibodies for immunofluorescence | | | |
| KIF11 | 1:1,000 | – | (224) |
| p-Histone H3 (Ser10) | 1:200 | Cell Signaling Technology | #9701 |
| Caspase-3 cleaved | 1:500 | Cell Signaling Technology | #9664 |
| Secondary antibodies for immunofluorescence | | | |
| α -Tubulin | 1:150 | Sigma-Aldrich | F2168 |
| Anti-Rabbit IgG-Alexa Fluor ® 555 | 1:500 | Thermo Fisher Scientific | A-21428 |

3.9. Cell cycle analysis

SK-N-BE(2) (2.5×10^6) and SH-SY5Y (3.5×10^6) cells were seeded in 100-mm dishes and treated 14 hours later with either vehicle (dimethyl sulfoxide, DMSO) or 25 nM 4SC-205. At the indicated time points, cells were harvested and fixed with cold 70% ethanol and kept at 4°C for at least 24 hours. Prior to flow cytometry analyses, cells were washed twice with PBS and resuspended in staining solution [0.19 mM sodium citrate (Sigma-Aldrich; W302600), 500 μ g/mL propidium iodide (Thermo Fisher Scientific; P1304MP) and 10 mg/mL RNase DNase-free (AppliChem; A3832)]. The DNA content was analyzed using a FACScalibur flow cytometer (BD Biosciences) and data by BD CellQuest™ Pro Software (BD Biosciences).

3.10. *In vitro* drug sensitivity assays

Between 3.5×10^3 and 14×10^3 neuroblastoma cells/well were seeded in 96-well plates. After 24 hours, cells were treated with vehicle (DMSO) or different concentrations of the indicated drug. Cells were then fixed with 1% glutaraldehyde for 20 minutes (Fisher Scientific; #11448900), washed once with PBS, stained with 0.5% crystal violet for 15 minutes (Sigma-Aldrich; C0775) and washed with distilled water. Crystals were dissolved with 15% acetic acid (Fisher Scientific; #10041250) and absorbance was read at 590 nm using an Epoch plate reader (Biotek). Dose-response curves were calculated using nonlinear regression approximation in GraphPad Prism 6.0 (GraphPad Software, Inc).

3.11. Hoechst staining

SK-N-BE(2) and SH-SY5Y (3×10^5) cells were reverse-transfected with control or siKIF11 at 25 nM using 5 μ L/plate of Lipofectamine 2000 and seeded in 6-well plates in triplicates.

For the pharmacological inhibition of KIF11, cells were seeded in 6-well plates and treated 24 hours later with DMSO or 25 nM 4SC-205. At the indicated times, cells were stained with 0.05 µg/mL Hoechst 33258 dye (Sigma-Aldrich; #94403) and photographed. Apoptosis quantification was made from 8 representative images/well ($n = 3$ replicates/condition). Cells with fragmented or condensed chromatin were considered apoptotic cells whereas uniformly-stained chromatin cells were scored as healthy.

3.12. Differentiation of SH-SY5Y

The protocol followed was adapted from Encinas M et al. (279). Briefly, 1×10^4 SH-SY5Y/cm² were seeded in 12-well plates and 60-mm dishes pre-coated with poly-D-lysine (Fisher Scientific, #11436632) and collagen (Fisher Scientific; #11563550). After 24 hours, cells were treated with all-trans retinoic acid (Selleckchem; #S1653) 10 µM in IMDM 10% fetal bovine serum (FBS) without antibiotics for 5 days. Cells were then washed with IMDM without FBS and incubated with fresh medium 0.5% FBS and 50 ng/mL brain derived neurotrophic factor (BDNF) (Sigma-Aldrich; SRP3014). After three days, cells were treated with vehicle (DMSO) or 4SC-205 at 25 nM. Cells were fixed with 1% glutaraldehyde or recollected for western blot analysis at the indicated time points.

3.13. Three-dimensional spheroid culture

For tumor spheroids, SH-SY5Y (4.5×10^4) and SK-N-BE(2) (6×10^4) cells were seeded in non-adherent 6-well plates and let them grow in spheroids for 48-72 hours. Spheroids were then treated with vehicle or 4SC-205. Forty-eight hours later, spheroids were disaggregated with 0.5 mL of 1x StemPro®Accutase® (ThermoFisher; #15323609) and incubated with a mixture of PMS:MTS (1:20) for 2-5 hours. Optical density was read at 490 nm using an Epoch Microplate Spectrophotometer (Biotek).

3.14. Lentivirus production, transduction and isolation of clones

Lentiviruses containing pTRIPZ (Dharmacon, GE Healthcare) or pTRIPZ-shKIF11 (Dharmacon, GE Healthcare; V3THS_391757) were produced using previously described methods in HEK293T (280). SK-N-BE(2) were seeded (3×10^5 cells/dish) in 60-mm dishes and incubated overnight with lentiviruses. Infected cells were selected with 1 µg/mL

Materials and methods

puromycin (Sigma-Aldrich; P8833). To isolate monoclonal population of pTRIPZ-KIF11, transduced SK-N-BE(2) were seeded at very low density into 100-mm dishes. After 10 days, isolated colonies were sorted and amplified in 96-well plates. pTRIPZ is engineered to be a Tet-on system that express the shRNA and the turboRFP fluorescent reporter in the presence of doxycycline. For western blot analysis, SK-N-BE(2) clones transduced with pTRIPZ-control or pTRIPZ-KIF11 were cultured with 1 $\mu\text{g}/\text{mL}$ doxycycline for five days. For cell proliferation assays, 1.5×10^5 cells/well were seeded in 6-well plates in the presence or absence of doxycycline, and fixed with 1% glutaraldehyde at the indicated time points.

3.15. *In vivo* experiments

3.15.1. Subcutaneous xenografts

SK-N-BE(2) and SK-N-AS (5×10^6 cells/flank) were subcutaneously injected into the right flank of 6-week old female Fox Chase SCID mice (Charles River) in 300 μL of PBS:Matrigel (1:1). For genetic KIF11 silencing, when tumor size reached $\sim 100 \text{ mm}^3$, mice were randomized into control (2% sucrose) and shKIF11 (1 mg/mL doxycycline into the drinking water) groups.

For pharmacological experiments, mice were randomized into two groups and treated three times per week by oral gavage with vehicle (5% polyethylene glycol 400 (PEG400, Fisher Scientific, #11449467), 0.9% NaCl, pH 3-4) or with 40 mg/kg 4SC-205. Tumor volume was measured every 2-3 days using an electronic caliper. At the end of the experiment, tumors were dissected, weighed and frozen in liquid nitrogen or fixed in 10% formalin, and embedded in paraffin.

3.15.2. Patient-derived orthotopic xenograft model

The human tumor sample was a small biopsy of the primary tumor located in the left adrenal gland of a 7-months old patient with high-risk metastatic neuroblastoma. The biopsy was performed at diagnosis at Vall d'Hebron University Hospital, Barcelona, Spain. The specimen was aseptically isolated and placed at room temperature in IMDM. The protocol for the use of patient's tumor sample were reviewed and approved according to Ethical Committee of

Clinical Research and written informed consent was collected from the patient to implant the tumor in mice.

Immediately after biopsy, the trucut was implanted into nude mice (strain Crl:NU-Foxn1nu) (Harlan) at the animal core facility of Bellvitge Biomedical Research Institute (IDIBELL)_ICO. To generate the patient-derived orthotopic xenograft model (PDOX), female mice of 5 to 7 weeks were anesthetized with a continuous flow of 2% of isoflurane/oxygen mixture, the sample was implanted without enzymatic digestion, in the left adrenal gland of the mice using a 7.0 suture. Mice were monitored twice weekly measuring their body weight and by palpation of tumors. At mice sacrifice (177 days after inoculation), the tumor was extracted, cut into small fragments and serially implanted into 3 to 5 new animals. Engrafted tumors were also cryopreserved in a solution of 90% non-inactivated FBS and 10% DMSO and stored in liquid nitrogen for subsequent future implantations and also frozen for advanced molecular analysis. Representative tumor fragments were fixed and then processed for paraffin embedding. All animal protocols were reviewed and approved according to regional Institutional Animal Care and Ethical Committee of Animal Experimentation.

For drug efficacy experiment, PDOX at passage #2 was orthotopically implanted into the adrenal gland. 65 days after implantation, when tumors measured 300-400 mm³, mice were randomized and assigned to vehicle and 4SC-205 groups and treated three times per week with either vehicle or 4SC-205 for three weeks. At the end of the experiment, tumors were dissected, weighed and frozen in liquid nitrogen or fixed in 10% formalin, and embedded in paraffin.

3.15.3. Neuroblastoma liver metastases model

Firefly luciferase-transduced SK-N-BE(2) cells were injected into the lateral tail vein (2.5 × 10⁵ cells/mouse in 150 µL of PBS) of 5-6-week-old female Fox Chase SCID Beige mice (Charles River). Twenty-four days after injection, mice were randomized into vehicle and treatment groups. Metastases growth was followed by *in vivo* bioluminescence imaging (IVIS) once a week. 4SC-205 was administered orally alone (40 mg/kg) or in combination (20

Materials and methods

mg/kg) with topotecan (5 mg/kg). 4SC-205 and topotecan were injected three times and once a week, respectively. For *in vivo* experiments, χ^2 test was used to determine whether there were statistically significant differences between the treatment group (i.e. vehicle, 4SC-205, topotecan and combo) and tumor response (complete response or progressive disease) (GraphPad Prism 6.0).

3.16. Genomic analyses

3.16.1. RNA sequencing

For transcriptomic analyses, total RNA was isolated from SK-N-BE(2) subcutaneous tumors treated with vehicle or 4SC-205 ($n = 3/\text{group}$) for 24 hours using the miRNeasy mini kit (Qiagen). RNA quality and quantity was determined using Qubit® RNA HS Assay (Life Technologies) and RNA 6000 Nano Assay on a Bioanalyzer 2100 (Agilent). RNA sequencing was performed by CNAG-CRG. Briefly, RNASeq libraries were prepared following the TruSeq® Stranded mRNA LT Sample Prep Kit protocol (Illumina) and sequenced on NovaSeq 6000 (Illumina). RNAseq reads were mapped against human reference genome (GRCh38) using STAR software version 2.5.3a (281) with ENCODE parameters. Genes were quantified using RSEM version 1.3.0 (282) with default parameters and annotation file from GENCODE version 34. Differential expression analysis was performed with DESeq2 v1.26.0 R package (283) using a Wald test to compare vehicle and treated samples. We considered differentially expressed genes those with P value adjusted < 0.05 and absolute fold-change > 1.5 . Functional enrichment analysis of “Hallmarks” gene set collections from MSigDB were performed using GSEA software (284,285). The accession number for RNA sequencing is GSE166984.

3.16.2. Whole exome sequencing

Genomic DNA from patient’s blood, tumor and PDOX (passage 2) samples was extracted using DNeasy Blood & Tissue Kit (Qiagen) and quantified using Qubit (Thermo Fisher Scientific). Genomic DNA was fragmented and sample library was prepared using KAPA library kit (Roche), hybridized with SeqCap EZ MedExome capture kit (Roche) and sequenced in a NextSeq500 sequencing machine (Illumina). The R-package Xenofilter to

remove sequence reads of mouse origin while retaining human sequences (Mismatch threshold = 8) (286) was used. Whole genome sequencing (WES) was carried out by qGenomics (Barcelona).

Copy number alterations (CNA), single nucleotide variants (SNV), small insertions/deletions (Indel) and tumor mutational burden (TMB) from somatic samples as well as SNV and Indel from germline sample were detected by bioinformatics analysis. The bioinformatics workflow started mapping sequence reads to the Human genome build (hg19) by using the BWA tool (287). Variant calling for the identification of SNV and Indel was carried out via the GATK Haplotype Caller tool (288) together with FreeBayes and Strelka2 (289) for constitutional DNA and via the VarDict tool (290) together with MuTect2 (291), Strelka2 and VarScan2 (292) for somatic DNA. Germline and somatic variants are considered when are called by at least two callers. To determine the effect of variants we used SnpEff annotation (293). Other information, including count of variant allele reads, the variant allele frequency. The TMB was calculated according to Chalmers et al. (294) counting all coding, SNV and Indels in the targeted regions, including synonymous alterations. Variants were filtered following Maximum Population Frequency < 1%, cancer genes list, Tumor Variant Allele Frequency > 10%, Germline Allele Frequency > 30% and variant consequence (missense, frameshift, splicing and stop). Filtering parameters for amplifications were number copy > 4 and for deletions number copy < 1.5.

3.17. Drug combination studies

For drug combination studies with neuroblastoma standard of care, SK-N-BE(2) (2×10^3 cells/well) and SH-SY5Y (2.5×10^3 cells/well) were seeded in 96-well plates. The next day, cells were treated with the indicated concentration of 4SC-205. 24 hours later, cell medium was replaced with medium containing the indicated concentration of cisplatin, topotecan and doxorubicin, and incubated for additional five days.

For drug combination studies with targeted therapies, neuroblastoma cells (6×10^3 - 14×10^3 cells/well) were seeded in 96-well plates. 24 hours later, cells were treated with increasing concentrations of 4SC-205 plus/minus the ALK or MEK1/2 inhibitor. 48 hours later, cells

Materials and methods

were fixed with 1% glutaraldehyde and stained with 0.5% crystal violet. Pharmacological agents and their respective solvents used throughout this project are listed in Table 17.

Table 17. List of pharmacological agents.

| <i>In vitro</i> experiments | | | |
|-----------------------------|-----------------------------|---------------------|----------------------------|
| Pharmacological agent | Solvent | Stock concentration | Reference |
| 4SC-205 | DMSO | 50 mM | 4SC AG |
| Cisplatin | Saline | 1.67 mM | MedChemExpress (HY-17394) |
| Topotecan | Water | 50 mM | MedChemExpress (HY-13768A) |
| Doxorubicin | DMSO | 10 mM | Selleckchem |
| Lorlatinib | DMSO | 10 mM | MedChemExpress (HY-12215) |
| Ceritinib | DMSO | 10 mM | MedChemExpress (HY-15656) |
| Selumetinib | DMSO | 10 mM | MedChemExpress (HY-50706) |
| <i>In vivo</i> experiments | | | |
| Pharmacological agent | Solvent | Dose | |
| 4SC-205 | 5% PEG400, saline, pH 3 - 4 | 40 mg/kg | |
| Topotecan | Saline | 5 mg/kg | |

The Bliss independence model from SynergyFinder (version 2.0) was used to evaluate if the pharmacological combination of 4SC-205 with chemotherapeutic agents and targeted therapies was synergistic, additive or antagonistic (295).

3.18. Statistical analysis

Unless otherwise indicated, statistical significance was determined by unpaired two-tailed Student's t-test. Half-maximal inhibitory concentration (IC₅₀) was calculated using nonlinear regression approximation in GraphPad Prism 6.0 (GraphPad Software, Inc). Differences in survival times among mice treated with vehicle or 4SC-205 were analyzed using Gehan-Breslow-Wilcoxon test (GraphPad Prism 6.0). * Means $P < 0.05$, ** means $P < 0.01$ and *** means $P < 0.001$.

RESULTS



4. Results

4.1. KIF11 is an independent factor of survival in neuroblastoma

In order to characterize the expression profile of KIF11 in neuroblastoma human samples, we mined gene expression data from publicly available datasets such as the SEQC patient cohort. KIF11 expression was found to be higher in the high-risk neuroblastoma group than in the low- and intermediate-risk groups (Figure 13A). Overall survival was significantly poorer in patients with high KIF11 expression ($P < 0.001$, Figure 13B), with a hazard ratio (HR) of 8.190 (Table 18). Interestingly, the association between KIF11 expression and a worse outcome was maintained in both cohorts: low-intermediate and high risk (Figure 13C, D).

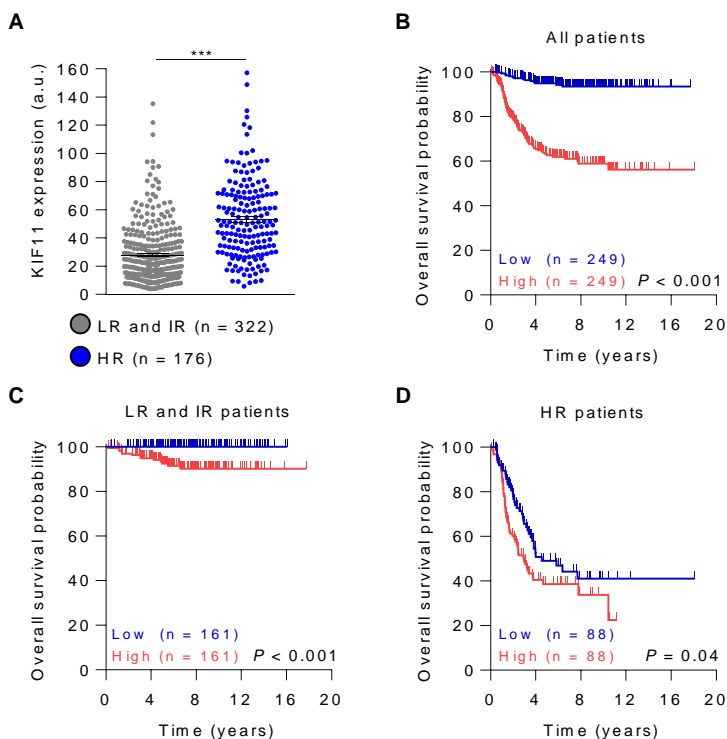


Figure 13. KIF11 mRNA expression correlates with poor outcome in neuroblastoma. (A) KIF11 mRNA expression levels comparing low-/intermediate- with high-risk neuroblastoma (SEQC; GSE62564; $n = 498$). (B-D) Kaplan-Meier overall survival curve in a cohort of 498 patients based on KIF11 mRNA expression (B) or stratified in low- (LR) and intermediate-risk (IR) (C) or high-risk (HR) (D) neuroblastoma subcohorts.

Results

KIF11 is an independent factor of survival in neuroblastoma

Table 18. Univariate and multivariate regression analysis.

| Univariate regression analysis | | |
|---|------------------------|-----------|
| Factors | Overall survival | |
| | HR (95% CI) | P value |
| Sex (M vs. F) | - | 0.252 |
| Age (≥ 18 months vs. < 18 months) | 8.114 (4.980-13.221) | < 0.001 |
| MYCN (MNA vs. Non-MNA) | 7.793 (5.262-11.542) | < 0.001 |
| ISSN Stage (4 vs. others) | 8.660 (5.441-13.783) | < 0.001 |
| KIF11 (High vs. low) | 8.190 (4.663-14.387) | < 0.001 |
| Risk (High vs. others) | 21.423 (11.932-38.464) | < 0.001 |
| Multivariate regression analysis | | |
| Factors | Overall survival | |
| | HR (95% CI) | P value |
| KIF11 (High vs. low) | 3.051 (1.693-5.497) | < 0.001 |
| Risk (High vs. others) | 14.182 (7.695-26.137) | < 0.001 |

Abbreviations: HR, hazard ratio; M, male; F, female; MNA, MYCN amplification.

Furthermore, KIF11 high expression was identified as an independent prognostic factor of survival in neuroblastoma, together with cancer risk assessment (HR = 3.051, $P < 0.001$, Table 18). These results highlighted the importance of KIF11 expression to predict the outcome of patients with neuroblastoma and indicated its potential inclusion in current risk-based management. Next, we analyzed KIF11 levels in patients with distinct genetic alterations associated with aggressive clinical behavior (296). KIF11 expression was found to be higher in patients with amplification of *MYCN*, 1p36 LOH or 17q23 gain (Figure 14).

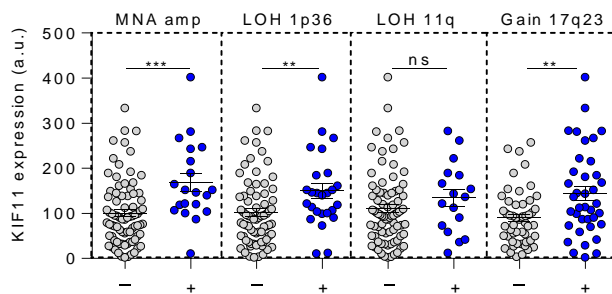


Figure 14. KIF11 mRNA is more expressed in patients with common neuroblastoma genetic alterations. KIF11 mRNA expression values are extracted from Maris (GSE3960, n = 101).

To confirm whether these associations were maintained at the protein level, KIF11 expression was assessed in an independent cohort of 25 primary neuroblastoma samples by immunohistochemistry (Table A1). KIF11 was detected mainly in the cytoplasm of neuroblastic cells (Figure 15A). Consistent with the previous mRNA analyses, patients diagnosed with high-risk neuroblastoma showed higher expression of KIF11 protein

compared to low- or intermediate-risk neuroblastoma samples ($P < 0.05$). Moreover, patients with SCA such as 1p36, 11q LOH and gain of 17q23 showed higher KIF11 protein expression ($P = 0.001$). (Table 19). The Kaplan-Meier analysis confirmed that high KIF11 protein expression was associated with poorer event-free (100% vs. 41.7%, $P = 0.025$) and overall survival (100% vs. 31.3%, $P = 0.016$) (Figure 15B, C).

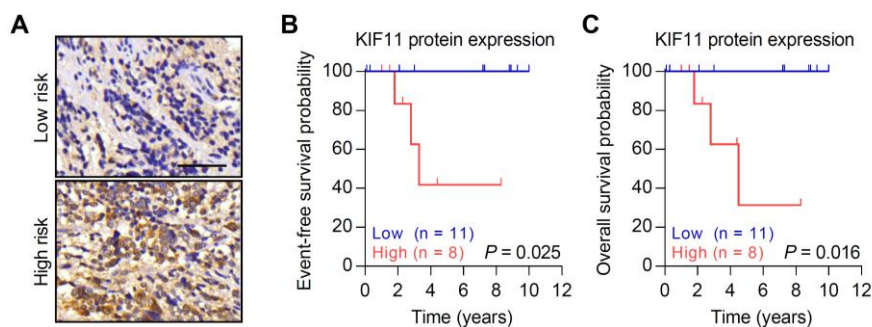


Figure 15. KIF11 protein expression is associated with worse overall survival in neuroblastoma. (A) Representative images of KIF11 immunohistochemistry in low- and high-risk neuroblastoma tissues. Scale bar indicates 50 μ m. (B, C) Kaplan-Meier curves of event-free survival (B) and overall survival (C) based on KIF11 protein expression.

Table 19. Relationships between KIF11 expression and clinico-biological characteristics

| Variable and category | Total, n | KIF11 expression | | P value | |
|-----------------------|-----------------|------------------|------------|-----------|-------|
| | | Low | High | | |
| Age | <18months | 7 | 6 (85.7%) | 1 (14.3%) | 0.132 |
| | \geq 18months | 17 | 9 (53%) | 8 (47%) | |
| Stage | L1,L2,MS | 15 | 10 (66.7%) | 5 (33.3%) | 0.179 |
| | M | 8 | 3 (37.5%) | 5 (62.5%) | |
| Hist. C. | GNB | 7 | 4 (57.1%) | 3 (42.9%) | 0.856 |
| | NB | 18 | 11 (61.1%) | 7 (38.9%) | |
| Hist. D. | dNB | 4 | 3 (75%) | 1 (25%) | 0.387 |
| | pdNB | 13 | 8 (61.5%) | 5 (38.5%) | |
| | uNB | 1 | 0 (0%) | 1 (100%) | |
| 11q | ND | 20 | 14 (70%) | 6 (30%) | 0.041 |
| | D | 5 | 1 (20%) | 4 (80%) | |
| 1p | ND | 18 | 14 (77.8%) | 4 (22.2%) | 0.008 |
| | D | 3 | 0 (0%) | 3 (100%) | |
| 17p | NG | 16 | 13 (81.2%) | 3 (18.8%) | 0.011 |
| | G | 5 | 1 (20%) | 4 (80%) | |
| Gen. profile | NCA | 14 | 13 (93%) | 1 (7%) | 0.001 |
| | SCA | 8 | 2 (25%) | 6 (75%) | |
| Ploidy | Hiperp. | 10 | 8 (80%) | 2 (20%) | 0.277 |
| | Dip+tetrap | 12 | 7 (58.3%) | 5 (41.7%) | |
| Risk group | Non-HR | 18 | 13 (72.2%) | 5 (27.8%) | 0.045 |
| | HR | 7 | 2 (28.6%) | 5 (71.4%) | |

L1 and L2, localized; MS, special metastasis; M, metastatic; Hist. C., histopathologic category; GNB, ganglioneuroblastoma; NB, neuroblastoma; Hist. D., histopathologic differentiation; dNB, differentiating neuroblastoma; pdNB, poorly differentiated neuroblastoma; uNB, undifferentiated neuroblastoma; ND, non deletion; D, deletion; NG, no gain; G, gain; Gen. Profile, genetic profile; NCA, numerical chromosomal aberration; SCA, segmental chromosomal aberration; Hiperp., Hiperploidy; Dip., diploid; Tetrap., tetraploid; HR, High risk.

Results

KIF11 expression correlates with MYCN mRNA levels

4.2. KIF11 expression correlates with MYCN mRNA levels

The correlation between KIF11 and MYCN mRNA expression suggested that KIF11 could be directly regulated by MYCN in neuroblastoma (Figure 16A). High KIF11 mRNA levels were also detected in patients with *MYCN* amplification in multiple datasets (Figure 16B).

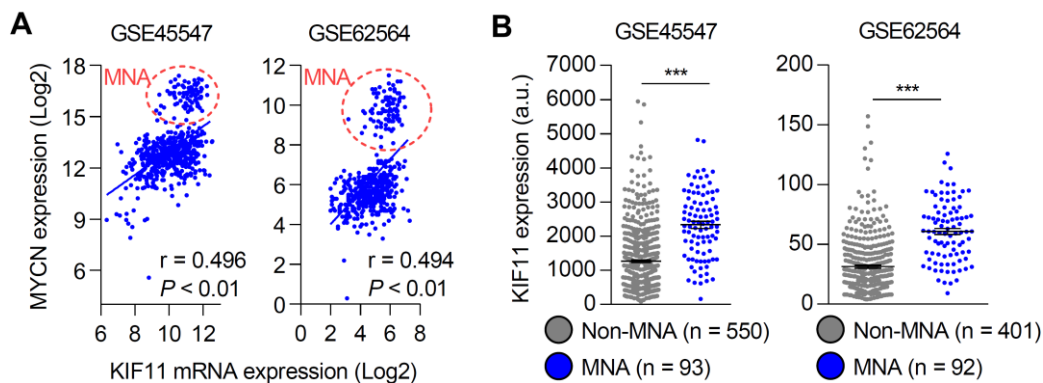


Figure 16. KIF11 mRNA expression correlates with MYCN in distinct neuroblastoma datasets. (A) Linear correlation between MYCN and KIF11 mRNA expression in the indicated neuroblastoma datasets. Data from patients with amplification of *MYCN* is encircled. (B) KIF11 mRNA expression levels comparing neuroblastoma tumors with amplification of *MYCN* (MNA) vs. no *MYCN* amplification (Non-MNA) in two different datasets.

Furthermore, ChIP on chip analysis showed that MYCN was bound to the promoter of *KIF11* in Tet21N cells (297). Thus, to verify whether MYCN was necessary and/or sufficient to drive KIF11 expression, we first analyzed the expression of KIF11 in a panel of neuroblastoma cell lines with and without *MYCN* amplification (Figure 17A). However, we did not observe any correlation between KIF11 and MYCN protein expression (Figure 17B).

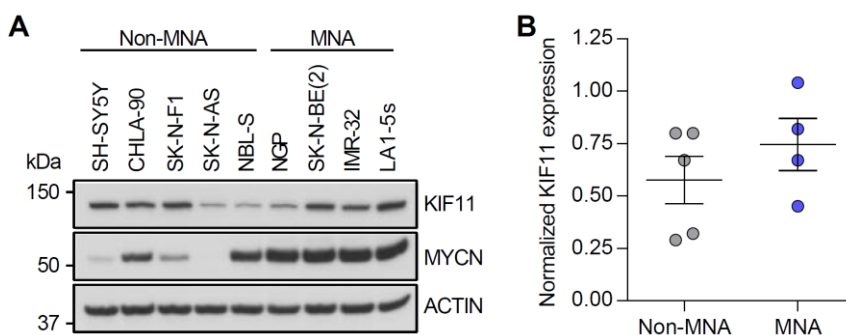


Figure 17. There is no correlation between KIF11 and MYCN protein expression in multiple neuroblastoma cell lines. (A) Western blot analysis of KIF11 and MYCN in a panel of neuroblastoma cell lines. (B) Normalized KIF11 expression in neuroblastoma cells without *MYCN* amplification (Non-MNA) and with *MYCN* amplification (MNA).

Doxycycline-mediated knockdown of MYCN in the conditional MYCN expressing SHEP Tet21N cells caused a reduction in KIF11 mRNA and protein levels (Figure 18A, B). Nevertheless, when MYCN was silenced using siRNA in other neuroblastoma cell lines, KIF11 protein remained unaltered (Figure 18C), suggesting that, in general, MYCN was not necessary for KIF11 expression.

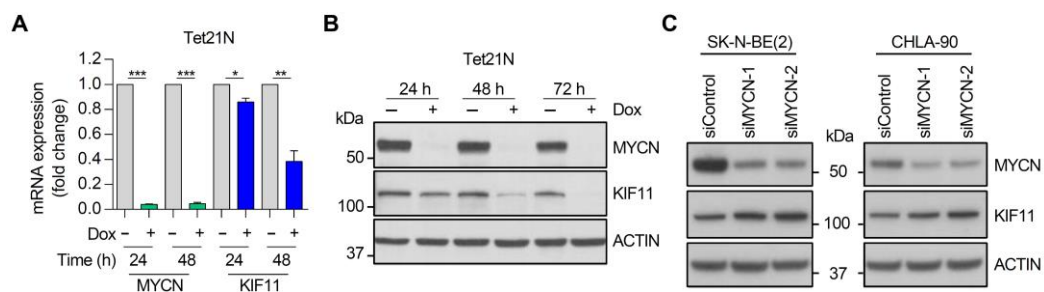


Figure 18. MYCN silencing induces KIF11 downregulation in Tet21N but not in SK-N-BE(2) and CHLA-90. (A) Analysis of MYCN and KIF11 mRNA expression in the Tet21N neuroblastoma model with the doxycycline (Dox) inducible silencing of MYCN. Results are representative of three independent experiments \pm standard error of the mean (SEM). * $P < 0.05$, ** $P < 0.01$ and *** $P < 0.01$, two-tailed student's t-test. (B) Western blot analysis of KIF11 in Tet21N cells in the presence of doxycycline (i.e. MYCN depletion) or absence (i.e. MYCN expression). (C) Immunoblot analysis of MYCN and KIF11 in SK-N-BE(2) and CHLA-90 cells transfected with two independent siRNAs targeting MYCN for 72 hours.

In order to study whether ectopic expression of MYCN resulted in an increase of KIF11 protein levels, we transfected a vector containing the human *MYCN* gene in two neuroblastoma cell lines that presented undetectable levels of MYCN protein expression. We observed that ectopic expression of MYCN was not sufficient to increase the levels of KIF11 (Figure 19). Our results suggested that, despite the existing correlation between MYCN and KIF11 mRNA expression, other transcription factors may also be implicated in its regulation in neuroblastoma.

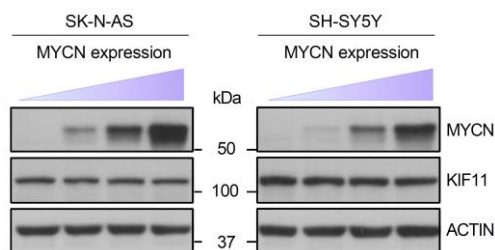


Figure 19. Ectopic expression of MYCN does not increase KIF11 protein levels. KIF11 and MYCN protein expression in SK-N-AS and SH-SY5Y transfected with increasing concentrations of a MYCN-overexpression vector.

Results

4SC-205 mirrors KIF11 depletion phenotype

4.3. 4SC-205 mirrors KIF11 depletion phenotype

4SC-205 is a potent and specific novel chemical class of KIF11 inhibitor with no structural similarities to previous KIF11 inhibitors (Figure 20). It is a chiral indole derivative with two stereogenic centers that are synthesized in multiple steps from methoxygramine. Docking experiments indicated that 4SC-205 is an allosteric inhibitor of the KIF11 protein (unpublished data). 4SC-205 is the only oral KIF11 inhibitor that has been tested in clinical studies. Moreover, its daily administration showed signs of efficacy in patients with relapsed solid malignancies and malignant lymphomas (272). To characterize whether 4SC-205 specifically inhibited KIF11, we compared the molecular effects of KIF11 genetic silencing using two different siRNAs with the pharmacological inhibition using 4SC-205.

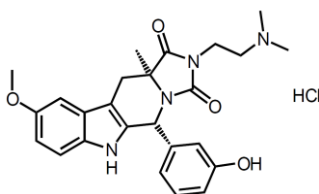


Figure 20. 4SC-205 structure. The molecular formula of 4SC-205 is $C_{25}H_{28}N_4O_4 \times HCl$. Its molecular weight is 484.99 g/mol.

It is well established that KIF11 inhibition leads to abnormal monopolar spindle formation and cell cycle arrest during mitosis (175). Immunofluorescence staining with α -TUBULIN showed that neuroblastoma cells treated with 4SC-205 were not able to self-organize microtubules into bipolar spindles and, as well as cells transfected with siKIF11, they induced aberrant spindles with monopolar morphology (Figure 21).

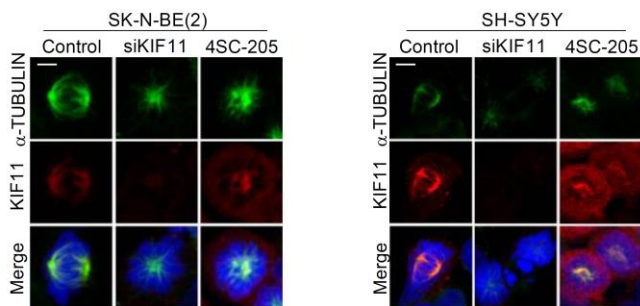


Figure 21. KIF11 inhibition using 4SC-205 induces monopolar spindle phenotype in neuroblastoma cells. Mitotic spindle immunofluorescence of SK-N-BE(2) and SH-SY5Y transfected with siKIF11 or treated with 4SC-205 (25 nM) for 24 hours. KIF11: red, α -TUBULIN: green, DAPI: blue. Scale bar, 5 μ m.

Next, we proceeded to analyze the cell cycle profile of neuroblastoma cells treated with 4S-205. Cell cycle analysis by flow cytometry showed that a large fraction of 4SC-205-treated neuroblastoma cells were arrested in the G₂/M phase (Figure 22).

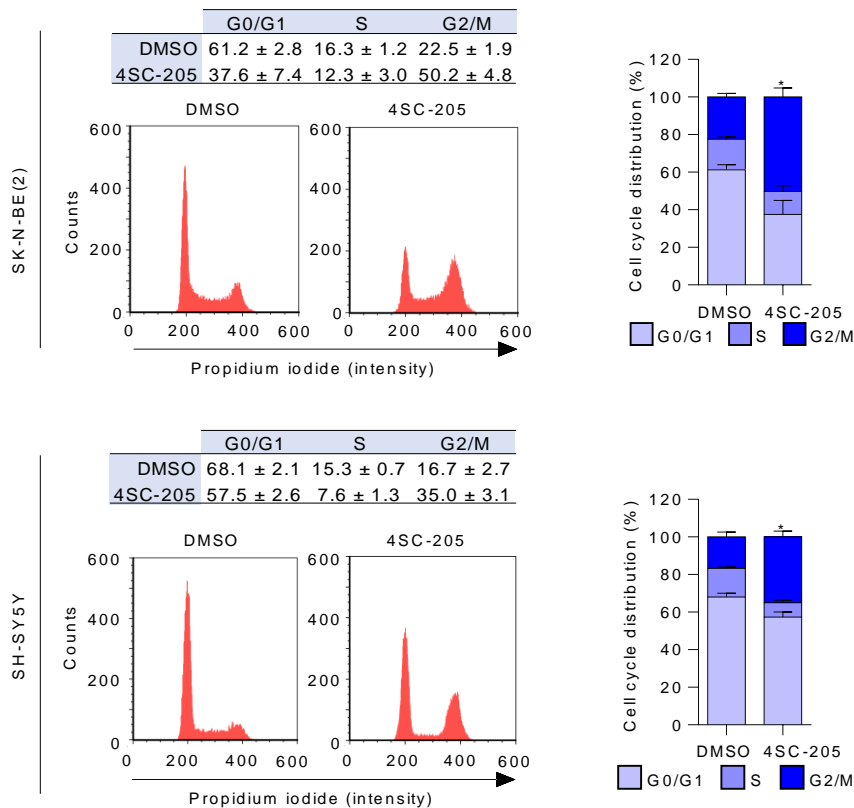


Figure 22. 4SC-205 blocks cell cycle progression in mitosis. Cell cycle analysis of SK-N-BE(2) and SH-SY5Y treated with DMSO or 4SC-205 (25 nM) for 24 hours analyzed by FACS. Histograms show one representative experiment (from three independent experiments). Graphs represent the average percentage of living cells in G₀/G₁, S or G₂/M phases of three independent experiments ± SEM. * *P* < 0.05, two-tailed student's t-test.

Results

4SC-205 mirrors KIF11 depletion phenotype

Consistent with flow cytometry analysis, siKIF11-depleted and 4SC-205-treated cells showed phosphorylation of histone H3 at serine 10 and accumulation of CCNB1, both typical markers of mitotic cells (Figure 23) (298,299).

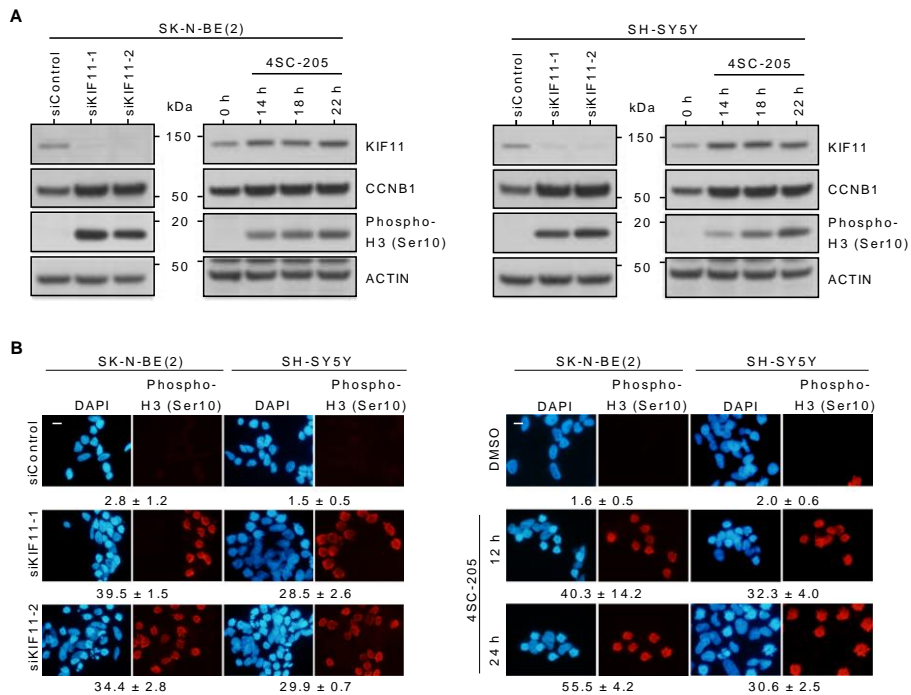


Figure 23. Genetic and pharmacological inhibition of KIF11 induce histone H3 phosphorylation of serine 10. (A) Western blot analysis of KIF11 and cell cycle-related proteins CCNB1 and phospho-histone H3 at serine 10 in cells transfected with siControl, siKIF11 or treated with 25 nM 4SC-205 at the indicated time points. (B) Representative immunofluorescence images of phospho-histone H3 in the indicated neuroblastoma cell lines transfected with two independent KIF11-targeting siRNA or treated with 4SC-205 at 25 nM for 12 and 24 hours. Scale bar, 10 μ m. The percentage of phospho-histone H3 positive cells is shown below each condition and represents the average of 7 representative fields \pm SEM.

These results demonstrated that 4SC-205 strongly interfered with mitotic spindle formation, thereby impeding the progression through mitosis. These effects mirrored those observed with the genetic depletion of KIF11.

4.4. KIF11 inhibition reduces neuroblastoma proliferation

Since neuroblastomas are molecularly diverse tumors, we sought to investigate the effect of inhibiting KIF11, both genetically and pharmacologically, in a panel of well-characterized neuroblastoma cell lines (Table 20). This panel contained multiple cell lines with numerous genetic alterations frequently found in neuroblastoma, including *MYCN* amplification (18), 11q LOH (43) and activating mutations in *ALK* (300).

Table 20. List of neuroblastoma cell lines used in this study.

| Cell line | Stage | <i>MYCN</i> | 11q | P53 | <i>ALK</i> |
|------------|-------|---------------|-----|----------------|---------------------|
| SK-N-AS | 4 | Non amplified | del | Non-functional | WT |
| SH-SY5Y | 4 | Non amplified | WT | Functional | ALK mut (F1174L) |
| SK-N-BE(2) | 4 | Amplified | WT | Non-functional | WT |
| LA1-5s | 4 | Amplified | WT | Non-functional | No expression (301) |
| IMR-32 | 4 | Amplified | WT | Functional | PA, WT |
| KELLY | 4 | Amplified | ND | Non-functional | ALK mut (F1174L) |
| BE(2)-C | 4 | Amplified | ND | Non-functional | WT |

Abbreviations: del, deletion; WT, wild type; ND, not determined; PA, partial amplification

Neuroblastoma cells were transfected with siRNA targeting KIF11 or treated with 4SC-205 for 96 and 48 hours, respectively. Crystal violet staining was performed to assess the effect of KIF11 genetic and pharmacological inhibition on cell proliferation. We observed that all cell lines exhibited comparable sensitivity to KIF11 genetic or pharmacological inhibition regardless of their respective genetic background (Figure 24). These results suggested that KIF11 inhibition may be effective in a broad spectrum of neuroblastomas, including the most aggressive subtypes, characterized by the amplification of *MYCN* (18).

Results

KIF11 inhibition reduces neuroblastoma proliferation

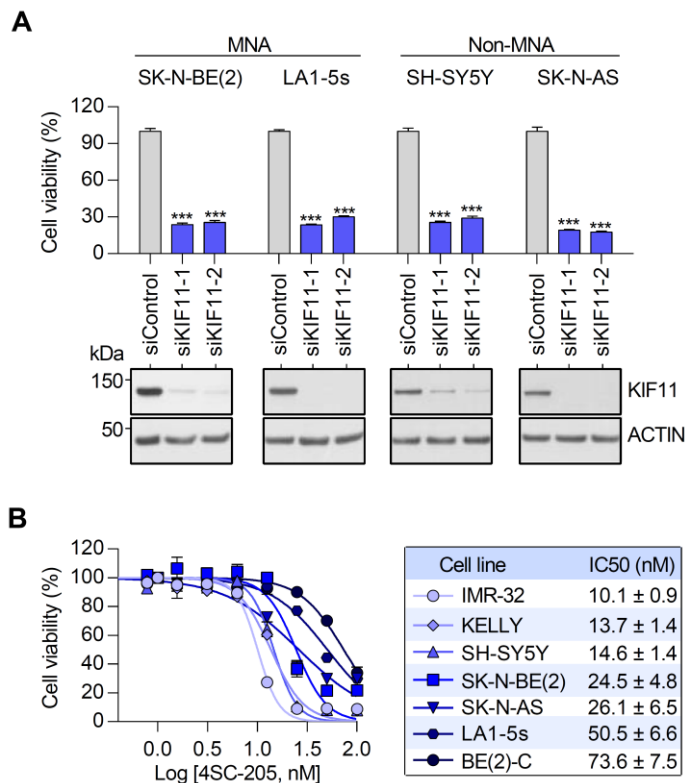


Figure 24. Genetic and pharmacological inhibition of KIF11 reduce cell proliferation. (A) Cell viability assay in the indicated cell lines transfected with 25 nM of siControl or siKIF11 for 96 hours. Protein knock-down was analyzed by western blot 72 hours post-transfection (lower panels). (B) Dose-response curves of neuroblastoma cell lines treated with increasing concentrations of 4SC-205 for 48 hours. IC50 values are presented as the average of three independent experiments ± SEM.

4.5. KIF11 inhibition induces apoptosis in neuroblastoma cells

Since cell proliferation assays demonstrated a significant reduction in cell number, we proceeded to analyze whether the effects of KIF11 inhibition on cell proliferation were induced by loss of viability. While control cells presented uniform chromatin staining, a significant proportion of neuroblastoma cells treated with 4SC-205 or transfected with siKIF11 displayed fragmented or condensed chromatin, indicating that these cells underwent apoptosis (Figure 25A, B).

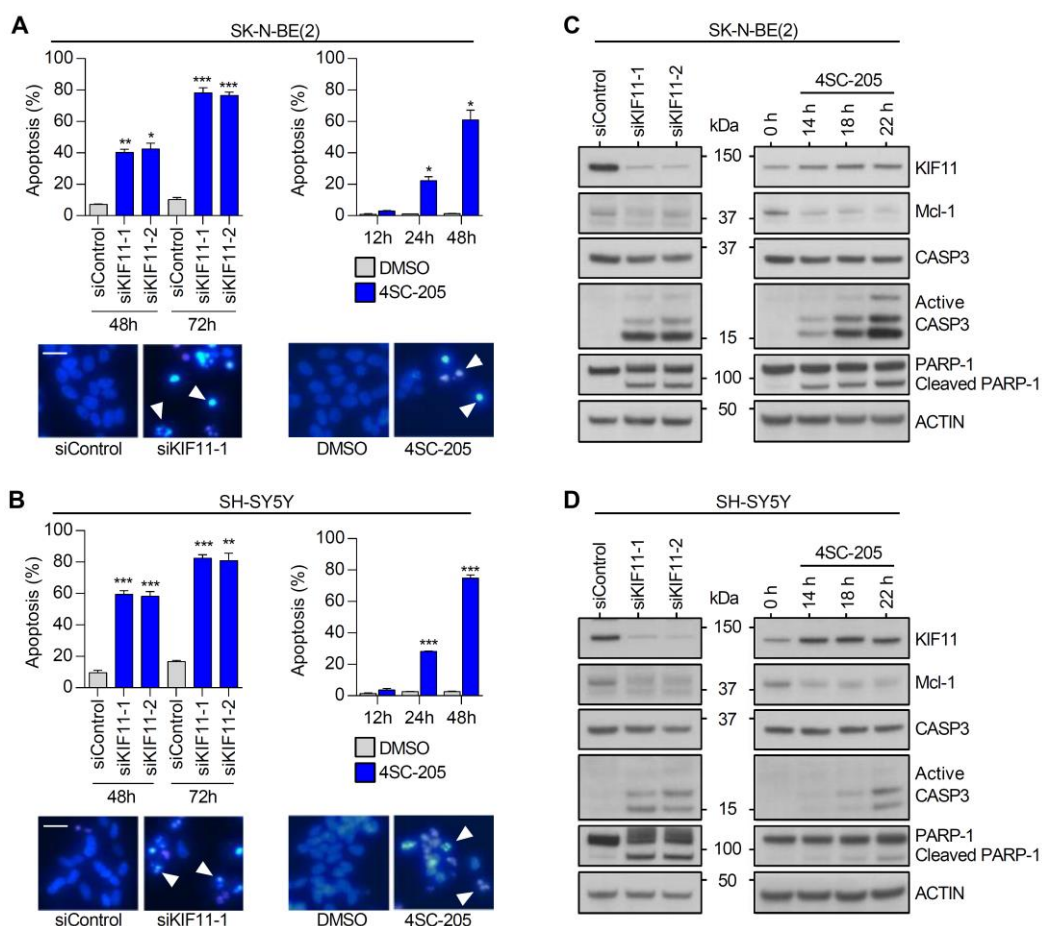


Figure 25. KIF11 inhibition induces apoptosis in neuroblastoma cells. (A, B) Apoptosis assay in SK-N-BE(2) (A) and SH-SY5Y (B) transfected with siControl / siKIF11 or treated with 25 nM 4SC-205. Each graph represents the mean of three independent experiments ($n = 6$ per experiment). * $P < 0.05$, ** $P < 0.01$, *** $P < 0.001$, two tailed Student's t-test. Lower images are representative pictures of Hoechst chromatin staining. White arrowheads point to cells with condensed and/or fragmented chromatin. Scale bar, 50 μm . (C, D) Western blot analysis of the indicated apoptosis-related proteins in SK-N-BE(2) (C) and SH-SY5Y (D) transfected with siControl / siKIF11 or treated with 4SC-205 (25 nM) at the indicated time points.

Results

KIF11 inhibition induces apoptosis in neuroblastoma cells

It has been described that the arrest in mitosis leads to the activation of the intrinsic apoptotic pathway which is induced by a progressive degradation of the anti-apoptotic protein Myeloid cell leukemia 1 (Mcl-1) (302,303). Here, we showed by western blot analysis that KIF11 inhibition resulted in the degradation of Mcl-1 with the concomitant cleavage of caspase-3 and the processing of its substrate PARP (Figure 25C, D and Figure 26). All this data confirmed the orchestrated induction of apoptosis upon KIF11 inhibition.

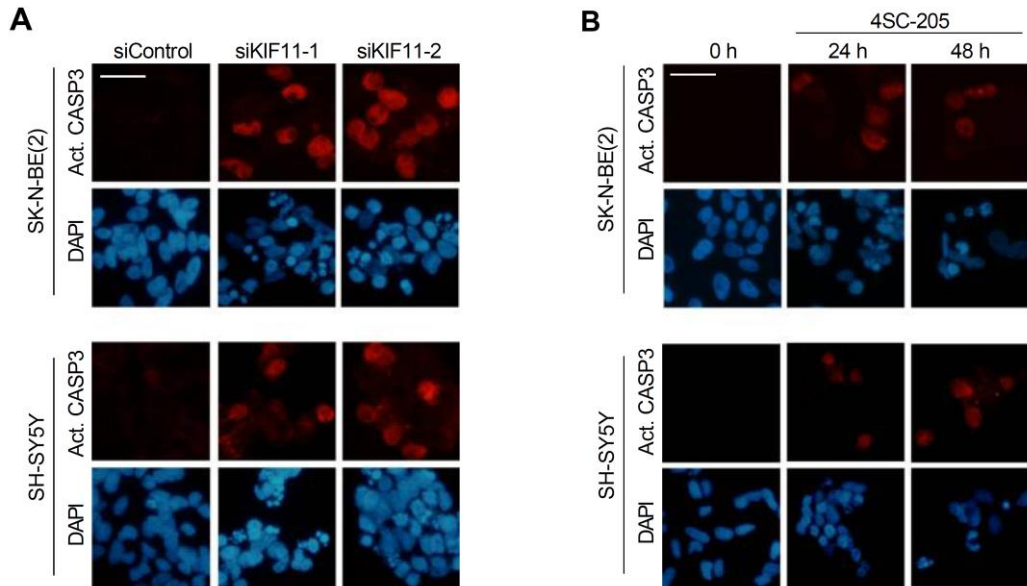


Figure 26. KIF11 inhibition increases the levels of active caspase-3. Active caspase-3 immunostaining of SK-N-BE(2) and SH-SY5Y transfected with siKIF11 (A) or treated with 25 nM of 4SC-205 at the indicated time points (B). Scale bar, 50 μ m.

4.6. 4SC-205 is a reversible inhibitor of KIF11

To clarify whether 4SC-205 binding to KIF11 was reversible, SK-N-BE(2) and SH-SY5Y were treated with 4SC-205 for 12 hours, washed and refeed with fresh medium in the presence or absence of 4SC-205. After 12 hours, cells were fixed and analyzed by flow cytometry. In this scenario, if 4SC-205 binding to KIF11 is reversible we would see that cells cultured for 12 hours with 4SC-205 and 12 additional hours with fresh medium without the inhibitor are able to reenter into G1 phase (Figure 27A). On the other hand, if 4SC-205 binding to KIF11 is irreversible, cells would remain arrested in mitosis after removal of 4SC-205 (Figure 27B).

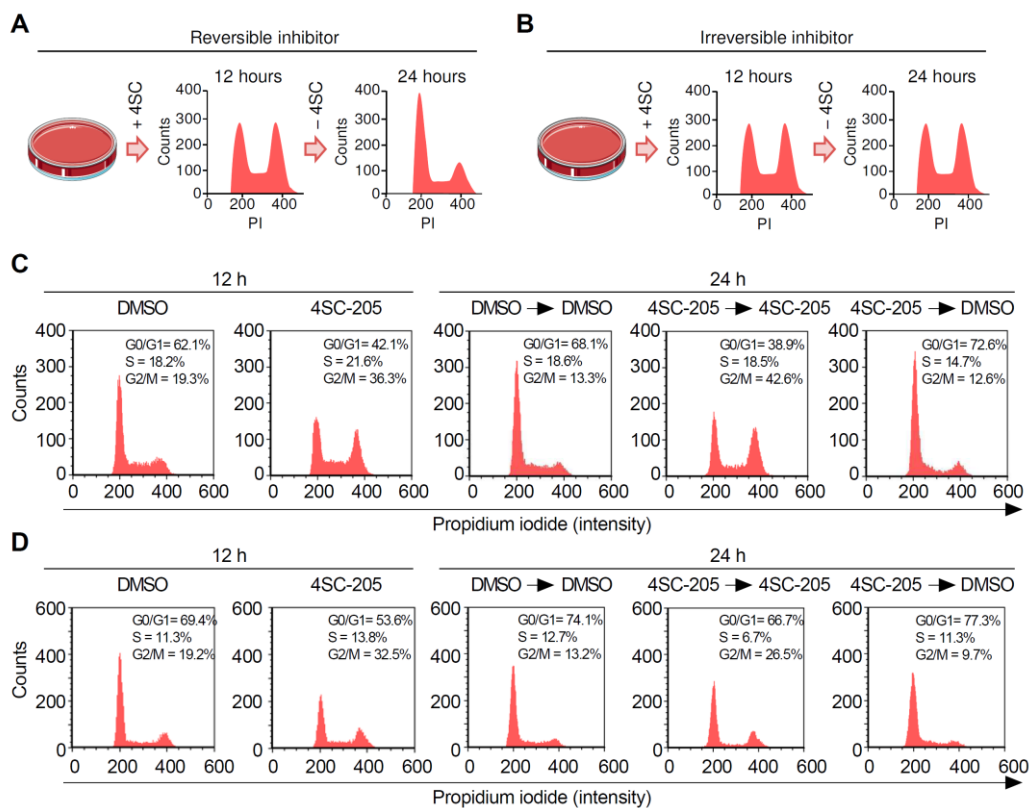


Figure 27. Effects of 4SC-205 on cell cycle are reversible. (A, B) Schematic representation of the expected results of reversible (A) and irreversible (B) KIF11 inhibition. (C, D) SK-N-BE(2) (C) and SH-SY5Y (D) cells were treated with DMSO or 25 nM of 4SC-205. After 12 hours, cell medium was replaced for fresh medium in the presence or absence (i.e. DMSO) of 4SC-205 and incubated for additional 12 hours. Cell cycle profile was analyzed by flow cytometry.

Results

KIF11 inhibition does not reduce cell viability of differentiated cells

We observed that 4SC-205 interaction with KIF11 was reversible as cells treated with 4SC-205 for 12 hours and cultured in fresh cell medium for additional 12 hours were able to reenter into the cell cycle (Figure 27C, D). Therefore, continuous dosing of 4SC-205 to ensure steady bioavailability will be necessary to maintain the therapeutic effect *in vivo*.

4.7. KIF11 inhibition does not reduce cell viability of differentiated cells

Vincristine, a vinca alkaloid, is currently being used as a standard treatment for neuroblastoma (104). Vincristine is an antimetabolic chemotherapeutic agent that inhibits microtubule assembly, which target both proliferating and non-proliferating cells (95). This mechanism of action leads to severe dose-limiting side effects such as neurotoxicity derived from interfering with the axonal integrity and microtubule's transport function (181). Specific inhibition of mitosis by targeting proteins that function exclusively during cell division is thought to improve the specificity for tumor cells and leave the majority of non-proliferating tissues in the body unaffected. Conceptually, this should provide a better therapeutic index (understood as a better efficacy-to-toxicity ratio). To investigate whether KIF11 inhibition using 4SC-205 specifically induced cell death in proliferating rather than non-proliferating cells, we tested the effects of 4SC-205 in differentiated SH-SY5Y cells. To differentiate SH-SY5Y cells, they were sequentially cultured with retinoic acid and brain-derived neurotrophic factor (BDNF) in serum-free medium. This procedure resulted in homogeneous differentiated cell population withdrawn from the cell cycle with neuronal morphology (Figure 28A, B) (279).

We found that KIF11 inhibition did not reduce cell viability of differentiated SH-SY5Y (Figure 28C). Concordantly, immunoblot analysis revealed that differentiated cells treated with 4SC-205 presented less phosphorylation of histone H3 at serine 10 and apoptosis activation (Figure 28D). These findings suggested that 4SC-205 exclusively induces cell death in proliferating cells and therefore, might avoid one of the most frequent dose-limiting side effects of microtubule poisons (i.e. neurotoxicity).

KIF11 inhibition does not reduce cell viability of differentiated cells

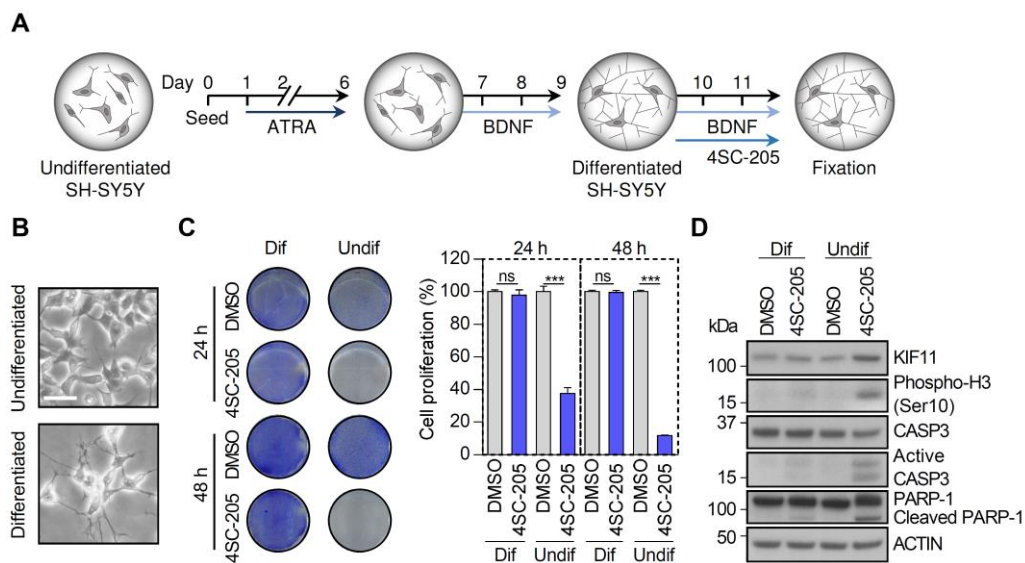


Figure 28. 4SC-205 does not affect cell viability of differentiated SH-SY5Y cells. (A) Overview of the experimental design. ATRA means all-trans-retinoic acid. (B) Representative images of SH-SY5Y before (upper image) and after 10 μ M all-trans-retinoic acid / 50 ng/mL BDNF-induced differentiation (lower image). Scale bar, 50 μ m. (C) Left, representative images of crystal violet staining. Right, cell proliferation of SH-SY5Y treated with DMSO or 4SC-205 in proliferating vs. differentiated cells. Results are expressed as the average of three independent experiments ($n = 2$ condition) \pm SEM. *** $P < 0.001$, two-tailed student's t -test. (D) Western blot analysis of phosphorylation of histone H3 and apoptosis-related proteins in differentiated and undifferentiated SH-SY5Y cells treated with 25 nM 4SC-205 for 24 hours

Results

4SC-205 reduces cell proliferation of tumor spheroids

4.8. 4SC-205 reduces cell proliferation of tumor spheroids

Since cells grown in three-dimensional (3D) spheroid culture have been described to predict more accurately *in vivo* efficacy (304), we generated 3D neuroblastoma spheroids by culturing SK-N-BE(2) and SH-SY5Y in non-adherent 6-well plates and let them grow in spheroids for 48-72 hours. Then, we proceeded to treat neuroblastoma spheroids with 4SC-205. We found that spheroid cultures of SK-N-BE(2) and SH-SY5Y were sensitive to KIF11 inhibition with slightly higher IC_{50} values than in adherent cells, i.e. IC_{50} (15-25 nM vs. ~50 nM) for both cell lines (Figure 29A, B). The increment of histone H3 phosphorylation at serine 10 and caspase-3 activation confirmed the antitumor activity of 4SC-205 in 3D cultures (Figure 29C).

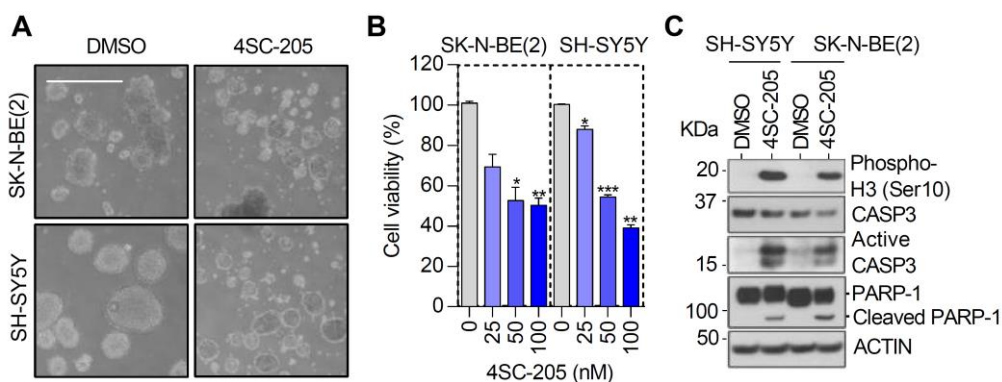


Figure 29. 4SC-205 reduces the viability of 3D neuroblastoma spheroid cultures. (A) Representative images of 3D spheroid cultures of SK-N-BE(2) and SH-SY5Y. Scale bar, 100 μ m. (B) Cell viability assay of neuroblastoma spheroids treated with DMSO or the indicated doses of 4SC-205 for 48 hours. Cell viability was measured by MTS. Graphs represent the average of three independent experiments \pm SEM. * $P < 0.05$; ** $P < 0.01$; *** $P < 0.001$. (C) Western blot analysis of phosphorylation of histone H3 at serine 10 and apoptosis-related proteins in SH-SY5Y and SK-N-BE(2) spheres treated with 25 nM 4SC-205.

4.9. KIF11 silencing inhibits neuroblastoma growth *in vivo*

To evaluate the effects of silencing KIF11 *in vivo*, SK-N-BE(2) cells were transduced with a doxycycline-inducible shKIF11 lentiviral vector. Monoclonal populations of SK-N-BE(2) transduced with pTRIPZ-shKIF11 were isolated, and KIF11 expression was analyzed by western blot in 3 independent shKIF11 clonal cell lines (Figure 30A). In the presence of doxycycline, SK-N-BE(2)-shKIF11 clones knocked down expression of KIF11 and mirrored the phenotype of siKIF11 transfected cells (Figure 30B, C).

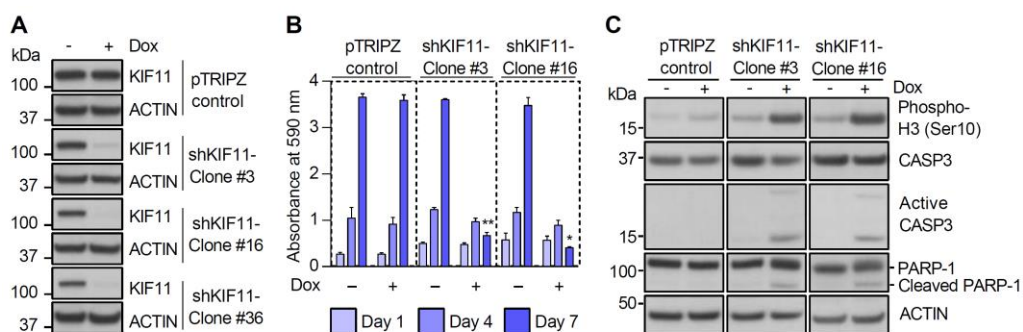


Figure 30. Genetic silencing of KIF11 using inducible shRNA mirrors siKIF11 phenotype. (A) Western blot analysis of KIF11 expression in SK-N-BE(2) cells transduced with pTRIPZ-control (pool) or in the indicated clones of pTRIPZ-shKIF11 transduced cells. Cells were treated with doxycycline (+) or not (-) for 96 hours. (B) Cell proliferation assay, after 1, 4 and 7 days upon doxycycline treatment. Results are expressed as average of three independent experiments \pm SEM. * $P < 0.05$; ** $P < 0.01$, two-tailed Student's t-test. (C) Immunoblot analysis of transduced neuroblastoma cells in presence (+ Dox) or absence (- Dox) of 1 μ g/mL doxycycline for 5 days.

SK-N-BE(2) transduced with pTRIPZ-control or pTRIPZ-shKIF11 were injected subcutaneously into the right flank of NMRI-nude mice. Once tumors reached \sim 100-200 mm³ in size, mice were randomized to receive 1 mg/mL doxycycline and 2% sucrose (+ doxycycline) or 2% sucrose (- doxycycline). As expected, doxycycline itself did not produce any significant change neither in tumor volume nor in tumor weight of mice with pTRIPZ-control SK-N-BE(2) tumors (Figure 31).

Results

KIF11 silencing inhibits neuroblastoma growth *in vivo*

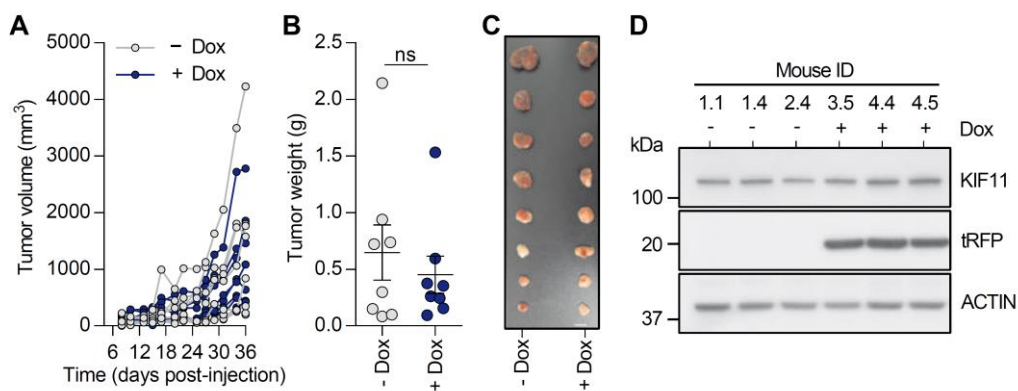


Figure 31. Doxycycline does not reduce tumor growth of pTRIPZ-control xenografts. (A) Analysis of individual tumor growth of pTRIPZ-control transduced SK-N-BE(2) xenografts. (B) Tumor weight at the end of the experiment. (C) Image of the dissected tumors. Scale bar, 1 cm. (D) Western blot analysis of resected-tumor samples from pTRIPZ-control. TurboRFP was used as a control of shRNA transgene induction.

Sixteen mice were then injected with SK-N-BE(2) cells previously transduced with pTRIPZ-shKIF11. When tumor size was ~ 100 mm³ (day 18), mice were randomized into control and shKIF11 groups. At the end of the experiment (day 28), we observed that KIF11 silencing caused a 3-4-fold reduction in tumor volume (Figure 32A) and weight (Figure 32B). Images of dissected tumors at day 28 corroborated the decrease in the tumor size between the control and shKIF11 groups (Figure 32C). We additionally estimated the tumor growth fold change for each mice between day 18 (beginning of doxycycline treatment) and day 28 (end of the experiment). Interestingly, we observed that all control mice presented a higher tumor growth fold change compared to any of the animals randomized into the shKIF11 group (Figure 32D). Western blot analysis also revealed an increase of PARP-1 cleavage in the shKIF11 group, which indicated that neuroblastoma cells underwent apoptosis after KIF11 depletion *in vivo*. Western blot analyses and immunohistochemistry confirmed KIF11 depletion and the induction of the reporter gene turboRFP, which was co-expressed with the shRNA that targets KIF11 (Figure 32E, F). Moreover, immunohistochemistry of formalin fixed paraffin-embedded samples showed a marked increase in the phosphorylation of histone H3 at serine 10 in tumor cells, thereby indicating that a significant number of cells were arrested during mitosis in KIF11 silenced tumors (Figure 32G, H).

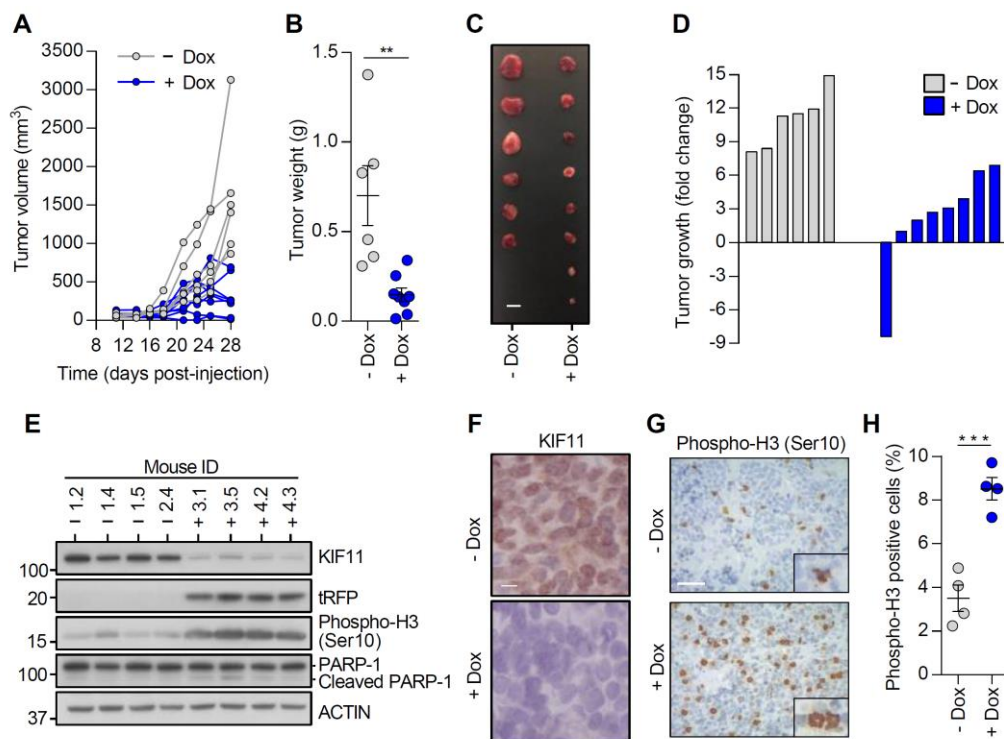


Figure 32. Genetic silencing of KIF11 reduces tumor growth in neuroblastoma xenografts. (A) Analysis of tumor volume of SK-N-BE(2) cells transduced with an inducible shKIF11 lentiviral construct comparing the effects of KIF11 silencing (+ Dox) vs. control (- Dox). (B) Tumor weight at the end of the experiment. (C) Image of the dissected tumors. Scale bar, 1 cm. (D) Waterfall plot comparing the change in tumor volume at day 18 (first day of treatment) and day 28 (end of the experiment). (E) Western blot analysis of excised tumors at the termination of the experiment. (F) Representative image of KIF11 immunohistochemistry in control (- Dox) vs. KIF11 silenced tumors (+ Dox). Scale bar, 10 μ m. (G) Representative image of phosphorylation of histone H3 immunohistochemistry from control (- Dox) vs. KIF11-depleted tumors (+ Dox). Scale bar, 100 μ m. (H) Quantification of phosphorylation of histone H3 at serine 10 positive cells in formalin-fixed paraffin-embedded tumor sections ($n = 4$ /condition). *** $P < 0.001$, two-tailed Student's t-test.

Results

4SC-205 reduces tumor growth of subcutaneous xenografts

4.10. 4SC-205 reduces tumor growth of subcutaneous xenografts

To investigate whether 4SC-205 mirrored shKIF11 effects *in vivo*, we used two subcutaneous xenografts of neuroblastoma cell lines harboring genomic alterations currently associated with poor outcome, such as *MYCN* amplification (SK-N-BE(2)) or 11q LOH (SK-N-AS) (18,43). While SK-N-BE(2) tumors from vehicle-treated mice grew exponentially, tumors from the 4SC-205-treated mice showed a remarkable shrinkage of the original tumors (Figure 33A). Of note, 9 out of 10 mice from the 4SC-205 group presented tumor regression and 1 out of 10 presented stable disease (Figure 33B). Western blot analysis showed a significant increase in phosphorylation of histone H3 at serine 10 and the cleavage of PARP-1 in the 4SC-205-treated group, thereby indicating that tumor cells were arrested during mitosis and died by apoptosis after 4SC-205 treatment (Figure 33C).

On the other hand, SK-N-AS subcutaneous xenografts of mice treated with 4SC-205 showed a significant delay in tumor growth compared to the vehicle group (Figure 33D). Even though we did not see neither tumor regression nor stabilization in SK-N-AS xenografts after 4SC-205 treatment, we observed that the highest fold change tumor growth of 4SC-205-treated mice was lower than the lowest of the vehicle-treated group (Figure 33E). Increased phosphorylation of histone H3 at serine 10 and apoptotic hallmarks (i.e. cleavage of PARP-1) were also found in SK-N-AS xenografts after 4SC-205 treatment (Figure 33F). We suspect that the difference between SK-N-BE(2) and SK-N-AS response to 4SC-205 could be caused by the rapid growth of the SK-N-AS subcutaneous tumors, which were treated with 4SC-205 only for 7 days.

These results confirmed that the antitumor effect of 4SC-205 was comparable to genetic KIF11 silencing *in vivo*.

4SC-205 reduces tumor growth of subcutaneous xenografts

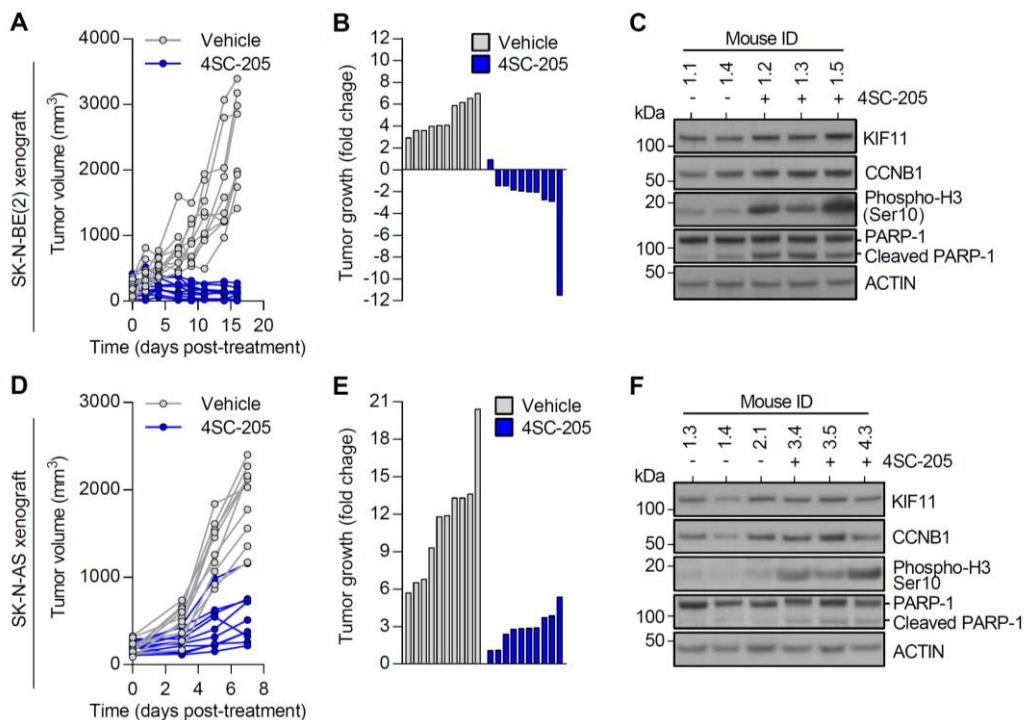


Figure 33. 4SC-205 impairs tumor growth in subcutaneous xenografts. (A) Individual tumor growth of xenograft derived from SK-N-BE(2) comparing vehicle (n = 10) vs. 4SC-205 (40 mg/kg, n = 10). (B) Waterfall plot comparing the change in tumor volume at day 16 post-treatment vs. day 4. (C) Western blot analysis of cell-cycle and apoptosis-related proteins in SK-N-BE(2) resected tumors. (D) Tumor growth of subcutaneous xenografts derived from SK-N-AS treated with vehicle (n = 10) or 4SC-205 (40 mg/kg, n = 10). (E) Tumor volume fold change at day 7 post-treatment. (F) Western blot analysis of resected tumors at the end of the experiment.

To elucidate the molecular effects of KIF11 inhibition in neuroblastoma subcutaneous xenografts, we proceeded to perform a transcriptomic analysis by RNA-seq of SK-N-BE(2) xenografts treated with 4SC-205 for 24 hours. We found that 582 genes were downregulated and 125 were upregulated after 4SC-205 treatment (Figure 34A). Then, we used gene set enrichment analysis to find functionally related genes that were upregulated or downregulated upon KIF11 inhibition (Figure 34B). We observed a downregulation of certain proteins involved in mTOR signaling pathway (Figure 34C, D). Moreover, we confirmed the upregulation of genes with crucial functions during mitosis, including mitotic kinases (i.e. PLK1, BUB1, NEK2 and AURKA), mitotic phosphatases (CDKN3), spindle assembly factors (TPX2, DLGAP5, CENPA and HMMR), kinesins (CENPE, KIF2C and KIF4A),

Results

4SC-205 reduces tumor growth of subcutaneous xenografts

and components of the APC/C complex (CDC20) in tumors treated with 4SC-205 (Figure 34E, F).

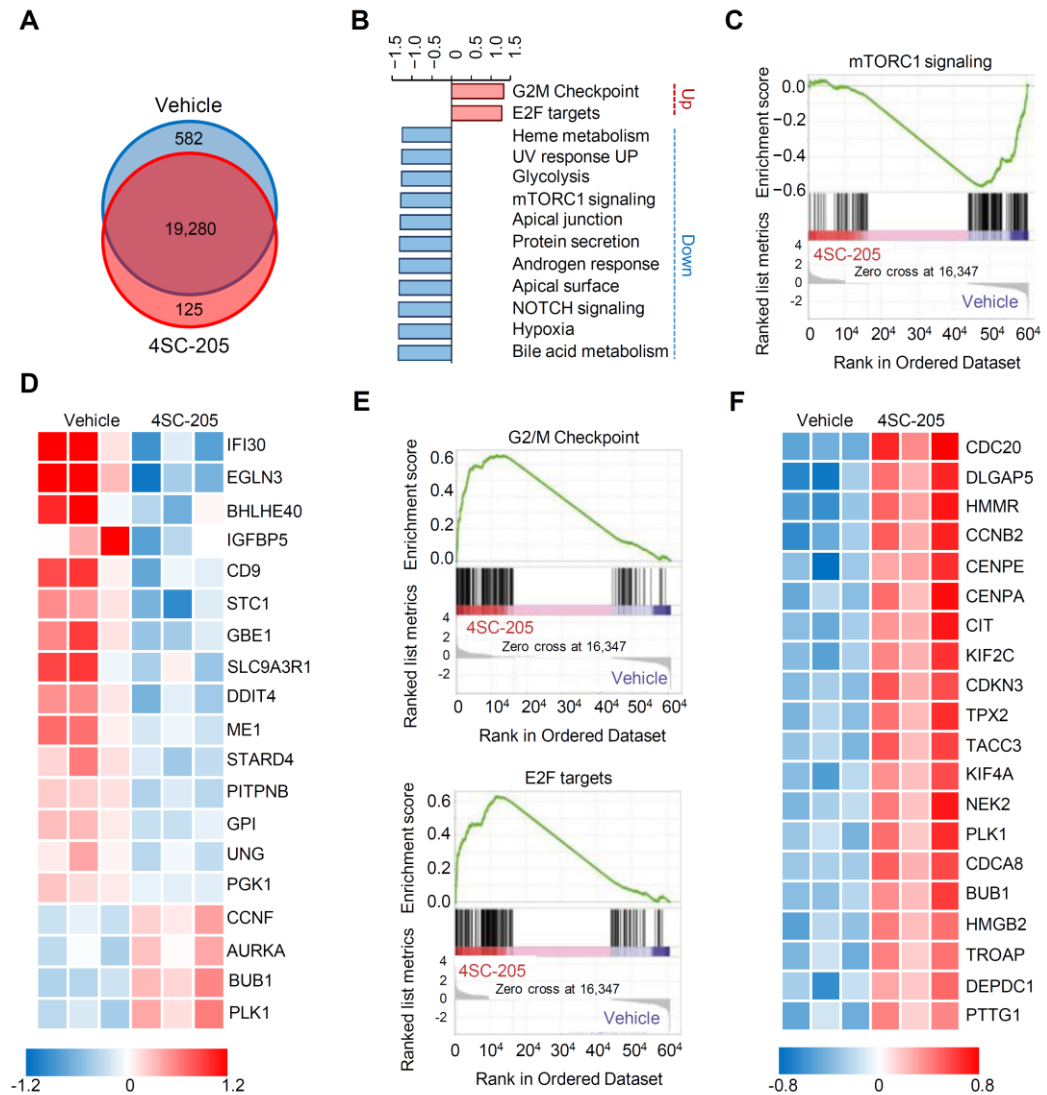


Figure 34. Transcriptomic analysis confirms that 4SC-205 arrests xenograft tumors in mitosis. (A) Venn diagram of the upregulated and downregulated genes after 4SC-205 treatment. (B) Gene set enrichment analysis (GSEA) of SK-N-BE(2) xenografts treated with vehicle or 4SC-205. Graph represents normalized enrichment score (NES) values of enriched sets with $P < 0.05$. Up and down mean upregulated or downregulated after 4SC-205 treatment. (C) GSEA of the “mTORC1 signaling” gene set of tumors from mice treated with vehicle or 4SC-205. (D) Heat map representing differentially expressed mTOR signaling related genes. (E) GSEA of “G2M checkpoint” and E2F “targets” gene sets of tumors from vehicle- and 4SC-205-treated mice. (F) Heat map representing top 20 differentially expressed genes of G2/M checkpoint and E2F targets.

Tumor volume of subcutaneous xenografts significantly correlated with tumor weight at the end of the experiment (Figure 35), which confirmed the accuracy of the measurements.

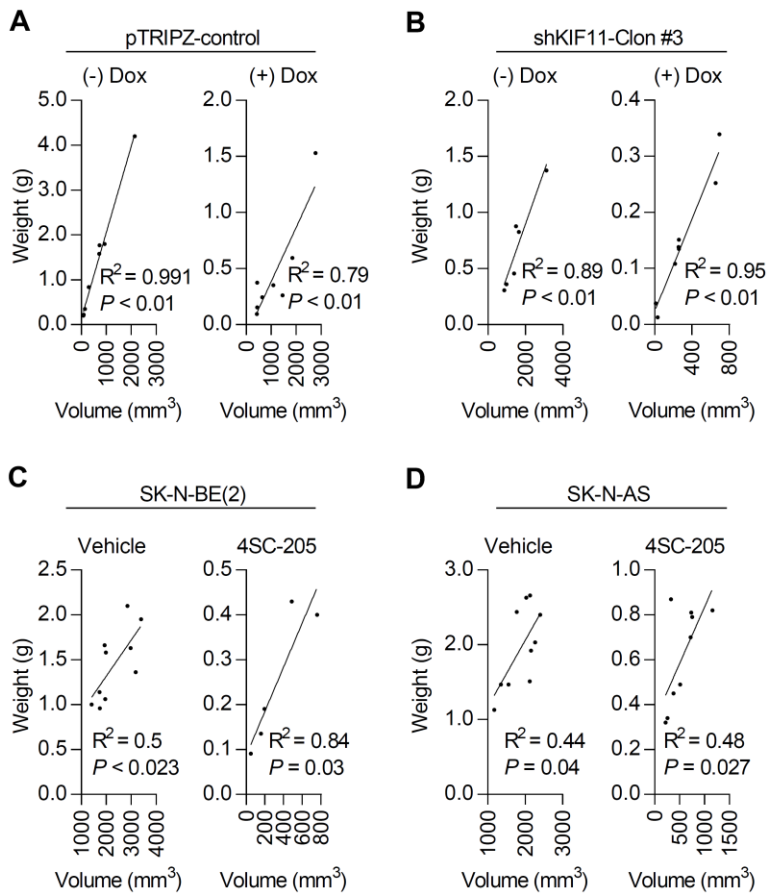


Figure 35. Tumor weight of subcutaneous xenografts correlates with tumor volume measurements. Correlation between tumor weight and tumor volume measurements in pTRIPZ-control (A), shKIF11-Clone #3 (B), SK-N-BE(2) (C) and SK-N-AS (D) xenografts treated with vehicle or 4SC-205.

4.11. KIF11 pharmacological inhibition is effective in neuroblastoma PDOX

PDOX have been described to recapitulate the genetic heterogeneity of the original tumor, as well as its response to therapy (305). To address whether 4SC-205 was also effective in a model that could closely recapitulate the aggressive behavior of high-risk neuroblastomas, a fragment of a tumor obtained at the time of diagnosis was implanted in the suprarenal gland of immunocompromised mice and further expanded into a larger cohort (Figure 36A). Of note, the PDOX model was derived from a very high-risk neuroblastoma patient who died 6 months after diagnosis due to the lack of response to the standard therapy. To investigate if the PDOX retained the histopathological features of the original tumor, we compared the histology of the PDOX and the patient's tumor. The majority of the original tumor sections were comprised of round undifferentiated small cells with a high nucleocytoplasmic ratio, typical features of the undifferentiated neuroblastoma subtype (306). Hematoxylin and eosin staining revealed that the PDOX preserved all these features (Figure 36B). We additionally performed the immunohistochemistry staining of synaptophysin and chromogranin A, both markers of neuroblastoma cells (307,308). Chromogranin A is a hydrophilic acidic protein expressed in neuroendocrine tissues and malignancies derived from them (309). Synaptophysin, a glycoprotein expressed in neuroendocrine cells, is also expressed in neuroendocrine tumors of neural type (310). We detected both synaptophysin and chromogranin A in the original tumor and the PDOX sections by immunohistochemistry.

Next, we evaluated by WES whether the PDOX conserved the key molecular features of the original tumor. The copy number analysis revealed that both PDOX and the original tumor presented chromosome alterations frequently found in neuroblastoma (i.e. 1p loss, gain of 7q and 17q) (43,311,312). Moreover, the PDOX and the original tumor harbored genetic alterations such as amplification of *MYCN*, *ABCB1* and *ALK^{G1128A}* mutation (300,313) (Figure 36C).

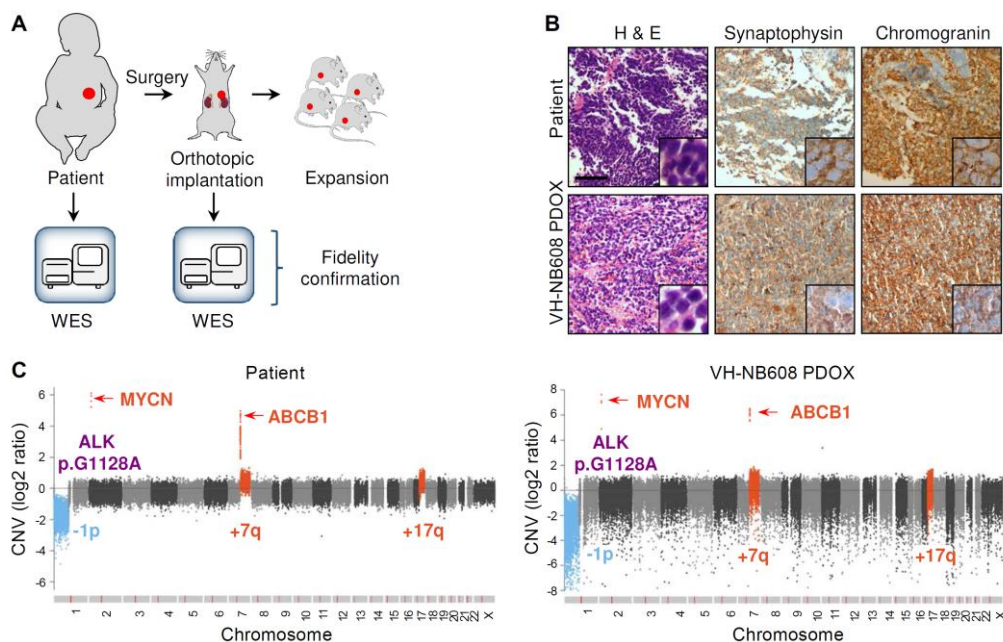


Figure 36. VH-NB608 PDOX model retains most of histological and molecular features of the original tumor. (A) Schematic representation of PDOX generation and characterization. (B) Immunohistochemistry of neuroblastoma markers in formalin-fixed paraffin-embedded tumors sections from the original tumor (upper panels) and after implantation in mice (lower panels). H&E: hematoxylin and eosin staining. Bar represents 110 μm . (C) Copy number analysis of the original tumor and after implantation in mice. CNA commonly found in neuroblastoma are highlighted.

When tumors were detected by palpation ($\sim 300\text{-}400\text{ mm}^3$), mice were randomized and treated 3 times per week for 3 weeks with 40 mg/kg 4SC-205 (Figure 37A). At the end of the experiment, 4SC-205-treated mice displayed a 14.75 fold reduction in tumor weight compared to the vehicle group (Figure 37B). Mice treated with 4SC-205 presented small tumors located in the adrenal gland, whereas vehicle-treated mice had big tumors with the kidney totally surrounded by the tumor (Figure 37C). Furthermore, 4SC-205 tumors had a larger fraction of cells with phosphorylation of histone H3 at serine 10, thereby indicating a specific targeting of KIF11 in those tumors, and suggesting that tumors were still sensitive to the inhibitor after 3 weeks (Figure 37D, E).

Results

KIF11 pharmacological inhibition is effective in neuroblastoma PDOX and metastases model

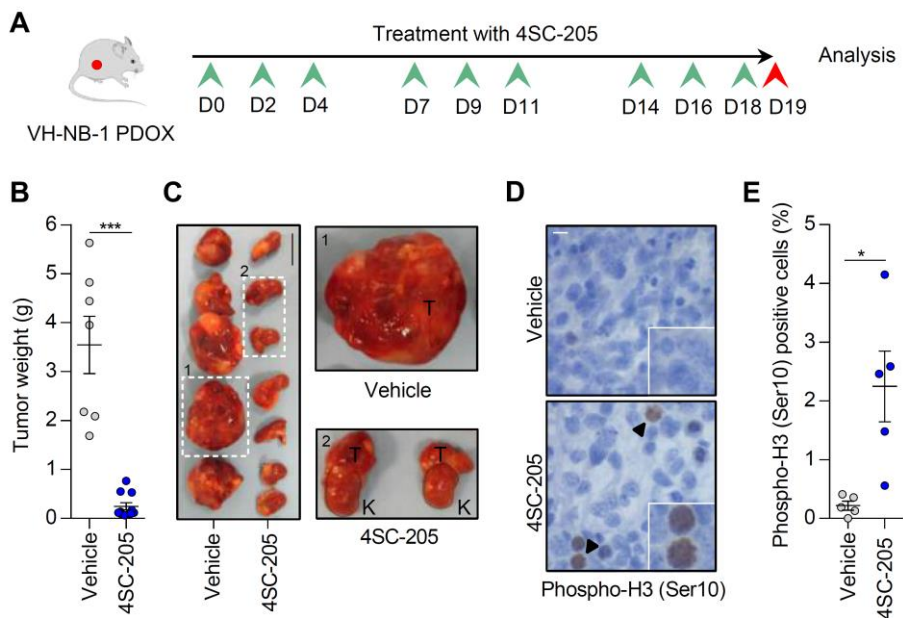


Figure 37. 4SC-205 impairs PDOX growth. (A) Schematic illustration of the treatment schedule. Mice bearing PDOX were treated for 3 weeks with either vehicle (n = 7) or 4SC-205 (40 mg/kg, n = 11). (B) Tumor weight at the end of the experiment. (C) Representative pictures of excised tumors (T: tumor; K: kidney). Scale bar: 1 cm. (D) Representative images of phosphorylated histone H3 immunohistochemistry. Scale bar: 10 μm . (E) Quantification of phospho-histone H3 positive cells in histological sections from vehicle- and 4SC-205-treated tumors. Graph represents the average percentage of positive cells \pm SEM from vehicle or 4SC-205-treated tumors (10 representative fields/tumor) (n = 5/group). * $P < 0.05$, *** $P < 0.001$, two-tailed Student's t-test.

4.12. 4SC-205 improves overall survival in a metastases mouse model

Since approximately half of neuroblastoma patients present metastases at the time of diagnosis (306), we proceeded to test the efficacy of 4SC-205 in a neuroblastoma metastases model. The most frequent sites of metastases in neuroblastoma are bone marrow, bones, regional lymph nodes, liver and skin (67). We found that SK-N-BE(2) injected into the tail vein of immunocompromised mice formed metastases mainly into the liver and bone marrow.

After SK-N-BE(2) cells were injected, metastatic growth was followed by *in vivo* bioluminescence imaging. Metastases were developed for three weeks and then, mice were randomized and treated with either vehicle or 40 mg/kg of 4SC-205 three times per week for one month (Figure 38A). Mice treated with 4SC-205 displayed a smaller increment of bioluminescence signal compared to mice treated with vehicle, indicating a significant delay

4SC-205 improves overall survival in a metastases mouse model

in metastatic outgrowth (Figure 38B, C). As a consequence, the median lifespan of the animals treated with 4SC-205 was significantly expanded (Figure 38D; vehicle: 33 days vs. 4SC-205: 42 days, $P = 0.008$).

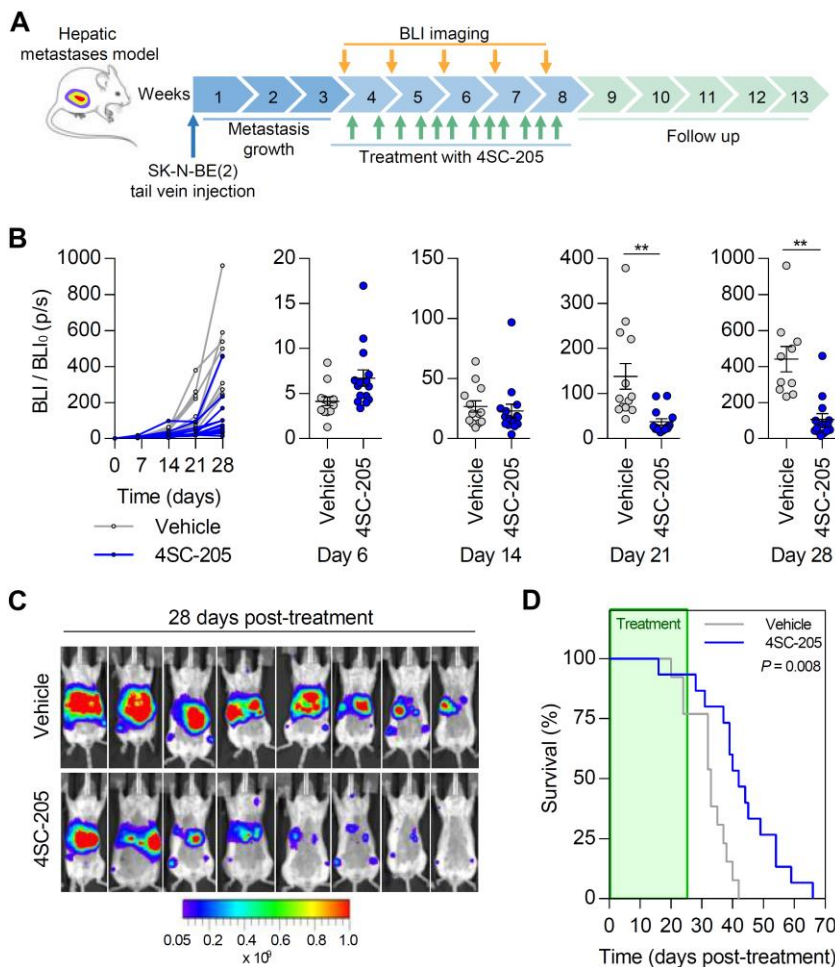


Figure 38. KIF11 inhibition prolongs survival of mice bearing neuroblastoma metastases. (A) Scheme of the experimental design. SK-N-BE(2) cells were injected into the tail vein and 21 days later, mice were randomized into vehicle ($n = 13$) and 40 mg/kg 4SC-205 groups ($n = 15$). Mice received oral administration three times per week during five weeks. (B) Quantification of individual tumor bioluminescence (left panel). Scatter dot plots represent the average quantification of tumor bioluminescence \pm SEM at the indicated time post-treatment (right panels). ** $P < 0.01$, two-tailed student's t-test. (C) Representative images of luciferase activity in 8 mice from vehicle and 4SC-205 treatment groups at 28 days post-treatment. (D) Kaplan-Meier survival curve of mice with neuroblastoma liver metastases treated with either vehicle or 40 mg/kg 4SC-205 for one month. Statistical differences were calculated using the Gehan-Breslow-Wilcoxon test.

Results

4SC-205 has a manageable toxicity profile in mice

4.13. 4SC-205 has a manageable toxicity profile in mice

Pharmaceutical compounds have to be safe and effective to succeed in the clinical trials. Safety refers that adverse effects can be tolerated by patients and potential benefits outweigh the risks of the treatment. To evaluate whether 4SC-205 was well tolerated in mice, we proceeded to analyze the evolution of body weight of control and 4SC-205-treated mice. We found that 4SC-205 minimally affected mice weight (< 10%) during the treatment (Figure 39A-D), thus offering a new potential therapeutic option for neuroblastoma patients.

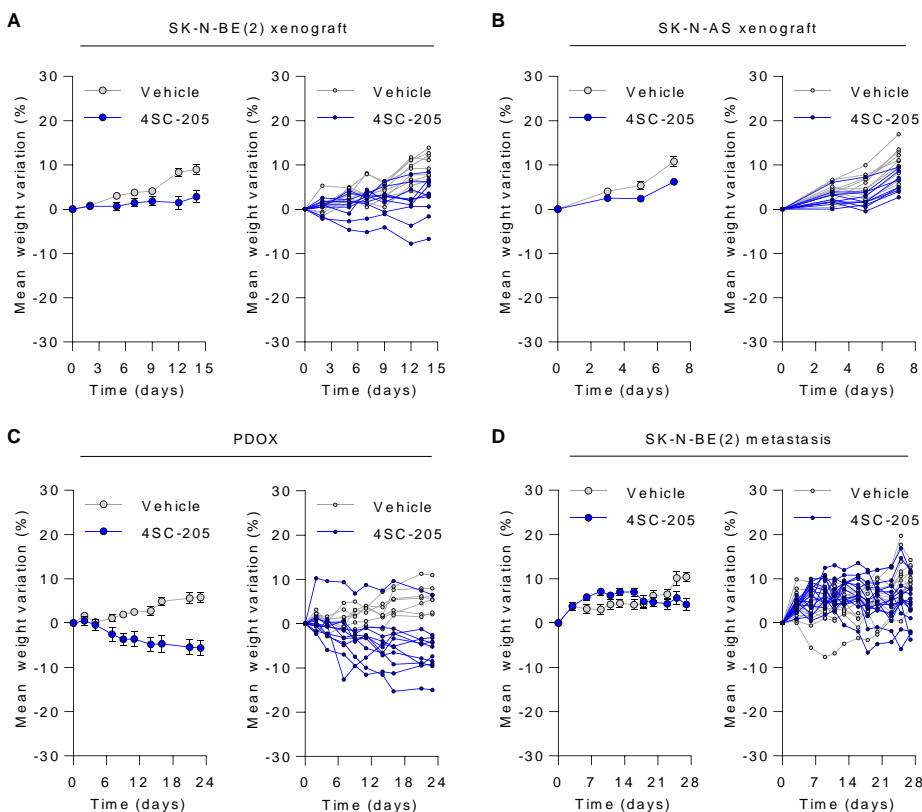


Figure 39. 4S-205 is well tolerated in mice. Average (left panels) and individual (right panels) mouse weight variation during vehicle or 4SC-205 oral administration in SK-N-BE(2) (A), SK-N-AS (B), PDOX (C) or metastases (D) xenograft models.

4.14. 4SC-205 enhances standard chemotherapy efficacy

The clinical management of high-risk neuroblastoma patients require the combination of multiple chemotherapeutic agents with different mechanisms of action, including alkylating agents (i.e. cisplatin and carboplatin), microtubule poisons (i.e. vincristine), topoisomerase I inhibitors (topotecan and irinotecan), and topoisomerase II inhibitors (etoposide and doxorubicin).

In an attempt to investigate whether KIF11 inhibition in combination with standard chemotherapy displayed enhanced efficacy, we selected three chemotherapeutic agents (i.e. cisplatin, topotecan and doxorubicin) to evaluate their respective combinations with 4SC-205.

First, we observed that topotecan and doxorubicin alone induced a strong reduction of cell viability at very low concentrations (10-35 nM). On the other hand, much higher doses of cisplatin were required to inhibit cell growth (900-1,500 nM) (Table 21).

Table 21. IC₅₀ values for cisplatin, doxorubicin and topotecan in neuroblastoma cell lines.

| Cell line | IC ₅₀ cisplatin (nM) | IC ₅₀ doxorubicin (nM) | IC ₅₀ topotecan (nM) |
|------------|---------------------------------|-----------------------------------|---------------------------------|
| SH-SY5Y | 925 ± 76 | 10.4 ± 0.7 | 11.2 ± 0.8 |
| SK-N-BE(2) | 1511 ± 143 | 34.8 ± 7.5 | 11.9 ± 1.5 |

Several studies suggest that combination of pharmaceutical agents targeting different cell cycle events can lead to a phenomenon known as cell-cycle mediated drug resistance. These studies described that a better therapeutic outcome was achieved when antimitotic drugs (i.e. taxanes) were administered prior to DNA damaging agents (314). Thus, we proceeded to treat neuroblastoma cells with a sequential combination of 4SC-205 for 24 hours and then add the chemotherapeutic drugs cisplatin, topotecan or doxorubicin for additional 5 days (Figure 40A). In all cases, the combination of 4SC-205 with chemotherapy almost doubled therapeutic effect of the single drug treatments (Figure 40B, C).

Results

4SC-205 enhances standard chemotherapy efficacy

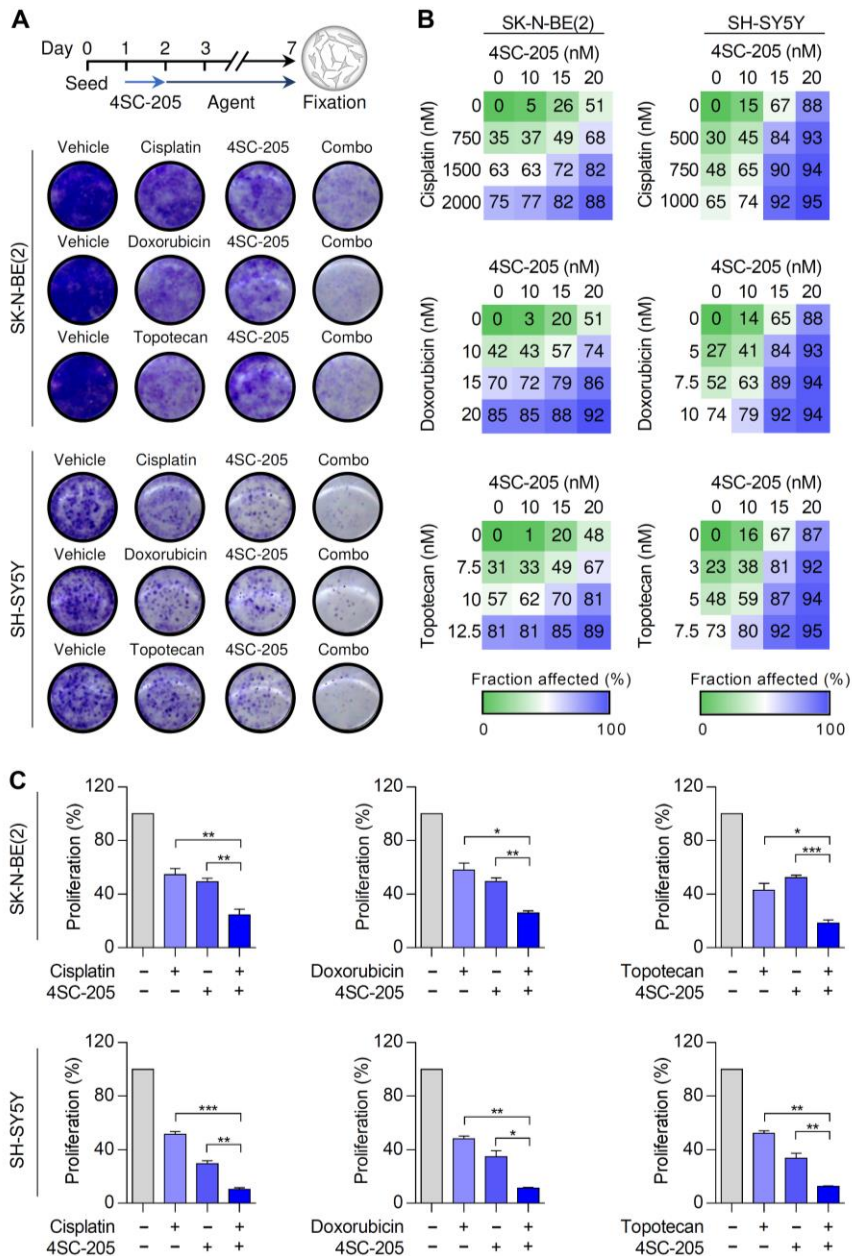


Figure 40. Combination of 4SC-205 with chemotherapy leads to enhanced efficacy. (A) Scheme of the experimental design. Images are representative of crystal violet staining of SK-N-BE(2) and SH-SY5Y cells treated with the indicated fraction drugs and their corresponding combinations (Combo). (B) Heatmaps showing the percentage of the cellular fraction affected. (C) Graphs represent the average effect on cell viability from of three independent experiments \pm SEM. * $P < 0.05$, ** $P < 0.01$, *** $P < 0.001$, two tailed Student's t-test.

To study if the combination of 4SC-205 with cisplatin, doxorubicin and topotecan exerted synergistic or additive antitumor effects, we analyzed the synergy score using the SynergyFinder tool (version 2.0) (295). We performed the analysis using the Bliss independence model, which assumes that the effect of two drugs are independent (315). In this model, if the synergy score is larger than 10, the combination between two drugs is likely to be synergistic. If the score value ranges from -10 to 10, the combination is likely to be additive. Finally, if the synergy score value is smaller than -10, it is likely to be antagonistic.

We observed that the combination between 4SC-205 and cisplatin, doxorubicin and topotecan exerted additive antiproliferative effects in SK-N-BE(2) and SH-SY5Y cell lines, as nearly all synergy score values ranged between 0 and 10 (Figure 41).

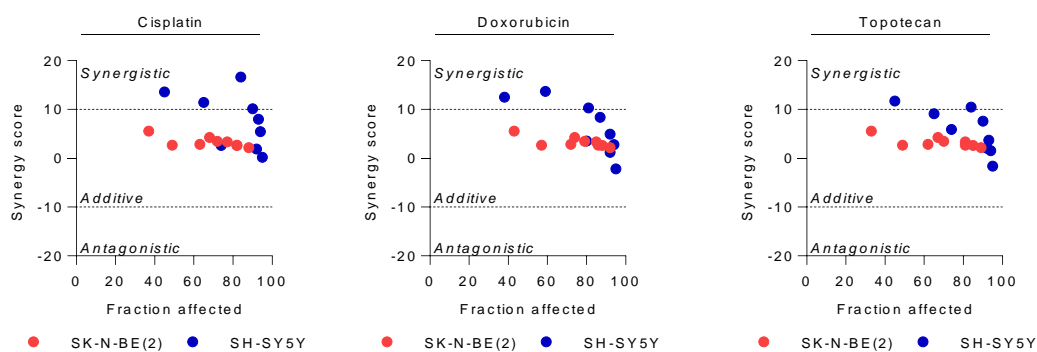


Figure 41. Combination of 4SC-205 with standard chemotherapy exerts additive antitumor effects in neuroblastoma.

The common induction regimen in Europe to treat high-risk neuroblastoma consist of a rapid and dose intensive chemotherapy, which include cisplatin, vincristine, carboplatin, etoposide and cyclophosphamide (104). Patients who relapse or do not respond to the standard chemotherapy schedule are treated with non-cross-resistant drugs such as topotecan and doxorubicin (125). The underlying assumption is that tumor cells have become resistant to previously used drugs (316). If 4SC-205 alone or in combination with chemotherapy enter in clinical studies, it will be used after relapse in patients with advanced neuroblastoma. Therefore, second-line chemotherapy, such as topotecan or doxorubicin, should be prioritized to evaluate the combination with 4SC-205 in mice over drugs used in the induction phase (i.e. cisplatin).

Results

4SC-205 enhances standard chemotherapy efficacy

Since nearly all neuroblastoma patients who relapse present metastatic disease (317), we tested the combination of 4SC-205 and chemotherapy in the SK-N-BE(2) metastases model. SK-N-BE(2) cells showed to be very sensitive to topotecan (Table 21). For that reason, we selected this drug to test the combination with 4SC-205 *in vivo*.

As both 4SC-205 and topotecan induce hematologic side effects such as neutropenia (318), we first evaluated the safety of this combination by testing four dosing regimens for topotecan in combination with 20 mg/kg of 4SC-205 three times per week. We observed that both topotecan 10 mg/kg once weekly and 5 mg/kg twice weekly caused a rapid decrease in mice weight. On the other hand, the dose of 2.5 and 5 mg/kg of topotecan once weekly alone or in combination with 4SC-205 did not cause any noticeable side effect (Figure 42). For that reason, we selected the schedule of 5 mg/kg of topotecan once a week and 20 mg/kg 4SC-205 three times a week to evaluate the efficacy of the combination.

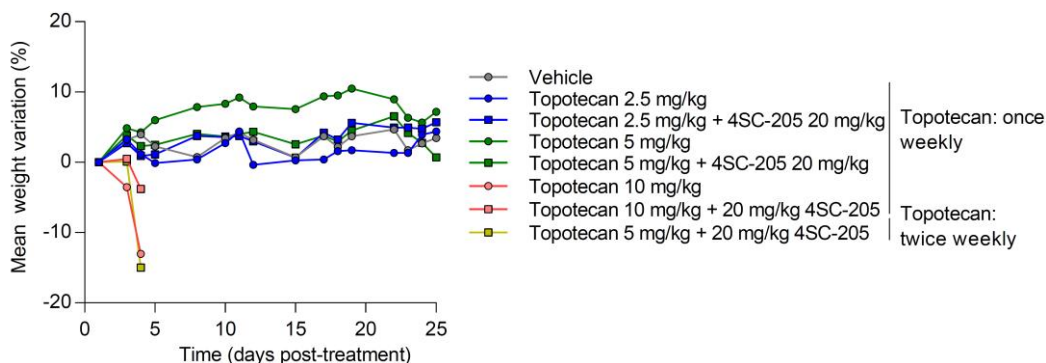


Figure 42. Combination of 5 mg/kg of topotecan once weekly and 20 mg/kg of 4SC-205 three times per week is well-tolerated in mice.

SK-N-BE(2) cells were injected into the tail vein of 35 SCID-Beige mice. After 11 days, mice were randomized into vehicle ($n = 7$), 20 mg/kg 4SC-205 ($n = 10$), 5 mg/kg topotecan ($n = 8$) and combo ($n = 10$) groups. Mice received oral administration of 4SC-205 three times per week and intraperitoneal injection of topotecan once weekly (Figure 43A). At 28 days post-treatment, we observed a ~25 and 3,000 fold reduction in bioluminescence activity in mice treated with 4SC-205 and topotecan alone, respectively. Of note, mice treated with the combination of 4SC-205 and topotecan presented a 10,000 fold reduction in the bioluminescence activity (Figure 43B, C). In this line, mice treated with vehicle, 4SC-205,

topotecan and the combination presented a median survival of 45, 59, 87 and 120 days, respectively (Figure 43D).

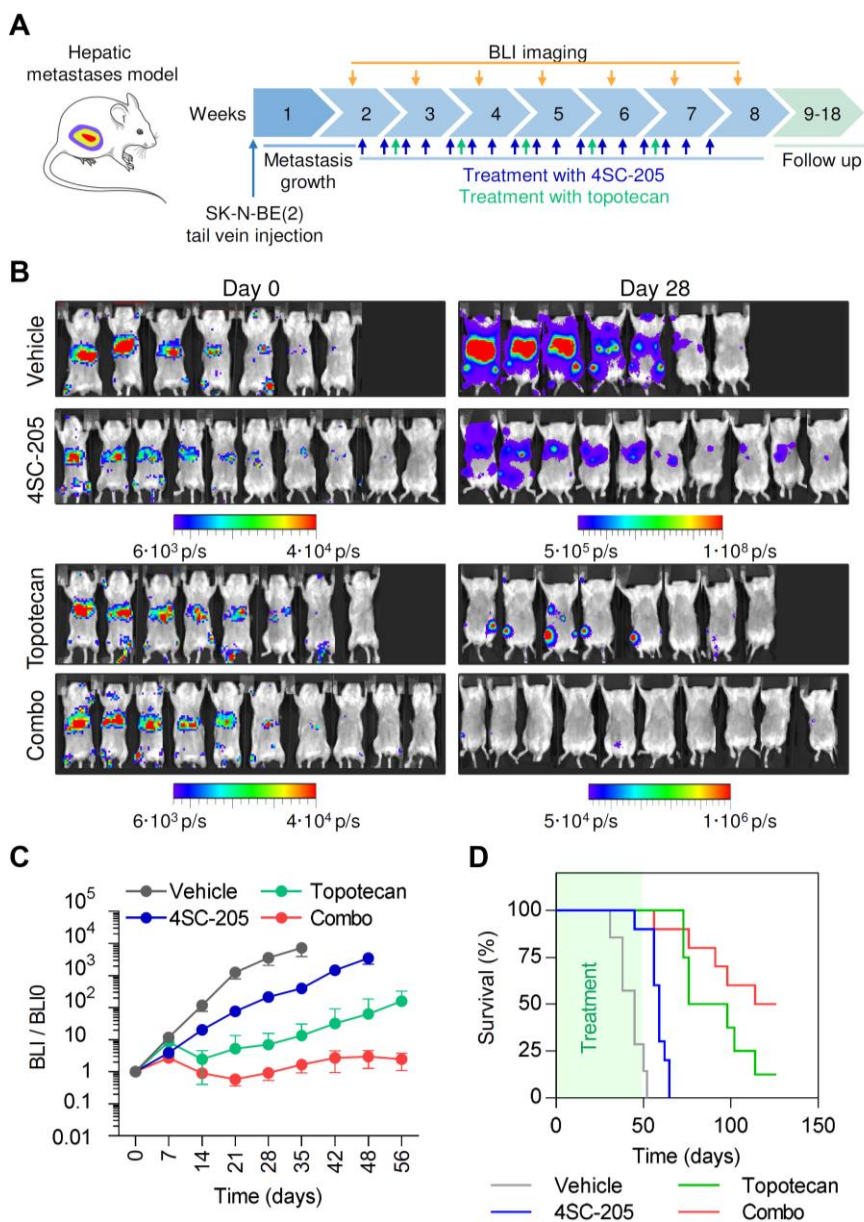


Figure 43. Combination of 4SC-205 and topotecan expands the lifespan of mice bearing SK-N-BE(2) metastases. (A) Scheme of the experimental design. (B) Images of luciferase activity at day 0 and 28 post-treatment. (C) Quantification of luminescence signal \pm SEM from all imaged mice. (D) Kaplan-Meier survival curves of each group of mice.

Results

4SC-205 enhances standard chemotherapy efficacy

Even though no substantial changes were found in the liver bioluminescence activity between topotecan and combination cohorts during treatment (Figure 44A), significant differences were observed at the end of the experiment where 80% (8 out of 10) of mice treated with the combination and only 25% (2 out of 8) treated with topotecan presented a complete remission of liver metastases (Table 22; $P = 0.0002$). These results indicated that although topotecan alone efficiently reduced the size of liver metastases during treatment, the combination of both drugs improved the overall response rate.

Table 22. Relationship between tumor response and treatment.

| Site of metastasis | Response | Vehicle | 4SC-205 | Topotecan | Combo | P value (χ^2) |
|------------------------|----------|------------|--------------|-------------|-------------|------------------------|
| Liver metastasis | PD | 7/7 (100%) | 10/10 (100%) | 6/8 (75%) | 2/10 (20%) | 0.0002 |
| | CR | 0/7 (0%) | 0/10 (0%) | 2/8 (25%) | 8/10 (80%) | |
| Bone marrow metastasis | PD | 6/6 (100%) | 4/4 (100%) | 6/7 (85.7%) | 1/8 (12.5%) | 0.0007 |
| | CR | 0/6 (0%) | 0/4 (0%) | 1/7 (14.3%) | 7/8 (87.5%) | |

Abbreviations: PD, progressive disease; CR, complete response

Of note, 87.5% (7 out of 8) of mice treated with the combination presented complete remission of bone marrow metastases at the end of the experiment. On the contrary, only 14.3% (1 out of 7) of topotecan-, 0% (0 out of 6) of vehicle- and 0% (0 out of 4) of 4SC-205-treated mice were in complete remission (Table 22; $P = 0.0007$). In this line, mice treated with the combination presented less bone marrow bioluminescence activity compared to the other groups (Figure 44B).

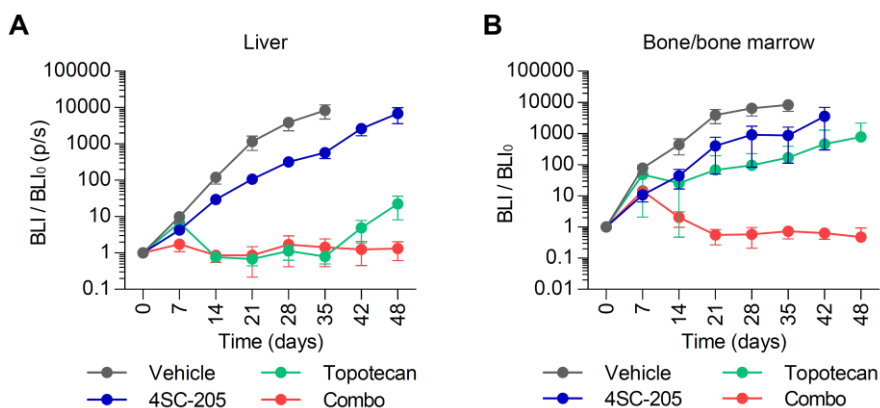


Figure 44. Combination of 4SC-205 and topotecan efficiently removes liver and bone marrow metastases. Bioluminescence activity of liver (A) and bone marrow metastases (B).

4.15. 4SC-205 and ALK inhibitors cooperate to impair neuroblastoma growth

Pediatric precision medicine programs led to the discovery of a small number of recurrent mutations that constitute the basis for the development of targeted therapies against high-risk neuroblastoma tumors. Among them, *ALK* activating mutations or amplifications are found in a significant number of neuroblastoma patients (32). Thus, we proceeded to combine 4SC-205 with two ALK inhibitors currently used in clinical trials for neuroblastoma patients (i.e. ceritinib and lorlatinib). The combination of 4SC-205 with ALK inhibitors was conducted in SH-SY5Y and KELLY cell lines, which harbor the constitutively activated mutant ALK protein (F1174L). We found that both cell lines showed a similar reduction of cell proliferation when were treated with ceritinib and lorlatinib alone (Table 23).

Table 23. IC50 values for ceritinib and lorlatinib in *ALK* mutated neuroblastoma cell lines.

| Cell line | Molecular alteration | IC50 ceritinib (nM) | IC50 lorlatinib (nM) |
|-----------|----------------------|---------------------|----------------------|
| SH-SY5Y | ALK mut (F1174L) | 74.4 ± 11.6 | 59.8 ± 10.8 |
| KELLY | ALK mut (F1174L) | 162.8 ± 28.7 | 51.9 ± 6 |

Abbreviations: mut, mutated

Interestingly, when both ALK inhibitors were combined with 4SC-205, a ~2-3 fold reduction in cell proliferation was observed compared to lorlatinib and ceritinib alone (Figure 45A-D). To identify if simultaneous inhibition of KIF11 and ALK exerted synergistic or additive antiproliferative effects, we treated SH-SY5Y and KELLY cell lines with different concentrations of 4SC-205 and lorlatinib/ceritinib and calculated the synergy score using the SingergyFinder tool. We found that the combination of 4SC-205 and ceritinib exerted synergistic antitumor effects in SH-SY5Y and additive effects in KELLY. On the other hand, lorlatinib exerted additive antiproliferative effects in both cell lines (Figure 45E).

Results

4SC-205 and ALK inhibitors cooperate to impair neuroblastoma growth

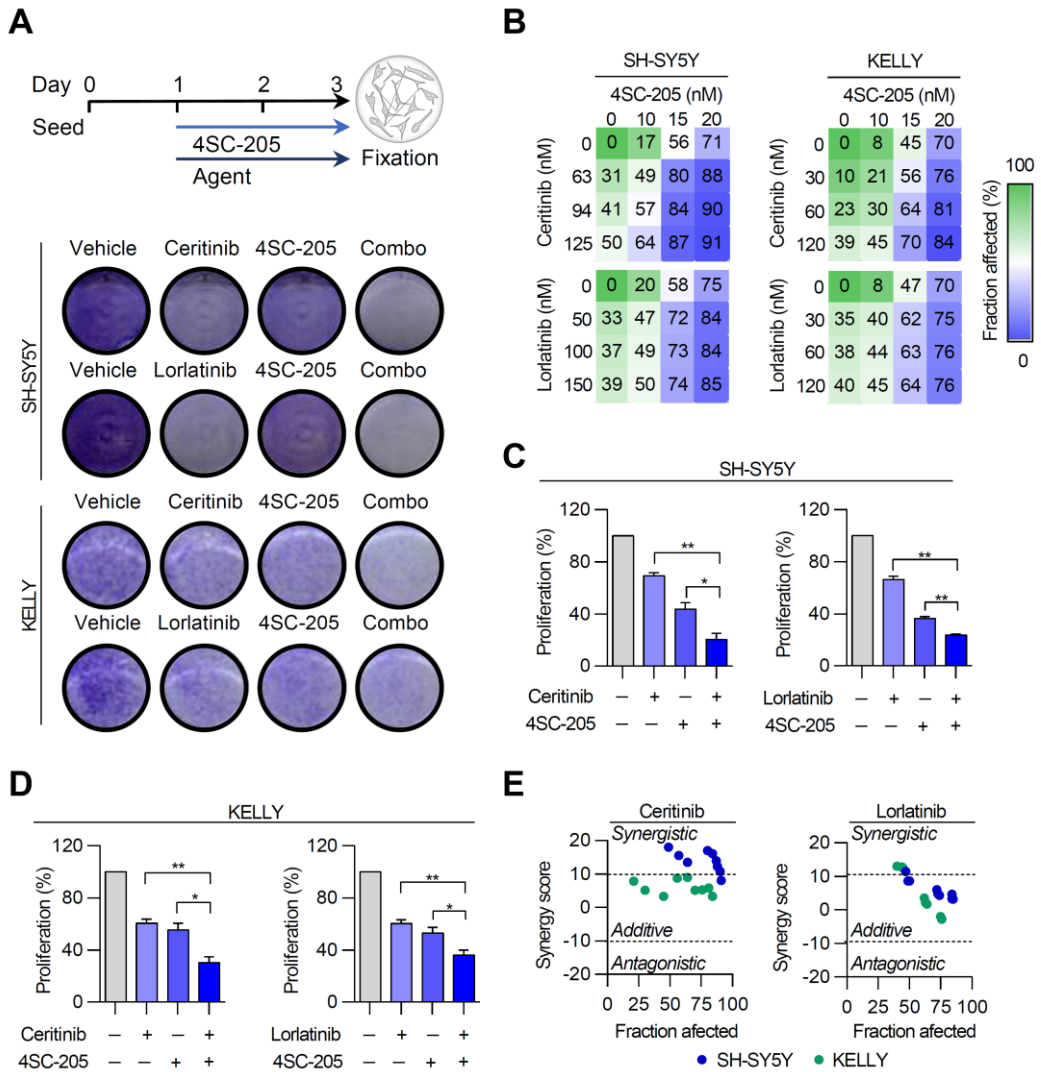


Figure 45. 4SC-205 and ALK inhibitors combination impairs neuroblastoma proliferation. (A) Schematic representation of the experimental design combining 4SC-205 and ALK inhibitors. Representative images of crystal violet of the *ALK* mutated SH-SY5Y and KELLY cell lines treated with ceritinib and lorlatinib with or without 4SC-205. (B) Heatmaps show the percentage of the cellular fraction affected by the drug combination treatments. (C, D) Graphs represent the average \pm SEM of cell proliferation after combination of 4SC-205 and ceritinib/lorlatinib in SH-SY5Y (C) and KELLY (D). * $P < 0.05$, ** $P < 0.01$, two tailed Student's t-test. (E) Combinatorial analysis performed using SynergyFinder tool (version 2.0).

4.16. 4SC-205 and selumetinib cooperate to reduce neuroblastoma growth

Only 3-5% of newly diagnosed neuroblastoma display mutations in the canonical MAPK pathway. However, around 80% of relapsed tumors could present genetic alterations predicted to activate RAS signaling (150).

We first selected two neuroblastoma cell lines with alterations on the RAS/MAPK pathway. SK-N-BE(2) has a genomic loss of the tumor suppressor *NF1*, which leads to increased RAS/MAPK signaling (319); and SK-N-AS harbors the *NRAS* (Q61K) activating mutation (320).

For combination studies with 4SC-205, we selected the MEK1/2 inhibitor selumetinib. Selumetinib has shown promising results in children with recurrent low-grade gliomas (151), and it is currently being tested in phase II studies for children with solid malignancies, including neuroblastoma, harboring mutations in MAPK pathway (NCT03155620). We found that selumetinib alone induced a strong reduction in cell growth in both neuroblastoma cell lines. However, SK-N-AS were much more sensitive to selumetinib than SK-N-BE(2), 54.5 nM and 330 nM, respectively (Table 24).

Table 24. IC50 values for selumetinib in neuroblastoma cell lines.

| Cell line | Molecular alteration | IC50 selumetinib (nM) |
|------------|----------------------|-----------------------|
| SK-N-BE(2) | NF1 copy number loss | 330 ± 55 |
| SK-N-AS | NRAS mut (Q61K) | 54.5 ± 15 |

Abbreviations: mut, mutated

Neuroblastoma cells were then treated with selumetinib combined with 4SC-205 (Figure 46A). We observed that the combination of 4SC-205 with selumetinib exerted additive anti-tumor effects in both neuroblastoma cell lines (Figure 46B-D).

Results

4SC-205 and selumetinib cooperate to reduce neuroblastoma growth

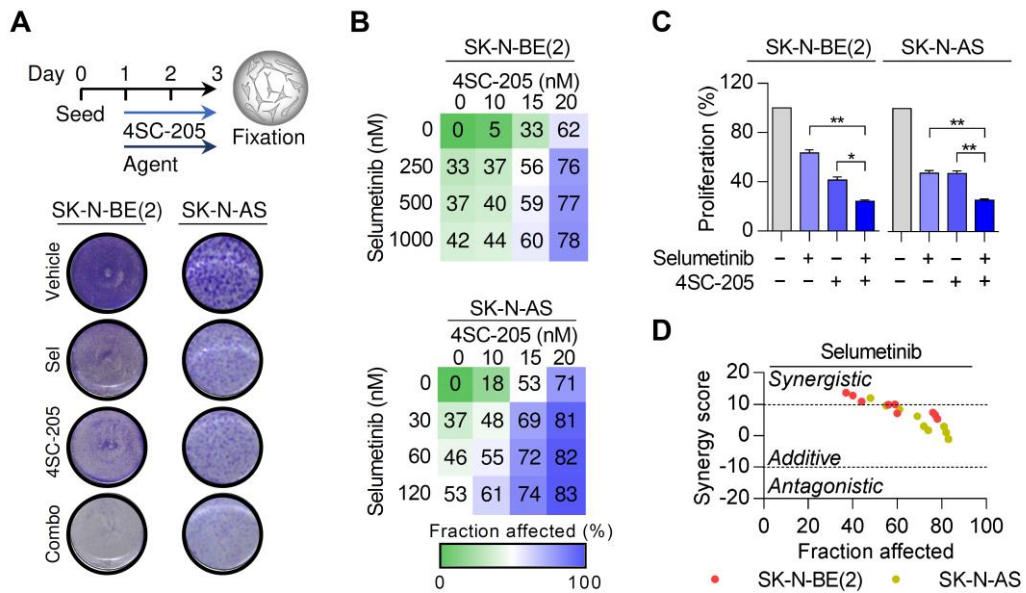


Figure 46. Combination of 4SC-205 and MEK1/2 inhibitors impairs neuroblastoma growth. (A) Schematic representation of the experimental design combining 4SC-205 and selumetinib. Representative images of crystal violet of SK-N-BE(2) and SK-N-AS treated with selumetinib, 4SC-205 or their combination. (B) Heatmaps showing the fraction of cells affected after the combination of 4SC-205 and selumetinib at the indicated concentrations for 48 hours. (C) Graph representing the average percentage of cell proliferation ($n = 2/\text{condition}$) \pm SEM from crystal violet staining. * $P < 0.05$, ** $P < 0.01$, two tailed Student's t-test. (D) Combinatorial analysis performed using SynergyFinder tool (version 2.0).

DISCUSSION



5. Discussion

5.1. Clinical challenges in the management of high-risk neuroblastomas

Neuroblastoma is a highly heterogeneous rare malignancy, ranging from spontaneous regression to high-risk disease. Standard treatment of high-risk neuroblastoma patients consists in multimodal therapy which includes high doses of chemotherapy, surgical resection, and radiotherapy followed by biological and immunological treatments (91). Although around 80% of patients respond to induction chemotherapy (102), 10-20% will not achieve remission, and between 50% and 60% of patients who complete treatment will relapse (321). These relapsed tumors are significantly different from untreated malignancies due to the presence of acquired molecular and genetic aberrations induced or selected by prior therapies (322,323), and to date, there are no curative treatments for these patients (324,325). Therefore, better induction chemotherapy schedules are necessary to improve the initial response rates, and standard curative second-line therapies must be developed for refractory and relapsed disease. Thus, high-risk neuroblastoma clinical management remains a challenge for both oncologists and researchers.

Genome-wide sequencing studies have been conducted to find molecular alterations that lead to the identification of new therapeutic targets. However, the small number of recurrent somatic alterations found in neuroblastoma at diagnosis, limits these precision therapies to a small subset of patients (53). Thus, it is clinically necessary to find therapeutic agents that can work in a broader number of neuroblastoma patients. Mitotic spindle is a validated target for cancer therapy in some types of malignancies (326). For instance, in neuroblastoma, vincristine is used as a standard of care during the induction chemotherapy (104). Classic antimitotic drugs disrupt microtubule dynamics by stabilizing or destabilizing tubulin polymers (95). Microtubules are dynamic structural components involved in several cellular processes, such as cell shape, intracellular trafficking, motility and generating mitotic spindle (327). Hinder microtubule dynamics not only induces cell death in proliferating cells, but also affects other cellular processes leading to severe side effects, such as peripheral neuropathy, which is frequent in patients treated regularly with these drugs (328). For this reason,

Discussion

development of mitotic-specific inhibitors has been thought to be a valid strategy to overcome dose-limiting toxicities.

In this present work, we propose KIF11 as a therapeutic target for high-risk neuroblastoma due to: (i) its key role in the mitotic spindle assembly (329), and (ii) the possibility to use the 4SC-205 inhibitor, a KIF11-inhibiting drug that can be orally administered (NCT01065025). Even though KIF11 mRNA expression has recently been reported to be upregulated in high-risk neuroblastoma (252), no data regarding the status of KIF11 protein expression has been published yet in this disease. In this line, we found that KIF11 expression levels, both mRNA and protein, were consistently upregulated in the high-risk neuroblastoma group. Loss-of-function approaches using siRNA, shRNA and 4SC-205 demonstrated that KIF11 was an attractive therapeutic target for this particular malignancy. We also examined the efficacy of 4SC-205 in multiple high-risk neuroblastoma models, including subcutaneous xenografts, a PDOX, and a mouse model for metastatic disease. Our findings validated that 4SC-205 impaired primary and metastatic neuroblastoma growth *in vivo*. Moreover, our research also revealed that KIF11 inhibition using 4SC-205 cooperated with standard of care chemotherapy (i.e. cisplatin, topotecan and doxorubicin) and targeted anticancer agents (ALK and MEK1/2 inhibitors) that are currently being tested in neuroblastoma patients (e.g. NCT03213691, NCT03107988 and NCT02559778).

5.2. KIF11 as a potential prognostic biomarker of survival

KIF11 has been reported to harbor heterozygous truncation mutations in familial exudative vitreoretinopathy, a rare hereditary disease that cause blindness (330,331), and microcephaly associated with congenital lymphedema and chorioretinopathy (332,333). In cancer, even though the specific role of KIF11 has not been fully characterized, several studies showed that KIF11 was upregulated in several adult malignancies compared to healthy tissues, and high expression levels correlated with poor survival rates in certain tumors. For instance, in breast cancer, KIF11 was upregulated in nearly all breast cancer biopsies, and multivariate analysis showed that KIF11 expression could be an independent prognostic marker for the survival of these patients (245,246). In hepatocellular carcinoma, Li and colleagues described

that the upregulation of eight kinesins, including KIF11, was significantly associated with the tumor stage, pathological tumor grade, and shorter overall survival. KIF11 expression was also found to be increased in hepatocellular carcinoma compared to normal liver tissues (247). In oral cancer, KIF11 was expressed in 65% of oral cancer tissues but not in healthy oral epithelia. Moreover, the authors showed that KIF11 expression correlated with poor outcome and could be an independent biomarker for survival (248). Additionally, KIF11 was found to be upregulated compared to healthy tissue in malignant pleural mesothelioma (249), glioblastoma (254), gallbladder (257), and pancreatic cancer (261).

Accordingly, here we demonstrated that KIF11 is widely expressed in neuroblastoma, and high mRNA and protein expression levels correlated with high-risk clinical stage and poor survival. Furthermore, we reported that KIF11 was significantly upregulated in patients with unfavorable features, including SCA (i.e. 1p36, 11q LOH and gain 17q23), and *MYCN* amplification, linked to tumor progression and chemoresistance (18,42). Our results evidenced that KIF11 expression, both at mRNA and protein levels, could be an independent biomarker of survival in neuroblastoma, a fact that could be particularly relevant to predict the prognosis of patients within the already low/intermediate- or within high-risk groups.

All these findings indicated that KIF11 upregulation could be required for cancer cell proliferation, and its overexpression might cooperate in developing a more aggressive malignancy. An important issue will be to determine whether KIF11 expression can distinguish between neuroblastoma patients that do not relapse and those who eventually relapse and become resistant to additional therapies. Interestingly, data mining using R2 visualization platform revealed that tumors from relapsed patients presented higher levels of KIF11 mRNA (Figure 47). Nevertheless, additional studies have to be performed to elucidate if KIF11 upregulation in those tumors occurred due to a role of this protein in neuroblastoma aggressiveness or was a mere consequence of its overexpression in high-risk disease.

Discussion

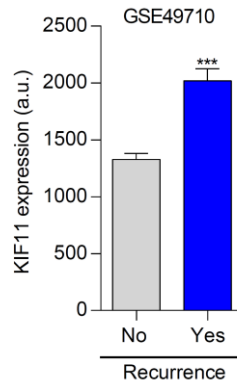


Figure 47. High expression of KIF11 correlates with neuroblastoma patient recurrence. KIF11 expression in neuroblastoma patients who did not relapse compared with patients who relapse (n = 498). *** $P < 0.001$.

5.3. Why is KIF11 more expressed in high-risk neuroblastoma?

Our data determined KIF11 as an independent prognostic marker for high-risk disease. In this context, a question remains to be elucidated: Why is KIF11 more expressed in patients with high-risk neuroblastoma? We still do not know if the consistent KIF11 overexpression is due to its role in tumorigenesis or is a consequence of the higher proliferation rate of these tumors.

There are multiple studies supporting that KIF11 overexpression could contribute to tumorigenesis in distinct cell types. For instance, Castillo and colleagues reported that a transgenic mice model overexpressing Kif11 under control of Pim1 promoter generated a broad spectrum of tumors with genetic instability and aneuploidy (244). Specifically, 24% (41/170) of these mice generated hematologic or solid malignancies. These results suggested that the aberrant expression of KIF11 led to cancer malignant transformation in multiple cell types. The authors did not report any case of neuroblastoma, which indicated that (i) KIF11 by itself may not be a main driver oncogene in this particular neoplasm or (ii) that Pim1 promoter might not induce sufficient Kif11 overexpression in neural crest cells to induce tumorigenesis in this specific cell type. Genetically engineered mouse models that overexpress Kif11 under tyrosine hydroxylase promoter would elucidate whether Kif11 aberrant expression is sufficient to drive neuroblastoma onset.

KIF11 is located on the long arm of chromosome 10 (10q23.33). Even though SCA and genetic amplifications are frequent in neuroblastoma (334), no 10q23 gains or *KIF11* amplifications have been described in this malignancy, suggesting that 10q23 genomic alterations are not the cause of *KIF11* increased expression in high-risk neuroblastoma. In the same line, according to cBioportal for Cancer Genomics (<http://www.cbioportal.org/>), among 240 neuroblastoma patients, no mutations were detected in *KIF11*. Thus, we suggest that other mechanisms of regulation may explain *KIF11* overexpression rather than genomic amplifications or mutations.

Another mechanism that might lead to *KIF11* overexpression could be a defective degradation of the protein. *KIF11* is degraded by the APC/C-CDH1 complex (233), which has been described to act as a tumor suppressor (335,336). Unfortunately, no data regarding APC/C-CDH1 activity in neuroblastoma has been published yet.

Another option would be to investigate which transcription factors could bind to *KIF11* promoter and contribute to its overexpression in high-risk neuroblastoma. Transcription factors are transcriptional regulators whose aberrant activation and/or expression can lead to deregulation of their target genes (337). *MYCN* is a transcription factor that promote cell growth and proliferation. About 20% of all neuroblastoma patients present *MYCN* amplification (> 10 copies), and its amplification is one of the most important markers associated with poor outcome (4,19,50). We found a positive correlation between *KIF11* and *MYCN* mRNA levels. Additionally, tumors with *MYCN* amplification presented increased *KIF11* mRNA levels compared to *MYCN* non-amplified neuroblastomas. Of note, Murphy and colleagues showed using CHIP-on-chip analyses that *MYCN* binds to the promoter of *KIF11* in Tet21N neuroblastoma cells (297). All these findings suggested that *MYCN* could regulate *KIF11* expression in neuroblastoma. When we analyzed *KIF11* protein expression in Tet21N cell line, we found that *KIF11* mRNA and protein were downregulated after *MYCN* silencing. However, we did not observe any clear association between *KIF11* and *MYCN* protein levels in a panel of nine neuroblastoma cell lines, and when *MYCN* was silenced or overexpressed in other neuroblastoma cell lines, *KIF11* protein levels remained unaltered. These results suggested that even though *KIF11* may be regulated by *MYCN*,

Discussion

other transcription factors might be more relevant to control KIF11 expression in neuroblastoma.

To date, only AP-1 transcription factor, an heterodimer composed by the Jun, Fos and ATF protein families, has been described to regulate KIF11 (338). To evaluate if AP-1 could be controlling KIF11 in neuroblastoma, we carried out an *in silico* analysis using the R2 visualization platform to correlate the expression of KIF11 and members of Jun, Fos and ATF protein families. We did not find any positive correlation between KIF11 and these proteins (Table 25). These evidences suggested that the AP-1 complex may not regulate KIF11 in this particular tumor.

Table 25. *In silico* correlation analysis between the expression of KIF11 and the AP-1 complex subunits.

| Transcription factor | GSE45547 (n = 649) | | GSE62564 (n = 498) | |
|----------------------|-----------------------------|---------|-----------------------------|---------|
| | Correlation coefficient (R) | P value | Correlation coefficient (R) | P value |
| c-Jun | -0.301 | 4.5E-15 | -0.051 | 0.260 |
| JunD | -0.198 | 3.7E-07 | -0.228 | 2.7E-07 |
| JunB | -0.413 | 4.2E-28 | -0.004 | 0.927 |
| c-Fos | -0.333 | 3.1E-18 | -0.208 | 2.7E-06 |
| FosB | -0.301 | 4.2E-15 | -0.203 | 4.9E-06 |
| Fra-1 | -0.018 | 0.64 | 0.143 | 1.4E-03 |
| Fra-2 | -0.285 | 1.3E-13 | -0.102 | 0.023 |
| ATF2 | 0.039 | 0.32 | 0.184 | 3.6E-05 |
| ATF3 | -0.375 | 3.7E-23 | 0.198 | 8.2E-06 |
| ATF4 | -0.119 | 2.4E-03 | 0.171 | 1.2E-04 |
| B-ATF | -0.296 | 1.3E-14 | -0.18 | 5.4E-05 |

To identify transcription factors that induce KIF11 overexpression in neuroblastoma, we carried out an *in silico* analysis correlating KIF11 expression with 720 proteins with transcriptional regulation activity through the R2 visualization platform. Interestingly, FOXM1, MYBL2 and E2Fs were the transcription factors with higher Pearson's correlation coefficient with KIF11. All of them are related to oncogenesis (Table 26).

Table 26. *In silico* correlation analysis between the expression of KIF11 and 720 transcription factors. Only transcription factors with positive correlation are listed in the table.

| Gene | GSE45547 (n = 649) | | GSE62564 (n = 498) | |
|---------------|-----------------------------|-----------|-----------------------------|-----------|
| | Correlation coefficient (R) | P value | Correlation coefficient (R) | P value |
| <i>FOXM1</i> | 0.843 | 1.57E-173 | 0.927 | 1.21E-210 |
| <i>E2F7</i> | 0.829 | 3.02E-163 | 0.832 | 6.39E-127 |
| <i>E2F8</i> | 0.821 | 2.57E+157 | 0.857 | 6.54E-143 |
| <i>MYBL2</i> | 0.79 | 1.91E-137 | 0.91 | 3.80E-189 |
| <i>E2F1</i> | 0.773 | 5.42E-128 | 0.899 | 9.01E-178 |
| <i>ZNF93</i> | 0.767 | 1.31E-124 | 0.743 | 1.04E-96 |
| <i>E2F2</i> | 0.764 | 1.89E-123 | 0.837 | 7.16E-130 |
| <i>TCF19</i> | 0.744 | 1.37E-113 | 0.783 | 2.08E-102 |
| <i>E2F3</i> | 0.679 | 4.37E-87 | 0.735 | 8.78E-84 |
| <i>ZNF367</i> | 0.661 | 6.05E-81 | 0.887 | 3.71E-166 |

FOXM1 is a transcriptional regulator essential for cell proliferation and cell cycle progression through the activation of several genes involved in mitosis (339). FOXM1 was found to be overexpressed in most human cancers, and it is a promising molecular target for cancer therapy (340), including neuroblastoma (341). Interestingly, Thiru and colleagues reported that cell division genes are usually coordinately regulated as part of a general activation of the cell division program that seems to occur downstream of FOXM1 (342). These results suggested that KIF11 might be a member of a large cluster of mitotic proteins regulated by FOXM1 and/or other transcription factors involved in mitosis. In this line, chromatin immunoprecipitation followed by sequencing (ChIP-seq) to study the chromatin binding profile of FOXM1 revealed its interaction in genes involved in controlling late cell cycle events in G2/M phases (343,344). Coordinated expression of mitotic genes suggests that KIF11 overexpression itself is unlikely to activate the cell division program and induce genomic instability in malignant cells. Supporting these results, Carter and colleagues described a signature of cell cycle genes whose overexpression predicted poor clinical outcome in various cancer types (345). In this line, we found that 13 of the 16 previously described mitotic kinesins (175), such as KIF11, KIF20A, CENPE, KIF18A, were significantly more expressed in high-risk than low- and intermediate-risk neuroblastoma (Table 27). Thus, mitotic genes, including kinesins, seem to be frequently upregulated together in human cancer as a result of malignant transformation.

Discussion

Table 27. Fold change of the expression of mitotic kinesins in high-risk vs. low- and intermediate-risk neuroblastoma patients. The analysis was assessed using SEQC498 dataset (GSE62564; n = 498).

| Gene symbol | Family | Fold change (high-risk vs. low- and intermediate-risk neuroblastoma) | P value |
|---------------|--------|--|----------|
| <i>KIF4A</i> | 4 | 2.25 | 5.37E-47 |
| <i>CENP-E</i> | 7 | 2.24 | 4.88E-33 |
| <i>KIF18A</i> | 8 | 2.20 | 1.09E-43 |
| <i>KIF15</i> | 12 | 2.19 | 5.97E-31 |
| <i>KIF4B</i> | 4 | 2.18 | 5.91E-42 |
| <i>KIF20A</i> | 6 | 2.04 | 1.60E-32 |
| <i>KIF18B</i> | 8 | 1.94 | 2.69E-24 |
| <i>KIF11</i> | 5 | 1.92 | 2.36E-27 |
| <i>KIFC1</i> | 14A | 1.83 | 3.78E-24 |
| <i>KIF23</i> | 6 | 1.82 | 4.97E-28 |
| <i>KIF14</i> | 3 | 1.72 | 5.20E-21 |
| <i>KIF2C</i> | 13 | 1.60 | 5.15E-15 |
| <i>KIF22</i> | 10 | 1.50 | 5.85E-31 |
| <i>KIF20B</i> | 6 | 1.49 | 9.21E-18 |
| <i>KIF2A</i> | 13 | -1.06 | 2.70E-02 |
| <i>KIF2B</i> | 13 | - | - |

Overall, it is unlikely that KIF11 deregulation itself induce neuroblastoma tumorigenesis. However, coordinated overexpression of KIF11 together with other cell division components may be necessary to maintain the cell division program and induce genomic instability in this particular tumor.

5.4. Targeting KIF11: exploring mitotic arrest and apoptotic cell death

Several studies have investigated the therapeutic potential of KIF11 inhibition in multiple types of human cancer. Overall, results indicate that KIF11 inhibition halts cell cycle progression in mitosis, and subsequently, induces apoptosis through the activation of executioner caspases (e.g. CASP3) (346). In this line, a study recently published in Science Translational Medicine by Hansson and colleagues, showed that neuroblastoma cells treated with filanesib stopped proliferating and died through this particular mechanism (252). Our results are consistent with these previous findings. KIF11 loss-of-function experiments using both genetic (i.e. siRNA and shRNA) and pharmacological tools (4SC-205) indicated that

neuroblastoma cells are highly sensitive to KIF11 depletion, and strengthened the essential role of KIF11 in neuroblastoma proliferation.

In this thesis, we provided a complete preclinical characterization of the KIF11 inhibitor 4SC-205. We observed that neuroblastoma cells treated with 4SC-205 displayed the morphological features expected for KIF11 loss of function, i.e., incapacity of forming bipolar spindles. Moreover, we reported that 4SC-205 caused G2/M cell cycle arrest, which subsequently induced accumulation of CCNB1, an essential cyclin to initiate and sustain mitosis and also for inhibiting mitotic exit (347), and increased histone H3 phosphorylation at serine 10, a serine residue phosphorylated during mitosis (348). Interestingly, neuroblastoma cells treated with 4SC-205 displayed high KIF11 protein levels. That could be explained by the fact that KIF11 is regulated during cell cycle being more expressed in mitosis and being degraded by APC/C-CDH1 during mitotic exit (233). These results confirmed the high KIF11 specificity of 4SC-205.

It has been described that the death of cells arrested in mitosis is generally mediated by the caspase-dependent apoptotic pathway controlled by BCL-2 family proteins (349-351). This family is divided into three groups based on their function (i) anti-apoptotic proteins, including BCL-2, BCL-xL and Mcl-1, (ii) pro-apoptotic pore-formers proteins, such as BAK and BAX, and (iii) pro-apoptotic BH3 proteins, e.g. NOXA and PUMA. The BCL-2 family members mediate apoptosis by direct binding interactions that control mitochondrial outer membrane permeabilization (MOMP) which results in caspase activation and apoptosis. The affinities and the relative abundance of these proteins dictate the prevalent interactions between anti-apoptotic and pro-apoptotic BCL-2 family members that control MOMP (352). In cells arrested in mitosis, the CDK1-CCNB1 complex mediates BCL-2 and BCL-xL phosphorylation, which does not affect protein levels but could prevent their association with the pro-apoptotic BCL-2 family members, such as BAX (353). Moreover, phosphorylation of Mcl-1 during mitosis by CDK1 and other kinases leads to Mcl-1 degradation which enables the release of pro-apoptotic proteins, such as BAK, and thus promotes apoptosis (354-356). Of note, it has been reported that NOXA accumulates in G2 phase, and binds to Mcl-1 during mitosis triggering co-degradation of both proteins (351). Interestingly, we found that

Discussion

KIF11 inhibition using 4SC-205 resulted in Mcl-1 and NOXA degradation, and no changes in BCL-2 and BCL-xL protein expression were observed upon KIF11 inhibition (Figure 48 and 49). Collectively, our data suggested that KIF11 loss-of-function using 4SC-205 led to cell cycle arrest in mitosis, and a subsequent cell death induced by the inhibition and degradation of the anti-apoptotic BCL-2 family protein Mcl-1. However, as the particular mechanism that induce mitotic cell death is still controversial (357), additional experiments should be performed to elucidate the exact mechanism that promote apoptosis in neuroblastoma cells arrested in mitosis.

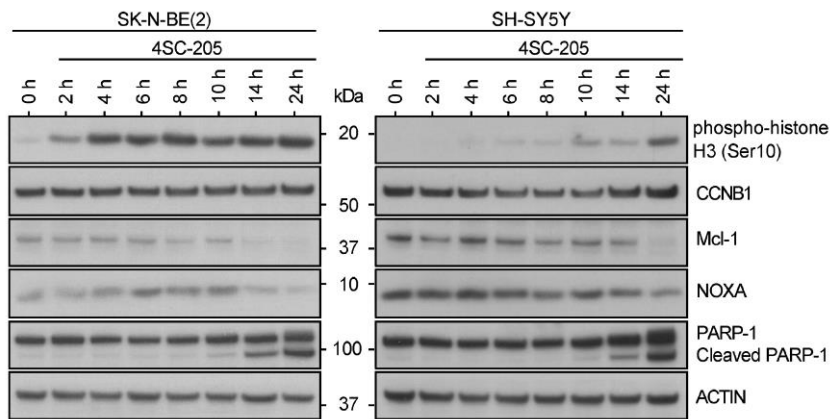


Figure 48. KIF11 inhibition results in Mcl-1 and NOXA degradation. SK-N-BE(2) and SH-SY5Y were treated with 4SC-205 at 25 nM and recollected at the indicated time points for western blot analysis.

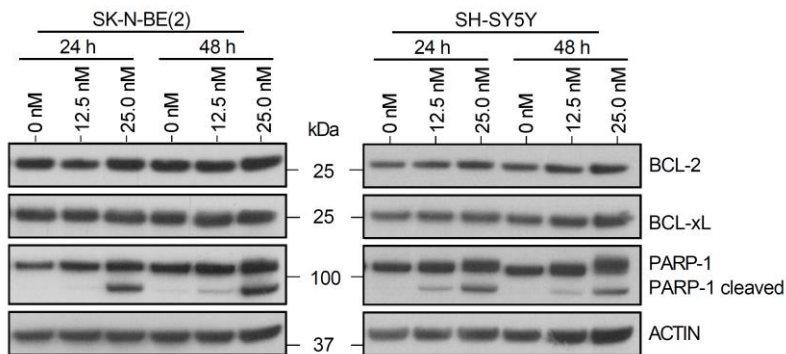


Figure 49. KIF11 inhibition does not reduce BCL-2 and BCL-xL protein levels. SK-N-BE(2) and SH-SY5Y were treated with the indicated concentrations of 4SC-205 for 24 and 48 hours and recollected for western blot analysis.

5.5. 4SC-205 is a candidate therapeutic agent for high-risk neuroblastoma

KIF11 inhibition using different pharmacological agents has been evaluated in multiple preclinical models representing different malignancies. For instance, filanesib showed to be effective in preclinical studies of hematologic malignancies (358,359) and solid malignancies (360), including neuroblastoma (252). Similarly, ispinesib demonstrated efficacy in several preclinical studies in solid adult malignancies such as breast cancer (361), glioblastoma (254,362), and in a panel of diverse pediatric hematologic and solid malignancies (363).

In this study, 4SC-205 has shown significant antitumor activity in different preclinical models of neuroblastoma, supporting its potential for therapeutic intervention in high-risk disease. *In vitro*, 4SC-205 presented a broad antiproliferative effect in a panel of 7 neuroblastoma cell lines with distinct genetic alterations. The *in vitro* activity profile of 4SC-205 was characterized by nanomolar concentration range IC₅₀ values for all cell lines. Interestingly, 4SC-205 exhibited no apparent specificity for *MYCN* and *TP53* status. *In vivo*, we tested this inhibitor in different types of tumor xenograft mouse models, including a PDOX and a metastatic mouse model. 4SC-205 proved to be effective in subcutaneous xenografts from SK-N-BE(2) and SK-N-AS cell lines, both of them derived from high-risk neuroblastoma. Moreover, we evaluated 4SC-205 efficacy in a PDOX derived from a very high-risk neuroblastoma patient who did not respond to the standard of care. In line with the subcutaneous xenografts, mice treated with 4SC-205 presented smaller tumors than vehicle-treated mice. Interestingly, we observed an increased ratio of cells with phosphorylation of histone H3 at serine 10, thereby suggesting that these tumors were still sensitive to 4SC-205 after 3 weeks of treatment. As most high-risk neuroblastomas display metastatic lesions at diagnosis, and metastases remains the main cause of the deaths of solid cancer patients (364), inhibition of metastatic growth is crucial to improving a person's chance of survival. For this reason, we tested 4SC-205 efficacy in mice with SK-N-BE(2) metastases. We observed that KIF11 inhibition using 4SC-205 resulted in metastases growth attenuation and extended survival of the animals. In conclusion, 4SC-205 was effective in diverse preclinical xenograft models, including tumors with *MYCN* amplification (SK-N-BE(2) and VH-NB608 PDOX), 11q LOH (SK-N-AS), *ALK* activating mutations (VH-NB608 PDOX), and *TP53* mutations (SK-N-BE(2) and SK-

Discussion

N-AS), suggesting that it might be useful in the treatment of a broad range of high-risk neuroblastomas.

One of the major concerns of cancer survivors is the long term side effects derived from cancer treatment. Standard therapeutic strategies and salvage treatments for high-risk neuroblastoma are based on high doses of chemotherapeutic agents and radiotherapy. Although these regimens have led to a significant improvement in survival and relapse rates, almost all patients experience treatment-associated acute side effects, including chemotherapy-induced renal dysfunction, pain and impaired growth. Furthermore, serious late side effects, such as hearing loss, hypothyroidism and an increased risk of developing a second neoplasm, are common in these children (160). The vast majority of side effects are derived from the mechanism of action of the chemotherapeutic agents and radiotherapy. Radiation and most chemotherapy disrupt DNA strings, which cause cell cycle arrest and the activation of the DNA damage response machinery. Cell death is ultimately activated with the aim of eliminating irreversibly damaged cells (365). Standard chemotherapy and radiotherapy not only target rapidly dividing cancer cells but also certain healthy tissues. Mutations and chromosome aberrations in normal cells can lead to the development of second neoplasms (366-368). Therefore, alternative therapies safer than standard chemotherapy and radiotherapy are necessary for these children.

At this point, a question regarding the safety of KIF11 inhibitors remains to be elucidated: Are KIF11 inhibitors safer than conventional chemotherapy and radiotherapy? Conventional anti-tubulin agents and antimetabolic inhibitors display a similar mechanism of action to induce mitotic arrest and a subsequent cell death *in vitro* (369). However, microtubule poisons have limitations, including innate or acquired resistance and dose-limiting neurotoxicity derived from interfering with the axonal integrity and transport (328,370). For this reason, inhibition of proteins specifically involved in mitosis, such as KIF11, without affecting other cellular processes has been thought to (i) improve response rates, and (ii) avoid acute and late side effects derived from the toxicity of these drugs in non-proliferating tissues.

In this study we reported that differentiated SH-SY5Y remained unaltered after KIF11 inhibition, whereas only ~10% of undifferentiated SH-SY5Y cells were alive after 48 hours

at the same dose. Therefore, 4SC-205 seemed to be specifically effective in neuroblastoma proliferating cells rather than in differentiated cells. Nevertheless, we should take into account that certain healthy tissues, such as bone marrow and gut, display higher proliferation rates than most tumors, and KIF11 inhibition is likely to cause mitotic arrest and cell death in these particular tissues (371). In this line, Castillo and colleagues reported that KIF11 is fundamental for maintenance of embryogenesis (372). Therefore, KIF11 seems to be essential for cell cycle progression of most human cells, both malignant and non-malignant. For this reason, we cannot discard dose-limiting toxicities derived from those tissues with high proliferation rates. Clinical trials using distinct KIF11 inhibitors (e.g. filanesib, ispinesib and 4SC-205) showed that all of them are generally well-tolerated with no indications of neurotoxicity; however, side effects such as neutropenia, anemia, leukopenia, thrombocytopenia, fatigue, diarrhea, nausea and vomiting are frequent (373,374). Therefore, KIF11 inhibition seems to affect hematopoietic precursors inducing a decrease in the number of leukocytes, platelets and red blood cells, also common in patients treated with chemotherapy (375). Concerning second neoplasms derived from cytotoxic drugs, KIF11 inhibition using siRNA and monastrol has been described to increase chromosome instability in different cell lines (376). Chromosome instability is well-known for its contribution with oncogenesis and disease aggressiveness by enhancing tumor heterogeneity and clonal evolution, which ultimately facilitate tumor adaptation to stressful environments and cytotoxic anticancer drugs (377). Therefore, it would be interesting to carry out *in vivo* experiments to investigate if KIF11 inhibition using distinct pharmacological agents can lead to the development of second neoplasms caused by KIF11 loss of function. A positive aspect of 4SC-205 is that its continuous daily treatment might enable the administration of lower doses compared to other KIF11 inhibitors, and thereby reduce the main side effects of inhibiting KIF11 in healthy tissues.

5.6. Overcoming treatment resistance: combination therapies

5.6.1. Results of clinical trials of KIF11 inhibitors

Even though KIF11 inhibitors showed promising preclinical results with low nanomolar biochemical potency and tumor regression, clinical efficacy has been insufficient for most agents (184). More specifically, in the case of AZD4877 (378), in a phase I clinical study, only four out of the 22 patients (18%) with relapsed/refractory solid tumors and lymphoma presented stable disease, and no complete or partial responses were observed among these patients (379). In a phase II study of patients with advanced urothelial cancer, only one out of the 39 patients (2.6%) treated with AZD4877 achieved a partial objective response, and seven patients (18%) presented stable disease for more than eight weeks (271). In a phase I/II study of AZD4877 in patients with acute myeloid leukemia, no objective responses were observed in evaluable patients (380). In case of MK-0731 (381), although no objective tumor responses were achieved, four out of 28 patients (14%) with solid tumors treated with the maximum tolerated dose (MTD) presented disease stabilization for more than 5 months (382). Similar results were obtained in a phase I study of ARQ 621 (383) in patients with solid malignancies, where six out of 48 patients (12.5%) achieved disease stabilization for more than 4 months (384). In the case of LY2523355 (litronesib) (385), a phase I study showed that two out of 7 evaluable patients (28.6%) with advanced solid tumors achieved disease stabilization (386). In this line, seventeen out of 86 evaluable patients (20%) maintained stable disease for more than 6 cycles, and only two patients (2%) achieved partial response in a phase II study of LY2523355 in patients with advanced malignancies (387).

Ispinesib (SB-715992) has been extensively evaluated clinically in multiple tumor types showing good safety and tolerability profile. However, limited responses were achieved after administration of ispinesib, being stable disease the best response in most cases, including melanoma (35% of patients) (270), metastatic squamous cell carcinoma of the head and neck (25%) (388), hepatocellular carcinoma (47%) (389), renal cell cancer (30%) (390), pediatric solid tumors (12.5%) (391), and in distinct advanced solid tumors (30%) (392). In the case of breast cancer, the results were slightly better for ispinesib, as one out of 15 patients (6.7%)

achieved partial response and nine out of 15 (60%) showed stable disease lasting at least 42 days (373). Interestingly, ispinesib did not show neither objective responses nor stable disease in androgen-independent prostate cancer patients previously treated with taxanes (393). The authors suggested that the lack of efficacy of ispinesib was caused by the low mitotic index of primary prostate tumors and the poor levels of the KIF11 protein in these cancer. On the contrary, when ispinesib was combined with docetaxel, seven out of 24 patients (29%) (six of them with androgen-independent prostate cancer) showed stable disease lasting more than 18 weeks (394).

A phase I study using the inhibitor SB-743921 in patients with advanced solid tumors or relapsed/refractory lymphomas provided similar results. Six out of 41 patients (28.6%) had stable disease for over four cycles, and one patient (2.4%) with metastatic cholangiocarcinoma achieved partial response and remained in the study until disease progression after nearly 12 months (395). As neutropenia was detected as the only dose limiting toxicity, SB-74921 was combined with the granulocyte-colony stimulating factor (G-CSF) to stimulate the bone marrow, specifically the proliferation and differentiation of the neutrophilic granulocyte lineage. Interestingly, patients supported by G-CSF presented a MTD 50% higher than patients treated with SB-74921 alone, 9 mg/m² and 6 mg/m², respectively. In this clinical study, four out of 56 patients (7.1%) achieved partial response, 19 experienced stable disease (34%), and 33 had progressive disease (59%). These results showed that stimulation of bone marrow with G-CSF enabled the increase of the MTD of SB-74921, which ultimately increased the efficacy of this drug (396).

ALN-VSP is a lipid nanoparticle formulation of siRNA targeting KIF11 and VEGF. In a phase I trial in cancer patients with liver involvement, ALN-VSP was well tolerated and reached liver tumors and multiple metastases. Interestingly, one out of 37 evaluable patients achieved complete response. This particular patient presented an endometrial cancer with multiple hepatic and lymph node metastases. The complete regression was obtained after 40 doses. The patient remained in remission and completed the treatment after receiving 50 doses. Three additional patients achieved stable disease for at least 8 months (397). These results highlight the importance of testing combination therapies with the aim to potentiate

Discussion

the efficacy of each drug. Unfortunately, no further clinical studies of ALN-VSP have been performed to date.

Filanesib is a potent KIF11 inhibitor that showed promising results in multiple preclinical studies in distinct tumor types; specifically, partial or complete responses were reported in thirteen out of 16 xenograft models (81%). Of note, hematologic tumors were especially sensitive to the inhibitor with a 100% complete response in some models (359). Filanesib was eventually tested in multiple clinical studies, including solid and hematologic malignancies. Filanesib was first tested as monotherapy in a phase I study in patients with advanced or refractory myeloid leukemia. Of 34 evaluable patients, one (3%) achieved partial response, and 10 (28%) had stable disease (398). For solid malignancies, stable disease was the best response observed in seven out of 39 evaluable patients (18%) (374). On the other hand, a phase 2 clinical study of multiple myeloma patients showed encouraging results. Response rates (\geq partial response) were observed in 16% of patients treated with filanesib alone, and 15% in patients treated with filanesib in combination with dexamethasone, a steroid drug frequently used in the treatment of multiple myeloma (399). Interestingly, combination of filanesib with bortezomib, a proteasome inhibitor approved for patients with multiple myeloma, and dexamethasone, showed promising results in a phase I clinical study in multiple myeloma patients. Of 19 patients treated with ≥ 1.25 mg/m² of filanesib (days 1, 2, 15 and 16 of a 28-day cycle), and 1.3 mg/m² of bortezomib and 40 mg/m² of dexamethasone (days 1, 8 and 15), one patient (5%) achieved nearly complete response, four (21%) experienced very good partial responses, and 3 (16%) had partial response. Prophylactic G-CSF was incorporated to avoid hematologic toxicities (400). Similar results were obtained when filanesib was combined with the second generation proteasome inhibitor carfilzomib and dexamethasone. Five out of 63 patients (8%) with multiple myeloma achieved very good partial response, and eighteen (29%) experienced partial response (401). Importantly, the efficacy of filanesib was found to be better in patients with low levels of α -1 acidic glycoprotein (AAG), as they had superior response (overall response rate of 62% vs. 17%) and longer median progression-free survival (9 vs. 2 months) than patients with high AAG levels (> 800 mg/l) (402). Therefore, AAG levels in serum could be used as a biomarker

of response to filanesib, and specific selection of patients depending on AAG levels might increase filanesib response rates.

In the case of 4SC-205, a phase I clinical study involving 59 patients with advanced solid malignancies and malignant lymphomas refractory to prior standard therapies was performed. Patients were randomized in different cohorts and treated once weekly, twice weekly or daily with different doses of 4SC-205. Fifteen patients (25.4%) showed stable disease as their best response during the course of this study. Best response results were observed in the 20 mg continuous daily dosing group, with 4 out of 6 patients (66.7%) achieving stable disease, and in the 50 mg once-weekly dosing group with 3 out of 3 patients (100%). Interestingly, daily dosing scheme was better tolerated than the other treatment schedules, and 10 and 20 mg seemed to be the doses of the daily dosing regimen that were best tolerated (272,403). Importantly, prophylactic G-CSF could still be incorporated to increase the MTD of 4SC-205 in order to increase its efficacy.

5.6.2. Why excellent KIF11 inhibitors failed in clinical trials?

The proliferation rate paradox

Among all KIF11 inhibitors tested in clinical trials, filanesib showed the best results. This brings up an important question: why did filanesib work and the others did not? We know that the other compounds, i.e. ispinesib, AZD4877, LY2523355, SB-743921, ARQ 621, and MK-0731 were targeting KIF11 as they targeted normal cell proliferation inducing neutropenia. However, pharmacokinetics properties between these compounds were very distinct (Table 28). The elimination half-life of filanesib was more than 90 hours, whereas other compounds presented a half-life below 30 hours. Therefore, the longer half-life of filanesib compared to other KIF11 compounds might be one determining factor for the better efficacy of filanesib in clinical studies.

Discussion

Table 28. Pharmacokinetics properties and administration schedules of KIF11 inhibitors (modified from (184)).

| Inhibitor | Company | Maximal tolerated dose | Elimination half-lives | Administration schedule |
|-----------|-----------------|------------------------|------------------------|------------------------------------|
| Filanesib | Array BioPharma | 1.5 mg/m ² | > 90 h | 1, 2, 15, and 16 of a 28-day cycle |
| LY2523355 | Eli Lilly & Co. | 8 mg/m ² | 10-31 h | 1, 5 and 9 of a 21-day cycle |
| 4SC-205 | 4SC AG | 20 mg | 10 h | Daily |
| ALN-VSP02 | Alnylam | 1 mg/kg | 10 h | Two times weekly |
| Ispinesib | Cytokinetics | 18 mg/m ² | 16 h | Day 1 of each 21-day cycle |
| AZD4877 | AstraZeneca | 11 mg | 16 h | 1, 4, 8 and 11 of a 21-day cycle |
| SB-743921 | Cytokinetics | 4-6 mg/m ² | 29 h | Day 1 of each 21-day cycle |
| ARQ 621 | Merck & Co. | 280mg/m ² | - | Once weekly |
| MK-0731 | Merck & Co. | 16 mg/m ² | 6 h | Day 1 of each 21-day cycle |

Another key factor for the efficacy of KIF11 inhibitors might be the proliferation status of the tumor. It is known that most solid tumors, including the chemo-sensitive ones, have low proliferation rates. This phenomenon, which became known as the proliferation rate paradox (371), may be determinant for antimetabolic targeted drugs. Antimetabolic compounds, including KIF11 inhibitors, are only effective during mitosis and, therefore, have to be present long enough to be effective in patients with slow proliferating tumors. Specifically, the agent should remain in the tumor in sufficient concentration longer than the duration of the cell cycle in the particular tumor. Filanesib, with a half-life of more than 90 hours, seemed to accomplish that objective in some malignancies with high proliferation rates, i.e. multiple myeloma. Supporting this hypothesis, promising results were obtained with the continuous dosing schedule of 20 mg/daily of 4SC-205, where 67% of patients presented stable disease for more than 100 days (272). Therefore, continuous administration of antimetabolic drugs could overcome the proliferation rate paradox and improve the therapeutic index of these compounds.

Functional plasticity of mitotic kinesins to replace KIF11 function

There are 45 members of the kinesin superfamily, and at least 16 of them play important roles during mitosis (175). Among them, KIF11 is essential for spindle formation during mitosis through crosslinking antiparallel microtubules and providing the forces for centrosome separation. Another one, KIF15, was described to enable centrosome separation during bipolar spindle assembly (404). KIF15 was found to be able to change its normal

localization in the spindle microtubules and contribute to bipolar spindle formation during prometaphase (405). Raaijmaker and colleagues elegantly demonstrated that KIF15 could replace KIF11 activity during mitosis. The authors generated human cells that could grow in the complete absence of KIF11 activity (406). Surprisingly, they observed that KIF11-independent cells needed KIF15 in prometaphase but not in prophase, where nuclear envelope-associated dynein drove prophase centrosome separation. Therefore, combination of KIF11 and KIF15 inhibitors could be a promising therapeutic strategy to target rapidly proliferating cancer cells.

In the same line, KIF11 inhibition sensitivity could be related to the timing of centrosome separation. Mardin and colleagues described that epidermal growth factor (EGF) signaling stimulated early centrosome separation in S phase, which ultimately impaired mitotic arrest upon KIF11 inhibition (407). In this model, KIF11 was also not required in prometaphase, since KIF15 replaced KIF11 to drive spindle assembly.

Alterations of proteins that antagonize KIF11 function during prophase were found to confer resistance to mitotic arrest induced by KIF11 inhibition. CDK1 is the master regulator that drive and oppose centrosome separation to control the appropriate balance for correct chromosome alignment during prophase. Specifically, CDK1 stimulates KIF11 proper localization by phosphorylating its C-terminal. KIF11 phosphorylation induces its binding to microtubules, and drives centrosome separation. On the other hand, CDK1 also phosphorylates Tiam1 (S1466), which antagonize KIF11 function by activating Pak1/2. Whalley and colleagues reported that depletion of Pak1/2 enabled cells to evade monopolar arrest induced by KIF11 inhibition (408). Thus, the modulation of Tiam1-Pak axis might potentially confer resistance to KIF11 inhibitors. However, further studies of this pathway need to be performed to elucidate whether this modulation is one of the factors that confers resistance against KIF11 inhibitors.

KIF11 point mutations

Genomic instability, a feature of most tumors, might be one of the reasons for the lack of efficacy of KIF11 inhibitors. Genomic instability includes aneuploidy, chromosome rearrangements and mutations in nucleic acid sequences (409). Preexisting mutations within the L5 loop of *KIF11* in the tumor could lead to a reduction of affinity between the KIF11 inhibitor and the protein. In fact, amino acid changes in the binding pocket have been reported to induce resistance to monastrol, BRD9647, STLC, SB-743921, filanesib and ispinesib (reviewed in (184)). However, it is difficult to think that most tumors harbor preexisting specific mutations within the *KIF11* that result in resistance to KIF11-inhibiting agents. In fact, to find those particular mutations, most authors had to perform extensive mutagenesis analysis in the allosteric binding site (410,411) or clonal selection of tumor cells exposed to KIF11 inhibitors (412,413). Interestingly, Wacker and colleagues reported that only 4 out of 14 (28.5%) clones resistant to STLC harbored mutations within *KIF11* (413). In the same line, no clinically relevant *KIF11* mutations have been reported to date in any clinical trial testing KIF11-inhibiting agents. This data suggest that the proliferation rate paradox and the functional plasticity of KIF15 to replace KIF11 function might be more relevant for the lack of efficacy of KIF11 inhibitors than point mutations in *KIF11*.

5.6.3. Combination of KIF11 inhibitors with standard and targeted therapies

Drug resistance is one of the major problems in the oncology field. Even though most tumors initially go into remission, they frequently develop resistance, which results in disease relapse. It is well-known that malignant cells become resistant to anticancer agents by distinct mechanisms, such as suppression of cell death, altering the drug metabolism, epigenetic changes, mutations, among others (414). The initial solution to overcome cancer drug resistance against single-agent chemotherapy was the combination of multiple chemotherapeutic agents with distinct mechanism of action. Since then, complex schedules combining different chemotherapeutic drugs with radiotherapy and surgery have become the standard regimen for most malignancies (415). In fact, the standard therapy for high-risk neuroblastoma includes the combination of multiple chemotherapeutic agents (i.e. cisplatin, vincristine, carboplatin, etoposide, and cyclophosphamide).

Resistance to targeted monotherapy is very common, and is frequently derived from reactivation of the signaling pathway. For this reason, rational combinations of targeted therapies with chemotherapy or other targeted therapies need to be studied (416). In this line, some combination treatments using KIF11 inhibitors with chemotherapy and other targeted therapies have been tested in preclinical models. For example, Purcell and colleagues reported that ispinesib enhanced the antitumor activity of doxorubicin, trastuzumab (a monoclonal antibody that specifically target the human epidermal growth factor receptor 2 (HER2)) and lapatinib (which binds to the ATP-binding pocket of the EGFR/HER2) in breast cancer (361). Similarly, the KIF11 inhibitor SCH 2047069 was found to potentiate paclitaxel, gemcitabine, or vincristine antitumor activity in ovarian xenograft tumors (417). Our findings showed that 4SC-205 had a good combination profile with standard chemotherapeutic agents for high-risk neuroblastoma (i.e. cisplatin, doxorubicin and topotecan). Moreover, we demonstrated that the combination of 4SC-205 and topotecan efficiently induced complete regression of neuroblastoma liver and bone marrow metastases compared to single treatments. We additionally found that 4SC-205 enhanced the antitumoral activity of ALK and MEK1/2 inhibitors, which are currently being tested in clinical trials for relapsed neuroblastoma patients. Thus, the combination of 4SC-205 with distinct chemotherapeutic agents and targeted inhibitors could reduce the ability of cancer cells to develop resistance against each inhibitor as monotherapy and improve the results of clinical trials of KIF11 inhibitors performed to date.

5.7. Future directions: 4SC-205, from bench to bedside

In this thesis we provided a full molecular and functional characterization of the 4SC-205 compound. We also investigated the combination of this compound with standard chemotherapy and targeted therapies. In particular, we found that 4SC-205 potentiated the anti-tumor effects of both chemotherapy (i.e. cisplatin, topotecan and doxorubicin) and targeted therapies (i.e. ALK and MEK1/2 inhibitors) in multiple neuroblastoma cell lines *in vitro*, and we evaluated the efficacy of the combination of topotecan and 4SC-205 *in vivo*. Interestingly, the combination of both agents effectively induced complete tumor regression of liver and bone marrow metastases compared to each single treatment regimen. These

Discussion

results are particularly interesting as neuroblastoma bone marrow metastases are highly tumorigenic and are still difficult to remove with the standard therapies (418).

On the other hand, we still have to test the combination of 4SC-205 with ALK and MEK1/2 inhibitors *in vivo*. In order to conduct these experiments, we will select clinically representative models that harbor activating mutations in *ALK* (i.e. the PDOX VH-NB608) or alterations on the RAS/MAPK pathway (i.e. SK-N-BE(2) or SK-N-AS). The result that we would expect to obtain is a reduction of tumor growth of the primary and metastatic lesions in the combination group compared to the single treatment regimens.

We also would like to test 4SC-205 alone and in combination in a clinical trial of patients with relapsed or refractory high-risk neuroblastomas. First, we would have to determine the recommended dose and dosing schedule of 4SC-205 as single agent in pediatric patients. This clinical study would also assess the safety and antitumor activity of 4SC-205 in a small cohort of neuroblastoma patients. Considering previous clinical studies testing distinct KIF11 inhibitors, daily administration of 4SC-205 to ensure uninterrupted KIF11 inhibition could be the best strategy to overcome the proliferation rate paradox, and in the same time, increase the therapeutic index of KIF11 inhibition. If this first stage achieves positive results, such as partial objective clinical responses or consistent stable disease, we could start a second clinical study testing the safety and efficacy of the combination between 4SC-205 and other therapeutic agents (i.e. chemotherapy and/or targeted therapies).

CONCLUSIONS



6. Conclusions

First: KIF11 mRNA and protein expression are independent prognostic factors of survival in neuroblastoma.

Second: Proliferative neuroblastoma cells are sensitive to the genetic and pharmacological inhibition of KIF11.

Third: 4SC-205 is safe and effective in multiple *in vivo* primary and metastatic neuroblastoma models.

Fourth: 4SC-205 enhances the antitumor activity of neuroblastoma standard of care and targeted therapies.

REFERENCES



7. References

1. Steliarova-Foucher E, Fidler MM, Colombet M, Lacour B, Kaatsch P, Piñeros M, *et al.* Changing geographical patterns and trends in cancer incidence in children and adolescents in Europe, 1991-2010 (Automated Childhood Cancer Information System): a population-based study. *The Lancet Oncology* **2018**;19:1159-69
2. Kaatsch P. Epidemiology of childhood cancer. *Cancer treatment reviews* **2010**;36:277-85
3. Bethesda. 2021 22/06/2021. Rare Cancers of Childhood Treatment (PDQ®). DQ Cancer Information Summaries <www.ncbi.nlm.nih.gov/books/NBK65876/>. Accessed 2021 22/06/2021.
4. Maris JM. Recent advances in neuroblastoma. *The New England journal of medicine* **2010**;362:2202-11
5. London WB, Castleberry RP, Matthay KK, Look AT, Seeger RC, Shimada H, *et al.* Evidence for an age cutoff greater than 365 days for neuroblastoma risk group stratification in the Children's Oncology Group. *Journal of Clinical Oncology* **2005**;23:6459-65
6. Mossé YP, Deyell RJ, Berthold F, Nagakawara A, Ambros PF, Monclair T, *et al.* Neuroblastoma in older children, adolescents and young adults: a report from the International Neuroblastoma Risk Group project. *Pediatric blood & cancer* **2014**;61:627-35
7. Schilling F, Spix C, Berthold F, Erttmann R, Fehse N, Hero B, *et al.* Neuroblastoma screening at one year of age. *The New England journal of medicine* **2002**;346:1047-53
8. Gamazon ER, Pinto N, Konkashbaev A, Im HK, Diskin SJ, London WB, *et al.* Trans-population analysis of genetic mechanisms of ethnic disparities in neuroblastoma survival. *Journal of the National Cancer Institute* **2013**;105:302-9
9. Bluhm EC, Daniels J, Pollock BH, Olshan AF, Children's Oncology G. Maternal use of recreational drugs and neuroblastoma in offspring: a report from the Children's Oncology Group (United States). *Cancer causes & control : CCC* **2006**;17:663-9
10. Matthay KK, Maris JM, Schleiermacher G, Nakagawara A, Mackall CL, Diller L, *et al.* Neuroblastoma. *Nature reviews Disease primers* **2016**;2:16078
11. Spix C, Pastore G, Sankila R, Stiller CA, Steliarova-Foucher E. Neuroblastoma incidence and survival in European children (1978–1997): Report from the Automated Childhood Cancer Information System project. *European Journal of Cancer* **2006**;42:2081-91
12. Cheung NK, Dyer MA. Neuroblastoma: developmental biology, cancer genomics and immunotherapy. *Nature reviews Cancer* **2013**;13:397-411
13. Tomolonis JA, Agarwal S, Shohet JM. Neuroblastoma pathogenesis: deregulation of embryonic neural crest development. *Cell and tissue research* **2018**;372:245-62
14. Johnsen JI, Dyberg C, Wickström M. Neuroblastoma-A neural crest derived embryonal malignancy. *Frontiers in Molecular Neuroscience* **2019**;12:9
15. Stutterheim J, Gerritsen A, Zappeij-Kanngieter I, Kleijn I, Dee R, Hooft L, *et al.* PHOX2B is a novel and specific marker for minimal residual disease testing in neuroblastoma. *Journal of Clinical Oncology* **2008**;26:5443-9

References

16. Weiss WA, Aldape K, Mohapatra G, Feuerstein BG, Bishop JM. Targeted expression of MYCN causes neuroblastoma in transgenic mice. *EMBO J* **1997**;16:2985-95
17. Olsen RR, Otero JH, Garcia-Lopez J, Wallace K, Finkelstein D, Reh J, *et al.* MYCN induces neuroblastoma in primary neural crest cells. *Oncogene* **2017**;36:5075-82
18. Huang M, Weiss WA. Neuroblastoma and MYCN. *Cold Spring Harbor perspectives in medicine* **2013**;3:a014415
19. Brodeur GM, Seeger RC, Schwab M, Varmus HE, Bishop JM. Amplification of N-myc in untreated human neuroblastomas correlates with advanced disease stage. *Science* **1984**;224:1121-4
20. Marshall GM, Carter DR, Cheung BB, Liu T, Mateos MK, Meyerowitz JG, *et al.* The prenatal origins of cancer. *Nature reviews Cancer* **2014**;14:277-89
21. Mosse YP, Laudenslager M, Longo L, Cole KA, Wood A, Attiyeh EF, *et al.* Identification of ALK as a major familial neuroblastoma predisposition gene. *Nature* **2008**;455:930-5
22. Mosse YP, Laudenslager M, Khazi D, Carlisle AJ, Winter CL, Rappaport E, *et al.* Germline PHOX2B mutation in hereditary neuroblastoma. *American journal of human genetics* **2004**;75:727-30
23. Knudson AG, C Strong LC. Mutation and cancer: neuroblastoma and pheochromocytoma. *Am J Hum Genet* **1972**;24:514-32
24. Barr EK, Applebaum MA. Genetic Predisposition to Neuroblastoma. *Children* **2018**;5:119
25. Trochet D, Bourdeaut F, Janoueix-Lerosey I, Deville A, de Pontual L, Schleiermacher G, *et al.* Germline mutations of the paired-like homeobox 2B (PHOX2B) gene in neuroblastoma. *Am J Hum Genet* **2004**;74:761-4
26. Bourdeaut F, Trochet D, Janoueix-Lerosey I, Ribeiro A, Deville A, Coz C, *et al.* Germline mutations of the paired-like homeobox 2B (PHOX2B) gene in neuroblastoma. *Cancer letters* **2005**;228:51-8
27. Pattyn A, Morin X, Cremer H, Goridis C, Brunet JF. The homeobox gene Phox2b is essential for the development of autonomic neural crest derivatives. *Nature* **1999**;399:366-70
28. Croaker G, Shi E, Simpson E, Cartmill T, Cass D. Congenital central hypoventilation syndrome and Hirschsprung's disease. *Arch Dis Child* **1998**;78:316-22
29. Iwahara T, Fujimoto J, Wen D, Cupples R, Bucay N, Arakawa T, *et al.* Molecular characterization of ALK, a receptor tyrosine kinase expressed specifically in the nervous system. *Oncogene* **1997**;14:439-49
30. Janoueix-Lerosey I, Lequin D, Brugieres L, Ribeiro A, de Pontual L, Combaret V, *et al.* Somatic and germline activating mutations of the ALK kinase receptor in neuroblastoma. *Nature* **2008**;455:967-70
31. Chen Y, Takita J, Choi YL, Kato M, Ohira M, Sanada M, *et al.* Oncogenic mutations of ALK kinase in neuroblastoma. *Nature* **2008**;455:971-4
32. George RE, Sanda T, Hanna M, Frohling S, Luther W, 2nd, Zhang J, *et al.* Activating mutations in ALK provide a therapeutic target in neuroblastoma. *Nature* **2008**;455:975-8
33. Schuldt A. Motors to deliver the goods. *Nature Reviews Molecular Cell Biology* **2001**;2:489

34. Schlisio S, Kenchappa RS, Vredevelde LC, George RE, Stewart R, Greulich H, *et al.* The kinesin KIF1Bbeta acts downstream from EglN3 to induce apoptosis and is a potential 1p36 tumor suppressor. *Genes & development* **2008**;22:884-93
35. Dinsmore CJ, Soriano P. MAPK and PI3K signaling: At the crossroads of neural crest development. *Developmental biology* **2018**;444 Suppl 1:S79-S97
36. Kamihara J, Bourdeaut F, Foulkes WD, Molenaar JJ, Mosse YP, Nakagawara A, *et al.* Retinoblastoma and Neuroblastoma Predisposition and Surveillance. *Clinical cancer research* **2017**;23:e98-e106
37. Birch JM, Alston RD, McNally RJ, Evans DG, Kelsey AM, Harris M, *et al.* Relative frequency and morphology of cancers in carriers of germline TP53 mutations. *Oncogene* **2001**;20:4621-8
38. Diskin SJ, Capasso M, Diamond M, Oldridge DA, Conkrite K, Bosse KR, *et al.* Rare variants in TP53 and susceptibility to neuroblastoma. *Journal of the National Cancer Institute* **2014**;106:dju047
39. Maas SM, Vansenne F, Kadouch DJ, Ibrahim A, Bliet J, Hopman S, *et al.* Phenotype, cancer risk, and surveillance in Beckwith-Wiedemann syndrome depending on molecular genetic subgroups. *American journal of medical genetics Part A* **2016**;170:2248-60
40. Mussa A, Molinatto C, Baldassarre G, Riberi E, Russo S, Larizza L, *et al.* Cancer Risk in Beckwith-Wiedemann Syndrome: A Systematic Review and Meta-Analysis Outlining a Novel (Epi)Genotype Specific Histotype Targeted Screening Protocol. *The Journal of pediatrics* **2016**;176:142-9 e1
41. Manolio TA, Collins FS, Cox NJ, Goldstein DB, Hindorff LA, Hunter DJ, *et al.* Finding the missing heritability of complex diseases. *Nature* **2009**;461:747-53
42. Janoueix-Lerosey I, Schleiermacher G, Michels E, Mosseri V, Ribeiro A, Lequin D, *et al.* Overall genomic pattern is a predictor of outcome in neuroblastoma. *Journal of Clinical Oncology* **2009**;27:1026-33
43. Attiyeh EF, London WB, Mossé YP, Wang Q, Winter C, Khazi D, *et al.* Chromosome 1p and 11q deletions and outcome in neuroblastoma. *The New England journal of medicine* **2005**;353:2243-53
44. Bown N, Cotterill S, Lastowska M, O'Neill S, Pearson AD, Plantaz D, *et al.* Gain of chromosome arm 17q and adverse outcome in patients with neuroblastoma. *The New England journal of medicine* **1999**;340:1954-61
45. Carén H, Kryh H, Nethander M, Sjoberg RM, Trager C, Nilsson S, *et al.* High-risk neuroblastoma tumors with 11q-deletion display a poor prognostic, chromosome instability phenotype with later onset. *Proc Natl Acad Sci U S A* **2010**;107:4323-8
46. Mlakar V, Jurkovic Mlakar S, Lopez G, Maris JM, Ansari M, Gumy-Pause F. 11q deletion in neuroblastoma: a review of biological and clinical implications. *Molecular cancer* **2017**;16:114
47. Henrich KO, Schwab M, Westermann F. 1p36 tumor suppression-a matter of dosage? *Cancer research* **2012**;72:6079-88
48. Mandriota SJ, Valentijn LJ, Lesne L, Betts DR, Marino D, Boudal-Khoshbeen M, *et al.* Ataxia-telangiectasia mutated (ATM) silencing promotes neuroblastoma progression through a MYCN independent mechanism. *Oncotarget* **2015**;6:18558-76

References

49. Ruiz-Perez MV, Henley AB, Arsenian-Henriksson M. The MYCN protein in health and disease. *Genes* **2017**;8:113
50. Cohn SL, Pearson AD, London WB, Monclair T, Ambros PF, Brodeur GM, *et al.* The International Neuroblastoma Risk Group (INRG) classification system: an INRG Task Force report. *Journal of Clinical Oncology* **2009**;27:289-97
51. Schulte JH, Bachmann HS, Brockmeyer B, Depreter K, Oberthur A, Ackermann S, *et al.* High ALK receptor tyrosine kinase expression supersedes ALK mutation as a determining factor of an unfavorable phenotype in primary neuroblastoma. *Clinical cancer research* **2011**;17:5082-92
52. Berry T, Luther W, Bhatnagar N, Jamin Y, Poon E, Sanda T, *et al.* The ALK(F1174L) mutation potentiates the oncogenic activity of MYCN in neuroblastoma. *Cancer cell* **2012**;22:117-30
53. Pugh TJ, Morozova O, Attiyeh EF, Asgharzadeh S, Wei JS, Auclair D, *et al.* The genetic landscape of high-risk neuroblastoma. *Nature genetics* **2013**;45:279-84
54. Heaphy CM, de Wilde RF, Jiao Y, Klein AP, Edil BH, Shi C, *et al.* Altered Telomeres in Tumors with ATRX and DAXX Mutations. *Science* **2011**;333:425
55. Valentijn LJ, Koster J, Zwijnenburg DA, Hasselt NE, van Sluis P, Volckmann R, *et al.* TERT rearrangements are frequent in neuroblastoma and identify aggressive tumors. *Nature genetics* **2015**;47:1411-4
56. Cheung NK, Cheung IY, Kushner BH, Ostrovskaya I, Chamberlain E, Kramer K, *et al.* Murine anti-GD2 monoclonal antibody 3F8 combined with granulocyte-macrophage colony-stimulating factor and 13-cis-retinoic acid in high-risk patients with stage 4 neuroblastoma in first remission. *Journal of Clinical Oncology* **2012**;30:3264-70
57. Peifer M, Hertwig F, Roels F, Dreidax D, Gartlgruber M, Menon R, *et al.* Telomerase activation by genomic rearrangements in high-risk neuroblastoma. *Nature* **2015**;526:700-4
58. Sausen M, Leary RJ, Jones S, Wu J, Reynolds CP, Liu X, *et al.* Integrated genomic analyses identify ARID1A and ARID1B alterations in the childhood cancer neuroblastoma. *Nature genetics* **2013**;45:12-7
59. Mayr F, Heinemann U. Mechanisms of Lin28-mediated miRNA and mRNA regulation—a structural and functional perspective. *Int J Mol Sci* **2013**;14:16532-53
60. Diskin SJ, Capasso M, Schnepf RW, Cole KA, Attiyeh EF, Hou C, *et al.* Common variation at 6q16 within HACE1 and LIN28B influences susceptibility to neuroblastoma. *Nature genetics* **2012**;44:1126-30
61. Molenaar JJ, Domingo-Fernández R, Ebus ME, Lindner S, Koster J, Drabek K, *et al.* LIN28B induces neuroblastoma and enhances MYCN levels via let-7 suppression. *Nature genetics* **2012**;44:1199-206
62. Powers JT, Tsanov KM, Pearson DS, Roels F, Spina CS, Ebright R, *et al.* Multiple mechanisms disrupt the let-7 microRNA family in neuroblastoma. *Nature* **2016**;535:246-51
63. Corallo D, Donadon M, Pantile M, Sidarovich V, Cocchi S, Ori M, *et al.* LIN28B increases neural crest cell migration and leads to transformation of trunk sympathoadrenal precursors. *Cell Death & Differentiation* **2019**;27:1225-42

64. Tao T, Shi H, Mariani L, Abraham BJ, Durbin AD, Zimmerman MW, *et al.* LIN28B regulates transcription and potentiates MYCN-induced neuroblastoma through binding to ZNF143 at target gene promoters. *Proc Natl Acad Sci U S A* **2020**;117:16516-26
65. Schnepf RW, Khurana P, Attiyeh EF, Raman P, Chodosh SE, Oldridge DA, *et al.* A LIN28B-RAN-AURKA signaling network promotes neuroblastoma tumorigenesis. *Cancer cell* **2015**;28:599-609
66. Vo KT, Matthay KK, Neuhaus J, London WB, Hero B, Ambros PF, *et al.* Clinical, biologic, and prognostic differences on the basis of primary tumor site in neuroblastoma: a report from the international neuroblastoma risk group project. *Journal of Clinical Oncology* **2014**;32:3169-76
67. Tolbert VP, Matthay KK. Neuroblastoma: clinical and biological approach to risk stratification and treatment. *Cell and tissue research* **2018**;372:195-209
68. Park JR, Bagatell R, Cohn SL, Pearson AD, Villablanca JG, Berthold F, *et al.* Revisions to the International Neuroblastoma Response Criteria: A Consensus Statement From the National Cancer Institute Clinical Trials Planning Meeting. *Journal of Clinical Oncology* **2017**;35:2580-7
69. Lonergan GJ, Schwab CM, Suarez ES, Carlson CL. Neuroblastoma, ganglioneuroblastoma, and ganglioneuroma: radiologic-pathologic correlation. *Radiographics* **2002**;22:911-34
70. Irwin MS, Park JR. Neuroblastoma: paradigm for precision medicine. *Pediatric clinics of North America* **2015**;62:225-56
71. Strenger V, Kerbl R, Dornbusch HJ, Ladenstein R, Ambros PF, Ambros IM, *et al.* Diagnostic and prognostic impact of urinary catecholamines in neuroblastoma patients. *Pediatric blood & cancer* **2007**;48:504-9
72. Monclair T, Brodeur GM, Ambros PF, Brisse HJ, Cecchetto G, Holmes K, *et al.* The International Neuroblastoma Risk Group (INRG) staging system: an INRG Task Force report. *Journal of Clinical Oncology* **2009**;27:298-303
73. Dubois SG, Geier E, Batra V, Yee SW, Neuhaus J, Segal M, *et al.* Evaluation of norepinephrine transporter expression and metaiodobenzylguanidine avidity in neuroblastoma: A report from the Children's Oncology Group. *International journal of molecular imaging* **2012**:250834
74. Biermann M, Schwarzlmuller T, Fasmer KE, Reitan BC, Johnsen B, Rosendahl K. Is there a role for PET-CT and SPECT-CT in pediatric oncology? *Acta radiologica* **2013**;54:1037-45
75. Sharp SE, Shulkin BL, Gelfand MJ, Salisbury S, Furman WL. 123I-MIBG scintigraphy and 18F-FDG PET in neuroblastoma. *Journal of nuclear medicine* **2009**;50:1237-43
76. London WB, Castel V, Monclair T, Ambros PF, Pearson AD, Cohn SL, *et al.* Clinical and biologic features predictive of survival after relapse of neuroblastoma: a report from the International Neuroblastoma Risk Group project. *Journal of Clinical Oncology* **2011**;29:3286-92
77. Brodeur GM, Seeger RC, Barrett A, Berthold F, Castleberry RP, D'Angio G, *et al.* International criteria for diagnosis, staging, and response to treatment in patients with neuroblastoma. *Journal of Clinical Oncology* **1988**;6:1874-81

References

78. Brodeur GM, Pritchard J, Berthold F, Carlsen NL, Castel V, Castelberry RP, *et al*. Revisions of the international criteria for neuroblastoma diagnosis, staging, and response to treatment. *Journal of Clinical Oncology* **1993**;11:1466-77
79. Coldman AJ, Fryer CJ, Elwood JM, Sonley MJ. Neuroblastoma: Influence of age at diagnosis, stage, tumor site, and sex on prognosis. *Cancer* **1980**;46:1896-901
80. George RE, London WB, Cohn SL, Maris JM, Kretschmar C, Diller L, *et al*. Hyperdiploidy plus nonamplified MYCN confers a favorable prognosis in children 12 to 18 months old with disseminated neuroblastoma: a Pediatric Oncology Group study. *Journal of Clinical Oncology* **2005**;23:6466-73
81. Schmidt ML, Lal A, Seeger RC, Maris JM, Shimada H, O'Leary M, *et al*. Favorable prognosis for patients 12 to 18 months of age with stage 4 nonamplified MYCN neuroblastoma: a Children's Cancer Group Study. *Journal of Clinical Oncology* **2005**;23:6474-80
82. Shimada H, Chatten J, Newton WA, Sachs N, Hamoudi AB, Chiba T, *et al*. Histopathologic prognostic factors in neuroblastic tumors: definition of subtypes of ganglioneuroblastoma and an age-linked classification of neuroblastomas. *J Natl Cancer Inst* **1984**;73:405-16
83. Shimada H, Ambros IM, Dehner LP, Hata J, Joshi VV, Roald B. Terminology and morphologic criteria of neuroblastic tumors: recommendations by the International Neuroblastoma Pathology Committee. *Cancer* **1999**;86:349-63
84. Shimada H, Ambros IM, Dehner LP, Hata J, Joshi VV, Roald B, *et al*. The International Neuroblastoma Pathology Classification (the Shimada system). *Cancer* **1999**;86:364-72
85. Shimada H, Umehara S, Monobe Y, Hachitanda Y, Nakagawa A, Goto S, *et al*. International neuroblastoma pathology classification for prognostic evaluation of patients with peripheral neuroblastic tumors: a report from the Children's Cancer Group. *Cancer* **2001**;92:2451-61
86. Schwab M, Alitalo K, Klempnauer KH, Varmus HE, Bishop JM, Gilbert F, *et al*. Amplified DNA with limited homology to myc cellular oncogene is shared by human neuroblastoma cell lines and a neuroblastoma tumour. *Nature* **1983** 305:245-8
87. Kohl NE, Kanda N, Schreck RR, Bruns G, Latt SA, Gilbert F, *et al*. Transposition and amplification of oncogene-related sequences in human neuroblastomas. *Cell* **1983** 35:359-67
88. Plantaz D, Vandesompele J, Van Roy N, Lastowska M, Bown N, Combaret V, *et al*. Comparative genomic hybridization (CGH) analysis of stage 4 neuroblastoma reveals high frequency of 11q deletion in tumors lacking MYCN amplification. *International journal of cancer* **2001** 91:680-6
89. Moreno L, Vaidya SJ, Pinkerton CR, Lewis IJ, Imeson J, Machin D, *et al*. Long-term follow-up of children with high-risk neuroblastoma: the ENSG5 trial experience. *Pediatric blood & cancer* **2013**;60:1135-40
90. Laverdière C, Liu Q, Yasui Y, Nathan PC, Gurney JG, Stovall M, *et al*. Long-term outcomes in survivors of neuroblastoma: a report from the Childhood Cancer Survivor Study. *Journal of the National Cancer Institute* **2009**;101:1131-40
91. Smith V, Foster J. High-Risk Neuroblastoma Treatment Review. *Children* **2018**;5:114
92. Strother DR, London WB, Schmidt ML, Brodeur GM, Shimada H, Thorner P, *et al*. Outcome After Surgery Alone or With Restricted Use of Chemotherapy for Patients With Low-Risk

- Neuroblastoma: Results of Children's Oncology Group Study P9641. *Journal of Clinical Oncology* **2012**;30:1842-8
93. De Bernardi B, Mosseri V, Rubie H, Castel V, Foot A, Ladenstein R, *et al.* Treatment of localised resectable neuroblastoma. Results of the LNESG1 study by the SIOP Europe Neuroblastoma Group. *British journal of cancer* **2008**;99:1027-33
94. Whittle SB, Smith V, Doherty E, Zhao S, McCarty S, Zage PE. Overview and recent advances in the treatment of neuroblastoma. *Expert review of anticancer therapy* **2017**;17:369-86
95. Perez EA. Microtubule inhibitors: Differentiating tubulin-inhibiting agents based on mechanisms of action, clinical activity, and resistance. *Mol Cancer Ther* **2009**;8:2086-95
96. Nuchtern JG, London WB, Barnewolt CE, Naranjo A, McGrady PW, Geiger JD, *et al.* A prospective study of expectant observation as primary therapy for neuroblastoma in young infants: a Children's Oncology Group study. *Annals of surgery* **2012**;256:573-80
97. Meany HJ, London WB, Ambros PF, Matthay KK, Monclair T, Simon T, *et al.* Significance of clinical and biologic features in Stage 3 neuroblastoma: a report from the International Neuroblastoma Risk Group project. *Pediatric blood & cancer* **2014**;61:1932-9
98. Baker DL, L. SM, Cohn SL, Maris JM, London WB, Buxton A, *et al.* Outcome after reduced chemotherapy for intermediate-risk neuroblastoma. *The New England journal of medicine* **2010** 363:1313-23
99. Kohler JA, Rubie H, Castel V, Beiske K, Holmes K, Gambini C, *et al.* Treatment of children over the age of one year with unresectable localised neuroblastoma without MYCN amplification: results of the SIOPEN study. *Eur J Cancer* **2013**;49:3671-9
100. Strother D, van Hoff J, Rao PV, Smith EI, Shamberger RC, Halperin EC, *et al.* Event-free survival of children with biologically favourable neuroblastoma based on the degree of initial tumour resection: results from the Pediatric Oncology Group. *Eur J Cancer* **1997** 33:2121-5
101. Defferrari R, Mazzocco K, Ambros IM, Ambros PF, Bedwell C, Beiske K, *et al.* Influence of segmental chromosome abnormalities on survival in children over the age of 12 months with unresectable localised peripheral neuroblastic tumours without MYCN amplification. *British journal of cancer* **2015**;112:290-5
102. Pinto NR, Applebaum MA, Volchenboum SL, Matthay KK, London WB, Ambros PF, *et al.* Advances in risk classification and treatment strategies for neuroblastoma. *Journal of Clinical Oncology* **2015**;33:3008-17
103. Park JR, Kreissman SG, London WB, Naranjo A, Cohn SL, Hogarty MD, *et al.* A phase III randomized clinical trial (RCT) of tandem myeloablative autologous stem cell transplant (ASCT) using peripheral blood stem cell (PBSC) as consolidation therapy for high-risk neuroblastoma (HR-NB): A Children's Oncology Group (COG) study. *Journal of Clinical Oncology* **2016**;34:LBA3-LBA
104. Pearson ADJ, Pinkerton CR, Lewis IJ, Imeson J, Ellershaw C, Machin D. High-dose rapid and standard induction chemotherapy for patients aged over 1 year with stage 4 neuroblastoma: a randomised trial. *The Lancet Oncology* **2008**;9:247-56
105. Yanik GA, Parisi MT, Shulkin BL, Naranjo A, Kreissman SG, London WB, *et al.* Semiquantitative mIBG scoring as a prognostic indicator in patients with stage 4

References

- neuroblastoma: a report from the Children's oncology group. *Journal of nuclear medicine* **2013**;54:541-8
106. Sorrentino S, Gigliotti AR, Sementa AR, Morsellino V, Conte M, Erminio G, *et al.* Neuroblastoma in the adult: the Italian experience with 21 patients. *Journal of pediatric hematology/oncology* **2014**;36:e499-505
107. Castel V, Tovar JA, Costa E, Cuadros J, Ruiz A, Rollan V, *et al.* The role of surgery in stage IV neuroblastoma. *Journal of pediatric surgery* **2002**;37:1574-8
108. Simon T, Haberle B, Hero B, von Schweinitz D, Berthold F. Role of surgery in the treatment of patients with stage 4 neuroblastoma age 18 months or older at diagnosis. *Journal of Clinical Oncology* **2013**;31:752-8
109. Du L, Liu L, Zhang C, Cai W, Wu Y, Wang J, *et al.* Role of surgery in the treatment of patients with high-risk neuroblastoma who have a poor response to induction chemotherapy. *Journal of pediatric surgery* **2014**;49:528-33
110. Ladenstein RL, Poetschger U, Luksch R, Brock P, Castel V, Yaniv I, *et al.* Busulphan-melphalan as a myeloablative therapy (MAT) for high-risk neuroblastoma: Results from the HR-NBL1/SIOPEN trial. *Journal of Clinical Oncology* **2011**;29:2
111. Berthold F, Boos J, Burdach S, Erttmann R, Henze G, Hermann J, *et al.* Myeloablative megatherapy with autologous stem-cell rescue versus oral maintenance chemotherapy as consolidation treatment in patients with high-risk neuroblastoma: a randomised controlled trial. *The Lancet Oncology* **2005**;6:649-58
112. Matthay KK, Reynolds CP, Seeger RC, Shimada H, Adkins ES, Haas-Kogan D, *et al.* Long-term results for children with high-risk neuroblastoma treated on a randomized trial of myeloablative therapy followed by 13-cis-retinoic acid: a children's oncology group study. *Journal of Clinical Oncology* **2009**;27:1007-13
113. Matthay KK, Villablanca JG, Seeger RC, Stram DO, Harris RE, Ramsay NK, *et al.* Treatment of high-risk neuroblastoma with intensive chemotherapy, radiotherapy, autologous bone marrow transplantation, and 13-cis-retinoic acid. Children's Cancer Group. *The New England journal of medicine* **1999** 341:1165-73
114. Yu AL, Gilman AL, Ozkaynak MF, London WB, Kreissman SG, Chen HX, *et al.* Anti-GD2 antibody with GM-CSF, interleukin-2, and isotretinoin for neuroblastoma. *The New England journal of medicine* **2010** 363:1324-34
115. Sait S, Modak S. Anti-GD2 immunotherapy for neuroblastoma. *Expert review of anticancer therapy* **2017**;17:889-904
116. Mitra S, Leonard WJ. Biology of IL-2 and its therapeutic modulation: Mechanisms and strategies. *Journal of leukocyte biology* **2018**;103:643-55
117. Waller EK. The role of sargramostim (rhGM-CSF) as immunotherapy. *The oncologist* **2007**;12 Suppl 2:22-6
118. Garaventa A, Parodi S, De Bernardi B, Dau D, Manzitti C, Conte M, *et al.* Outcome of children with neuroblastoma after progression or relapse. A retrospective study of the Italian neuroblastoma registry. *Eur J Cancer* **2009**;45:2835-42

119. Moreno L, Rubie H, Varo A, Le Deley MC, Amoroso L, Chevance A, *et al.* Outcome of children with relapsed or refractory neuroblastoma: A meta-analysis of ITCC/SIOPEN European phase II clinical trials. *Pediatric blood & cancer* **2017**;64:25-31
120. Di Giannatale A, Dias-Gastellier N, Devos A, Mc Hugh K, Boubaker A, Courbon F, *et al.* Phase II study of temozolomide in combination with topotecan (TOTEM) in relapsed or refractory neuroblastoma: a European Innovative Therapies for Children with Cancer-SIOP-European Neuroblastoma study. *Eur J Cancer* **2014**;50:170-7
121. London WB, Frantz CN, Campbell LA, Seeger RC, Brumback BA, Cohn SL, *et al.* Phase II randomized comparison of topotecan plus cyclophosphamide versus topotecan alone in children with recurrent or refractory neuroblastoma: a Children's Oncology Group study. *Journal of Clinical Oncology* **2010**;28:3808-15
122. Simon T, Langer A, Harnischmacher U, Fruhwald MC, Jorch N, Claviez A, *et al.* Topotecan, cyclophosphamide, and etoposide (TCE) in the treatment of high-risk neuroblastoma. Results of a phase-II trial. *Journal of cancer research and clinical oncology* **2007**;133:653-61
123. Kushner BH, Kramer K, Modak S, Qin LX, Cheung NK. Differential impact of high-dose cyclophosphamide, topotecan, and vincristine in clinical subsets of patients with chemoresistant neuroblastoma. *Cancer* **2010**;116:3054-60
124. Garaventa A, Luksch R, Biasotti S, Severi G, Pizzitola MR, Viscardi E, *et al.* A phase II study of topotecan with vincristine and doxorubicin in children with recurrent/refractory neuroblastoma. *Cancer* **2003**;98:2488-94
125. Amoroso L, Erminio G, Makin G, Pearson ADJ, Brock P, Valteau-Couanet D, *et al.* Topotecan-Vincristine-Doxorubicin in stage 4 high-risk neuroblastoma patients failing to achieve a complete metastatic response to rapid COJEC: A SIOPEN study. *Cancer research and treatment* **2018**;50:148-55
126. Bagatell R, London WB, Wagner LM, Voss SD, Stewart CF, Maris JM, *et al.* Phase II study of irinotecan and temozolomide in children with relapsed or refractory neuroblastoma: a Children's Oncology Group study. *Journal of Clinical Oncology* **2011**;29:208-13
127. Kushner BH, Kramer K, Modak S, Cheung NK. Irinotecan plus temozolomide for relapsed or refractory neuroblastoma. *Journal of Clinical Oncology* **2006**;24:5271-6
128. Kushner BH, Modak S, Kramer K, Basu EM, Roberts SS, Cheung NK. Ifosfamide, carboplatin, and etoposide for neuroblastoma: a high-dose salvage regimen and review of the literature. *Cancer* **2013**;119:665-71
129. Donfrancesco A, Jenkner A, Castellano A, Ilari I, Milano GM, De Sio L, *et al.* Ifosfamide/carboplatin/etoposide (ICE) as front-line, topotecan/cyclophosphamide as second-line and oral temozolomide as third-line treatment for advanced neuroblastoma over one year of age. *Acta Paediatr Suppl* **2004**;93:6-11
130. Hutchinson RJ, Sisson JC, Shapiro B, Miser JS, Normole D, Shulkin BL, *et al.* 131-I-metaiodobenzylguanidine treatment in patients with refractory advanced neuroblastoma. *Am J Clin Oncol* **1992**;15:226-32
131. Klingebiel T, Berthold F, Treuner J, Schwabe D, Fischer M, Feine U, *et al.* Metaiodobenzylguanidine (mIBG) in treatment of 47 patients with neuroblastoma: results of the German Neuroblastoma Trial. *Med Pediatr Oncol* **1991**;19:84-8

References

132. Matthay KK, Yanik G, Messina J, Quach A, Huberty J, Cheng SC, *et al.* Phase II study on the effect of disease sites, age, and prior therapy on response to iodine-131-metaiodobenzylguanidine therapy in refractory neuroblastoma. *Journal of Clinical Oncology* **2007**;25:1054-60
133. Lee JW, Lee S, Cho HW, Ma Y, Yoo KH, Sung KW, *et al.* Incorporation of high-dose (131)I-metaiodobenzylguanidine treatment into tandem high-dose chemotherapy and autologous stem cell transplantation for high-risk neuroblastoma: results of the SMC NB-2009 study. *Journal of hematology & oncology* **2017**;10:108
134. Moreno L, Caron H, Georger B, Eggert A, Schleiermacher G, Brock P, *et al.* Accelerating drug development for neuroblastoma - New Drug Development Strategy: an Innovative Therapies for Children with Cancer, European Network for Cancer Research in Children and Adolescents and International Society of Paediatric Oncology Europe Neuroblastoma project. *Expert opinion on drug discovery* **2017**;12:801-11
135. Moreno L, Barone G, DuBois SG, Molenaar J, Fischer M, Schulte J, *et al.* Accelerating drug development for neuroblastoma: Summary of the Second Neuroblastoma Drug Development Strategy forum from Innovative Therapies for Children with Cancer and International Society of Paediatric Oncology Europe Neuroblastoma. *Eur J Cancer* **2020**;136:52-68
136. Caren H, Abel F, Kogner P, Martinsson T. High incidence of DNA mutations and gene amplifications of the ALK gene in advanced sporadic neuroblastoma tumours. *The Biochemical journal* **2008**;416:153-9
137. Passoni L, Longo L, Collini P, Coluccia AM, Bozzi F, Podda M, *et al.* Mutation-independent anaplastic lymphoma kinase overexpression in poor prognosis neuroblastoma patients. *Cancer research* **2009**;69:7338-46
138. Mossé YP, Lim MS, Voss SD, Wilner K, Ruffner K, Laliberte J, *et al.* Safety and activity of crizotinib for paediatric patients with refractory solid tumours or anaplastic large-cell lymphoma: a Children's Oncology Group phase 1 consortium study. *The Lancet Oncology* **2013**;14:472-80
139. Puissant A, Frumm SM, Alexe G, Bassil CF, Qi J, Chanthery YH, *et al.* Targeting MYCN in neuroblastoma by BET bromodomain inhibition. *Cancer discovery* **2013**;3:308-23
140. Otto T, Horn S, Brockmann M, Eilers U, Schuttrumpf L, Popov N, *et al.* Stabilization of N-Myc is a critical function of Aurora A in human neuroblastoma. *Cancer cell* **2009**;15:67-78
141. Cowley DO, Rivera-Pérez JA, Schliekelman M, He YJ, Oliver TG, Lu L, *et al.* Aurora-A kinase is essential for bipolar spindle formation and early development. *Molecular and cellular biology* **2009**;29:1059-71
142. Mosse YP, Lipsitz E, Fox E, Teachey DT, Maris JM, Weigel B, *et al.* Pediatric phase I trial and pharmacokinetic study of MLN8237, an investigational oral selective small-molecule inhibitor of Aurora kinase A: a Children's Oncology Group Phase I Consortium study. *Clinical cancer research* **2012**;18:6058-64
143. DuBois SG, Marachelian A, Fox E, Kudgus RA, Reid JM, Groshen S, *et al.* Phase I study of the Aurora A kinase inhibitor alisertib in combination with irinotecan and temozolomide for patients with relapsed or refractory neuroblastoma: A NANT (New Approaches to Neuroblastoma Therapy) trial. *Journal of Clinical Oncology* **2016**;34:1368-75

144. DuBois SG, Mosse YP, Fox E, Kudgus RA, Reid JM, McGovern R, *et al.* Phase II trial of alisertib in combination with irinotecan and temozolomide for patients with relapsed or refractory neuroblastoma. *Clinical cancer research* **2018**;24:6142-9
145. Felgenhauer J, Tomino L, Selich-Anderson J, Bopp E, Shah N. Dual BRD4 and AURKA inhibition is synergistic against MYCN-amplified and nonamplified neuroblastoma. *Neoplasia* **2018**;20:965-74
146. Vaughan L, Clarke PA, Barker K, Chanthery Y, Gustafson CW, Tucker E, *et al.* Inhibition of mTOR-kinase destabilizes MYCN and is a potential therapy for MYCN-dependent tumors. *Oncotarget* **2016**;7(36):57525–44
147. Geoerger B, Bourdeaut F, DuBois SG, Fischer M, Geller JI, Gottardo NG, *et al.* A phase I study of the CDK4/6 inhibitor ribociclib (LEE011) in pediatric patients with malignant rhabdoid tumors, neuroblastoma, and other solid tumors. *Clinical cancer research* **2017**;23:2433-41
148. Lowery CD, Dowless M, Renschler M, Blosser W, VanWye AB, Stephens JR, *et al.* Broad spectrum activity of the checkpoint kinase 1 inhibitor prexasertib as a single agent or chemopotentiator across a range of preclinical pediatric tumor models. *Clinical cancer research* **2019**;25:2278-89
149. Lee J-M, Nair J, Zimmer A, Lipkowitz S, Annunziata CM, Merino MJ, *et al.* Prexasertib, a cell cycle checkpoint kinase 1 and 2 inhibitor, in BRCA wild-type recurrent high-grade serous ovarian cancer: a first-in-class proof-of-concept phase 2 study. *The Lancet Oncology* **2018**;19:207-15
150. Eleveld TF, Oldridge DA, Bernard V, Koster J, Daage LC, Diskin SJ, *et al.* Relapsed neuroblastomas show frequent RAS-MAPK pathway mutations. *Nature genetics* **2015**;47:864-71
151. Fangusaro J, Onar-Thomas A, Young Poussaint T, Wu S, Ligon AH, Lindeman N, *et al.* Selumetinib in paediatric patients with BRAF-aberrant or neurofibromatosis type 1-associated recurrent, refractory, or progressive low-grade glioma: a multicentre, phase 2 trial. *The Lancet Oncology* **2019**;20:1011-22
152. Carr-Wilkinson J, O'Toole K, Wood KM, Challen CC, Baker AG, Board JR, *et al.* High frequency of p53/MDM2/p14ARF pathway abnormalities in relapsed neuroblastoma. *Clinical Cancer Research* **2010**;16:1108-18
153. Carr J, Bell E, Pearson AD, Kees UR, Beris H, Lunec J, *et al.* Increased frequency of aberrations in the p53/MDM2/p14(ARF) pathway in neuroblastoma cell lines established at relapse. *Cancer research* **2006**;66:2138-45
154. Mody R, Naranjo A, Van Ryn C, Yu AL, London WB, Shulkin BL, *et al.* Irinotecan–temozolomide with temsirolimus or dinutuximab in children with refractory or relapsed neuroblastoma (COG ANBL1221): an open-label, randomised, phase 2 trial. *The Lancet Oncology* **2017**;18:946-57
155. Yang RK, Sondel PM. Anti-GD2 strategy in the treatment of neuroblastoma. *Drugs Future* **2010**;35:665
156. Russell HV, Strother D, Mei Z, Rill D, Popek E, Biagi E, *et al.* Phase I trial of vaccination with autologous neuroblastoma tumor cells genetically modified to secrete IL-2 and lymphotactin. *J Immunother* **2007**;30:227-33

References

157. Krishnadas DK, Shapiro T, Lucas K. Complete remission following decitabine/dendritic cell vaccine for relapsed neuroblastoma. *Pediatrics* **2013**;131:e336-41
158. Kanold J, Paillard C, Tchirkov A, Lang P, Kelly A, Halle P, *et al.* NK cell immunotherapy for high-risk neuroblastoma relapse after haploidentical HSCT. *Pediatric blood & cancer* **2012**;59:739-42
159. Merchant MS, Wright M, Baird K, Wexler LH, Rodriguez-Galindo C, Bernstein D, *et al.* Phase I clinical trial of ipilimumab in pediatric patients with advanced solid tumors. *Clinical cancer research* **2016**;22:1364-70
160. Laverdière C, Cheung NK, Kushner BH, Kramer K, Modak S, LaQuaglia MP, *et al.* Long-term complications in survivors of advanced stage neuroblastoma. *Pediatric blood & cancer* **2005**;45:324-32
161. Martin A, Schneiderman J, Helenowski IB, Morgan E, Dilley K, Danner-Koptik K, *et al.* Secondary malignant neoplasms after high-dose chemotherapy and autologous stem cell rescue for high-risk neuroblastoma. *Pediatric blood & cancer* **2014**;61:1350-6
162. Trahair TN, Vowels MR, Johnston K, Cohn RJ, Russell SJ, Neville KA, *et al.* Long-term outcomes in children with high-risk neuroblastoma treated with autologous stem cell transplantation. *Bone marrow transplantation* **2007**;40:741-6
163. Perwein T, Lackner H, Sovinz P, Benesch M, Schmidt S, Schwinger W, *et al.* Survival and late effects in children with stage 4 neuroblastoma. *Pediatric blood & cancer* **2011**;57:629-35
164. Friedman DN, Henderson TO. Late effects and survivorship issues in patients with neuroblastoma. *Children* **2018**;5:107
165. Barnum KJ, O'Connell MJ. Cell cycle regulation by checkpoints. *Methods in molecular biology* **2014**;1170:29-40
166. Hanahan D, Weinberg RA. Hallmarks of cancer: the next generation. *Cell* **2011**;144:646-74
167. Vermeulen K, Van Bockstaele DR, Berneman ZN. The cell cycle: a review of regulation, deregulation and therapeutic targets in cancer. *Cell Prolif* **2003**;36: 131–49
168. Burgess A, Vuong J, Rogers S, Malumbres M, O'Donoghue SI. SnapShot: phosphoregulation of mitosis. *Cell* **2017**;169:1358.e1
169. Gavet O, Pines J. Progressive activation of CyclinB1-Cdk1 coordinates entry to mitosis. *Developmental cell* **2010**;18:533-43
170. Takizawa CG, Morgan DO. Control of mitosis by changes in the subcellular location of cyclin-B1–Cdk1 and Cdc25C. *Curr Opin Cell Biol* **2000**;12:658-65
171. Crncec A, Hochegger H. Triggering mitosis. *FEBS letters* **2019**;593:2868-88
172. Bollen M, Gerlich DW, Lesage B. Mitotic phosphatases: from entry guards to exit guides. *Trends in cell biology* **2009**;19:531-41
173. Kim HS, Fernandes G, Lee CW. Protein phosphatases involved in regulating mitosis: facts and hypotheses. *Molecules and cells* **2016**;39:654-62
174. Acquaviva C, Pines J. The anaphase-promoting complex/cyclosome: APC/C. *Journal of cell science* **2006**;119:2401-4
175. Rath O, Kozielski F. Kinesins and cancer. *Nature reviews Cancer* **2012**;12:527-39

176. Dumontet C, Jordan MA. Microtubule-binding agents: a dynamic field of cancer therapeutics. *Nature reviews Drug discovery* **2010**;9:790-803
177. Dominguez-Brauer C, Thu KL, Mason JM, Blaser H, Bray MR, Mak TW. Targeting mitosis in cancer: emerging strategies. *Molecular cell* **2015**;60:524-36
178. Risinger AL, Giles FJ, Mooberry SL. Microtubule dynamics as a target in oncology. *Cancer treatment reviews* **2009**;35:255-61
179. Kline-Smith SL, Walczak CE. Mitotic spindle assembly and chromosome segregation: refocusing on microtubule dynamics. *Molecular cell* **2004**;15:317-27
180. Mukhtar E, Adhami VM, Mukhtar H. Targeting microtubules by natural agents for cancer therapy. *Mol Cancer Ther* **2014**;13:275-84
181. Canta A, Chiorazzi A, Cavaletti G. Tubulin: a target for antineoplastic drugs into the cancer cells but also in the peripheral nervous system. *Curr Med Chem* **2009**;16:1315-24
182. Hirokawa N, Takemura R. Kinesin superfamily proteins and their various functions and dynamics. *Experimental cell research* **2004**;301:50-9
183. Hirokawa N, Noda Y, Tanaka Y, Niwa S. Kinesin superfamily motor proteins and intracellular transport. *Nature Reviews Molecular Cell Biology* **2009**;10:682-96
184. Garcia-Saez I, Skoufias DA. Eg5 targeting agents: From new anti-mitotic based inhibitor discovery to cancer therapy and resistance. *Biochemical pharmacology* **2021**;184:114364
185. Algarin EM, Hernandez-Garcia S, Garayoa M, Ocio EM. Filanesib for the treatment of multiple myeloma. *Expert opinion on investigational drugs* **2020**;29:5-14
186. Yen TJ, Compton DA, Wise D, Zinkowski RP, Brinkley BR, Earnshaw WC, *et al.* CENP-E, a novel human centromere-associated protein required for progression from metaphase to anaphase. *The EMBO journal* **1991**;10:1245-54
187. Schaar BT, Chan GK, Maddox P, Salmon ED, Yen TJ. CENP-E function at kinetochores is essential for chromosome alignment. *The Journal of cell biology* **1997**;139:1373-82
188. Chung V, Heath EI, Schelman WR, Johnson BM, Kirby LC, Lynch KM, *et al.* First-time-in-human study of GSK923295, a novel antimitotic inhibitor of centromere-associated protein E (CENP-E), in patients with refractory cancer. *Cancer chemotherapy and pharmacology* **2012**;69:733-41
189. Wang J, Guo X, Xie C, Jiang J. KIF15 promotes pancreatic cancer proliferation via the MEK-ERK signalling pathway. *British journal of cancer* **2017**;117:245-55
190. Luo W, Liao M, Liao Y, Chen X, Huang C, Fan J, *et al.* The role of kinesin KIF18A in the invasion and metastasis of hepatocellular carcinoma. *World journal of surgical oncology* **2018**;16:36
191. Malumbres M, Barbacid M. Cell cycle, CDKs and cancer: a changing paradigm. *Nature reviews Cancer* **2009**;9:153-66
192. Santamaria D, Barriere C, Cerqueira A, Hunt S, Tardy C, Newton K, *et al.* Cdk1 is sufficient to drive the mammalian cell cycle. *Nature* **2007**;448:811-5
193. Bednarek K, Kiwerska K, Szaumkessel M, Bodnar M, Kostrzewska-Poczekaj M, Marszalek A, *et al.* Recurrent CDK1 overexpression in laryngeal squamous cell carcinoma. *Tumor Biology* **2016**;37:11115-26

References

194. Piao J, Zhu L, Sun J, Li N, Dong B, Yang Y, *et al.* High expression of CDK1 and BUB1 predicts poor prognosis of pancreatic ductal adenocarcinoma. *Gene* **2019**;701:15-22
195. Li J, Wang Y, Wang X, Yang Q. CDK1 and CDC20 overexpression in patients with colorectal cancer are associated with poor prognosis: evidence from integrated bioinformatics analysis. *World journal of surgical oncology* **2020**;18:50
196. Asghar U, Witkiewicz AK, Turner NC, Knudsen ES. The history and future of targeting cyclin-dependent kinases in cancer therapy. *Nature Reviews Drug Discovery* **2015**;14:130-46
197. Serra F, Lapidari P, Quaquareni E, Tagliaferri B, Sottotetti F, Palumbo R. Palbociclib in metastatic breast cancer: current evidence and real-life data. *Drugs in Context* **2019**;8:1-16
198. Ditchfield C, Johnson VL, Tighe A, Ellston R, Haworth C, Johnson T, *et al.* Aurora B couples chromosome alignment with anaphase by targeting BubR1, Mad2, and Cenp-E to kinetochores. *The Journal of cell biology* **2003**;161:267-80
199. Vader G, Medema RH, Lens SMA. The chromosomal passenger complex: guiding Aurora-B through mitosis. *The Journal of cell biology* **2006**;173:833-7
200. Xu J, Yue CF, Zhou WH, Qian YM, Zhang Y, Wang SW, *et al.* Aurora-A contributes to cisplatin resistance and lymphatic metastasis in non-small cell lung cancer and predicts poor prognosis. *Journal of translational medicine* **2014**;12:200
201. Larsen SL, Yde CW, Laenkholm AV, Rasmussen BB, Duun-Henriksen AK, Bak M, *et al.* Aurora kinase B is important for antiestrogen resistant cell growth and a potential biomarker for tamoxifen resistant breast cancer. *BMC cancer* **2015**;15:239
202. Tang A, Gao K, Chu L, Zhang R, Yang J, Zheng J. Aurora kinases: novel therapy targets in cancers. *Oncotarget* **2017**;8:23937-54
203. O'Connor OA, Özcan M, Jacobsen ED, Roncero JM, Trotman J, Demeter J, *et al.* Randomized phase III study of alisertib or investigator's choice (selected single agent) in patients with relapsed or refractory peripheral T-Cell lymphoma. *Journal of Clinical Oncology* **2019**;37:613-23
204. Collins GP, Eyre TA, Linton KM, Radford J, Vallance GD, Soilleux E, *et al.* A phase II trial of AZD1152 in relapsed/refractory diffuse large B-cell lymphoma. *British journal of haematology* **2015**;170:886-90
205. Liu Z, Sun Q, Wang X. PLK1, a potential target for cancer therapy. *Transl Oncol* **2017**;10:22-32
206. Mross K, Dittrich C, Aulitzky WE, Strumberg D, Schutte J, Schmid RM, *et al.* A randomised phase II trial of the Polo-like kinase inhibitor BI 2536 in chemo-naïve patients with unresectable exocrine adenocarcinoma of the pancreas - a study within the Central European Society Anticancer Drug Research (CESAR) collaborative network. *British journal of cancer* **2012**;107:280-6
207. Stadler WM, Vaughn DJ, Sonpavde G, Vogelzang NJ, Tagawa ST, Petrylak DP, *et al.* An open-label, single-arm, phase 2 trial of the Polo-like kinase inhibitor volasertib (BI 6727) in patients with locally advanced or metastatic urothelial cancer. *Cancer* **2014**;120:976-82
208. Gjertsen BT, Schöffski P. Discovery and development of the Polo-like kinase inhibitor volasertib in cancer therapy. *Leukemia* **2015**;29:11-9

209. Doz F, Locatelli F, Baruchel A, Blin N, De Moerloose B, Frappaz D, *et al.* Phase I dose-escalation study of volasertib in pediatric patients with acute leukemia or advanced solid tumors. *Pediatric blood & cancer* **2019**;66:e27900
210. Luo J, Emanuele MJ, Li D, Creighton CJ, Schlabach MR, Westbrook TF, *et al.* A genome-wide RNAi screen identifies multiple synthetic lethal interactions with the Ras oncogene. *Cell* **2009**;137:835-48
211. Maia ARR, Linder S, Song JY, Vaarting C, Boon U, Pritchard CEJ, *et al.* Mps1 inhibitors synergise with low doses of taxanes in promoting tumour cell death by enhancement of errors in cell division. *British journal of cancer* **2018**;118:1586-95
212. Tannous BA, Kerami M, Van der Stoop PM, Kwiatkowski N, Wang J, Zhou W, *et al.* Effects of the selective MPS1 inhibitor MPS1-IN-3 on glioblastoma sensitivity to antimetabolic drugs. *Journal of the National Cancer Institute* **2013**;105:1322-31
213. Lorusso P, Chawla SP, Bendell J, Shields AF, Shapiro G, Rajagopalan P, *et al.* First-in-human study of the monopolar spindle 1 (Mps1) kinase inhibitor BAY 1161909 in combination with paclitaxel in subjects with advanced malignancies. *Annals of Oncology* **2018**;29:viii138
214. Siemeister G, Mengel A, Fernández-Montalván AE. Inhibition of BUB1 kinase by BAY 1816032 sensitizes tumor cells toward taxanes, ATR, and PARP inhibitors in vitro and in vivo. *Clinical cancer research* **2019**;25:1404-14
215. Ammarah U, Kumar A, Pal R, Bal NC, Misra G. Identification of new inhibitors against human Great wall kinase using in silico approaches. *Scientific reports* **2018**;8:4894
216. De Donato M, Righino B, Filippetti F, Battaglia A, Petrillo M, Piroli D, *et al.* Identification and antitumor activity of a novel inhibitor of the NIMA-related kinase NEK6. *Scientific reports* **2018**;8:16047
217. Liu M, Ran J, Zhou J. Non-canonical functions of the mitotic kinesin Eg5. *Thoracic cancer* **2018**;9:904-10
218. Gillmor CS, Roeder AH, Sieber P, Somerville C, Lukowitz W. A genetic screen for mutations affecting cell division in the arabidopsis thaliana embryo identifies seven loci required for cytokinesis. *PLoS One* **2016**;11:e0146492
219. Turner J, Anderson R, Guo J, Beraud C, Fletterick R, Sakowicz R. Crystal structure of the mitotic spindle kinesin Eg5 reveals a novel conformation of the neck-linker. *The Journal of biological chemistry* **2001**;276:25496-502
220. Waitzman JS, Rice SE. Mechanism and regulation of kinesin-5, an essential motor for the mitotic spindle. *Biol Cell* **2014**;106:1-12
221. Kapitein LC, Kwok BH, Weinger JS, Schmidt CF, Kapoor TM, Peterman EJ. Microtubule cross-linking triggers the directional motility of kinesin-5. *The Journal of cell biology* **2008**;182:421-8
222. Weinger JS, Qiu M, Yang G, Kapoor TM. A nonmotor microtubule binding site in kinesin-5 is required for filament crosslinking and sliding. *Curr Biol* **2011**;21:154-60
223. Chen Y, Hancock WO. Kinesin-5 is a microtubule polymerase. *Nature Communications* **2015**;6:8160

References

224. Blangy A, Lane HA, d'Herin P, Harper M, Kress M, Nigg EA. Phosphorylation by p34cdc2 regulates spindle association of human Eg5, a kinesin-related motor essential for bipolar spindle formation in vivo. *Cell* **1995**;83:1159–69
225. Kapoor TM, Mayer TU, Coughlin ML, Mitchison TJ. Probing spindle assembly mechanisms with monastrol, a small molecule inhibitor of the mitotic kinesin, Eg5. *J Cell Biol* **2000**;150:975-88
226. Cahu J, Olichon A, Hentrich C, Schek H, Drinjakovic J, Zhang C, *et al.* Phosphorylation by Cdk1 increases the binding of Eg5 to microtubules in vitro and in Xenopus egg extract spindles. *PLoS One* **2008**;3:e3936
227. Sawin KE, Mitchison TJ. Mutations in the kinesin-like protein Eg5 disrupting localization to the mitotic spindle. *Proc Natl Acad Sci U S A* **1995**;92:4289-93
228. Rapley J, Nicolás M, Groen A, Regué L, Bertran MT, Caelles C, *et al.* The NIMA-family kinase Nek6 phosphorylates the kinesin Eg5 at a novel site necessary for mitotic spindle formation. *Journal of cell science* **2008**;121:3912-21
229. Liu Y, Zhang Z, Liang H, Zhao X, Liang L, Wang G, *et al.* Protein Phosphatase 2A (PP2A) regulates EG5 to control mitotic progression. *Scientific reports* **2017**;7:1630
230. He J, Zhang Z, Ouyang M, Yang F, Hao H, Lamb KL, *et al.* PTEN regulates EG5 to control spindle architecture and chromosome congression during mitosis. *Nature communications* **2016**;7:12355-
231. Pines J. Cubism and the cell cycle: the many faces of the APC/C. *Nature reviews Molecular cell biology* **2011**;12:427-38
232. Musacchio A, Salmon ED. The spindle-assembly checkpoint in space and time. *Nature reviews Molecular cell biology* **2007**;8:379-93
233. Drosopoulos K, Tang C, Chao WC, Linardopoulos S. APC/C is an essential regulator of centrosome clustering. *Nature Communications* **2014**;5:3686
234. Eguren M, Álvarez-Fernández M, García F, López-Contreras AJ, Fujimitsu K, Yaguchi H, *et al.* A synthetic lethal interaction between APC/C and topoisomerase poisons uncovered by proteomic screens. *Cell reports* **2014**;6:670-83
235. Ma N, Titus J, Gable A, Ross JL, Wadsworth P. TPX2 regulates the localization and activity of Eg5 in the mammalian mitotic spindle. *The Journal of cell biology* **2011**;195:87-98
236. Gable A, Qiu M, Titus J, Balchand S, Ferenz NP, Ma N, *et al.* Dynamic reorganization of Eg5 in the mammalian spindle throughout mitosis requires dynein and TPX2. *Molecular biology of the cell* **2012**;23:1254-66
237. Blangy A, Arnaud L, Nigg EA. Phosphorylation by p34cdc2 protein kinase regulates binding of the kinesin-related motor HsEg5 to the dynactin subunit p150. *The Journal of biological chemistry* **1997**;272:19418-24
238. Bishop JD, Han Z, Schumacher JM. The *Caenorhabditis elegans* Aurora B kinase AIR-2 phosphorylates and is required for the localization of a BimC kinesin to meiotic and mitotic spindles. *Molecular biology of the cell* **2005**;16:742-56
239. Sawin KE, LeGuellec K, Philippe M, Mitchison TJ. Mitotic spindle organization by a plus-end-directed microtubule motor. *Nature* **1992**;359:540-3

240. Salemi JD, McGilvray PT, Maresca TJ. Development of a *Drosophila* cell-based error correction assay. *Frontiers in oncology* **2013**;3:187
241. Asada T, Kuriyama R, Shibaoka H. TKRP125, a kinesin-related protein involved in the centrosome-independent organization of the cytokinetic apparatus in tobacco BY-2 cells. *Journal of cell science* **1997**;110:179-89
242. Bannigan A, Scheible WR, Lukowitz W, Fagerstrom C, Wadsworth P, Somerville C, *et al.* A conserved role for kinesin-5 in plant mitosis. *Journal of cell science* **2007**;120:2819-27
243. Miki T, Naito H, Nishina M, Goshima G. Endogenous localizome identifies 43 mitotic kinesins in a plant cell. *Proc Natl Acad Sci U S A* **2014**;111:E1053-61
244. Castillo A, Morse HC, 3rd, Godfrey VL, Naeem R, Justice MJ. Overexpression of Eg5 causes genomic instability and tumor formation in mice. *Cancer research* **2007**;67:10138-47
245. Zhou J, Chen WR, Yang LC, Wang J, Sun JY, Zhang WW, *et al.* KIF11 functions as an oncogene and is associated with poor outcomes from breast cancer. *Cancer research and treatment* **2019**;51:1207-21
246. Pei YY, Li GC, Ran J, Wei FX. Kinesin family member 11 contributes to the progression and prognosis of human breast cancer. *Oncology letters* **2017**;14:6618-26
247. Li X, Huang W, Huang W, Wei T, Zhu W, Chen G, *et al.* Kinesin family members KIF2C/4A/10/11/14/18B/20A/23 predict poor prognosis and promote cell proliferation in hepatocellular carcinoma. *Am J Transl Res* **2020**;12:1614-39
248. Daigo K, Takano A, Thang PM, Yoshitake Y, Shinohara M, Tohnai I, *et al.* Characterization of KIF11 as a novel prognostic biomarker and therapeutic target for oral cancer. *International journal of oncology* **2018**;52:155-65
249. Kato T, Lee D, Wu L, Patel P, Young AJ, Wada H, *et al.* Kinesin family members KIF11 and KIF23 as potential therapeutic targets in malignant pleural mesothelioma. *International journal of oncology* **2016**;49:448-56
250. Jungwirth, Yu, Moustafa, Rapp, Warta, Jungk, *et al.* Identification of KIF11 as a novel target in meningioma. *Cancers* **2019**;11:545
251. Mo XC, Zhang ZT, Song MJ, Zhou ZQ, Zeng JX, Du YF, *et al.* Screening and identification of hub genes in bladder cancer by bioinformatics analysis and KIF11 is a potential prognostic biomarker. *Oncology letters* **2021**;21:205
252. Hansson K, Radke K, Aaltonen K, Saarela J, Mañas A, Sjölund J, *et al.* Therapeutic targeting of KSP in preclinical models of high-risk neuroblastoma. *Science translational medicine* **2020**;12
253. Liu B, Zhang G, Cui S, Du G. Upregulation of KIF11 in TP53 mutant glioma promotes tumor stemness and drug resistance. *Cellular and molecular neurobiology* **2021**
254. Venere M, Horbinski C, Crish JF, Jin X, Vasani A, Major J, *et al.* The mitotic kinesin KIF11 is a driver of invasion, proliferation, and self-renewal in glioblastoma. *Science translational medicine* **2015**;7:304ra143
255. Jin Q, Dai Y, Wang Y, Zhang S, Liu G. High kinesin family member 11 expression predicts poor prognosis in patients with clear cell renal cell carcinoma. *Journal of clinical pathology* **2019**;72:354-62

References

256. Sun D, Lu J, Ding K, Bi D, Niu Z, Cao Q, *et al.* The expression of Eg5 predicts a poor outcome for patients with renal cell carcinoma. *Medical oncology* **2013**;30:476
257. Wei D, Rui B, Qingquan F, Chen C, Ping HY, Xiaoling S, *et al.* KIF11 promotes cell proliferation via ERBB2/PI3K/AKT signaling pathway in gallbladder cancer. *International journal of biological sciences* **2021**;17:514-26
258. Liu J, Tian Y, Yi L, Gao Z, Lou M, Yuan K. High KIF11 expression is associated with poor outcome of NSCLC. *Tumori* **2021**:300891620988342
259. Lu M, Zhu H, Wang X, Zhang D, Xiong L, Xu L, *et al.* The prognostic role of Eg5 expression in laryngeal squamous cell carcinoma. *Pathology* **2016**;48:214-8
260. Nowicki MO, Pawlowski P, Fischer T, Hess G, Pawlowski T, Skorski T. Chronic myelogenous leukemia molecular signature. *Oncogene* **2003**;22:3952-63
261. Liu M, Wang X, Yang Y, Li D, Ren H, Zhu Q, *et al.* Ectopic expression of the microtubule-dependent motor protein Eg5 promotes pancreatic tumorigenesis. *The Journal of pathology* **2010**;221:221-8
262. Enos AP, Morris NR. Mutation of a gene that encodes a kinesin-like protein blocks nuclear division in *A. nidulans*. *Cell* **1990**;60:1019-27
263. Hoyt MA, He L, Loo KK, Saunders WS. Two *Saccharomyces cerevisiae* kinesin-related gene products required for mitotic spindle assembly. *The Journal of cell biology* **1992**;118:109-20
264. Mayer TU, Kapoor TM, Haggarty SJ, King RW, Schreiber SL, Mitchison TJ. Small molecule inhibitor of mitotic spindle bipolarity identified in a phenotype-based screen. *Science* **1999**;286:971-4
265. Myers SM, Collins I. Recent findings and future directions for inter-polar mitotic kinesin inhibitors in cancer therapy. *Future Med Chem* **2016**;8:463-89
266. El-Nassan HB. Advances in the discovery of kinesin spindle protein (Eg5) inhibitors as anti-tumor agents. *European journal of medicinal chemistry* **2013**;62:614-31
267. Yan Y, Sardana V, Xu B, Homnick C, Halczenko W, Buser CA, *et al.* Inhibition of a mitotic motor protein: where, how, and conformational consequences. *Journal of molecular biology* **2004**;335:547-54
268. Groen AC, Needleman D, Brangwynne C, Gradinaru C, Fowler B, Mazitschek R, *et al.* A novel small-molecule inhibitor reveals a possible role of kinesin-5 in anastral spindle-pole assembly. *Journal of cell science* **2008**;121:2293-300
269. Ulaganathan V, Talapatra SK, Rath O, Pannifer A, Hackney DD, Kozielski F. Structural insights into a unique inhibitor binding pocket in kinesin spindle protein. *Journal of the American Chemical Society* **2013**;135:2263-72
270. Lee CW, Bélanger K, Rao SC, Petrella TM, Tozer RG, Wood L, *et al.* A phase II study of ispinesib (SB-715992) in patients with metastatic or recurrent malignant melanoma: a National Cancer Institute of Canada Clinical Trials Group trial. *Investigational new drugs* **2008**;26:249-55
271. Jones R, Vuky J, Elliott T, Mead G, Arranz JA, Chester J, *et al.* Phase II study to assess the efficacy, safety and tolerability of the mitotic spindle kinesin inhibitor AZD4877 in patients with recurrent advanced urothelial cancer. *Investigational new drugs* **2013**;31:1001-7

272. Mross KB, Scharr D, Richly H, Bauer S, Krauss B, Krauss R, *et al.* Overcoming the proliferation rate paradox: Clinical evaluation of a continuous dosing scheme of the novel oral Eg5 inhibitor 4SC-205. *Journal of Clinical Oncology* **2015**;33:2528
273. Su Z, Fang H, Hong H, Shi L, Zhang W, Zhang W, *et al.* An investigation of biomarkers derived from legacy microarray data for their utility in the RNA-seq era. *Genome biology* **2014**;15:523
274. Wang Q, Diskin S, Rappaport E, Attiyeh E, Mosse Y, Shue D, *et al.* Integrative genomics identifies distinct molecular classes of neuroblastoma and shows that multiple genes are targeted by regional alterations in DNA copy number. *Cancer research* **2006**;66:6050-62
275. Kocak H, Ackermann S, Hero B, Kahlert Y, Oberthuer A, Juraeva D, *et al.* Hox-C9 activates the intrinsic pathway of apoptosis and is associated with spontaneous regression in neuroblastoma. *Cell death & disease* **2013**;4:e586
276. Schneider CA, Rasband WS, Eliceiri KW. NIH Image to ImageJ: 25 years of image analysis. *Nat Methods* **2012**;9:671-5
277. Livak KJ, Schmittgen TD. Analysis of relative gene expression data using real-time quantitative PCR and the 2(-Delta Delta C(T)) Method. *Methods* **2001**;25:402-8
278. Vo BT, Wolf E, Kawauchi D, Gebhardt A, Rehg JE, Finkelstein D, *et al.* The interaction of Myc with Miz1 defines medulloblastoma subgroup identity. *Cancer cell* **2016**;29:5-16
279. Encinas M, Iglesias M, Lui Y, Wang H, Muhaisen A, Ceña V, *et al.* Sequential treatment of SH-SY5Y cells with retinoic acid and brain-derived neurotrophic factor gives rise to fully differentiated, neurotrophic factor-dependent, human neuron-like cells. *J Neurochem* **2000**;75:991-1003
280. Zufferey R, Dull T, Mandel RJ, Bukovsky A, Quiroz D, Naldini L, *et al.* Self-inactivating lentivirus vector for safe and efficient in vivo gene delivery. *J Virol* **1998**;72:9873-80
281. Dobin A, Davis CA, Schlesinger F, Drenkow J, Zaleski C, Jha S, *et al.* STAR: ultrafast universal RNA-seq aligner. *Bioinformatics* **2013**;29:15-21
282. Li B, Dewey CN. RSEM: accurate transcript quantification from RNA-Seq data with or without a reference genome. *BMC Bioinformatics* **2011**;4:323
283. Love MI, Huber W, Anders S. Moderated estimation of fold change and dispersion for RNA-seq data with DESeq2. *Genome biology* **2014**;15:550
284. Subramanian A, Tamayo P, Mootha VK, Mukherjee S, Ebert BL, Gillette MA, *et al.* Gene set enrichment analysis: A knowledge-based approach for interpreting genome-wide expression profiles. *Proceedings of the National Academy of Sciences* **2005**;102:15545-50
285. Mootha VK, Lindgren CM, Eriksson KF, Subramanian A, Sihag S, Lehar J, *et al.* PGC-1 α -responsive genes involved in oxidative phosphorylation are coordinately downregulated in human diabetes. *Nature genetics* **2003**; 34:267-73
286. Kluin RJC, Kemper K, Kuilman T, de Ruiter JR, Iyer V, Forment JV, *et al.* Xenofilter: computational deconvolution of mouse and human reads in tumor xenograft sequence data. *BMC Bioinformatics* **2018**;19:366
287. Li H, Durbin R. Fast and accurate short read alignment with Burrows-Wheeler transform. *Bioinformatics* **2009**;25:1754-60

References

288. Van der Auwera GA, Carneiro MO, Hartl C, Poplin R, Del Angel G, Levy-Moonshine A, *et al.* From FastQ data to high confidence variant calls: the Genome Analysis Toolkit best practices pipeline. *Current protocols in bioinformatics* **2013**;43:11.0.1-0.33
289. Kim S, Scheffler K, Halpern AL, Bekritsky MA, Noh E, Källberg M, *et al.* Strelka2: fast and accurate calling of germline and somatic variants. *Nature Methods* **2018**;15:591-4
290. Lai Z, Markovets A, Ahdesmaki M, Chapman B, Hofmann O, McEwen R, *et al.* VarDict: a novel and versatile variant caller for next-generation sequencing in cancer research. *Nucleic acids research* **2016**;44:e108
291. Benjamin D, Sato T, Cibulskis K, Getz G, Stewart C, Lichtenstein L. Calling Somatic SNVs and Indels with Mutect2. *bioRxiv.* **2019**;861054
292. Koboldt DC, Zhang Q, Larson DE, Shen D, McLellan MD, Lin L, *et al.* VarScan 2: somatic mutation and copy number alteration discovery in cancer by exome sequencing. *Genome research* **2012**;22:568-76
293. Cingolani P, Platts A, Wang le L, Coon M, Nguyen T, Wang L, *et al.* A program for annotating and predicting the effects of single nucleotide polymorphisms, SnpEff: SNPs in the genome of *Drosophila melanogaster* strain w1118; iso-2; iso-3. *Fly* **2012**;6:80-92
294. Chalmers ZR, Connelly CF, Fabrizio D, Gay L, Ali SM, Ennis R, *et al.* Analysis of 100,000 human cancer genomes reveals the landscape of tumor mutational burden. *Genome Medicine* **2017**;9:34
295. Ianevski A, Giri AK, Aittokallio T. SynergyFinder 2.0: visual analytics of multi-drug combination synergies. *Nucleic acids research* **2020**;48:W488-W93
296. Domingo-Fernandez R, Watters K, Piskareva O, Stallings RL, Bray I. The role of genetic and epigenetic alterations in neuroblastoma disease pathogenesis. *Pediatric Surgery International* **2012**;29:101-19
297. Murphy DM, Buckley PG, Das S, Watters KM, Bryan K, Stallings RL. Co-localization of the oncogenic transcription factor MYCN and the DNA methyl binding protein MeCP2 at genomic sites in neuroblastoma. *PLoS One* **2011**;6:e21436
298. Prigent C, Dimitrov S. Phosphorylation of serine 10 in histone H3, what for? *Journal of cell science* **2003**;116:3677-85
299. Ling YH, Consoli U, Tornos C, Andreeff M, Perez-Soler R. Accumulation of cyclin B1, activation of cyclin B1-dependent kinase and induction of programmed cell death in human epidermoid carcinoma KB cells treated with taxol. *International journal of cancer* **1998**;75:925-32
300. Trigg RM, Turner SD. ALK in Neuroblastoma: Biological and Therapeutic Implications. *Cancers* **2018**;10:113
301. Del Grosso F, De Mariano M, Passoni L, Luksch R, Tonini GP, Longo L. Inhibition of N-linked glycosylation impairs ALK phosphorylation and disrupts pro-survival signaling in neuroblastoma cell lines. *BMC cancer* **2011**;11:525
302. Hain KO, Colin DJ, Rastogi S, Allan LA, Clarke PR. Prolonged mitotic arrest induces a caspase-dependent DNA damage response at telomeres that determines cell survival. *Scientific reports* **2016**;6:26766

303. Orth JD, Loewer A, Lahav G, Mitchison TJ. Prolonged mitotic arrest triggers partial activation of apoptosis, resulting in DNA damage and p53 induction. *Molecular biology of the cell* **2012**;23:567-76
304. Edmondson R, Broglie JJ, Adcock AF, Yang L. Three-dimensional cell culture systems and their applications in drug discovery and cell-based biosensors. *ASSAY and Drug Development Technologies* **2014**;12:207-18
305. Izumchenko E, Paz K, Ciznadija D, Sloma I, Katz A, Vasquez-Dunddel D, *et al.* Patient-derived xenografts effectively capture responses to oncology therapy in a heterogeneous cohort of patients with solid tumors. *Annals of oncology* **2017**;28:2595-605
306. Maris JM, Hogarty MD, Bagatell R, Cohn SL. Neuroblastoma. *The Lancet* **2007**;369:2106-20
307. Miettinen M, Rapola J. Synaptophysin - an immuno-histochemical marker for childhood neuroblastoma. *Acta pathologica, microbiologica, et immunologica Scandinavica Section A, Pathology* **1987**;95:167-70
308. Wirnsberger GH, Becker H, Ziervogel K, Höfler H. Diagnostic immunohistochemistry of neuroblastic tumors. *The American journal of surgical pathology* **1992**;16:49-57
309. Campana D, Nori F, Piscitelli L, Morselli-Labate AM, Pezzilli R, Corinaldesi R, *et al.* Chromogranin A: is it a useful marker of neuroendocrine tumors? *Journal of Clinical Oncology* **2007**;25:1967-73
310. Wiedenmann B, Franke WW, Kuhn C, Moll R, Gould VE. Synaptophysin: a marker protein for neuroendocrine cells and neoplasms. *Proc Natl Acad Sci U S A* **1986**;83:3500-4
311. Plantaz D, Mohapatra G, Matthay KK, Pellarin M, Seeger RC, Feuerstein BG. Gain of chromosome 17 is the most frequent abnormality detected in neuroblastoma by comparative genomic hybridization. *Am J Pathol* **1997**;150:81-9
312. Stallings RL, Howard J, Dunlop A, Mullarkey M, McDermott M, Breatnach F, *et al.* Are gains of chromosomal regions 7q and 11p important abnormalities in neuroblastoma? *Cancer genetics and cytogenetics* **2003**;140:133-7
313. Genovese I, Ilari A, Assaraf YG, Fazi F, Colotti G. Not only P-glycoprotein: Amplification of the ABCB1-containing chromosome region 7q21 confers multidrug resistance upon cancer cells by coordinated overexpression of an assortment of resistance-related proteins. *Drug Resistance Updates* **2017**;32:23-46
314. Shah MA, Schwartz GK. Cell cycle-mediated drug resistance: an emerging concept in cancer therapy. *Clinical cancer research* **2001**;7:2168-81
315. Goldoni M, Johansson C. A mathematical approach to study combined effects of toxicants in vitro: evaluation of the Bliss independence criterion and the Loewe additivity model. *Toxicology in vitro : an international journal published in association with BIBRA* **2007**;21:759-69
316. Komarova NL, Wodarz D. Drug resistance in cancer: principles of emergence and prevention. *Proc Natl Acad Sci U S A* **2005**;102:9714-9
317. Basta NO, Halliday GC, Makin G, Birch J, Feltbower R, Bown N, *et al.* Factors associated with recurrence and survival length following relapse in patients with neuroblastoma. *British journal of cancer* **2016**;115:1048-57

References

318. Armstrong DK, Spriggs D, Levin J, Poulin R, Lane S. Hematologic safety and tolerability of topotecan in recurrent ovarian cancer and small cell lung cancer: an integrated analysis. *The oncologist* **2005**;10:686-94
319. Holzel M, Huang S, Koster J, Ora I, Lakeman A, Caron H, *et al.* NF1 is a tumor suppressor in neuroblastoma that determines retinoic acid response and disease outcome. *Cell* **2010**;142:218-29
320. Hamilton M, Wolfman A. Ha-ras and N-ras regulate MAPK activity by distinct mechanisms in vivo. *Oncogene* **1998**;16:1417-28
321. Cole KA, Maris JM. New strategies in refractory and recurrent neuroblastoma: translational opportunities to impact patient outcome. *Clinical cancer research* **2012**;18:2423-8
322. Padovan-Merhar OM, Raman P. Enrichment of targetable mutations in the relapsed neuroblastoma genome. *PLoS Genet* **2016**;12:e1006501
323. Schramm A, Köster J, Assenov Y, Althoff K, Peifer M, Mahlow E, *et al.* Mutational dynamics between primary and relapse neuroblastomas. *Nature genetics* **2015**;47:872-7
324. Zage PE. Novel therapies for relapsed and refractory neuroblastoma. *Children* **2018**;5:148
325. London WB, Bagatell R, Weigel BJ, Fox E, Guo D, Van Ryn C, *et al.* Historical time to disease progression and progression-free survival in patients with recurrent/refractory neuroblastoma treated in the modern era on Children's Oncology Group early-phase trials. *Cancer* **2017**;123:4914-23
326. van Vuuren RJ, Visagie MH, Theron AE, Joubert AM. Antimitotic drugs in the treatment of cancer. *Cancer chemotherapy and pharmacology* **2015**;76:1101-12
327. Brouhard GJ, Rice LM. Microtubule dynamics: an interplay of biochemistry and mechanics. *Nature reviews Molecular cell biology* **2018**;19:451-63
328. Sioka C, Kyritsis AP. Central and peripheral nervous system toxicity of common chemotherapeutic agents. *Cancer chemotherapy and pharmacology* **2009**;63:761-7
329. Kapitein LC, Peterman EJ, Kwok BH, Kim JH, Kapoor TM, Schmidt CF. The bipolar mitotic kinesin Eg5 moves on both microtubules that it crosslinks. *Nature* **2005**;435:114-8
330. Hu H, Xiao X, Li S, Jia X, Guo X, Zhang Q. KIF11 mutations are a common cause of autosomal dominant familial exudative vitreoretinopathy. *The British journal of ophthalmology* **2016**;100:278-83
331. Rao FQ, Cai XB, Cheng FF, Cheng W, Fang XL, Li N, *et al.* Mutations in LRP5, FZD4, TSPAN12, NDP, ZNF408, or KIF11 genes account for 38.7% of Chinese patients with familial exudative vitreoretinopathy. *Investigative ophthalmology & visual science* **2017**;58:2623-9
332. Mears K, Bakall B, Harney LA, Penticoff JA, Stone EM. Autosomal dominant microcephaly associated with congenital lymphedema and chorioretinopathy due to a novel mutation in KIF11. *JAMA ophthalmology* **2015**;133:720-1
333. Schlögel MJ, Mendola A, Fastré E, Vasudevan P, Devriendt K, de Ravel TJ, *et al.* No evidence of locus heterogeneity in familial microcephaly with or without chorioretinopathy, lymphedema, or mental retardation syndrome. *Orphanet journal of rare diseases* **2015**;10:52

334. Fernández-Blanco B, Berbegall AP, Martín-Vañó S, Castel V, Navarro S, Noguera R. Imbalance between genomic gain and loss identifies high-risk neuroblastoma patients with worse outcomes. *Neoplasia* **2021**;23:12-20
335. García-Higuera I, Manchado E, Dubus P, Cañamero M, Méndez J, Moreno S, *et al.* Genomic stability and tumour suppression by the APC/C cofactor Cdh1. *Nature cell biology* **2008**;10:802-11
336. Penas C, Ramachandran V, Ayad NG. The APC/C ubiquitin ligase: from cell biology to tumorigenesis. *Frontiers in oncology* **2012**;1:60-
337. Bradner JE, Hnisz D, Young RA. Transcriptional Addiction in Cancer. *Cell* **2017**;168:629-43
338. Liu M, Aneja R, Sun X, Xie S, Wang H, Wu X, *et al.* Parkin regulates Eg5 expression by Hsp70 ubiquitination-dependent inactivation of c-Jun NH2-terminal kinase. *The Journal of biological chemistry* **2008**;283:35783-8
339. Costa RH. FoxM1 dances with mitosis. *Nature cell biology* **2005**;7:108-10
340. Liao G-B, Li X-Z, Zeng S, Liu C, Yang S-M, Yang L, *et al.* Regulation of the master regulator FOXM1 in cancer. *Cell Commun Signal* **2018**;16:57
341. Wang Z, Park HJ, Carr JR, Chen YJ, Zheng Y, Li J, *et al.* FoxM1 in tumorigenicity of the neuroblastoma cells and renewal of the neural progenitors. *Cancer research* **2011**;71:4292-302
342. Thiru P, Kern DM, McKinley KL, Monda JK, Rago F, Su K-C, *et al.* Kinetochores are coordinately up-regulated in human tumors as part of a FoxM1-related cell division program. *Molecular biology of the cell* **2014**;25:1983-94
343. Chen X, Müller GA, Quaaas M, Fischer M, Han N, Stutchbury B, *et al.* The forkhead transcription factor FOXM1 controls cell cycle-dependent gene expression through an atypical chromatin binding mechanism. *Molecular and cellular biology* **2013**;33:227-36
344. Grant GD, Brooks L, 3rd, Zhang X, Mahoney JM, Martyanov V, Wood TA, *et al.* Identification of cell cycle-regulated genes periodically expressed in U2OS cells and their regulation by FOXM1 and E2F transcription factors. *Molecular biology of the cell* **2013**;24:3634-50
345. Carter SL, Eklund AC, Kohane IS, Harris LN, Szallasi Z. A signature of chromosomal instability inferred from gene expression profiles predicts clinical outcome in multiple human cancers. *Nature genetics* **2006**;38:1043-8
346. Chin GM, Herbst R. Induction of apoptosis by monastrol, an inhibitor of the mitotic kinesin Eg5, is independent of the spindle checkpoint. *Mol Cancer Ther* **2006**;5:2580-91
347. Gong D, Ferrell JE, Jr. The roles of cyclin A2, B1, and B2 in early and late mitotic events. *Molecular biology of the cell* **2010**;21:3149-61
348. Wei Y, Mizzen CA, Cook RG, Gorovsky MA, Allis CD. Phosphorylation of histone H3 at serine 10 is correlated with chromosome condensation during mitosis and meiosis in *Tetrahymena*. *Proc Natl Acad Sci U S A* **1998**;95:7480-4
349. Eichhorn JM, Sakurikar N, Alford SE, Chu R, Chambers TC. Critical role of anti-apoptotic Bcl-2 protein phosphorylation in mitotic death. *Cell death & disease* **2013**;4:e834

References

350. Bah N, Mailliet L, Ryan J, Dubreil S, Gautier F, Letai A, *et al.* Bcl-xL controls a switch between cell death modes during mitotic arrest. *Cell death & disease* **2014**;5:e1291
351. Haschka MD, Soratroi C, Kirschnek S, Häcker G, Hilbe R, Geley S, *et al.* The NOXA–MCL1–BIM axis defines lifespan on extended mitotic arrest. *Nature Communications* **2015**;6:6891
352. Kale J, Osterlund EJ, Andrews DW. BCL-2 family proteins: changing partners in the dance towards death. *Cell death and differentiation* **2018**;25:65-80
353. Terrano DT, Upreti M, Chambers TC. Cyclin-dependent kinase 1-mediated Bcl-xL/Bcl-2 phosphorylation acts as a functional link coupling mitotic arrest and apoptosis. *Molecular and cellular biology* **2010**;30:640-56
354. Harley ME, Allan LA, Sanderson HS, Clarke PR. Phosphorylation of Mcl-1 by CDK1-cyclin B1 initiates its Cdc20-dependent destruction during mitotic arrest. *Embo j* **2010**;29:2407-20
355. Wertz IE, Kusam S, Lam C, Okamoto T, Sandoval W, Anderson DJ, *et al.* Sensitivity to antitubulin chemotherapeutics is regulated by MCL1 and FBW7. *Nature* **2011**;471:110-4
356. Chu R, Terrano DT, Chambers TC. Cdk1/cyclin B plays a key role in mitotic arrest-induced apoptosis by phosphorylation of Mcl-1, promoting its degradation and freeing Bak from sequestration. *Biochemical pharmacology* **2012**;83:199-206
357. Haschka M, Karbon G, Fava LL, Villunger A. Perturbing mitosis for anti-cancer therapy: is cell death the only answer? *EMBO reports* **2018**;19:e45440
358. Carter BZ, Mak DH, Woessner R, Gross S, Schober WD, Estrov Z, *et al.* Inhibition of KSP by ARRY-520 induces cell cycle block and cell death via the mitochondrial pathway in AML cells. *Leukemia* **2009**;23:1755-62
359. Woessner R, Tunquist B, Lemieux C, Chlipala E, Jackinsky S, Dewolf W, Jr., *et al.* ARRY-520, a novel KSP inhibitor with potent activity in hematological and taxane-resistant tumor models. *Anticancer research* **2009**;29:4373-80
360. Jungwirth G, Yu T, Cao J, Eddine MA, Moustafa M, Warta R, *et al.* KIF11 inhibitors filanesib and ispinesib inhibit meningioma growth in vitro and in vivo. *Cancer letters* **2021**;506:1-10
361. Purcell JW, Davis J, Reddy M, Martin S, Samayoa K, Vo H, *et al.* Activity of the kinesin spindle protein inhibitor ispinesib (SB-715992) in models of breast cancer. *Clinical cancer research* **2010**;16:566-76
362. Gampa G, Kenchappa RS, Mohammad AS, Parrish KE, Kim M, Crish JF, *et al.* Enhancing brain retention of a KIF11 inhibitor significantly improves its efficacy in a mouse model of glioblastoma. *Scientific reports* **2020**;10:6524
363. Carol H, Lock R, Houghton PJ, Morton CL, Kolb EA, Gorlick R, *et al.* Initial testing (stage 1) of the kinesin spindle protein inhibitor ispinesib by the pediatric preclinical testing program. *Pediatric blood & cancer* **2009**;53:1255-63
364. Dillekås H, Rogers MS, Straume O. Are 90% of deaths from cancer caused by metastases? *Cancer Med* **2019**;8:5574-6
365. Surova O, Zhivotovsky B. Various modes of cell death induced by DNA damage. *Oncogene* **2013**;32:3789-97

366. Bhatia S, Robison LL, Oberlin O, Greenberg M, Bunin G, Fossati-Bellani F, *et al.* Breast cancer and other second neoplasms after childhood Hodgkin's disease. *The New England journal of medicine* **1996**;334:745-51
367. Neglia JP, Meadows AT, Robison LL, Kim TH, Newton WA, Ruymann FB, *et al.* Second neoplasms after acute lymphoblastic leukemia in childhood. *The New England journal of medicine* **1991**;325:1330-6
368. Applebaum MA, Vaksman Z, Lee SM, Hungate EA, Henderson TO, London WB, *et al.* Neuroblastoma survivors are at increased risk for second malignancies: A report from the International Neuroblastoma Risk Group Project. *Eur J Cancer* **2017**;72:177-85
369. Marcus AI, Peters U, Thomas SL, Garrett S, Zelnak A, Kapoor TM, *et al.* Mitotic kinesin inhibitors induce mitotic arrest and cell death in Taxol-resistant and -sensitive cancer cells. *The Journal of biological chemistry* **2005**;280:11569-77
370. Kavallaris M. Microtubules and resistance to tubulin-binding agents. *Nature reviews Cancer* **2010**;10:194-204
371. Mitchison TJ. The proliferation rate paradox in antimetabolic chemotherapy. *Molecular biology of the cell* **2012**;23:1-6
372. Castillo A, Justice MJ. The kinesin related motor protein, Eg5, is essential for maintenance of pre-implantation embryogenesis. *Biochem Biophys Res Commun* **2007**;357:694-9
373. Gomez HL, Philco M, Pimentel P, Kiyani M, Monsalvo ML, Conlan MG, *et al.* Phase I dose-escalation and pharmacokinetic study of ispinesib, a kinesin spindle protein inhibitor, administered on days 1 and 15 of a 28-day schedule in patients with no prior treatment for advanced breast cancer. *Anti-cancer drugs* **2012**;23:335-41
374. LoRusso PM, Goncalves PH, Casetta L, Carter JA, Litwiler K, Roseberry D, *et al.* First-in-human phase 1 study of filanesib (ARRY-520), a kinesin spindle protein inhibitor, in patients with advanced solid tumors. *Investigational new drugs* **2015**;33:440-9
375. Shi J, Gao P, Song Y, Chen X, Li Y, Zhang C, *et al.* Efficacy and safety of taxane-based systemic chemotherapy of advanced gastric cancer: A systematic review and meta-analysis. *Scientific reports* **2017**;7:5319
376. Asbaghi Y, Thompson LL, Lichtensztejn Z, McManus KJ. KIF11 silencing and inhibition induces chromosome instability that may contribute to cancer. *Genes, chromosomes & cancer* **2017**;56:668-80
377. Vargas-Rondón N, Villegas VE, Rondón-Lagos M. The role of chromosomal instability in cancer and therapeutic responses. *Cancers* **2017**;10:4
378. Theoclitou ME, Aquila B, Block MH, Brassil PJ, Castriotta L, Code E, *et al.* Discovery of (+)-N-(3-aminopropyl)-N-[1-(5-benzyl-3-methyl-4-oxo-[1,2]thiazolo[5,4-d]pyrimidin-6-yl)-2-methylpropyl]-4-methylbenzamide (AZD4877), a kinesin spindle protein inhibitor and potential anticancer agent. *Journal of medicinal chemistry* **2011**;54:6734-50
379. Gerecitano JF, Stephenson JJ, Lewis NL, Osmukhina A, Li J, Wu K, *et al.* A Phase I trial of the kinesin spindle protein (Eg5) inhibitor AZD4877 in patients with solid and lymphoid malignancies. *Investigational new drugs* **2013**;31:355-62
380. Kantarjian HM, Padmanabhan S, Stock W, Tallman MS, Curt GA, Li J, *et al.* Phase I/II multicenter study to assess the safety, tolerability, pharmacokinetics and pharmacodynamics

References

- of AZD4877 in patients with refractory acute myeloid leukemia. *Investigational new drugs* **2012**;30:1107-15
381. Cox CD, Coleman PJ, Breslin MJ, Whitman DB, Garbaccio RM, Fraley ME, *et al.* Kinesin spindle protein (KSP) inhibitors. 9. Discovery of (2S)-4-(2,5-difluorophenyl)-n-[(3R,4S)-3-fluoro-1-methylpiperidin-4-yl]-2-(hydroxymethyl)-N-methyl-2-phenyl-2,5-dihydro-1H-pyrrole-1-carboxamide (MK-0731) for the treatment of taxane-refractory cancer. *Journal of medicinal chemistry* **2008**;51:4239-52
382. Holen K, DiPaola R, Liu G, Tan AR, Wilding G, Hsu K, *et al.* A phase I trial of MK-0731, a kinesin spindle protein (KSP) inhibitor, in patients with solid tumors. *Investigational new drugs* **2012**;30:1088-95
383. Jeay S, Ali S, Chen C-R, Uppalapati U, Senator D, Chan T, *et al.* Discovery of a novel Eg5 kinesin inhibitor, ARQ 621, with potent antitumor activity while sparing bone marrow-derived cells. *Cancer research* **2008**;68:656
384. Chen LC, Rosen LS, Iyengar T, Goldman JW, Savage R, Kazakin J, *et al.* First-in-human study with ARQ 621, a novel inhibitor of Eg5: Final results from the solid tumors cohort. *Journal of Clinical Oncology* **2011**;29:3076
385. Ye XS, Fan L, Van Horn RD, Nakai R, Ohta Y, Akinaga S, *et al.* A novel eg5 Inhibitor (LY2523355) causes mitotic arrest and apoptosis in cancer cells and shows potent antitumor activity in xenograft tumor models. *Molecular Cancer Therapeutics* **2015**;14:2463-72
386. Wakui H, Yamamoto N, Kitazono S, Mizugaki H, Nakamichi S, Fujiwara Y, *et al.* A phase 1 and dose-finding study of LY2523355 (litronesib), an Eg5 inhibitor, in Japanese patients with advanced solid tumors. *Cancer chemotherapy and pharmacology* **2014**;74:15-23
387. Infante JR, Patnaik A, Verschraegen CF, Olszanski AJ, Shaheen M, Burris HA, *et al.* Two Phase 1 dose-escalation studies exploring multiple regimens of litronesib (LY2523355), an Eg5 inhibitor, in patients with advanced cancer. *Cancer chemotherapy and pharmacology* **2017**;79:315-26
388. Tang PA, Siu LL, Chen EX, Hotte SJ, Chia S, Schwarz JK, *et al.* Phase II study of ispinesib in recurrent or metastatic squamous cell carcinoma of the head and neck. *Investigational new drugs* **2008**;26:257-64
389. Knox JJ, Gill S, Synold TW, Biagi JJ, Major P, Feld R, *et al.* A phase II and pharmacokinetic study of SB-715992, in patients with metastatic hepatocellular carcinoma: a study of the National Cancer Institute of Canada Clinical Trials Group (NCIC CTG IND.168). *Investigational new drugs* **2008**;26:265-72
390. Lee RT, Beekman KE, Hussain M, Davis NB, Clark JI, Thomas SP, *et al.* A University of Chicago consortium phase II trial of SB-715992 in advanced renal cell cancer. *Clinical genitourinary cancer* **2008**;6:21-4
391. Souid AK, Dubowy RL, Ingle AM, Conlan MG, Sun J, Blaney SM, *et al.* A pediatric phase I trial and pharmacokinetic study of ispinesib: a Children's Oncology Group phase I consortium study. *Pediatric blood & cancer* **2010**;55:1323-8
392. Burris HA, 3rd, Jones SF, Williams DD, Kathman SJ, Hodge JP, Pandite L, *et al.* A phase I study of ispinesib, a kinesin spindle protein inhibitor, administered weekly for three consecutive weeks of a 28-day cycle in patients with solid tumors. *Investigational new drugs* **2011**;29:467-72

393. Beer TM, Goldman B, Synold TW, Ryan CW, Vasist LS, Van Veldhuizen PJ, Jr., *et al.* Southwest Oncology Group phase II study of ispinesib in androgen-independent prostate cancer previously treated with taxanes. *Clinical genitourinary cancer* **2008**;6:103-9
394. Blagden SP, Molife LR, Seebaran A, Payne M, Reid AH, Protheroe AS, *et al.* A phase I trial of ispinesib, a kinesin spindle protein inhibitor, with docetaxel in patients with advanced solid tumours. *British journal of cancer* **2008**;98:894-9
395. Holen KD, Belani CP, Wilding G, Ramalingam S, Volkman JL, Ramanathan RK, *et al.* A first in human study of SB-743921, a kinesin spindle protein inhibitor, to determine pharmacokinetics, biologic effects and establish a recommended phase II dose. *Cancer chemotherapy and pharmacology* **2011**;67:447-54
396. O'Connor OA, Gerecitano J, Van Deventer H, Hainsworth J, Zullo KM, Saikali K, *et al.* The addition of granulocyte-colony stimulating factor shifts the dose limiting toxicity and markedly increases the maximum tolerated dose and activity of the kinesin spindle protein inhibitor SB-743921 in patients with relapsed or refractory lymphoma: results of an international, multicenter phase I/II study. *Leukemia & lymphoma* **2015**;56:2585-91
397. Taberero J, Shapiro GI, LoRusso PM, Cervantes A, Schwartz GK, Weiss GJ, *et al.* First-in-humans trial of an RNA interference therapeutic targeting VEGF and KSP in cancer patients with liver involvement. *Cancer discovery* **2013**;3:406-17
398. Khoury HJ, Garcia-Manero G, Borthakur G, Kadia T, Foudray MC, Arellano M, *et al.* A phase 1 dose-escalation study of ARRY-520, a kinesin spindle protein inhibitor, in patients with advanced myeloid leukemias. *Cancer* **2012**;118:3556-64
399. Shah JJ, Kaufman JL, Zonder JA, Cohen AD, Bensinger WI, Hilder BW, *et al.* A Phase 1 and 2 study of Filanesib alone and in combination with low-dose dexamethasone in relapsed/refractory multiple myeloma. *Cancer* **2017**;123:4617-30
400. Chari A, Htut M, Zonder JA, Fay JW, Jakubowiak AJ, Levy JB, *et al.* A phase 1 dose-escalation study of filanesib plus bortezomib and dexamethasone in patients with recurrent/refractory multiple myeloma. *Cancer* **2016**;122:3327-35
401. Lee HC, Shah JJ, Feng L, Manasanch EE, Lu R, Morphey A, *et al.* A phase 1 study of filanesib, carfilzomib, and dexamethasone in patients with relapsed and/or refractory multiple myeloma. *Blood cancer journal* **2019**;9:80
402. Ocio EM, Motlló C, Rodríguez-Otero P, Martínez-López J. Filanesib in combination with pomalidomide and dexamethasone in refractory MM patients: safety and efficacy, and association with alpha 1-acid glycoprotein (AAG) levels. Phase Ib/II Pomdefil clinical trial conducted by the Spanish MM group. *British journal of haematology* **2021**;192:522-30
403. Mross KB, Scharr D, Richly H, Frost A, Bauer S, Krauss B, *et al.* First-in-human study of 4SC-205 (AEGIS), a novel oral inhibitor of Eg5 kinesin spindle protein. *Journal of Clinical Oncology* **2014**;32:2564
404. Tanenbaum ME, Macůrek L, Janssen A, Geers EF, Alvarez-Fernández M, Medema RH. Kif15 cooperates with eg5 to promote bipolar spindle assembly. *Curr Biol* **2009**;19:1703-11
405. Sturgill EG, Norris SR, Guo Y, Ohi R. Kinesin-5 inhibitor resistance is driven by kinesin-12. *The Journal of cell biology* **2016**;213:213-27

References

406. Raaijmakers JA, van Heesbeen RG, Meaders JL, Geers EF, Fernandez-Garcia B, Medema RH, *et al.* Nuclear envelope-associated dynein drives prophase centrosome separation and enables Eg5-independent bipolar spindle formation. *Embo j* **2012**;31:4179-90
407. Mardin BR, Isokane M, Cosenza MR, Krämer A, Ellenberg J, Fry AM, *et al.* EGF-induced centrosome separation promotes mitotic progression and cell survival. *Developmental cell* **2013**;25:229-40
408. Whalley HJ, Porter AP, Diamantopoulou Z, White GR, Castañeda-Saucedo E, Malliri A. Cdk1 phosphorylates the Rac activator Tiam1 to activate centrosomal Pak and promote mitotic spindle formation. *Nature Communications* **2015**;6:7437
409. Negrini S, Gorgoulis VG, Halazonetis TD. Genomic instability—an evolving hallmark of cancer. *Nature reviews Molecular cell biology* **2010**;11:220-8
410. Maliga Z, Mitchison TJ. Small-molecule and mutational analysis of allosteric Eg5 inhibition by monastrol. *BMC Chem Biol* **2006**;6:2
411. Brier S, Lemaire D, DeBonis S, Forest E, Kozielski F. Molecular dissection of the inhibitor binding pocket of mitotic kinesin Eg5 reveals mutants that confer resistance to antimitotic agents. *Journal of molecular biology* **2006**;360:360-76
412. Kasap C, Elemento O, Kapoor TM. DrugTargetSeqR: a genomics- and CRISPR-Cas9-based method to analyze drug targets. *Nat Chem Biol* **2014**;10:626-8
413. Wacker SA, Houghtaling BR, Elemento O, Kapoor TM. Using transcriptome sequencing to identify mechanisms of drug action and resistance. *Nat Chem Biol* **2012**;8:235-7
414. Mansoori B, Mohammadi A, Davudian S, Shirjang S, Baradaran B. The Different Mechanisms of Cancer Drug Resistance: A Brief Review. *Adv Pharm Bull* **2017**;7:339-48
415. Vasan N, Baselga J, Hyman DM. A view on drug resistance in cancer. *Nature* **2019**;575:299-309
416. Groenendijk FH, Bernards R. Drug resistance to targeted therapies: déjà vu all over again. *Mol Oncol* **2014**;8:1067-83
417. Basso AD, Liu M, Dai C, Gray K, Nale L, Tevar S, *et al.* SCH 2047069, a novel oral kinesin spindle protein inhibitor, shows single-agent antitumor activity and enhances the efficacy of chemotherapeutics. *Mol Cancer Ther* **2010**;9:2993-3002
418. Hansford LM, McKee AE, Zhang L, George RE, Gerstle JT, Thorner PS, *et al.* Neuroblastoma cells isolated from bone marrow metastases contain a naturally enriched tumor-initiating cell. *Cancer research* **2007**;67:11234-43

ANNEXES



8. Annexes

Table A1. Characteristics of neuroblastoma patients analyzed by immunoblastochemistry.

| Patient | Category | Age (months) | Grade differentiation | Ploidy | MYCN | Genomic profile | LOH 1p36 | LOH 11q | Gain 17q23 | Stage | Stage M | Risk category | KIP11 expression |
|------------|----------------------|--------------|-----------------------|------------|---------------|-----------------|----------|---------|------------|-------|---------|---------------|------------------|
| Patient 1 | Neuroblastoma | ≥18 | pdNB | Triploid | Non amplified | NCA | No | No | No | 1 | 0 | Non high risk | Low |
| Patient 2 | Neuroblastoma | <18 | pdNB | Triploid | Non amplified | NCA | No | No | No | 2 | 0 | Non high risk | Low |
| Patient 3 | Neuroblastoma | <18 | pdNB | Triploid | Non amplified | SCA | No | No | Yes | 4S | 0 | Non high risk | Low |
| Patient 4 | Neuroblastoma | <18 | pdNB | Triploid | Non amplified | NCA | No | No | No | 4S | 0 | Non high risk | Low |
| Patient 5 | Neuroblastoma | <18 | pdNB | Triploid | Non amplified | NCA | No | No | No | 4 | 1 | Non high risk | Low |
| Patient 6 | Neuroblastoma | <18 | dNB | Triploid | Non amplified | NCA | No | No | No | 2 | 0 | Non high risk | Low |
| Patient 7 | Neuroblastoma | ≥18 | dNB | Triploid | Non amplified | NCA | No | No | No | 3 | 0 | Non high risk | Low |
| Patient 8 | Ganglioneuroblastoma | ≥18 | - | Triploid | Non amplified | NCA | No | No | No | 1 | 0 | Non high risk | Low |
| Patient 9 | Neuroblastoma | <18 | pdNB | Diploid | Non amplified | NCA | No | No | No | 1 | 0 | Non high risk | Low |
| Patient 10 | Neuroblastoma | ≥18 | dNB | Diploid | Non amplified | NCA | No | No | No | - | - | Non high risk | Low |
| Patient 11 | Ganglioneuroblastoma | ≥18 | - | Diploid | Non amplified | NCA | No | No | No | 1 | 0 | Non high risk | Low |
| Patient 12 | Ganglioneuroblastoma | ≥18 | - | Diploid | Non amplified | NCA | No | No | No | 1 | 0 | Non high risk | Low |
| Patient 13 | Neuroblastoma | ≥18 | pdNB | Tetraploid | Non amplified | NCA | No | No | No | - | - | Non high risk | Low |
| Patient 14 | Neuroblastoma | ≥18 | dNB | Diploid | Non amplified | - | - | No | - | 1 | 0 | Non high risk | High |
| Patient 15 | Ganglioneuroblastoma | - | - | - | Non amplified | SCA | Yes | No | No | 3 | 0 | Non high risk | High |
| Patient 16 | Neuroblastoma | <18 | pdNB | Diploid | Non amplified | SCA | No | No | Yes | 4S | 0 | Non high risk | High |
| Patient 17 | Ganglioneuroblastoma | ≥18 | - | Diploid | Non amplified | - | - | No | - | 1 | 0 | Non high risk | High |
| Patient 18 | Neuroblastoma | ≥18 | pdNB | - | Non amplified | - | - | No | - | 3 | 0 | Non high risk | High |
| Patient 19 | Ganglioneuroblastoma | ≥18 | - | Diploid | Non amplified | NCA | No | No | No | 4 | 1 | High risk | Low |
| Patient 20 | Neuroblastoma | ≥18 | pdNB | Diploid | Non amplified | SCA | No | Yes | Yes | 4 | 1 | High risk | Low |
| Patient 21 | Neuroblastoma | ≥18 | pdNB | - | Non amplified | SCA | Yes | Yes | Yes | 4 | 1 | High risk | High |
| Patient 22 | Neuroblastoma | ≥18 | uNB | Triploid | Non amplified | SCA | No | Yes | Yes | 4 | 1 | High risk | High |
| Patient 23 | Ganglioneuroblastoma | ≥18 | - | Diploid | Non amplified | SCA | Yes | Yes | No | 4 | 1 | High risk | High |
| Patient 24 | Neuroblastoma | ≥18 | pdNB | Triploid | Non amplified | SCA | No | Yes | Yes | 4 | 1 | High risk | High |
| Patient 25 | Neuroblastoma | ≥18 | pdNB | Tetraploid | Non amplified | NCA | No | No | No | 4 | 1 | High risk | High |

Abbreviations: uNB, undifferentiated neuroblastoma; pdNB, poorly differentiated neuroblastoma; dNB, differentiating neuroblastoma; NCA, numerical chromosomal alterations; YCA, segmental chromosomal alterations; M, metastasis.

PUBLICATIONS



9. Publications

1. **Masanas M**, Masiá N, Suárez-Cabrera L, Oliván M, Soriano A, Majem B, Devis-Jauregui L, Burgos-Panadero R, Jiménez C, Rodríguez-Sodupe P, Boloix A, Toledano I, Guillén G, Navarro A, Llobet-Navas D, Villanueva A, Sánchez de Toledo J, Roma J, Noguera R, Moreno L, Krauss R, Gallego S, Santamaria A, Segura MF. The oral KIF11 inhibitor 4SC-205 exhibits antitumor activity and potentiates standard and targeted therapies in primary and metastatic neuroblastoma models. *Clinical and Translational Medicine*. **2021**;11:e533.
2. Boloix A, Feiner-Gracia N, Köber M, Repetto J, Pascarella R, Soriano A, **Masanas M**, Segovia N, Vargas-Nadal G, Merlo-Mas J, Danino D, Abutbul-Ionita I, Foradada L, Roma J, Córdoba A, Sala S, Sánchez de Toledo J, Gallego S, Veciana J, Albertazzi L, Segura MF, Ventosa N. Engineering pH-sensitive stable nanovesicles for delivery of microRNA therapeutics. *Small*. **2021** (In press).
3. Jiménez C, Antonelli A, **Masanas M**, Soriano A, Devis-Jauregui L, Camacho J, Magdaleno A, Guillén G, Hladun R, Jubierre L, Roma J, Llobet-Navas D, Sánchez de Toledo J, Moreno L, Gallego S, Segura MF. Neuronal differentiation-related epigenetic regulator ZRF1 has independent prognostic value in neuroblastoma but is functionally dispensable *in vitro*. *Caners*. **2021**;13:4845.
4. Aguilera C, Hümmer S, **Masanas M**, Gabau E, Guitart M, Jeyaprakash AA, Segura MF, Santamaria A, Ruiz A. The novel KIF1A missense variant (R169T) strongly reduces microtubule stimulated ATPase activity and is associated with NESCAV syndrome. *Front Neurosci*. **2021**;15:618098.
5. Coccia E, **Masanas M**, López-Soriano J, Segura MF, Comella JX, Pérez-García MJ. FAIM Is Regulated by MiR-206, MiR-1-3p and MiR-133b. *Front Cell Dev Biol*. **2020**;8:584606.
6. París-Coderch L, Soriano A, Jiménez C, Erazo T, Muñoz-Guardiola P, **Masanas M**, Antonelli R, Boloix A, Alfón J, Pérez-Montoyo H, Yeste-Velasco M, Domènech C, Roma J, Sánchez de Toledo J, Moreno L, Lizcano JM, Gallego S, Segura MF. The antitumour drug ABTL0812 impairs neuroblastoma growth through endoplasmic reticulum stress-mediated autophagy and apoptosis. *Cell Death Dis*. **2020**;11:773.
7. Soriano A*, **Masanas M***, Boloix A, Masiá N, París-Coderch L, Piskareva O, Jiménez C, Henrich KO, Roma J, Westermann F, Stallings RL, Sábado C, de Toledo JS, Santamaria A, Gallego S, Segura MF. Functional high-throughput screening reveals miR-323a-5p and miR-342-5p as new tumor-suppressive microRNA for neuroblastoma. *Cell Mol Life Sci*. **2019**;6:2231-2243. (* authors contributed equally).
8. Boloix A, **Masanas M**, Jiménez C, Antonelli R, Soriano A, Roma J, Sánchez de Toledo J, Gallego S, Segura MF. Long Non-coding RNA PVT1 as a Prognostic and Therapeutic Target in Pediatric Cancer. *Front Oncol*. **2019**;9:1173.

Publications

9. Dopeso H, Rodrigues P, Bilic J, Bazzocco S, Cartón-García F, Macaya I, de Marcondes PG, Anguita E, **Masanas M**, Jiménez-Flores LM, Martínez-Barriocanal Á, Nieto R, Segura MF, Schwartz S Jr, Mariadason JM, Arango D. Mechanisms of inactivation of the tumour suppressor gene RHOA in colorectal cancer. *Br J Cancer*. **2018**;118:106-116.
10. Segura MF, Jubierre L, Li S, Soriano A, Koetz L, Gazieli-Sovran A, **Masanas M**, Kleffman K, Dankert JF, Walsh MJ, Hernando E. Krüppel-like factor 4 (KLF4) regulates the miR-183~96~182 cluster under physiologic and pathologic conditions. *Oncotarget*. **2017**;8:26298-26311.

THE ORAL KIF11 INHIBITOR 4SC-205 EXHIBITS ANTITUMOR
ACTIVITY AND POTENTIATES STANDARD AND TARGETED
THERAPIES IN PRIMARY AND METASTATIC
NEUROBLASTOMA MODELS

CLINICAL AND TRANSLATIONAL MEDICINE

Masanas M, Masiá N, Suárez-Cabrera L, Olivan M, Soriano A, Majem B, Devis-Jauregui L, Burgos-Panadero R, Jiménez C, Rodríguez-Sodupe P, Boloix A, Toledano I, Guillén G, Navarro A, Llobet-Navas D, Villanueva A, Sánchez de Toledo J, Roma J, Noguera R, Moreno L, Krauss R, Gallego S, Santamaria A, Segura MF.

DOI: 10.1002/ctm2.533

LETTER TO EDITOR

The oral KIF11 inhibitor 4SC-205 exhibits antitumor activity and potentiates standard and targeted therapies in primary and metastatic neuroblastoma models

Dear Editor,

Neuroblastoma remains incurable for most patients with high-risk disease.¹ Perturbation of transcription factors (MYCN and PHOX2B), kinases (ALK, MEK), and cell cycle regulators (CDK4/6, CHECK1), among other factors, make neuroblastoma cells highly proliferative, which is associated with poor patient outcomes.^{2,3} To circumvent the limitations of the classical microtubule poisons such as vinca alkaloids used in the treatment of neuroblastoma,¹ we sought to explore alternative mitotic regulators as new therapeutic targets for high-risk neuroblastoma patients. One of these mitotic spindle-specific proteins is kinesin family member 11 (KIF11), also known as kinesin spindle protein, kinesin-5, or Eg5, which is essential for bipolar spindle formation and mitotic progression in human cells.⁴

Transcriptomic analyses showed that the expression of multiple kinesins, including *KIF11* was higher in the high-risk neuroblastoma compared with low- and intermediate-risk groups (Figures 1A and S1; Table S1). Overall survival was significantly poorer in patients with high *KIF11* expression (Figure 1B–D; Table S2). *KIF11* high expression was identified as an independent prognostic factor of survival, together with risk assessment (HR = 3.051; Table S3) and found to be higher in patients with amplification of *MYCN*, 1p36 loss, or 17q23 gain (Figure 1E). At the protein level, KIF11 expression was detected in the cytoplasm of neuroblastic cells (Figure 1F) and showed higher expression compared to low- or intermediate-risk neuroblastoma samples ($p < 0.05$) and in tumors with segmental chromosome alterations such as 1p36, 11q deletion, and gain of 17q23 (Table S4). Kaplan–Meier analysis confirmed that high KIF11 protein expression was associated with shorter event-free and overall survival (Figures 1G and H). While there is a positive correlation between *KIF11* and *MYCN* mRNA expression levels, *MYCN* is neither sufficient, nor necessary for KIF11 expression (Figure S2).

According to functional genomics, neuroblastoma cells seem to be one of the cell types that are more dependent on the expression of KIF11 for survival being particularly sensitive to its pharmacological inhibition.⁵ Concurring with these observations, the silencing of KIF11 caused a reduction in cell viability (Figure S3A–C) and a 3–4 fold reduction in the growth of established neuroblastoma subcutaneous xenografts (Figure 2A–C and S3D–R). KIF11 inhibitors have moved forward toward phase 1 and 2 clinical trials in adult tumors,^{6,7} with very limited development for childhood cancer. Herein, we provide a complete pre-clinical characterization of the potent and highly selective KIF11 inhibitor, 4SC-205 (Figure 2D), the first oral KIF11 inhibitor that has been evaluated in phase I clinical trials in adult patients (NCT01065025). Compared to other KIF11 inhibitors, 4SC-205 can be administered daily, thus being able to hit the target in a more sustained manner. Neuroblastoma cells treated with 4SC-205 (Figure 2E; Table S5) displayed all the expected phenotypic features resulting from KIF11 inhibition such as the inability to form bipolar spindles (Figures 2F and S4A), cell cycle arrest during mitosis (Figure S4B–H), and induction of apoptosis (Figure S5), thereby confirming the high KIF11 specificity of this compound. While similar effects were observed in 3D spheroid cultures (Figure S6A–C), 4SC-205 did not affect the viability of differentiated cells (Figure S6D–G).

When used in vivo, 4SC-205 treated mice showed a remarkable shrinkage of the original SK-N-BE(2) subcutaneous xenograft (Figures 2G and 2H) or tumor growth delay in SK-N-AS xenografts (Figures 2J, 2K, and Figure S7). Increased phosphorylation of histone H3 and apoptotic hallmarks (i.e., processing of PARP) confirmed that the antitumor effect of 4SC-205 was comparable to that of genetic KIF11 silencing in vivo (Figures 2I, L). Transcriptomic analysis of the 4SC-205-treated tumors confirmed the expected genetic changes of arrested cells in mitosis

This is an open access article under the terms of the [Creative Commons Attribution](https://creativecommons.org/licenses/by/4.0/) License, which permits use, distribution and reproduction in any medium, provided the original work is properly cited.

© 2021 The Authors. *Clinical and Translational Medicine* published by John Wiley & Sons Australia, Ltd on behalf of Shanghai Institute of Clinical Bioinformatics

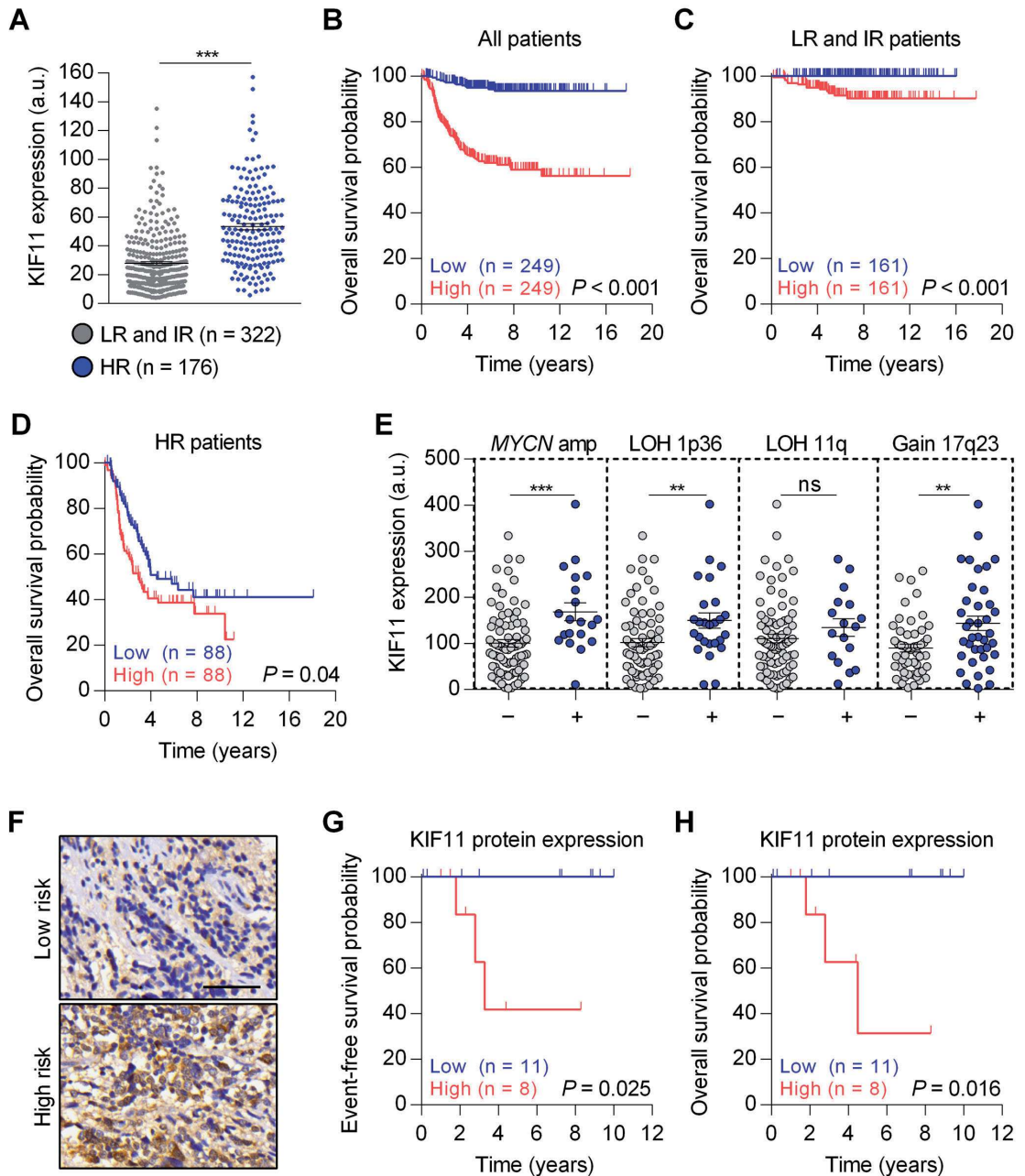


FIGURE 1 KIF11 expression is an independent prognostic factor of survival in neuroblastoma. (A) *KIF11* mRNA expression levels comparing low-/intermediate- with high-risk neuroblastoma tumors (GSE62564, $n = 498$). (B-D) Kaplan-Meier overall survival curve in a cohort of 498 patients based on *KIF11* mRNA expression (B) or stratified in low- and intermediate-risk (C) or high-risk (D) neuroblastoma subcohorts. (E) *KIF11* mRNA expression in neuroblastoma patients with different genomic alterations (GSE3960, $n = 101$). (F) Representative images of KIF11 immunohistochemistry in low- and high-risk neuroblastoma tissues. Scale bar indicates 50 μm . (G and H) Kaplan-Meier curves of event-free survival (G) and overall survival (H) based on KIF11 protein expression

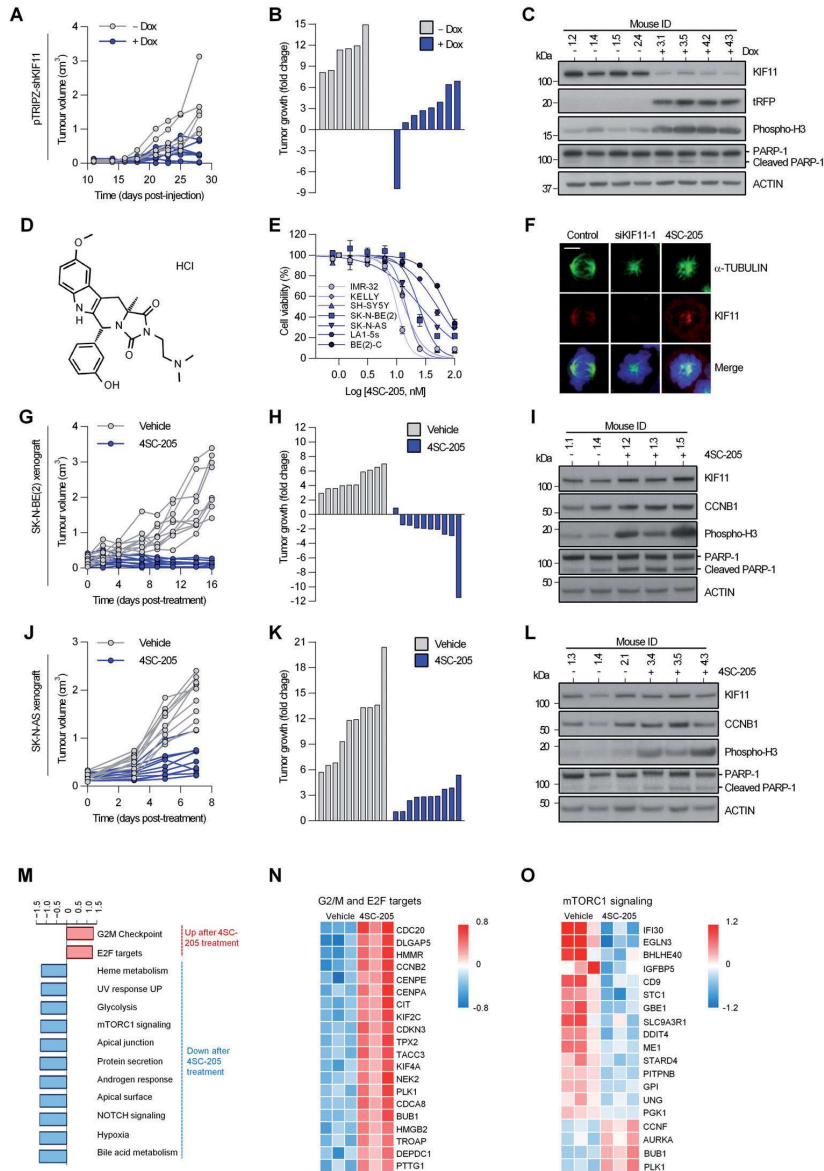


FIGURE 2 Genetic and pharmacological inhibition of KIF11 reduces tumor growth in subcutaneous neuroblastoma xenografts. (A) Analysis of tumor volume of SK-N-BE(2) cells transduced with an inducible shKIF11 lentiviral construct comparing the effects of KIF11 silencing (+Dox) versus control (-Dox). (B) Waterfall plot comparing the change in tumor volume at day 28 post-injection versus day 18, when doxycycline was added into the drinking water. (C) Western blot analysis of excised tumors at termination of the experiment. Turbo-RFP (tRFP) reporter expression was used as a control for shRNA transgene induction. (D) 4SC-205 chemical structure. (E) Dose-response curves of neuroblastoma cell lines treated with increasing concentrations of 4SC-205 for 48 h. IC₅₀ values are represented as the average of three independent experiments ± SEM. (F) Mitotic spindle immunofluorescence of SK-N-BE(2) cells transfected with siKIF11 or treated with 4SC-205 (25 nM) for 24 h. KIF11: red, α-TUBULIN: green, DAPI: blue. Scale bar, 5 μm. (G) Individual tumor growth of xenografts derived from SK-N-BE(2) comparing vehicle (*n* = 10) versus 40 mg/kg 4SC-205 (*n* = 10). (H) Waterfall plot comparing the change in tumor volume at day 16 post-treatment versus day 4. (I) Western blot analysis of cell-cycle and apoptosis-related proteins in SK-N-BE(2) resected tumors. (J) Tumor growth of subcutaneous xenograft derived from SK-N-AS treated with vehicle (*n* = 10) or 40 mg/kg 4SC-205 (*n* = 10). (K) Tumor volume fold change at day 7 post-treatment versus day 0. (L) Western blot analysis of resected tumors at the end of the experiment. (M) Gene set enrichment analysis of SK-N-BE(2) xenografts treated with vehicle or 4SC-205. Graph represents normalized enrichment score (NES) values of enriched sets with *p* < 0.05. (N and O) Heatmap representing top 20 differentially deregulated genes of G2/M checkpoint and E2F targets (N), and mTORC1 signaling-related genes (O)

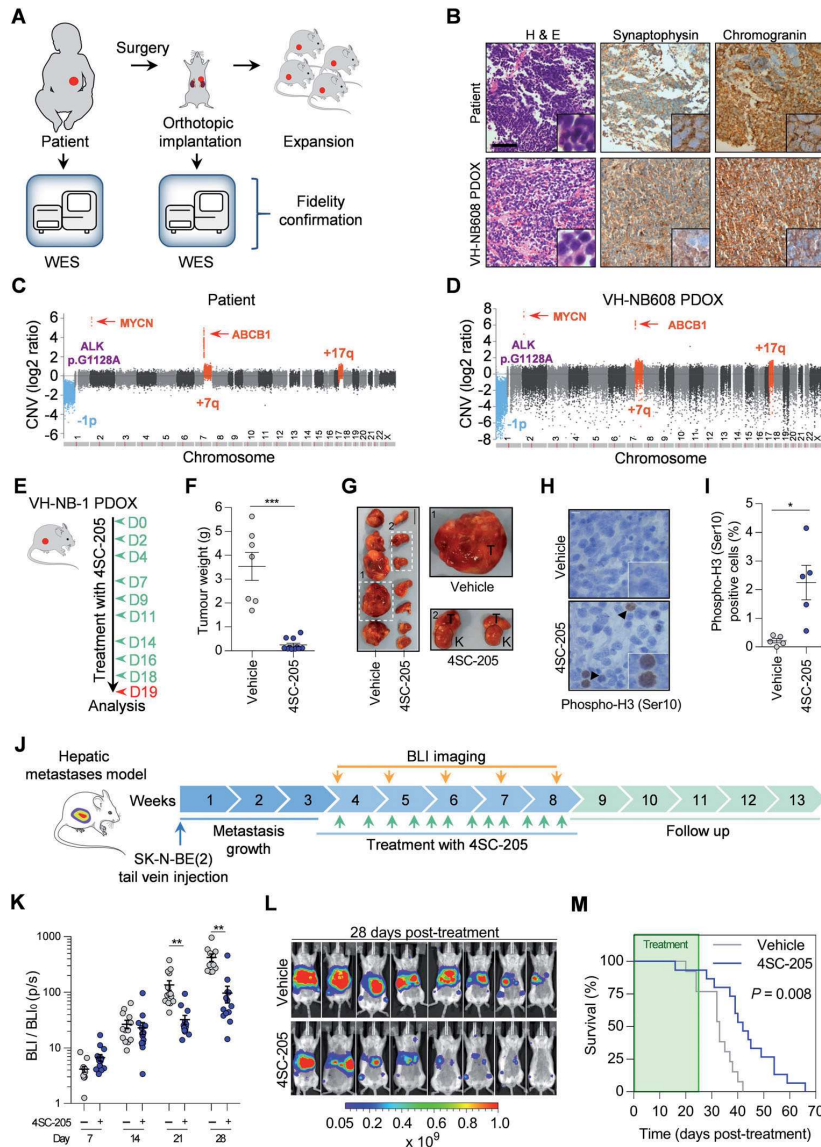


FIGURE 3 4SC-205 impairs PDXO growth and prolongs the survival of mice bearing neuroblastoma liver metastasis. (A) Schematic representation of PDXO generation and characterization. (B) Immunohistochemistry of neuroblastoma markers in FPPE tumor sections from the original tumor (upper panels) and after implantation in mice (lower panels). H&E: Hematoxylin and eosin staining. Scale bar represents 110 μm. (C and D) Chromosomal copy number variations (CNV) of the original tumor and after implantation in mice. The most relevant molecular pathogenic alterations found in the original tumor and PDXO are highlighted. (E) Schematic illustration of the treatment schedule. Mice bearing PDXO were treated for 3 weeks with either vehicle ($n = 7$) or 4SC-205 (40 mg/kg, $n = 11$). (F) Tumor weights at the end of the experiment. (G) Representative picture of the dissected tumors (T: tumor; K: kidney). Scale bar: 1 cm. (H) Representative images of phosphorylated histone H3. Scale bar: 10 μm. (I). Quantification of phospho-histone H3 positive cells in histological sections from vehicle- and 4SC-205-treated tumors. Graph represents the average percentage of positive cells ± SEM from vehicle- or 4SC-205 (10 representative fields/tumor)-treated tumors ($n = 5$ /group). (J) Scheme of the experimental design. SK-N-BE(2) cells were injected into the tail vein, and 21 days later, mice were randomized into vehicle ($n = 13$) and 40 mg/kg 4SC-205 groups ($n = 15$). The mice received oral administration of 4SC-205 three times a week for five consecutive weeks. (K) Scatter dot plots representing the average quantification of tumor bioluminescence ± SEM at the indicated days post-treatment. ** $p < 0.01$, two-tailed student's t -test. (L) Representative images of luciferase activity in eight mice from the vehicle and 4SC-205 treatment groups at 28 days posttreatment. (M) Kaplan–Meier survival curve of mice with neuroblastoma liver metastases treated with either vehicle or 40 mg/kg 4SC-205 for 5 weeks. Statistical differences were calculated using the Gehan–Breslow–Wilcoxon test. * $p < 0.05$, *** $p < 0.001$, two-tailed Student's t -test

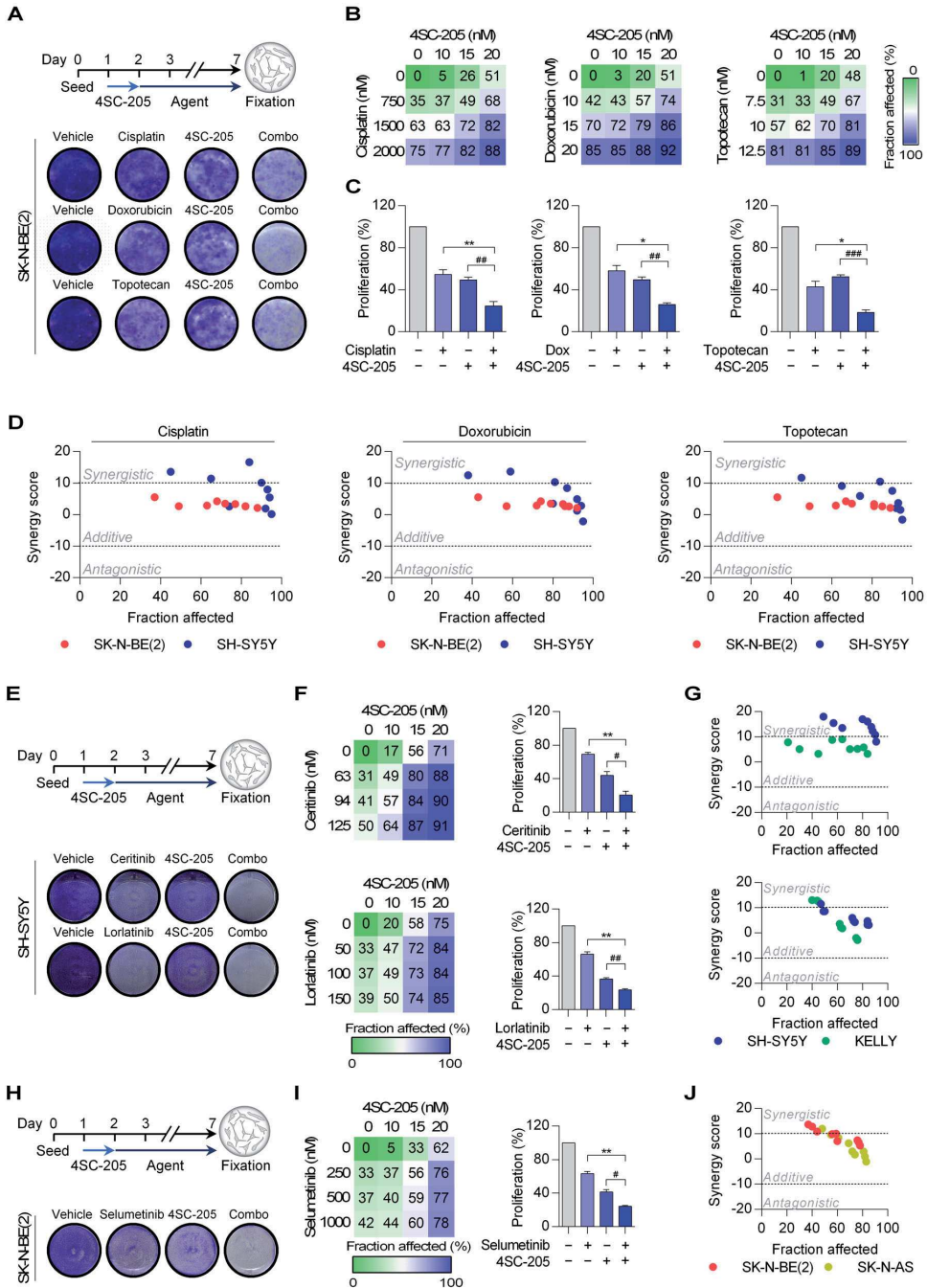


FIGURE 4 4SC-205 potentiates the effect of chemotherapy and neuroblastoma-targeted therapies. (A) Scheme of the experimental design for the combination of 4SC-205 and standard chemotherapies. Images are representative of crystal violet staining of SK-N-BE(2) cells treated with CDDP (1000 nM), doxorubicin (15 nM), topotecan (10 nM), 4SC-205 (17.5 nM) and their corresponding combinations (Combo). (B) Heatmaps showing the percentage of cellular fraction affected by drug combination treatments. (C) Graphs represent the average effect on cell viability from three independent experiments \pm SEM ($n = 3$ /condition). (D) Combinatorial analysis performed using SynergyFinder 2.0 software. (E) Schematic representation of the experimental design combining 4SC-205 and neuroblastoma-targeted therapies. Representative

and tumor cells with reduced proliferation or viability (Figure 2M–O). We next tested 4SC-205 in a patient-derived orthotopic xenografts (PDOX) derived from a very high-risk neuroblastoma patient. VH-NB608 PDOX retained most of the histological and molecular features of the original tumor (Figure 3A–D). 4SC-205-treated mice displayed a 14.75-fold reduction in tumor weight compared to the vehicle group (Figures 3E and 3F). Mice treated with 4SC-205 presented small tumors located in the adrenal gland, whereas vehicle-treated mice had large tumors with the kidney completely surrounded by the tumor (Figure 3G). Furthermore, 4SC-205 tumors had a larger fraction of cells with phosphorylation of histone H3, thereby indicating a specific targeting of KIF11 in these tumors, and suggesting that tumors were still sensitive to the inhibitor after 3 weeks (Figure 3H,I).

Half of neuroblastoma patients present metastases at the time of diagnosis.⁸ Therefore, we proceeded to test the efficacy of 4SC-205 in a neuroblastoma liver metastasis model. In response to treatment, a clear delay in metastatic outgrowth was observed in 4SC-205-treated mice (Figure 3J–L and S8). As a consequence, the median lifespan of the animals was significantly expanded by ~27% (Figure 3M; vehicle: 33 days vs. 4SC-205: 42 days). Noticeable, 4SC-205 administration minimally affected mice weight (<10%) during the course of the treatment (Figure S9). To achieve a better therapeutic effect and provide a rationale for further development of 4SC-205 in clinical trials, we combined 4SC-205 with chemotherapies, such as platine derivatives (cisplatin), doxorubicin, and topotecan, which are currently used as standard treatment for patients with high-risk neuroblastoma. In all cases, the combination of 4SC-205 with the chemotherapies showed additive effects (Figures 4A–D and S10A–C; Table S6). Pediatric precision medicine programs have discovered a small number of recurrent alterations such as *ALK* activating mutations or hyperactivation of the ERK Pathway,^{9,10} which constitute the basis for the development of targeted therapies against high-risk neuroblastoma tumors. Thus, we combined 4SC-205 with two *ALK* inhibitors (ceritinib and lorlatinib) or with the MEK1/2 inhibitor selumetinib. The combination of 4SC-205 with *ALK* or MEK inhibitors showed a ~2–3-fold reduction in cell proliferation compared with the

inhibitors alone, with most of the combination doses showing additive effects (Figures 4E–J and S10D–G; Table S7).

In summary, our study provides a rationale for the future therapeutic integration in clinical trials of 4SC-205, an structurally distinct oral KIF11 inhibitor that shows potent antitumor activity in multiple preclinical neuroblastoma models and sensitizes neuroblastoma cells to standard chemotherapy and specific neuroblastoma-targeted therapies.

ACKNOWLEDGMENTS

We are very thankful to Prof. Thomas U. Mayer for providing us with contact with the 4SC. We would like to acknowledge the members of the Laboratory Animal Service and High Technology Unit for technical support. We are grateful to the CNAG-CRG for technical and bioinformatics assistance with transcriptome analyses. We would like to thank *Editage* (www.editage.com) for English language editing.

CONFLICT OF INTEREST

Dr. Moreno participates in data monitoring committees of clinical trials sponsored by Novartis, Actuate Therapeutics, Shionogi, Incyte, the University of Southampton and the Royal Marsden NHS Foundation Trust; and had a consulting role for Novartis and Shionogi. Dr. Lucas Moreno is also a member of the Executive Committee of the European neuroblastoma research cooperative group (SIOPEN) which receives royalties for the sales of dinutuximab beta. Rolf Krauss (RK) is an employee of 4SC. Alberto Villanueva (AV) is co-founder of Xenopat S.L. No potential conflict of interest was disclosed by the rest of the authors.

AUTHOR CONTRIBUTIONS


Miguel F. Segura and Anna Santamaria conceived and designed the study. Marc Masanas, Nuria Masiá, Leticia Suárez-Cabrera, Mireia Olivan, Aroa Soriano, Blanca Majem, Carlos Jimenez, Ariadna Boloix, Ignasi Toloedano, Gabriela Guillén, Alexandra Navarro, and Alberto Villanueva carried out the experiments. Marc Masanas, Laura Devis-Jauregui, Rebeca Burgos-Panadero, Pau Rodriguez-Sodupe, and Aroa soriano analyzed the data. David

crystal violet staining images of the *ALK*-mutated SH-SY5Y cell line treated with the *ALK* inhibitors ceritinib (62.5 nM) or lorlatinib (50 nM) with or without 4SC-205 (15 nM). (F) Heatmaps show the percentage of the cellular fraction affected by the drug combination treatments at the indicated doses. The graph represents the average of three independent experiments ($n = 3/\text{condition}$) \pm SEM at 62.5 nM and 50 nM of ceritinib or lorlatinib, respectively. (G) Combinatorial analysis of 4SC-205 and ceritinib/lorlatinib in SH-SY5Y and KELLY cells. (H) Crystal violet staining images of SK-N-BE(2) cells treated with selumetinib (250 nM) and 4SC-205 (20 nM) and their respective combinations. (I) Heatmap showing the fraction of cells affected after the combination of 4SC-205 and selumetinib at the indicated concentrations for 48 h. Graph represents the average percentage of cell proliferation ($n = 3/\text{condition}$) \pm SEM at 250 nM of selumetinib. (J) Combinatorial analysis of 4SC-205 and selumetinib in SK-N-BE(2) and SK-N-AS. * $p < 0.05$, ** $p < 0.01$, *** $p < 0.001$, two tailed Student's *t*-test

Llobet-Navas, Josep Sánchez de Toledo, Josep Roma, Rosa Noguera, Lucas Moreno, and Soledad Gallego provided intellectual support for result interpretation and critical revision. Rolf Krauss provided the compound used in this study. Marc Masanas, Miguel F. Segura, and Anna Santamaria wrote the initial manuscript. All the authors read and approved the final manuscript.

DATA AVAILABILITY STATEMENT

The authors confirm that all data supporting the findings of this study are available within the article and the corresponding web servers. Further information from WES data analyses is available from the corresponding authors upon reasonable request.

Marc Masanas¹
 Nuria Masiá²
 Leticia Suárez-Cabrera²
 Mireia Olivan^{2,3}
 Aroa Soriano¹
 Blanca Majem²
 Laura Devis-Jauregui⁴
 Rebeca Burgos-Panadero^{5,6}
 Carlos Jiménez¹
 Pau Rodriguez-Sodupe⁷
 Ariadna Boloix¹
 Ignasi Toledano²
 Gabriela Guillén^{1,8}
 Alexandra Navarro⁹
 David Llobet-Navas^{4,6}
 Alberto Villanueva^{10,11}
 Josep Sánchez de Toledo^{1,12}
 Josep Roma¹
 Rosa Noguera^{5,6}
 Lucas Moreno^{1,13}
 Rolf Krauss¹⁴
 Soledad Gallego^{1,13}
 Anna Santamaria²
 Miguel F. Segura¹ 

¹ Group of Translational Research in Child and Adolescent Cancer, Vall d'Hebron Research Institute (VHIR) - Universitat Autònoma de Barcelona (UAB), Barcelona, Spain

² Cell Cycle and Cancer Laboratory, Biomedical Research Group in Urology, Vall d'Hebron Research Institute (VHIR) - Universitat Autònoma de Barcelona (UAB), Barcelona, Spain

³ Translational Oncology Laboratory, Anatomy Unit, Department of Pathology and Experimental Therapy, School of Medicine, Universitat de Barcelona (UB), L'Hospitalet de Llobregat, Spain

⁴ Molecular Mechanisms and Experimental Therapy in Oncology-Oncobell Program, Bellvitge Biomedical Research Institute (IDIBELL), L'Hospitalet de Llobregat, Spain

⁵ Group of Translational Research in Pediatric Solid Tumors Department of Pathology, Medical School, University of Valencia-INCLIVA Biomedical Health Research Institute, Valencia, Spain

⁶ Low Prevalence Tumors. Centro de Investigación Biomédica en Red de Cáncer (CIBERONC), Instituto de Salud Carlos III, Madrid, Spain

⁷ Quantitative Genomic Medicine Laboratory, qGenomics, Barcelona, Spain

⁸ Department of Surgery, Universitat Autònoma de Barcelona (UAB), Barcelona, Spain

⁹ Department of Pathology, Vall d'Hebron University Hospital, Universitat Autònoma de Barcelona, Barcelona, Spain

¹⁰ Group of Chemoresistance and Predictive Factors, Subprogram Against Cancer Therapeutic Resistance (ProCURE), ICO, Oncobell Program, IDIBELL, L'Hospitalet del Llobregat, Barcelona, Spain

¹¹ Xenopat S.L., Business Bioincubator, Bellvitge Health Science Campus, Barcelona, Spain

¹² Catalan Institute of Oncology (ICO), Barcelona, Spain

¹³ Pediatric Oncology and Hematology Department, Hospital Universitari Vall d'Hebron - Universitat Autònoma de Barcelona (UAB), Barcelona, Spain

¹⁴ 4SC, Martinsried, Germany

Correspondence

Miguel F. Segura, Group of Translational Research in Child and Adolescent Cancer, Passeig Vall d'Hebron 119–129, Collserola Building. Lab 207, 08035 Barcelona, Spain.

Email: miguel.segura@vhir.org

Anna Santamaria, Cell Cycle and Cancer Laboratory, Biomedical Research Group in Urology, Passeig Vall d'Hebron 119–129, Collserola Building. Lab 210, 08035 Barcelona, Spain.

Email: anna.santamaria@vhir.org

Funding information

The financial support for this research was provided by Instituto de Salud Carlos III (PI20/00530 to Miguel F. Segura; PI20/01107 to Rosa Noguera; PI17/02248 and CPII18/00027 to Anna Santamaria; PI19/01320 to Alberto Villanueva); Ministerio de Educación, Cultura y Deporte (Grant no. FPU16/01099 to Marc Masanas). This work was also supported by the Asociación NEN (Nico contra el cancer infantil 2017–PVR00157).

ORCID

Miguel F. Segura  <https://orcid.org/0000-0003-0916-3618>

REFERENCES

1. Matthay KK, Maris JM, Schleiermacher G, et al. Neuroblastoma. *Nat Rev Dis Primers*. 2016;2:16078.
2. Stafman LL, Beierle EA. Cell proliferation in neuroblastoma. *Cancers*. 2016;8:13.
3. London WB, Shimada H, d'Amore E, et al. Age, tumor grade, and mitosis-karyorrhexis index (MKI) are independently predictive of outcome in neuroblastoma (NB). *J Clin Oncol*. 2007;25(18_suppl):9558.
4. Blangy A, Lane HA, d'Herin P, Harper M, Kress M, Nigg EA. Phosphorylation by p34cdc2 regulates spindle association of human Eg5, a kinesin-related motor essential for bipolar spindle formation in vivo. *Cell*. 1995;83(7):1159–1169.
5. Hansson K, Radke K, Aaltonen K, et al. Therapeutic targeting of KSP in preclinical models of high-risk neuroblastoma. *Sci Transl Med*. 2020;12(562):eaba4434.
6. Shah JJ, Kaufman JL, Zonder JA, et al. A phase 1 and 2 study of Filanesib alone and in combination with low-dose dexamethasone in relapsed/refractory multiple myeloma. *Cancer*. 2017;123(23):4617–4630.
7. Garcia-Saez I, Skoufias DA. Eg5 targeting agents: from new anti-mitotic based inhibitor discovery to cancer therapy and resistance. *Biochem Pharmacol*. 2021;184:114364.
8. Maris JM, Hogarty MD, Bagatell R, Cohn SL. Neuroblastoma. *Lancet North Am Ed*. 2007;369(9579):2106–2120.
9. George RE, Sanda T, Hanna M, et al. Activating mutations in ALK provide a therapeutic target in neuroblastoma. *Nature*. 2008;455(7215):975–978.
10. Eleveld TF, Oldridge DA, Bernard V, et al. Relapsed neuroblastomas show frequent RAS-MAPK pathway mutations. *Nat Genet*. 2015;47(8):864–871.

SUPPORTING INFORMATION

Additional supporting information may be found online in the Supporting Information section at the end of the article.

The oral KIF11 inhibitor 4SC-205 exhibits antitumor activity and potentiates standard and targeted therapies in primary and metastatic neuroblastoma models

Marc Masanas et al.

SUPPORTING INFORMATION

Materials and methods

Analysis of mRNA neuroblastoma data sets

KIF11 mRNA expression was analyzed with the R2 software: Genomics Analysis and Visualization Platform (<http://r2.amc.nl>) using SEQC498 (GSE62564), Kocak (GSE45547), and Maris (GSE3960) datasets. Receiver operating characteristic curves were constructed to determine the diagnostic power of KIF11 expression for clinical outcome prediction using the SEQC498 dataset. The optimal cutoff value was defined according to the Youden index. *KIF11* expression was categorized as “high” (\geq median) and “low” ($<$ median). Overall survival (OS) and the cumulative survival rate were estimated using the Kaplan-Meier method, and the log-rank test was performed to assess differences between groups. Univariate and multivariate Cox proportional hazard regression analyses were used to assess the prognostic significance of *KIF11* on survival. The Maris (GSE3960) dataset was used to correlate *KIF11* mRNA expression with *MYCN* amplification, gain of 17q23, loss of heterozygosity of 1p36 and 11q genomic alterations. All statistical analyses were performed using the IBM SPSS 21. All reported *p* values were based on two-sided tests with *p* values <0.05 , which were considered statistically significant.

Immunohistochemistry

Twenty-five primary non-*MYCN*-amplified neuroblastoma samples (at least two representative cylinders of 1 mm² from each tumor) classified according to the International Neuroblastoma Risk Group (INRG) pre-treatment stratification criteria (1) were included in five tissue microarrays. Patient samples were referred to the Spanish Reference Center for Neuroblastoma Biological and Pathological studies (Department of Pathology, University of Valencia-INCLIVA) between 2008 and 2010. All patients, their relatives, or their legal guardians provided written informed consent. The present study was approved by the Clinical Research Ethics Committee of INCLIVA (ref. B.0000339).

For immunostaining, tissue sections were deparaffinized overnight at 60°C and rehydrated using graded alcohols. Heat-induced antigen retrieval was performed using citrate buffer (pH 6, 4 min, 115°C) in a pressurized heating chamber. Primary antibodies (Table S8) were incubated overnight at 4°C after blocking endogenous peroxidase. Tissue sections were incubated with secondary antibody for 30 min at room temperature (RT), developed using diaminobenzidine (Dako, K3468), and counterstained using hematoxylin. The assessment of immunostained sections was performed by two independent studies according to the intensity and percentage of KIF11-positive tumor cells. The intensity of positive cells was scored as 1 (weak), 2 (moderate), or 3 (strong), and the percentage of cells as 1 (1–25%), 2 (>25–50%), 3 (>50–75%), or 4 (>75–100%), as per previous studies (2). The sum of these parameters allowed us to categorize the samples as follows: a staining score of ≤ 3 was considered as low expression, and a score of ≥ 3 was considered as high expression. The association between KIF11 protein expression and INRG features was analyzed using the χ^2 test. Survival analysis was performed using Kaplan-Meier curves and log-rank tests. Statistical significance was set at $p < 0.05$. All data were analyzed using SPSS 26.0 statistical analysis software (SPSS, Inc., Chicago, IL, USA).

Cell lines

SK-N-AS, SH-SY5Y, IMR-32, SK-N-F1, SK-N-BE(2)-C, and HEK293T cell lines were purchased from the American Type Culture Collection. SK-N-BE(2), KELLY, and LA1-5s were purchased from Public Health England Culture Collection. The CHLA-90 cell line was acquired from the Children's Oncology Group Cell Culture and Xenograft Repository. NBL-S and NGP were provided by the Cell Bank DSMZ (German Collection of Microorganisms and Cell Cultures). All cell lines were amplified and stored in liquid nitrogen. Upon resuscitation, the cells were maintained in culture for no more than two months. Cell lines were cultured and maintained in Iscove's Modified Dulbecco's medium (Thermo Fisher Scientific) supplemented with 1% insulin-transferrin-selenium supplement (Thermo Fisher Scientific). KELLY cells were cultured in RPMI 1640 medium (Thermo Fisher Scientific). HEK293T cells were grown in Dulbecco's modified Eagle medium (Thermo Fisher Scientific). All media were supplemented with 10% heat-inactivated fetal bovine serum (South America Premium, Biowest), 100 U/mL penicillin, 100 µg/mL streptomycin (Thermo Fisher Scientific), and 5 µg/mL plasmocin (InvivoGen). All cultures were maintained at 37°C in a humidified atmosphere of 95% air and 5% CO₂ and periodically tested for mycoplasma contamination.

Inducible MYCN silencing

The MYCN-Tet-off-inducible Tet21N cell line was a generous gift from Manfred Schwab (DKFZ, Heidelberg, Germany). Cells were cultured in RPMI 1640 medium (Thermo Fisher Scientific) supplemented with 10% heat-inactivated fetal bovine serum (South America Premium, Biowest), 25 mM HEPES, 4 mM L-Glutamine, 200 µg/mL G418, 0.5 µg/mL amphotericin B, 10 µg/mL hygromycin B, 100 U/mL penicillin, 100 µg/mL streptomycin (Thermo Fisher Scientific), and 5 µg/mL plasmocin (InvivoGen). MYCN depletion was triggered by the addition of 100 ng/mL doxycycline.

MYCN overexpression

pCDNA3-HA-human MYCN was a gift from Martine Roussel (Addgene plasmid # 74163; <http://n2t.net/addgene:74163>; RRID:Addgene_74163)(3). For MYCN overexpression 2.5 x 10³ SK-N-AS or SH-SY5Y were seeded in 35 mm dishes and reverse transfected using Lipofectamine 2000 (Thermo Fisher Scientific; 3 µL/plate) with increasing concentrations of pCDNA3-HA-human MYCN or empty vector (0, 1, 2 or 4 µg/p35). Forty-eight h later, cells were harvested and protein was extracted for western blot analyses.

Quantitative real-time PCR

Total RNA was isolated using the miRNeasy Mini Kit (Qiagen). mRNA (1 µg) were reverse transcribed using a Taqman RT kit (Applied Biosystems, Thermo Fisher Scientific). Real-time PCR of KIF11 and MYCN was performed using 2X Power SYBR Green Master Mix (Applied Biosystems, Thermo Fisher Scientific). mRNA expression was normalized against the *GAPDH* housekeeping gene. Primer sequences are listed in Table S9. Relative quantification of gene expression was performed with a comparative 2^(-ΔΔCT) method (4).

Lentivirus production, transduction and isolation of clones

Lentiviruses containing pTRIPZ (Dharmacon, GE Healthcare) or pTRIPZ-shKIF11 (Dharmacon, GE Healthcare; V3THS_391757) were produced using previously described methods in HEK293T (5). Virus particles were concentrated by ultracentrifugation. SK-N-BE(2) were seeded (3 × 10⁵ cells/dish) in 60-mm dishes and incubated overnight with lentiviruses. Infected cells were selected with 1 µg/mL puromycin (Sigma-Aldrich). To isolate monoclonal population of pTRIPZ-KIF11, transduced SK-N-BE(2) were seeded at very low density into 100-mm dishes. After 10 days, isolated colonies were sorted and amplified in 96-well plates.

***In vivo* experiments**

Subcutaneous xenografts: SK-N-BE(2) and SK-N-AS were subcutaneously injected into the right flank (5×10^6 cells/flank) of 6-week old female Fox Chase SCID mice (Charles River) in 300 μ L of PBS: Matrigel (1:1). When tumor size reached 100–200 mm³, mice were randomized into control (2% sucrose) and shKIF11. KIF11 knockdown was induced by adding 1 mg/mL doxycycline to drinking water.

For drug efficacy experiments, mice bearing measurable tumors (~100–200 mm³) were randomized into two groups and treated three times per week by oral gavage with vehicle (5% polyethylene glycol 400 (PEG400, Fisher Scientific, 11449467), 0.9% NaCl, pH 3–4) or with 40 mg/kg 4SC-205. Tumor volume was measured every 2–3 days. At the end of the experiment, tumors were dissected, weighed, frozen in liquid nitrogen, fixed in 10% formalin, and embedded in paraffin.

Orthoxenografts or patient-derived orthotopic xenograft model (PDOX): A biopsy of a primary tumor located in left adrenal gland of a 7-month old female patient with high risk metastatic neuroblastoma was performed at diagnosis at the Vall d'Hebron University Hospital (VH), Barcelona, Spain. The specimen was aseptically isolated and placed at RT in IMDM (Life Technologies, Thermo Fisher Scientific) supplemented with 20% FBS (South America Premium, Biowest), 1% of insulin–transferrin–selenium supplement plus 100 U/ml penicillin and 100 μ g/ml streptomycin (Life Technologies, Thermo Fisher Scientific) and 5 μ g/mL plasmocin (InvivoGen). The protocol for the use of patient's tumor sample was reviewed and approved according to Ethical Committee of Clinical Research and written informed consent was collected.

Immediately after biopsy the trucut was implanted into a NU-Foxn1nu mouse (Harlan) at the animal core facility of Bellvitge Biomedical Research Institute (IDIBELL). A seven weeks-old female mouse was anesthetized with a continuous flow of 2% to isoflurane/oxygen mixture; the sample was implanted without enzymatic digestion in the left adrenal gland of the mice using a 7.0 suture and monitored twice weekly measuring their body weight and by palpation of tumors. At 177 days post-implantation, the tumor was extracted, cut into small fragments and serially implanted into 3 to 5 new animals. Engrafted tumors were also cryopreserved in a solution of 90% non-inactivated FBS and 10% dimethyl-sulfoxide, stored in liquid nitrogen for subsequent future implantations, and frozen for advanced molecular analysis. Representative tumor fragments were fixed and then processed for paraffin embedding.

For drug efficacy experiments, eighteen nude mice were implanted with PDOX at passage two. Sixty-five days after implantation, when tumors measured 300–400 mm³, mice were randomized and assigned to the vehicle and 4SC-205 groups. At the end of the experiment, tumors were dissected, weighed, frozen in liquid nitrogen, fixed in 10% formalin, and embedded in paraffin.

Neuroblastoma liver metastasis model: Firefly luciferase-transduced SK-N-BE(2) cells were injected into the lateral tail vein (2.5×10^5 cells/mouse in 150 μ L of PBS) of 5–6-week-old female Fox Chase SCID Beige mice (Charles River). Twenty-four days after injection, the mice were randomized into vehicle and 4SC-205 groups. Metastasis growth was monitored by *in vivo* bioluminescence imaging (IVIS) once a week during 5 weeks. All animal protocols were reviewed and approved according to regional Institutional Animal Care and Ethical Committee of Animal Experimentation.

Immunofluorescence

SK-N-BE(2) and SH-SY5Y cells were seeded in 6-well plates (2×10^5 cells/well) on 15 mm coverslips and left for 24 h before drug treatment. Cells were seeded in 6-well plates (7.5×10^5 cells/well), and for siRNA experiments, reverse transfected with control or KIF11 siRNA oligonucleotides (25 nM) (Table S10) using Lipofectamine 2000 (Thermo Fisher Scientific; 5 μ L/well). Alternatively, 24 h after seeding, cells were treated using 25 nM 4SC-205. At the end of the experiment, cells were fixed using PTEMF buffer (50 mM Pipes, 0.2%

Triton X-100, 10 mM EGTA, 1 mM MgCl₂, 4% formaldehyde) for 10 min and washed twice with PBS. The samples were then blocked with 3% BSA in PBS for 30 min at RT. Primary antibodies (Table S8) were diluted in 3% BSA in PBS and incubated for 1 h at RT. Secondary antibodies, DAPI and FITC- α -tubulin, were incubated for 1 h at RT in the dark. The coverslips were mounted with a mounting medium (P36965, Thermo Fisher Scientific).

Cell cycle analysis

SK-N-BE(2) (2.5×10^6) and SH-SY5Y (3.5×10^6) cells were seeded in 100-mm dishes. After 14 h, cells were treated with either vehicle (DMSO) or 25 nM 4SC-205. At 12 and 24 h post-treatment, cells were harvested and fixed with cold 70% ethanol and kept at 4°C for at least 24 h. Cells were washed with PBS and resuspended in propidium iodide (PI) buffer (500 μ g/mL PI, RNase 10 μ g/mL). DNA content was analyzed using a FACSCalibur flow cytometer (BD Biosciences) and data were analyzed using BD CellQuest™ Pro Software (BD Biosciences).

Western blot

Cells were harvested in RIPA buffer 1X (Thermo Fisher Scientific) supplemented with a 1X EDTA-free complete protease inhibitor cocktail (Roche). Tumors were cut into small pieces, disaggregated using a homogenizer (10 s, three times), and sonicated (5 s, three times) in RIPA buffer 1X with 1X EDTA-free complete protease inhibitor cocktail and phosphatase inhibitor cocktail 2 and 3 (Sigma-Aldrich; P5726 and P0044). Protein extracts (20–40 μ g of protein) were resolved on NuPAGE 4–12% Bis-Tris gels and transferred to PVDF membranes (Thermo Fisher Scientific). Membranes were blocked with Tris-buffered saline with Tween-20 containing 5% BSA or 5% non-fat dry milk for 1 h at RT and incubated overnight at 4°C with the appropriate primary antibody (Table S8). Membranes were incubated with the corresponding secondary antibodies for 1 h at RT. Actin was used as loading control. Membranes were developed using the EZ-ECL chemiluminescence detection kit (Fisher Scientific).

***In vitro* drug sensitivity assays**

For cell proliferation assays, neuroblastoma cells were seeded in 96-well plates ($3.5\text{--}14 \times 10^3$ cells/well) and treated 24 h later with vehicle (DMSO) or the indicated drugs. Cells were then fixed with 1% glutaraldehyde (Sigma-Aldrich) and stained with 0.5% crystal violet (Sigma-Aldrich). Crystals were dissolved in 15% acetic acid (Fisher Scientific) and the optical density was read at 590 nm using an Epoch microplate spectrophotometer (Biotek). Dose-response curves were calculated using nonlinear regression approximation in GraphPad Prism 6.0 (GraphPad Software, Inc.).

Cell death assay

For gene silencing experiments, SK-N-BE(2) and SH-SY5Y cells were seeded in 6-well plates (3×10^5 cells/well) in triplicate and reverse transfected with control or KIF11 siRNA (25 nM) using Lipofectamine 2000 (Thermo Fisher Scientific, 5 μ L/well). For drug-induced cell death, cells were seeded in 6-well plates (2×10^5 cells/well) and treated 24 h later with DMSO or 25 nM 4SC-205. At the indicated times, cells were stained using 0.05 μ g/mL Hoechst 33258 dye and photographed. Apoptosis quantification was performed using eight representative images per well ($n = 3$ replicates per condition). Cells with fragmented or condensed chromatin were scored as apoptotic cells, whereas uniformly stained chromatin cells were considered healthy.

Three-dimensional spheroid culture

For tumor spheroids, SH-SY5Y (4.5×10^4 cells/well) and SK-N-BE(2) (6×10^4 cells/well) cells were seeded in non-adherent 6-well plates and let them grow in spheroids for 48–72 h. Spheroids were then treated with DMSO or 25 nM 4SC-205. Forty-eight h later, spheroids were disaggregated with 0.5 mL of 1X

StemPro®Accutase® (Thermo Fisher Scientific) and incubated with a mixture of PMS:MTS (1:20) for 2-5 h. Optical density was read at 590 nm using an Epoch Microplate Spectrophotometer (Biotek).

Differentiation of neuroblastoma cells

The protocol followed was adapted from (6). 1×10^4 SH-SY5Y/cm² were seeded in 12-well plates and 60-mm dishes pre-coated with poly-D-lysine (Fisher Scientific) and collagen (Fisher Scientific). After 24 h, cells were treated with all-trans retinoic acid (ATRA) (Selleckchem) 10 μ M in IMDM 10% FBS without antibiotics for 5 days. Cells were then washed with IMDM without FBS and incubated with fresh media 0.5% FBS and 50 ng/mL brain-derived neurotrophic factor (BDNF) (Sigma-Aldrich). After three days, cells were treated with vehicle (DMSO) or 4SC-205 at 25 nM. Cells were fixed with 1% glutaraldehyde or recollected for western blot analysis at the indicated time points.

Genomic analyses

RNA sequencing. For transcriptomic analyses, total RNA was isolated from SK-N-BE(2) subcutaneous tumors treated with vehicle or 4SC-205 (n = 3/group) for 24 h using the miRNeasy mini kit (Qiagen). RNA quality and quantity were determined using a Qubit® RNA HS Assay (Life Technologies) and RNA 6000 Nano Assay on a Bioanalyzer 2100 (Agilent). RNASeq libraries were prepared following the TruSeq® Stranded mRNA LT Sample Prep Kit protocol (Illumina) and sequenced on a NovaSeq 6000 system (Illumina). RNASeq reads were mapped against the human reference genome (GRCh38) using STAR software version 2.5.3a (7) with ENCODE parameters. Genes were quantified using RSEM version 1.3.0 (8) with default parameters and annotation files from GENCODE version 34. Differential expression analysis was performed with the DESeq2 v1.26.0 R package (9) using a Wald test to compare the vehicle and treated samples. We considered differentially expressed genes with *p* values adjusted to < 0.05, and absolute fold-change (FC) > 1.5. Functional enrichment analysis of “Hallmarks” gene set collections from MSigDB was performed using GSEA software (10,11).

Whole exome sequencing (WES): Genomic DNA from the patient’s blood, tumor, and PDOX samples were extracted using the DNeasy Blood & Tissue Kit (Qiagen) and quantified using Qubit (Thermo Fisher Scientific). Genomic DNA was fragmented and a sample library was prepared using the KAPA library kit (Roche), hybridized with the SeqCap EZ MedExome capture kit (Roche), and sequenced on a NextSeq500 sequencing system (Illumina) with the 2 x 150 bp paired-end mode. The R-package XenofilteR to remove sequence reads of mouse origin while retaining human sequences (mismatch threshold=8) (12) was used.

Copy number variants (CNVs), single nucleotide variants (SNVs), and small insertions/deletions (indels) from somatic samples as well as SNV and indel from germline samples were detected by bioinformatics analysis. The bioinformatics workflow started mapping sequence reads to the human genome build (hg19) using the BWA tool (13). Variant calling for the identification of SNVs and indels was carried out using the GATK Haplotype Caller tool (14) together with FreeBayes and Strelka2 (15) for constitutional DNA and via the VarDict tool (16), together with MuTect2 (17) and Strelka2 and VarScan2 (18) for somatic DNA. Both germline and somatic variants were considered when called by at least two callers. To determine the effect of variants, we used the SnpEff annotation (19). Control-FREEC was used to investigate genomic CNV and B-allele frequency (20). Variants were filtered following maximum population frequency <1%, cancer genes list, tumor variant allele frequency >10%, germline allele frequency >30%, and variant consequence (missense, frameshift, splicing, and stop). Filtering parameters for amplifications were number copy >4 and deletions number copy <1.5. RNA sequencing is available at the GEO public repository (GSE166984), and WES data analyses will be available upon request.

Drug combination studies

For drug combination studies with standard chemotherapies, SK-N-BE(2) (2×10^3 cells/well) and SH-SY5Y (2.5×10^3 cells/well) cells were seeded in 96-well plates. The next day, the cells were treated with the indicated concentrations of 4SC-205. Twenty-four h later, cell medium was replaced with a medium containing the indicated concentrations of cisplatin, topotecan, and doxorubicin, and incubated for additional 5 days.

In combination with ALK inhibitors, SH-SY5Y (8×10^3 cells/well) and KELLY (1×10^4 cells/well) cells were seeded in 96-well plates and treated 24 h later with increasing concentrations of 4SC-205 plus/minus ceritinib or lorlatinib. For combinations with MEK inhibitors, SK-N-BE(2) and SK-N-AS (6×10^3 cells/well) cells were seeded in 96-well plates and treated 24 h later with the indicated doses of 4SC-205 plus/minus selumetinib. Forty-eight h later, cells were fixed with 1% glutaraldehyde (Sigma-Aldrich) and stained with 0.5% crystal violet (Sigma-Aldrich).

The Bliss independence model from SynergyFinder (version 2.0) was used to evaluate if the pharmacological combination of 4SC-205 with chemotherapeutic agents and targeted therapies was synergistic, additive or antagonistic (21).

Statistical analyses

Unless otherwise indicated, statistical significance was determined using an unpaired two-tailed Student's t-test. Half-maximal inhibitory concentration (IC₅₀) was calculated using nonlinear regression approximation in GraphPad Prism 6.0 (GraphPad Software, Inc.). Differences in survival times among mice treated with vehicle or 4SC-205 were analyzed using the Gehan-Breslow-Wilcoxon test (GraphPad Prism 6.0). * indicates $p < 0.05$, ** indicates $p < 0.01$, and *** indicates $p < 0.001$.

Supplementary references

1. Cohn SL, Pearson AD, London WB, Monclair T, Ambros PF, Brodeur GM, *et al.* The International Neuroblastoma Risk Group (INRG) classification system: an INRG Task Force report. *Journal of clinical oncology : official journal of the American Society of Clinical Oncology*. 2009; **27**(2): 289-97.
2. Jin Q, Dai Y, Wang Y, Zhang S, Liu G. High kinesin family member 11 expression predicts poor prognosis in patients with clear cell renal cell carcinoma. *Journal of clinical pathology*. 2019; **72**(5): 354-62.
3. Vo BT, Wolf E, Kawauchi D, Gebhardt A, Rehg JE, Finkelstein D, *et al.* The interaction of Myc with Miz1 defines medulloblastoma subgroup identity. *Cancer cell*. 2016; **29**(1): 5-16.
4. Livak KJ, Schmittgen TD. Analysis of relative gene expression data using real-time quantitative PCR and the 2(-Delta Delta C(T)) Method. *Methods*. 2001; **25**(4): 402-8.
5. Zufferey R, Dull T, Mandel RJ, Bukovsky A, Quiroz D, Naldini L, *et al.* Self-inactivating lentivirus vector for safe and efficient in vivo gene delivery. *J Virol*. 1998; **72**(12): 9873-80.
6. Encinas M, Iglesias M, Lui Y, Wang H, Muhaisen A, Ceña V, *et al.* Sequential treatment of SH-SY5Y cells with retinoic acid and brain-derived neurotrophic factor gives rise to fully differentiated, neurotrophic factor-dependent, human neuron-like cells. *J Neurochem*. 2000; **75**(3): 991-1003.
7. Dobin A, Davis CA, Schlesinger F, Drenkow J, Zaleski C, Jha S, *et al.* STAR: ultrafast universal RNA-seq aligner. *Bioinformatics*. 2013; **29**(1): 15-21.
8. Li B, Dewey CN. RSEM: accurate transcript quantification from RNA-Seq data with or without a reference genome. *BMC Bioinformatics*. 2011; **4**(12): 323.
9. Love MI, Huber W, Anders S. Moderated estimation of fold change and dispersion for RNA-seq data with DESeq2. *Genome biology*. 2014; **15**(12): 550.

10. Subramanian A, Tamayo P, Mootha VK, Mukherjee S, Ebert BL, Gillette MA, *et al.* Gene set enrichment analysis: A knowledge-based approach for interpreting genome-wide expression profiles. *Proceedings of the National Academy of Sciences*. 2005; **102**(43): 15545-50.
11. Mootha VK, Lindgren CM, Eriksson KF, Subramanian A, Sihag S, Lehar J, *et al.* PGC-1 α -responsive genes involved in oxidative phosphorylation are coordinately downregulated in human diabetes. *Nature genetics*. 2003; **34**(3): 267-73.
12. Kluin RJC, Kemper K, Kuilman T, de Ruiter JR, Iyer V, Forment JV, *et al.* XenofilterR: computational deconvolution of mouse and human reads in tumor xenograft sequence data. *BMC Bioinformatics*. 2018; **19**(1): 366.
13. Li H, Durbin R. Fast and accurate short read alignment with Burrows-Wheeler transform. *Bioinformatics*. 2009; **25**(14): 1754-60.
14. Van der Auwera GA, Carneiro MO, Hartl C, Poplin R, Del Angel G, Levy-Moonshine A, *et al.* From FastQ data to high confidence variant calls: the Genome Analysis Toolkit best practices pipeline. *Current protocols in bioinformatics*. 2013; **43**: 11.0.1-.0.33.
15. Kim S, Scheffler K, Halpern AL, Bekritsky MA, Noh E, Källberg M, *et al.* Strelka2: fast and accurate calling of germline and somatic variants. *Nature Methods*. 2018; **15**(8): 591-4.
16. Lai Z, Markovets A, Ahdesmaki M, Chapman B, Hofmann O, McEwen R, *et al.* VarDict: a novel and versatile variant caller for next-generation sequencing in cancer research. *Nucleic acids research*. 2016; **44**(11): e108.
17. Benjamin D, Sato T, Cibulskis K, Getz G, Stewart C, Lichtenstein L. Calling Somatic SNVs and Indels with Mutect2. *Preprint at bioRxiv* <https://www.biorxiv.org/content/101101/861054v1>. 2019.
18. Koboldt DC, Zhang Q, Larson DE, Shen D, McLellan MD, Lin L, *et al.* VarScan 2: somatic mutation and copy number alteration discovery in cancer by exome sequencing. *Genome research*. 2012; **22**(3): 568-76.
19. Cingolani P, Platts A, Wang le L, Coon M, Nguyen T, Wang L, *et al.* A program for annotating and predicting the effects of single nucleotide polymorphisms, SnpEff: SNPs in the genome of *Drosophila melanogaster* strain w1118; iso-2; iso-3. *Fly*. 2012; **6**(2): 80-92.
20. Boeva V, Popova T, Bleakley K, Chiche P, Cappelletti J, Schleiermacher G, *et al.* Control-FREEC: a tool for assessing copy number and allelic content using next-generation sequencing data. *Bioinformatics*. 2012; **28**(3): 423-5.
21. Ianevski A, Giri AK, Aittokallio T. SynergyFinder 2.0: visual analytics of multi-drug combination synergies. *Nucleic acids research*. 2020; **48**(W1): W488-w93.

Supplementary Figures

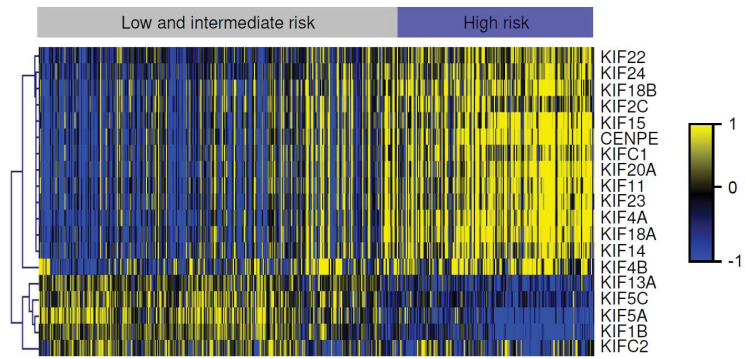


Figure S1. Multiple kinesins are highly expressed in high-risk neuroblastoma compared to low- and intermediate-risk groups. Heatmap and hierarchical clustering analysis of the expression of 19 kinesins in 498 NB samples (low- and intermediate-risk, n = 322; high-risk, n = 176) measured by RNAseq.

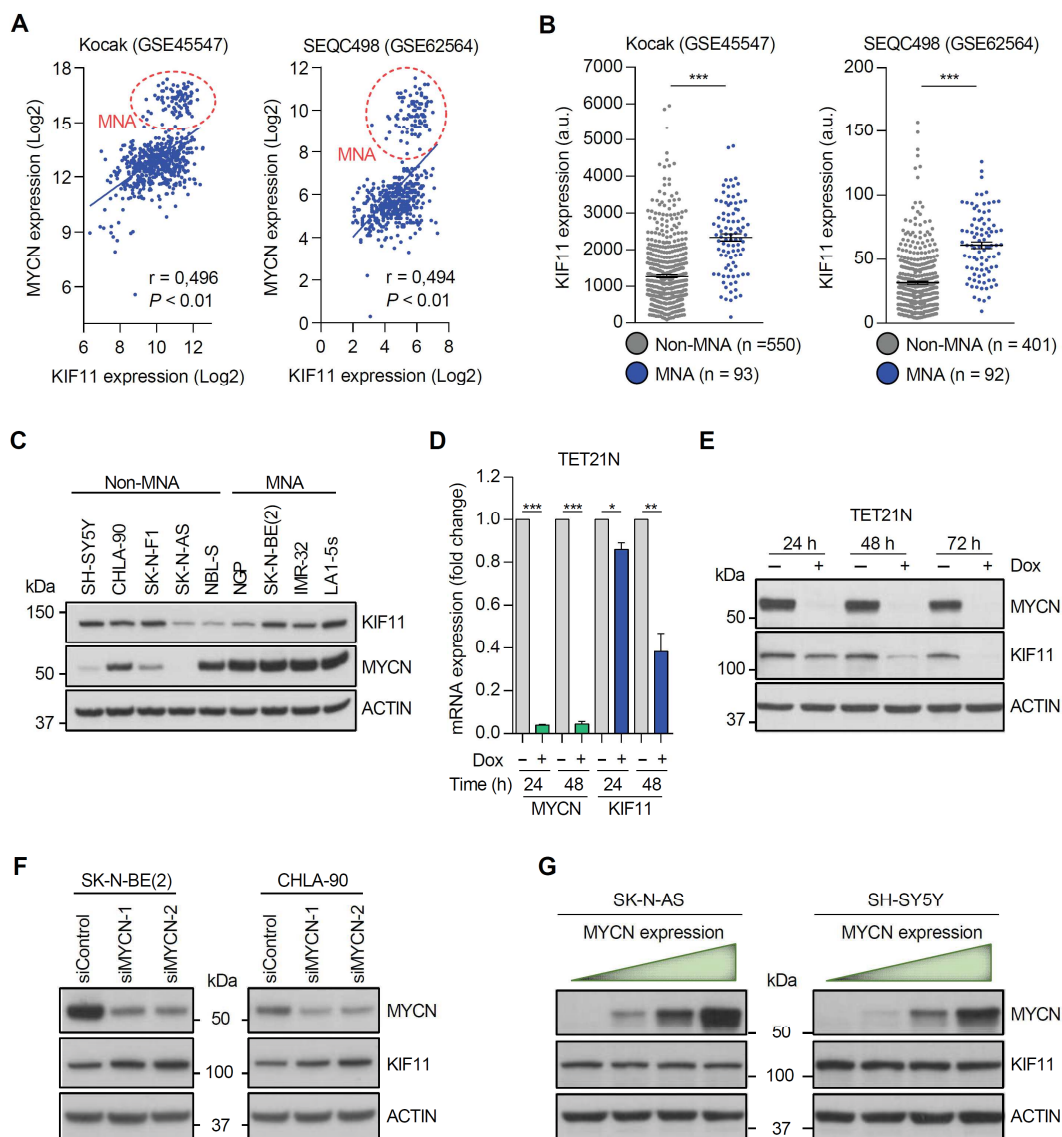


Figure S2. *KIF11* correlates with *MYCN* in distinct neuroblastoma datasets. (A) Linear correlation between *MYCN* and *KIF11* mRNA expression in the indicated neuroblastoma datasets. Data from patients with amplification of *MYCN* (MNA) is encircled. (B) *KIF11* mRNA expression levels comparing neuroblastoma tumors with amplification of *MYCN* versus no *MYCN* amplification (Non-MNA). (C) Western blot analysis of *KIF11* in a panel of neuroblastoma cell lines with and without *MYCN* amplification. (D) Analysis of *MYCN* and *KIF11* expression in the Tet21N neuroblastoma model with the doxycycline (Dox) inducible silencing of *MYCN*. Results are the mean of three independent experiments \pm SEM. * $p < 0,05$, ** $p < 0,01$ and *** $p < 0,01$ two-tailed student's t-test. (E) Western blot analysis of *KIF11* in Tet21N cells in the presence of doxycycline (i.e., *MYCN* depletion) or absence (i.e., *MYCN* expression). (F) Immunoblot analysis of *MYCN* and *KIF11* in SK-N-BE(2) and CHLA-90 cells transfected with two independent siRNAs targeting *MYCN* 72 h post-transfection. (G) *KIF11* and *MYCN* protein expression in SK-N-AS and SH-SY5Y cell lines transfected with increasing concentrations of a *MYCN*-overexpression vector.

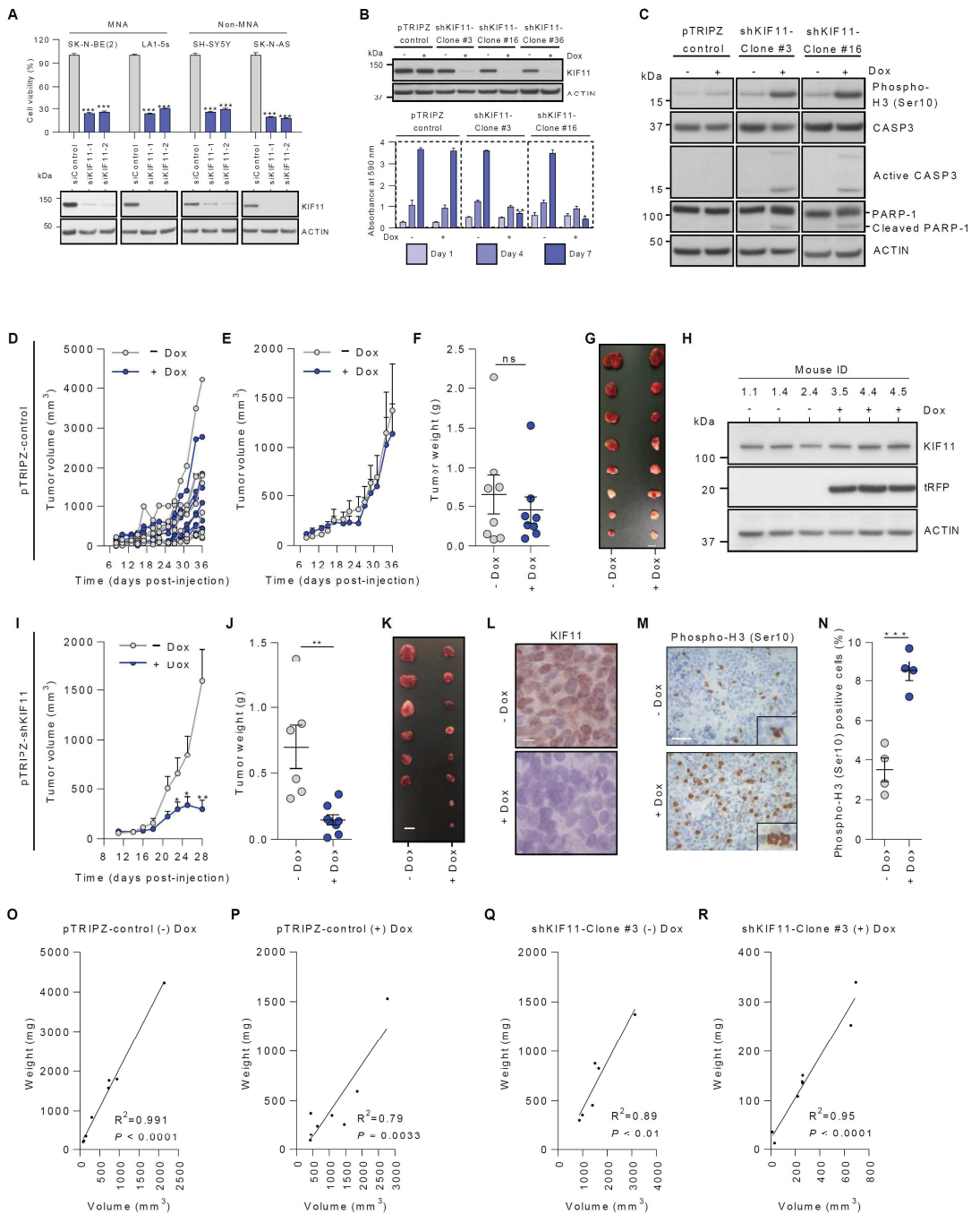


Figure S3. KIF11 knockdown halts tumor growth and induces apoptosis. (A) Cell viability assay in the indicated cell lines transfected with 25 nM of siControl or siKIF11 at 96 h post-transfection. Protein knock-down was analyzed by western blot 72 h post-transfection in the indicated cell lines. (B) Western blot analysis of KIF11 in SK-N-BE(2) cells transfected with pTRIPZ-control (pool) or pTRIPZ-shKIF11 lentiviral vectors (upper panel). Cells were treated with + / - doxycycline for 96 h. Graph representing cell proliferation after 1, 4 and 7 days upon doxycycline treatment (lower panel). Results are expressed as average of three independent experiments \pm SEM. * $p < 0.05$; ** $p < 0.01$; two-tailed Student's t-test. (C) Immunoblot analysis of transduced neuroblastoma cells in presence (+ dox) or absence (- dox) of 1 μ g/mL doxycycline

for 5 days. **(D, E)** Analysis of individual **(D)** or average **(E)** tumor growth of pTRIPZ-control transduced SK-N-BE(2) xenografts. **(F)** Tumor weight at the end of the experiment. **(G)** Image of the dissected tumors. Scale bar, 1 cm. **(H)** Western blot analysis of resected-tumor samples from pTRIPZ-control. TurboRFP (tRFP) was used as a control of shRNA transgene induction. **(I)** Tumor growth of shKIF11-clone #3 SK-N-BE(2) xenografts comparing control (- dox) vs silencing of KIF11 (+ dox). **(J)** Tumor weight at the end of the experiment. **(K)** Image of the dissected tumors. Scale bar, 1 cm. **(L)** Representative image of KIF11 immunohistochemistry in control (- dox) vs KIF11 silenced tumors (+ dox). Scale bar, 10 μ m. **(M)** Representative image of phospho-histone H3 immunohistochemistry from control (- dox) vs KIF11-depleted tumors (+ dox). Scale bar, 100 μ m. **(N)** Quantification of phospho-histone H3 positive cells in FFPE tumor sections (n = 4/condition). *** $p < 0.001$, two-tailed Student's t-test. **(O-R)** Correlation between tumor weight and tumor volume measurements in pTRIPZ-control and shKIF11-Clone #3 xenografts.

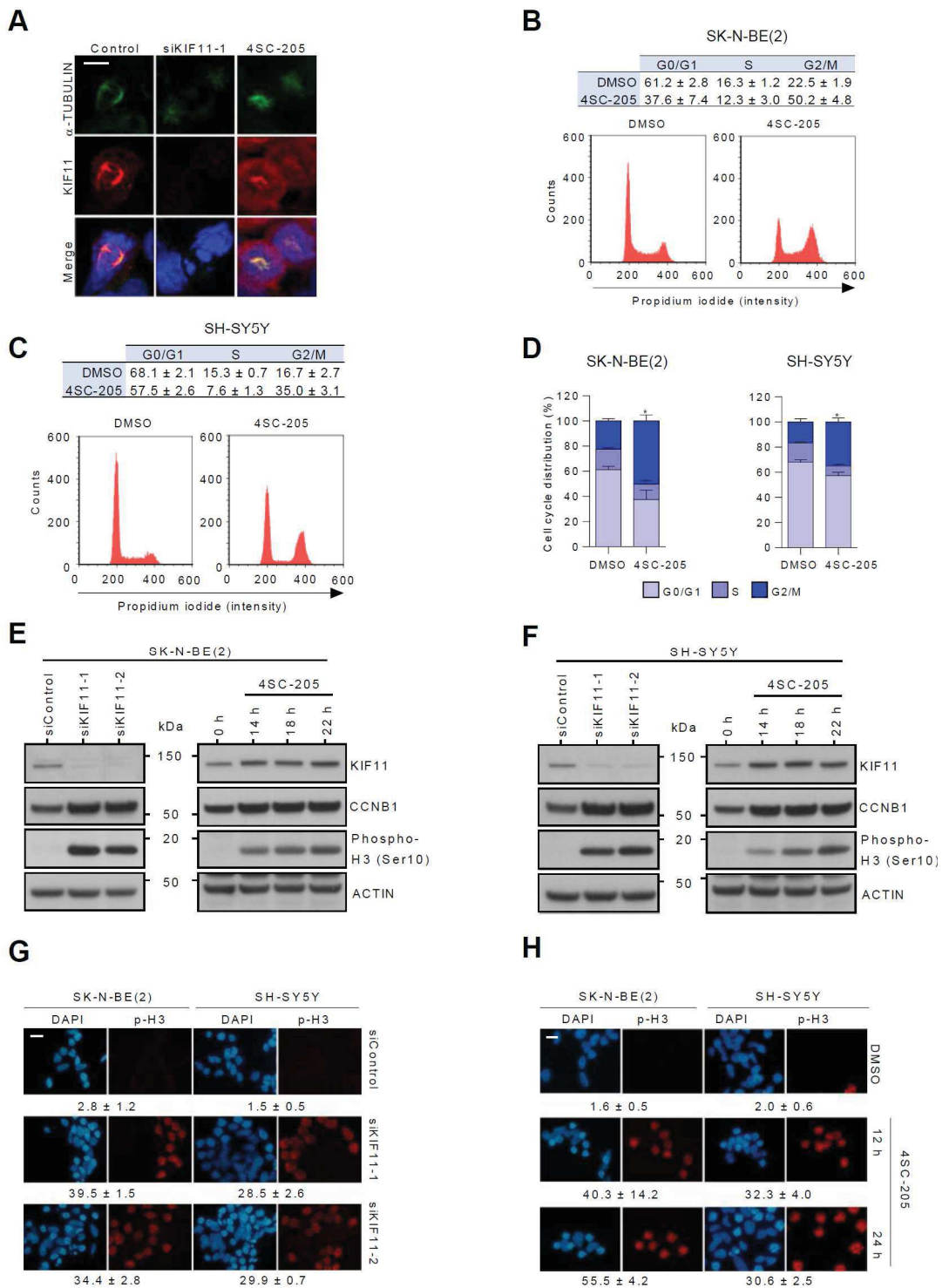


Figure S4. Genetic and pharmacological inhibition of KIF11 reduces neuroblastoma cell proliferation and induces cell cycle arrest in mitosis. (A) Mitotic spindle immunofluorescence of SH-SY5Y cells transfected with siKIF11 or

treated with 4SC-205 (25 nM) for 24 h. KIF11: red, α -TUBULIN: green, DAPI: blue. Scale bar, 5 μ m. **(B, C)** Cell cycle analysis of SK-N-BE(2) and SH-SY5Y cells treated with DMSO or 4SC-205 (25 nM) for 24 h analyzed by FACS. Histograms show one representative experiment from three independent experiments. **(D)** Graphs represent the average percentage of living neuroblastoma cells in G0/G1, S or G2/M phases of three independent experiments \pm SEM. **(E, F)** Western blot analysis of KIF11 and cell cycle-related proteins CCNB1 and phospho-histone H3 at serine 10 in cells transfected with siControl, siKIF11 or treated with 25 nM 4SC-205 at the indicated time points. **(G, H)** Representative immunofluorescence images of phospho-histone H3 in the indicated neuroblastoma cell lines transfected with two independent KIF11-targeting siRNA **(H)** or treated with 4SC-205 at 25 nM **(G)**. Scale bar, 10 μ m. The percentage of phospho-histone H3 positive cells is shown below each condition and represents the average of 7 representative fields \pm SEM. * $p < 0.05$, *** $p < 0.001$, two tailed Student's t-test.

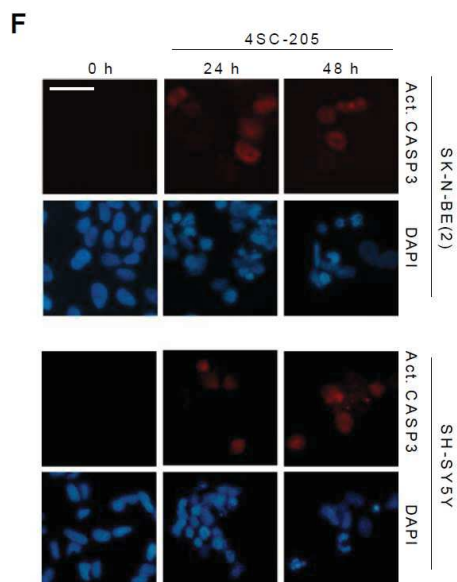
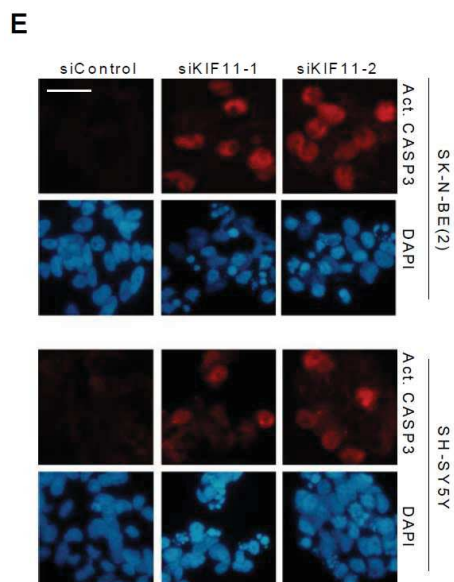
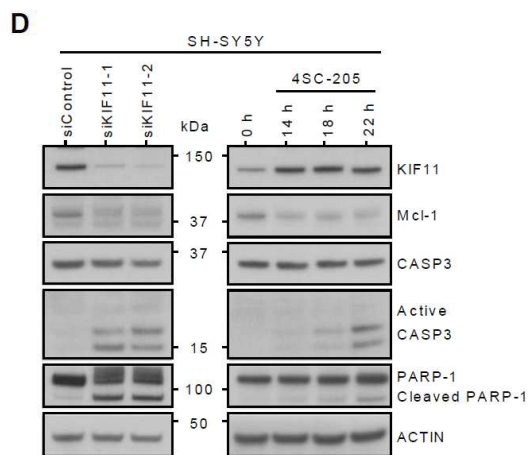
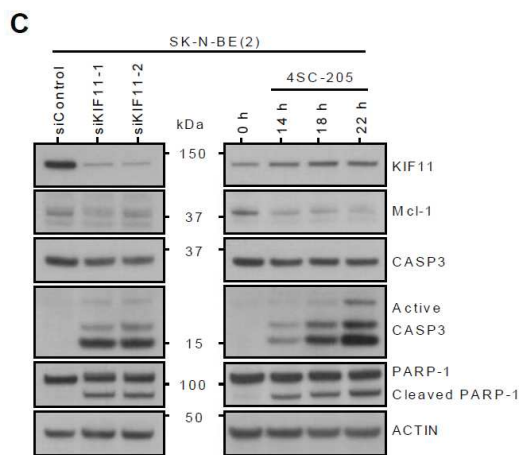
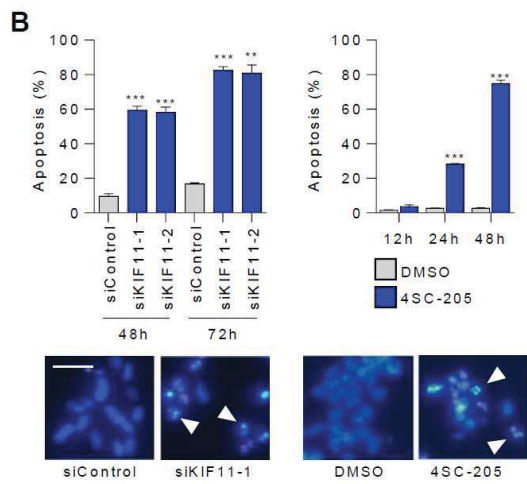
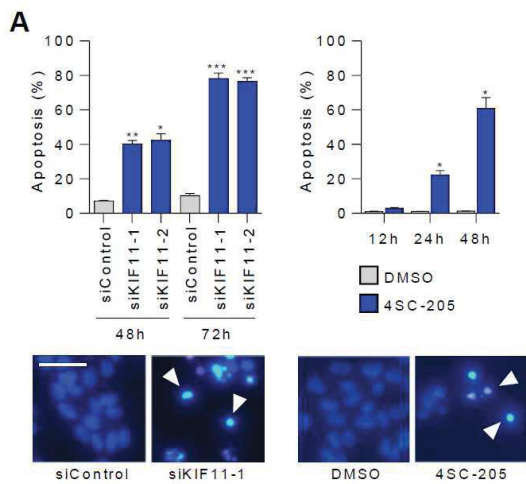


Figure S5. Genetic and pharmacologic inhibition of KIF11 induces apoptosis. (A, B) Quantification of apoptotic cells in SK-N-BE(2) (A) and SH-SY5Y (B) by Hoechst staining. Each graph represents the mean \pm SEM of three independent experiments (n = 6 per experiment). * $p < 0.05$; ** $p < 0.01$; *** $p < 0.001$, two-tailed Student's t-test. Lower panels show representative images of chromatin staining of neuroblastoma cells transfected with control siRNA (siControl) / siKIF11 or treated with 25 nM 4SC-205 for 48 h. White arrowheads point to cells with condensed and/or fragmented chromatin. Scale bar, 20 μ m. (C, D) Western blot analysis of the indicated apoptosis-related proteins in SK-N-BE(2) and SH-SY5Y cells transfected with siControl/siKIF11 or treated with 4SC-205 (25 nM) at the indicated time points. (E, F) Active caspase-3 immunostaining of SK-N-BE(2) and SH-SY5Y cells transfected with siKIF11 (E) or treated with 25 nM of 4SC-205 (F) for 48 h. Scale bar, 20 μ m.

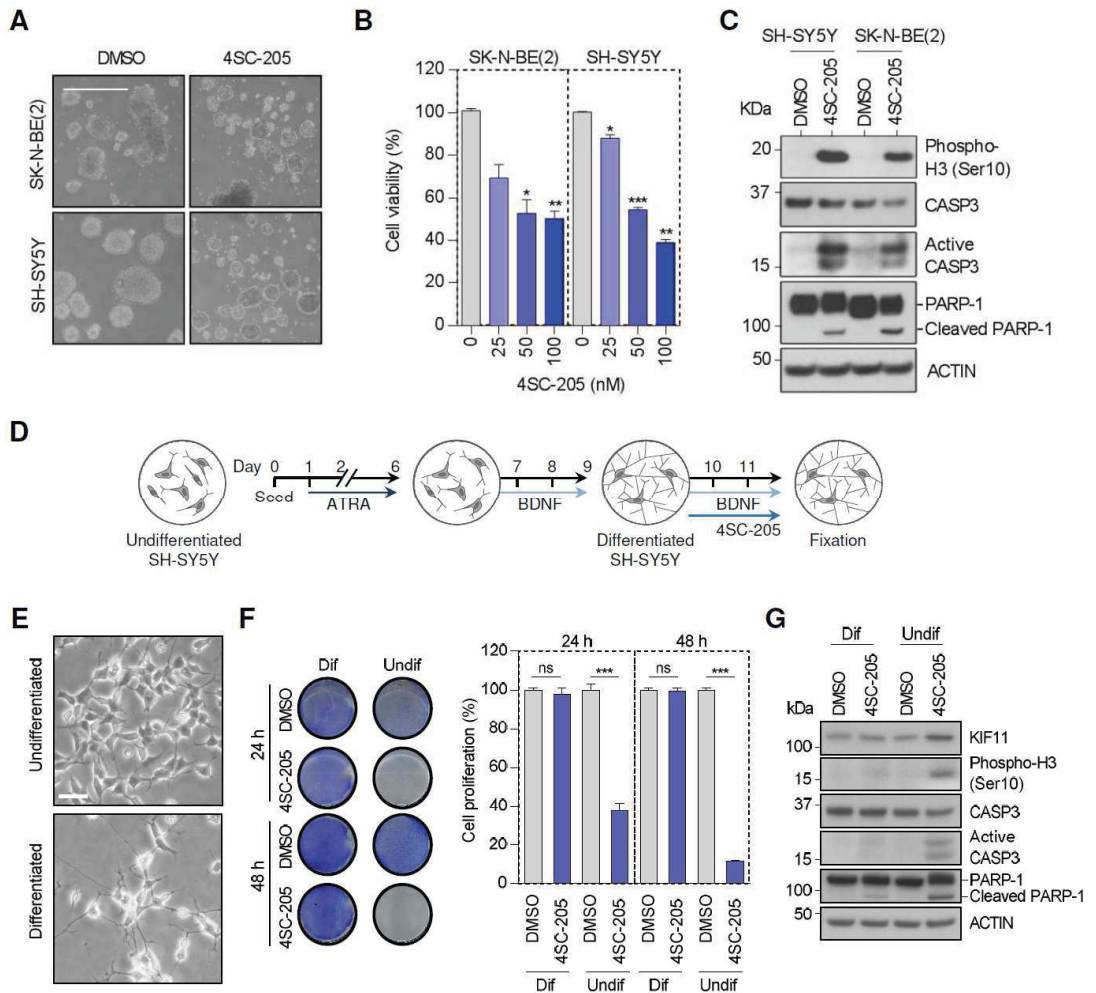


Figure S6. Characterization of the 4SC-205 inhibitor. (A) Representative images of three-dimensional (3D) spheroid culture of SK-N-BE(2) and SH-SY5Y. Scale bar, 100 μ m. (B) Cell viability assay of neuroblastoma spheroids treated with DMSO or the indicated doses of 4SC-205 for 48 h. Cell viability was measured by MTS. Graphs represent the average of three independent experiments \pm SEM * $p < 0.05$; ** $p < 0.01$; *** $p < 0.001$. (C) Western blot analysis of phospho-histone H3 at serine 10 and apoptosis-related proteins in SH-SY5Y and SK-N-BE(2) spheres treated with 25 nM 4SC-205. (D) Overview of the experimental design. (E) Representative images of SH-SY5Y cells before (upper image) and after 10 μ M all-trans-retinoic acid / 50 ng/mL BDNF-induced differentiation (lower image). Scale bar, 50 μ m. (F) Left, representative images of crystal violet staining. Right, cell proliferation of SH-SY5Y treated with DMSO or 4SC-205 in proliferating versus differentiated cells. Results are expressed as the average of three independent experiments ($n = 2$ /condition) \pm SEM. *** $p < 0.001$, two-tailed student's t-test. (G) Western blot analysis of phospho-histone H3 and apoptosis-related proteins in differentiated and undifferentiated SH-SY5Y cells treated for 24 h with 25 nM 4SC-205.

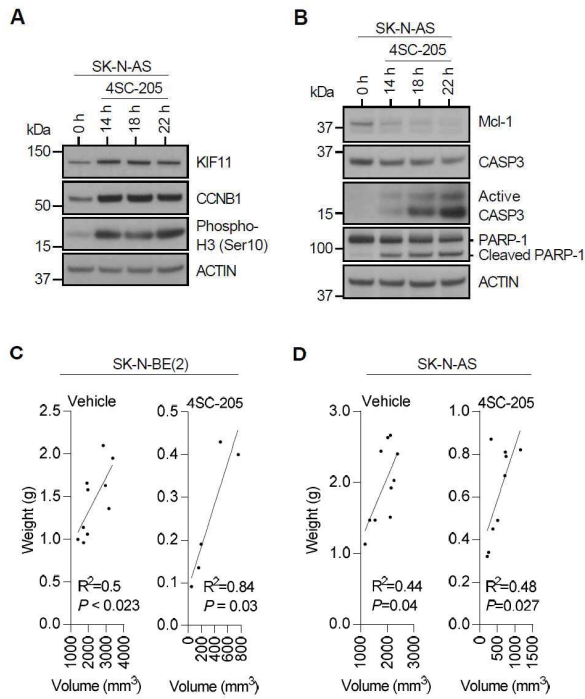


Figure S7. 4SC-205 impairs tumor growth *in vitro* and *in vivo*. (A, B) SK-N-AS cells were treated with 25 nM 4SC-205 at the indicated time points. Cell cycle-related genes (A) or apoptosis-related genes (B) were analyzed by western blot. (C, D) Correlation analysis between tumor weight and tumor volume in from SK-N-BE(2) and SK-N-AS subcutaneous xenografts.

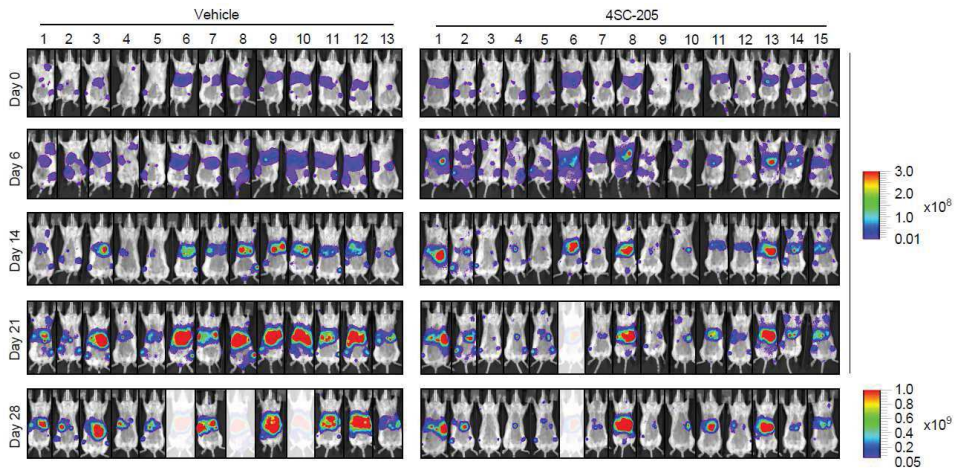


Figure S8. 4SC-205 delays neuroblastoma liver metastases growth. *In vivo* bioluminescence imaging of all mice bearing SK-N-BE(2) liver metastases at the indicated days. Mouse #6, #8, #10 from vehicle and #6 from 4SC-205 groups were euthanized before the last *in vivo* bioluminescence imaging.

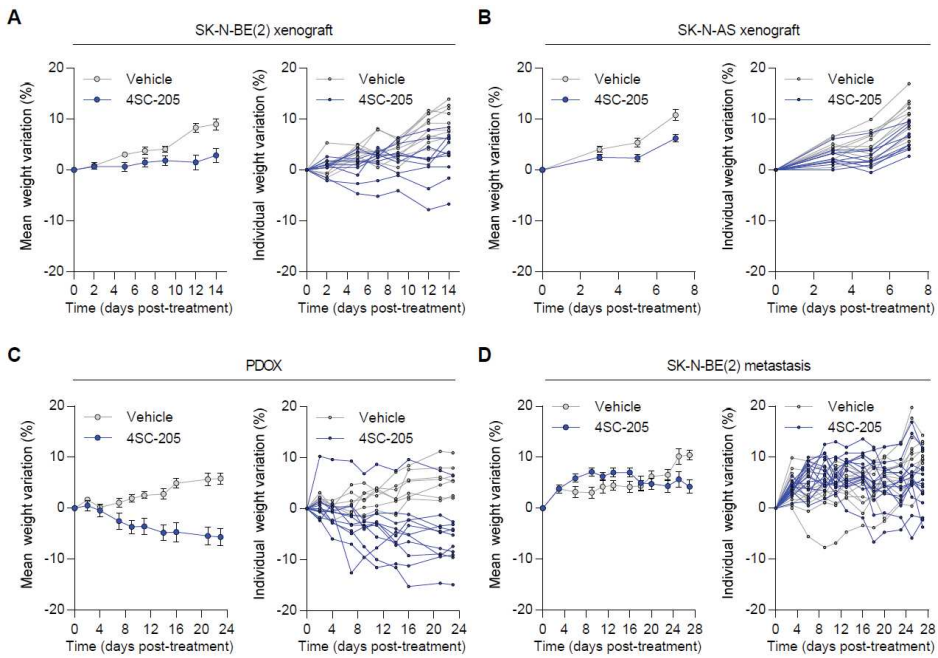
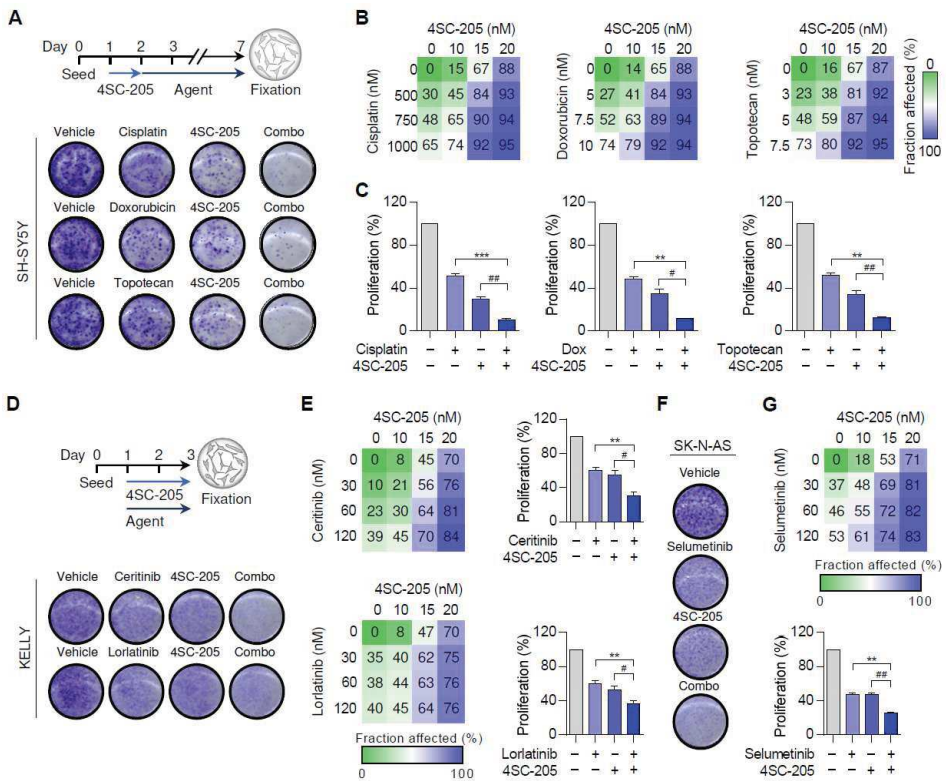


Figure S9. 4SC-205 is well tolerated in mice. Average (left panels) and individual (right panels) mouse weight variation during vehicle or 4SC-205 oral administration in SK-N-BE(2) (A), SK-N-AS (B), PDOX (C) or liver metastases (D) xenograft models.



Supplementary Tables

Table S1. Risk-associated expression of kinesin family members in neuroblastoma

| Gene symbol | Family | Fold change low and intermediate risk vs high risk | p value |
|-------------|--------|--|----------|
| KIF5A | 1 | -2.20 | 2.58E-40 |
| KIF1B | 3 | -1.95 | 3.29E-54 |
| KIFC2 | 14B | -1.90 | 1.89E-35 |
| KIF13A | 3 | -1.70 | 8.61E-45 |
| KIF12 | 12 | -1.66 | 2.60E-02 |
| KIF5C | 1 | -1.65 | 4.89E-26 |
| KIF13B | 3 | -1.48 | 4.01E-32 |
| KIF1A | 3 | -1.43 | 1.13E-24 |
| KIF3A | 2 | -1.42 | 3.25E-27 |
| STARD9 | 3 | -1.42 | 4.28E-17 |
| KIF3C | 2 | -1.38 | 4.97E-21 |
| KIF1C | 3 | -1.34 | 3.91E-14 |
| KIF25 | 14B | -1.23 | 1.00E-02 |
| KIF3B | 2 | -1.21 | 2.17E-09 |
| KIF16B | 3 | -1.20 | 5.75E-04 |
| KIF17 | 2 | -1.07 | 4.20E-01 |
| KIF2A | 13 | -1.06 | 2.70E-02 |
| KIF9 | 9 | -1.06 | 3.50E-02 |
| KIF5B | 1 | -1.02 | 3.60E-01 |
| KIFC3 | 14B | -1.01 | 8.59E-01 |
| KIF19A | 8 | 1.05 | 1.00E-01 |
| KIF21A | 4 | 1.07 | 1.80E-01 |
| KIF26B | 11 | 1.09 | 2.30E-01 |
| KIF27 | 4 | 1.14 | 7.66E-07 |
| KIF26A | 11 | 1.18 | 1.50E-02 |
| KIF21B | 4 | 1.28 | 1.20E-02 |
| KIF6 | 9 | 1.31 | 2.13E-25 |
| KIF7 | 4 | 1.46 | 1.05E-25 |
| KIF20B | 6 | 1.49 | 9.21E-18 |
| KIF22 | 10 | 1.50 | 5.85E-31 |
| KIF2C | 13 | 1.60 | 5.15E-15 |
| KIF24 | 13 | 1.61 | 4.19E-25 |
| KIF14 | 3 | 1.72 | 5.20E-21 |
| KIF23 | 6 | 1.82 | 4.97E-28 |
| KIFC1 | 14A | 1.83 | 3.78E-24 |
| KIF11 | 5 | 1.92 | 2.36E-27 |
| KIF18B | 8 | 1.94 | 2.69E-24 |
| KIF20A | 6 | 2.04 | 1.60E-32 |
| KIF4B | 4 | 2.18 | 5.91E-42 |
| KIF15 | 12 | 2.19 | 5.97E-31 |
| KIF18A | 8 | 2.20 | 1.09E-43 |
| CENP-E | 7 | 2.24 | 4.88E-33 |
| KIF4A | 4 | 2.25 | 5.37E-47 |
| KIF2B | 13 | n.d. | n.d. |
| KIF19B | 8 | n.d. | n.d. |

Abbreviations: FC, fold change; ND, not determined

Table S2. Univariate regression analysis

| Factors | Overall survival | |
|--|------------------------|-----------|
| | HR (95% CI) | p value |
| Sex (M vs F) | - | 0.252 |
| Age (≥ 18 months vs < 18 months) | 8.114 (4.980-13.221) | < 0.001 |
| MYCN (MNA vs Non-MNA) | 7.793 (5.262-11.542) | < 0.001 |
| ISSN Stage (4 vs others) | 8.660 (5.441-13.783) | < 0.001 |
| KIF11 (High vs low) | 8.190 (4.663-14.387) | < 0.001 |
| Risk (High vs others) | 21.423 (11.932-38.464) | < 0.001 |

Abbreviations: HR, hazard ratio; MNA, MYCN amplification

Table S3. Multivariate regression analysis

| Factors | Overall survival | |
|-----------------------|-----------------------|-----------|
| | HR (95% CI) | p value |
| KIF11 (High vs low) | 3.051 (1.693-5.497) | < 0.001 |
| Risk (High vs others) | 14.182 (7.695-26.137) | < 0.001 |

Abbreviations: HR, hazard ratio

Table S4. Relationships between KIF11 expression and clinico-biological characteristics

| Variable and category | Total, n | KIF11 expression | | p value | |
|-----------------------|------------------|------------------|------------|-----------|-------|
| | | Low | High | | |
| Age | < 18 months | 7 | 6 (85.7%) | 1 (14.3%) | 0.132 |
| | ≥ 18 months | 17 | 9 (53%) | 8 (47%) | |
| Stage | L1,L2,MS | 15 | 10 (66.7%) | 5 (33.3%) | 0.179 |
| | M | 8 | 3 (37.5%) | 5 (62.5%) | |
| Hist. C. | GNB | 7 | 4 (57.1%) | 3 (42.9%) | 0.856 |
| | NB | 18 | 11 (61.1%) | 7 (38.9%) | |
| Hist. D. | dNB | 4 | 3 (75%) | 1 (25%) | 0.387 |
| | pdNB | 13 | 8 (61.5%) | 5 (38.5%) | |
| | uNB | 1 | 0 (0%) | 1 (100%) | |
| 11q | ND | 20 | 14 (70%) | 6 (30%) | 0.041 |
| | D | 5 | 1 (20%) | 4 (80%) | |
| 1p | ND | 18 | 14 (77.8%) | 4 (22.2%) | 0.008 |
| | D | 3 | 0 (0%) | 3 (100%) | |
| 17p | NG | 16 | 13 (81.2%) | 3 (18.8%) | 0.011 |
| | G | 5 | 1 (20%) | 4 (80%) | |
| Gen. profile | NCA | 14 | 13 (93%) | 1 (7%) | 0.001 |
| | SCA | 8 | 2 (25%) | 6 (75%) | |
| Ploidy | Hiperp. | 10 | 8 (80%) | 2 (20%) | 0.277 |
| | Dip+tetrap | 12 | 7 (58.3%) | 5 (41.7%) | |
| Risk group | Non-HR | 18 | 13 (72.2%) | 5 (27.8%) | 0.045 |
| | HR | 7 | 2 (28.6%) | 5 (71.4%) | |

L1 and L2: localized; MS: special metastatic; M: metastatic; Hist. C.: histopathologic category; GNB: ganglioneuroblastoma; NB: neuroblastoma; Hist. D.: histopathologic differentiation; dNB: differentiating neuroblastoma; pdNB: poorly differentiated neuroblastoma; uNB: undifferentiated neuroblastoma; ND: non deletion; D: deletion; Hiperp.: Hiperploidy; Dip.: diploid; Tetrap.: tetraploid; Gen. Profile: genetic profile; NCA: numerical chromosomal aberration; SCA: segmental chromosomal aberration; HR: High risk; Gen. Instab.: genetic instability

Table S5. IC50 of 4SC-205 in neuroblastoma cell lines

| Cell line | Stage | MYCN | 11q | P53 | IC50 (nM) |
|------------|-------|---------------|-----|----------------|----------------|
| SK-N-AS | 4 | Non amplified | del | Non-functional | 26.1 \pm 6.5 |
| SH-SY5Y | 4 | Non amplified | WT | Functional | 14.6 \pm 1.4 |
| SK-N-BE(2) | 4 | Amplified | WT | Non-functional | 24.5 \pm 4.8 |
| LA1-5s | 4 | Amplified | WT | Non-functional | 50.5 \pm 6.6 |
| IMR-32 | 4 | Amplified | WT | Functional | 10.1 \pm 0.9 |
| KELLY | 4 | Amplified | ND | Non-functional | 13.7 \pm 1.4 |
| BE(2)-C | 4 | Amplified | ND | Non-functional | 73.6 \pm 7.5 |

Abbreviations: del, deletion; WT, wild type; ND, not determined

Table S6. IC50 values for cisplatin, doxorubicin and topotecan in neuroblastoma cell lines

| Cell line | IC50 cisplatin (nM) | IC50 doxorubicin (nM) | IC50 topotecan (nM) |
|------------|---------------------|-----------------------|---------------------|
| SH-SY5Y | 925 ± 76 | 10.4 ± 0.7 | 11.2 ± 0.8 |
| SK-N-BE(2) | 1511 ± 143 | 34.8 ± 7.5 | 11.9 ± 1.5 |

Table S7. IC50 values for ceritinib, lorlatinib and selumetinib in neuroblastoma cell lines

| Cell line | Molecular alteration | IC50 ceritinib (nM) | IC50 lorlatinib (nM) | IC50 selumetinib (nM) |
|------------|----------------------|---------------------|----------------------|-----------------------|
| SK-N-BE(2) | NF1 copy number loss | – | – | 330 ± 55 |
| SK-N-AS | NRAS mut (Q61K) | – | – | 54.5 ± 15 |
| SH-SY5Y | ALK mut (F1174L) | 74.4 ± 11.6 | 59.8 ± 10.8 | – |
| KELLY | ALK mut (F1174L) | 162.8 ± 28.7 | 51.9 ± 6 | – |

Abbreviations: mut, mutated

Table S8. Antibodies

| Primary antibodies for immunohistochemistry | | | | |
|---|----------|---------------|------------|--|
| Antibody | Dilution | Supplier | Reference | |
| KIF11 | 1:2,000 | Sigma-Aldrich | HPA006916 | |
| p-Histone H3 (Ser10) | 1:100 | CST | #9701 | |
| Chromogranin A | 1:20 | Roche | 760-2519 | |
| Synaptophysin | 1:20 | Roche | 790-4407 | |
| Secondary antibodies for immunohistochemistry | | | | |
| Anti-Rabbit HRP | – | Dako | K4003 | |
| Anti-Mouse HRP | – | Dako | K4001 | |
| Primary antibodies for western blot | | | | |
| KIF11 | 1:3,000 | – | 1 | |
| MYCN | 1:1,000 | SCBT | sc-53993 | |
| CCNB1 | 1:2,000 | Millipore | #05-373 | |
| p-Histone H3 (Ser10) | 1:1,000 | CST | #9701 | |
| MCL1 | 1:500 | SCBT | sc-12756 | |
| Caspase-3 | 1:3,000 | CST | #9662 | |
| Caspase-3 cleaved | 1:1,000 | CST | #9664 | |
| PARP | 1:2,500 | CST | #9542 | |
| mCherry | 1:1,000 | OriGene | AB0081-200 | |
| Actin HRP | 1:40,000 | SCBT | sc-1616 | |
| Secondary antibodies for western blot | | | | |
| Anti-Rabbit IgG-Peroxidase | 1:10,000 | Sigma-Aldrich | #A0545 | |
| Anti-Mouse IgG-Peroxidase | 1:10,000 | Sigma-Aldrich | #A9044 | |
| Anti-Goat IgG-Peroxidase | 1:5,000 | Dako | #P0449 | |
| Primary antibodies for immunofluorescence | | | | |
| KIF11 | 1:1,000 | – | 1 | |
| p-Histone H3 (Ser10) | 1:200 | CST | #9701 | |
| Caspase-3 cleaved | 1:500 | CST | #9664 | |
| Secondary antibodies for immunofluorescence | | | | |
| α-Tubulin | 1:150 | Sigma-Aldrich | F2168 | |
| Anti-Rabbit IgG-Alexa Fluor ® 555 | 1:500 | TFS | A-21428 | |

Abbreviations: SCBT, Santa Cruz Biotechnology; CST, Cell Signaling Technology; TFS, Thermo Fisher Scientific

Table S9. List of RT-qPCR primer sequences

| Gene | Primer sequence (5' to 3') | Amplicon (bp) |
|--------------|--------------------------------|---------------|
| KIF11 | Fw : AAAACAACAAAGAAGAGACAATTCC | 93 |
| | Rv : CAGATGGCTCTTGACTTAGAGGT | |
| MYCN | Fw : AGAGGAGACCCGCCCTAATC | 123 |
| | Rv : TCCAAACACGGCTCTCCGA | |
| GAPDH | Fw : CGCTCTCTGCTCCTCCTGTT | 100 |
| | Rv : CCA TGGTGTCTGAGCGA TGT | |

Table S10. List of siRNA

| Gene | siRNA | Sequence (5'-3') | Reference | Supplier | |
|-------|-----------|------------------|----------------------|-------------------|---------------------|
| - | siControl | BLOCK-iT | - | Fisher Scientific | |
| KIF11 | siKIF11-1 | KIF11 | CUAGAUGGCUUUCUCAGUA | - | Sigma-Aldrich |
| | | KIF11_as | UACUGAGAAAGCCAUCUAG | | |
| | siKIF11-2 | KIF11 | - | L-003317-00 | GE health Dharmacon |
| | | KIF11_as | - | | |
| MYCN | siMYCN-1 | MYCN | GAAGAAUUCGACGUGGUA | - | Sigma-Aldrich |
| | | MYCN_as | UGACCA CGUCGAUUUCUUC | | |
| | siMYCN-2 | MYCN | GAGAGGACACCCUGAGCGA | - | Sigma-Aldrich |
| | | MYCN_as | UCGCUCAGGGUGUCCUCUC | | |

FUNCTIONAL HIGH-THROUGHPUT SCREENING REVEALS
miR-323a-5p AND miR-342-5p AS TUMOR-SUPPRESSIVE
microRNA FOR NEUROBLASTOMA


CELLULAR AND MOLECULAR LIFE SCIENCE

Soriano A*, **Masanas M***, Boloix A, Masiá N, París-Coderch L, Piskareva O, Jiménez C,
Henrich KO, Roma J, Westermann F, Stallings RL, Sábado C, de Toledo JS,
Santamaria A, Gallego S, Segura MF. (* authors contributed equally)

DOI: 10.1007/s00018-019-03041-4



Functional high-throughput screening reveals miR-323a-5p and miR-342-5p as new tumor-suppressive microRNA for neuroblastoma

Aroa Soriano¹ · Marc Masanas¹ · Ariadna Boloix^{1,2} · Núria Masiá³ · Laia París-Coderch¹ · Olga Piskareva⁴ · Carlos Jiménez¹ · Kai-Oliver Henrich⁵ · Josep Roma¹ · Frank Westermann⁵ · Raymond L. Stallings⁴ · Constantino Sábado⁶ · Josep Sánchez de Toledo^{1,6} · Anna Santamaria³ · Soledad Gallego^{1,6} · Miguel F. Segura¹ 

Received: 1 October 2018 / Revised: 28 January 2019 / Accepted: 4 February 2019
© The Author(s) 2019

Abstract

Current therapies for most non-infectious diseases are directed at or affect functionality of the human translated genome, barely 2% of all genetic information. By contrast, the therapeutic potential of targeting the transcriptome, ~ 70% of the genome, remains largely unexplored. RNA therapeutics is an emerging field that widens the range of druggable targets and includes elements such as microRNA. Here, we sought to screen for microRNA with tumor-suppressive functions in neuroblastoma, an aggressive pediatric tumor of the sympathetic nervous system that requires the development of new therapies. We found miR-323a-5p and miR-342-5p to be capable of reducing cell proliferation in multiple neuroblastoma cell lines in vitro and in vivo, thereby providing a proof of concept for miRNA-based therapies for neuroblastoma. Furthermore, the combined inhibition of the direct identified targets such as CCND1, CHAF1A, INCENP and BCL-XL could reveal new vulnerabilities of high-risk neuroblastoma.

Keywords Pediatric cancer · Non-coding RNA · High-throughput screening · 14q32 · Epigenetics · Cancer therapy

Introduction

Approximately 15,000 new cases of pediatric cancers are diagnosed yearly in Europe, with around 10% corresponding to neuroblastoma (NB), an embryonal tumor of the sympathetic nervous system [1]. NB accounts for 15% of all cancer-related deaths in children, and is the embryonal tumor with the lowest 5-year relative survival [2]. Significant improvements are only foreseen in the field of new targeted

Aroa Soriano and Marc Masanas contributed equally to this work.

Electronic supplementary material The online version of this article (<https://doi.org/10.1007/s00018-019-03041-4>) contains supplementary material, which is available to authorized users.

✉ Miguel F. Segura
miguel.segura@vhir.org

- ¹ Group of Translational Research in Child and Adolescent Cancer, Vall d'Hebron Research Institute (VHIR)-Universitat Autònoma de Barcelona (UAB), Passeig Vall d'Hebron 119-129, Collserola Building, Lab 207, 08035 Barcelona, Spain
- ² Institut de Ciència de Materials de Barcelona (ICMAB-CSIC) and Nanomol Technologies SA, Mòdul de Recerca B, Campus UAB, 08193 Bellaterra, Spain
- ³ Cell Cycle and Cancer Laboratory, Biomedical Research Group in Urology, Vall d'Hebron Research Institute

(VHIR)-Universitat Autònoma de Barcelona (UAB), Passeig Vall d'Hebron 119, 08035 Barcelona, Spain

- ⁴ Molecular and Cellular Therapeutics, Royal College of Surgeons in Ireland and National Children's Research Centre Our Lady's Children's Hospital, Dublin, Ireland
- ⁵ Neuroblastoma Genomics Group, German Cancer Research Center (DKFZ), Im Neuenheimer Feld 280, 69120 Heidelberg, Germany
- ⁶ Pediatric Oncology and Hematology Department, Hospital Universitari Vall d'Hebron-Universitat Autònoma de Barcelona (UAB), Passeig Vall d'Hebron 119, 08035 Barcelona, Spain

therapies and personalized medicine programs which, at present, are effective for a small number of patients. Therefore, new approaches must be considered.

RNA therapeutics is an emerging field that widens the range of druggable targets and includes elements such as small interference RNA (i.e., siRNA, shRNA and microRNA). MicroRNA (miRNA) are small non-coding RNA that interfere with the translation and stability of coding mRNA in a sequence-specific manner [3]. Mounting evidence shows miRNA to be deregulated and functionally contributing to the development and progression of different human cancers, including NB [4, 5]. An overall reduction in miRNA is observed in advanced NB, mainly due to alterations in the miRNA-processing machinery [6]; therefore, miRNA restoration represents an attractive novel therapeutic approach.

To identify miRNA with therapeutic potential in NB, we carried out high-throughput functional screening of 2048 miRNA mimics. Several miRNA with potential tumor-suppressive functions were identified, among which miR-323a-5p and miR-342-5p had the highest therapeutic potential in multiple NB cell lines in vitro and in vivo. These

results support the use of miRNA-based restoration therapies as an alternative tool against NB resistant to conventional therapies.

Materials and methods

Cell lines

SK-N-AS, SH-SY5Y, IMR-32 and HEK293T cell lines were purchased from American Type Culture Collection (ATCC, Manassas, VA, USA), CHLA-90 cell line from the Children's Oncology Group Cell Culture and Xenograft Repository (Lubbock, TX, USA). SK-N-BE(2) and LA1-5s acquired from Public Health England Culture Collections (Salisbury, UK). All cell lines purchased from the tissue banks were amplified and stored in liquid nitrogen. Upon resuscitation, cells were maintained in culture for no more than 2 months. SK-N-AS, SK-N-BE(2), SH-SY5Y, IMR-32, CHLA-90 and LA1-5s were cultured and maintained in Iscove's modified Dulbecco's medium (Life Technologies,

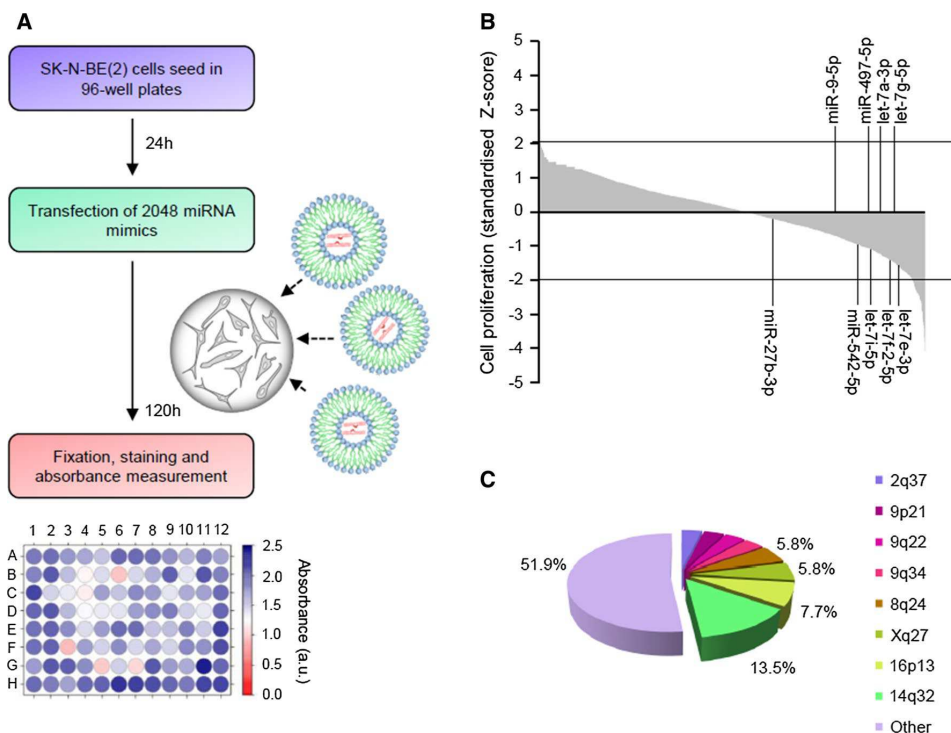


Fig. 1 Functional high-throughput miRNA screening identified several tumor-suppressive miRNA. **a** Screening design. **b** Graph representing the effects of 2048 individual miRNA on cell proliferation. The percentage of growth inhibition was obtained by comparing the average of three independent miRNA mimics replicates with mock-

transfected cells and standardized using the Z score transformation method. MiRNA previously reported as tumor-suppressive miRNA in NB are indicated. **c** Pie chart representing the genomic distribution of miRNA that were capable of reducing cell proliferation ~50% (Z score < -2)

Thermo Fisher Scientific) supplemented with 10% heat-inactivated fetal bovine serum (South America Premium, Biowest) and 1% of insulin–transferrin–selenium Supplement (Life Technologies, Thermo Fisher Scientific). HEK293T were grown in Dulbecco’s modified Eagle’s medium (Life Technologies, Thermo Fisher Scientific) supplemented with 10% heat-inactivated fetal bovine serum. All media were supplemented with 100 U/mL penicillin, 100 µg/mL streptomycin (Life Technologies, Thermo Fisher Scientific) and 5 µg/mL plasmocin (InvivoGen). All cultures were maintained at 37 °C in a saturated atmosphere of 95% air and 5% CO₂. All cell lines were frequently tested for mycoplasma contamination.

MicroRNA functional high-throughput library screening

Chemoresistant SK-N-BE(2) cells were seeded in 96-well plates at 5000 cells/well using the MultidropV2 dispenser (Finstruments). Twenty-four hours later cells were transfected with a microRNA library consisting of 2048 human miRNA mimics (Dharmacon, Lafayette, CO, USA, miRIDIAN® microRNA Library—Human Mimic (19.0) CS-001030 Lot 13112, GE Healthcare, 25 nM each miRNA

in technical triplicates using Lipofectamine 2000 (Life technologies, Thermo Fisher Scientific, Madrid, Spain, 0.2 µL per well) using the Robotic Platform Caliper SciClone (Caliper Life Sciences, Perkin Elmer, Waltham, Massachusetts, USA). At 96-h post-transfection, cells were fixed with 1% glutaraldehyde (Sigma-Aldrich) and stained with 0.5% crystal violet (Sigma-Aldrich, Madrid, Spain). Crystals were dissolved with 15% acetic acid (Fisher Scientific) and absorbance was measured at 590 nm using an Epoch Microplate Spectrophotometer (Biotek, Winooski, Vermont, USA).

Screening statistics

Data quality control and analysis of different factors (e.g., miRNA position, transfection time) was performed using “R” Statistical Software (Supplementary Fig. 1C).

The absorbance value of each mock- or miRNA-transfected well was normalized to the median of all non-transfected values of the corresponding replicate plate. To evaluate the effect of each miRNA on cell proliferation, the absorbance value (3 replicates) versus the median of all mock values was compared. The statistical significance was assessed by Student’s *t* test and the *p* value was adjusted by the false discovery rate “FDR” method. The percentage of

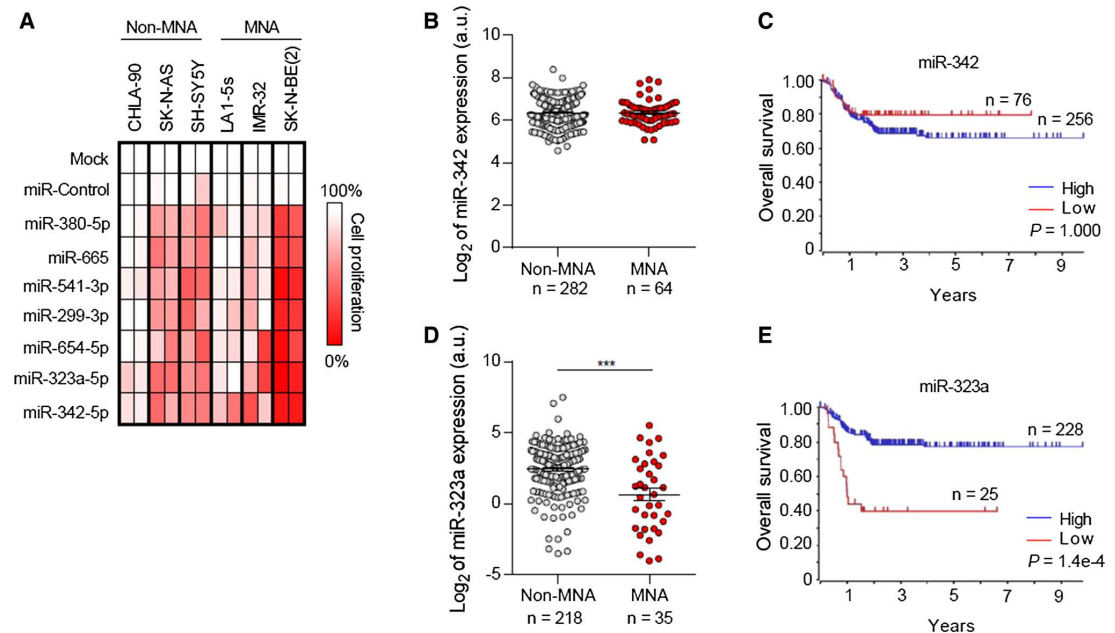
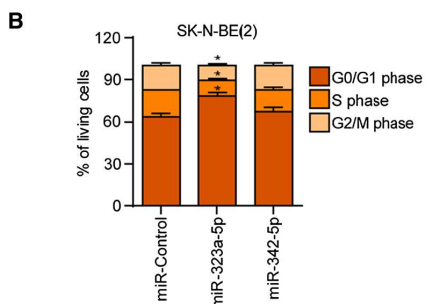
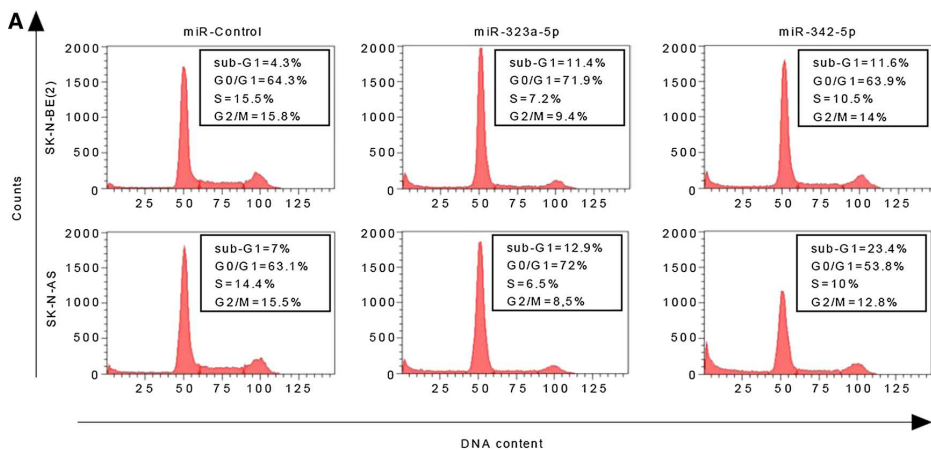
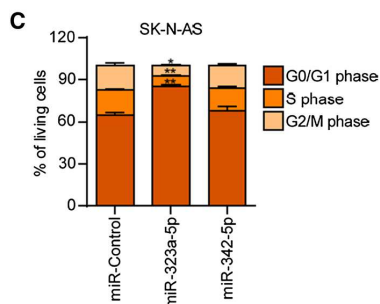


Fig. 2 Ectopic expression of miRNA located at 14q32 reduced cell proliferation in multiple NB cell lines. **a** Heatmap representing effects of the indicated miRNA on cell proliferation reduction in MYCN amplified (MNA) and MYCN non-amplified (non-MNA) cell lines. The overexpression effect of each miRNA on cell proliferation was

compared to mock-transfected cells. **b, d** Relative expression (log₂) of miR-342 (**b**) and miR-323a (**d**) in MNA and non-MNA NB tumors. **c, e** Overall survival Kaplan–Meier plot of the indicated miRNA expression in human NB tissues



| | miR-Control | miR-323a-5p | miR-342-5p |
|-------------|-------------|-------------|------------|
| G0/G1 phase | 63.7 ± 2.3 | 78.5 ± 2.4 | 67.0 ± 3.4 |
| S phase | 18.7 ± 0.5 | 10.9 ± 1.2 | 16.1 ± 1.6 |
| G2/M phase | 17.5 ± 1.9 | 10.6 ± 1.3 | 17.0 ± 1.9 |



| | miR-Control | miR-323a-5p | miR-342-5p |
|-------------|-------------|-------------|------------|
| G0/G1 phase | 64.8 ± 1.8 | 85.3 ± 1.3 | 67.4 ± 3.0 |
| S phase | 17.8 ± 0.5 | 7.3 ± 0.9 | 16.0 ± 1.8 |
| G2/M phase | 17.4 ± 1.8 | 7.3 ± 0.7 | 16.3 ± 1.6 |

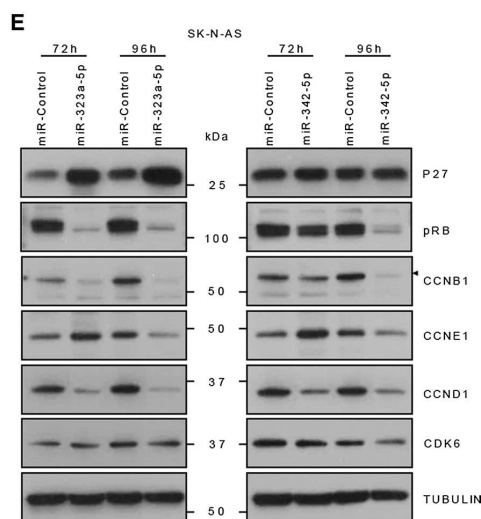
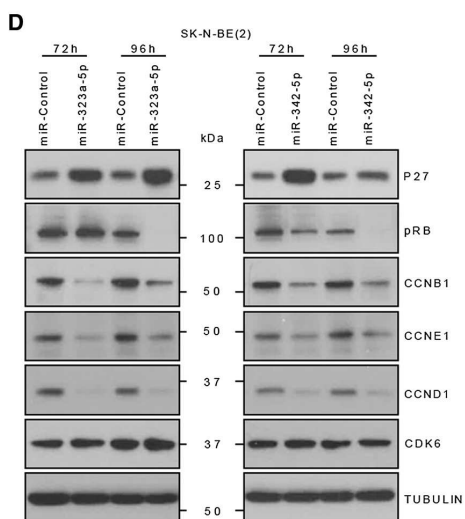


Fig. 3 MiR-323a-5p induced cell cycle arrest at G0/G1 phase. Cell cycle flow cytometry analysis of the indicated cell lines transfected with miR-control, miR-323a-5p or miR-342-5p at 25 nM for 96 h. **a** One representative histogram of three independent experiments. **b, c** Histograms representing the average percentage of living cell population from three independent experiments of SK-N-BE(2) (**b**) or SK-N-AS (**c**) cells in G0/G1, S, or G2/M phases. * $p < 0.05$, ** $p < 0.01$, two-tailed Student's *t* test. **d, e** Western blot of the indicated cell cycle regulatory proteins in SK-N-BE(2) (**d**) and SK-N-AS (**e**) transfected with miR-control, miR-323a-5p and miR-342-5p (25 nM) at 72 h and 96 h post-transfection

proliferation was standardized using the Z score equation $Z = \frac{x-\mu}{\sigma}$, where x is the value of cell proliferation after transfection of each single miRNA, μ is the mean cell proliferation of all miRNA and σ the standard deviation.

Mouse xenograft

SK-N-AS cells (4×10^6) were reverse transfected with 25 nM of miR-control, miR-323a-5p or miR-342-5p in 100-mm plates (25 μ L lipofectamine/dish). SK-N-BE(2) cells (4.7×10^6) were reverse transfected with 25 nM of miR-control, miR-323a-5p or miR-342-5p in T175 flasks (90 μ L lipofectamine/flask). Thirty-six hours post-transfection, 4×10^6 cells/flank of SK-N-AS and 5×10^6 cells/flank of SK-N-BE(2) were injected into the right flank of 6- to 8-week-old female NMRI-nude mice ($n = 13$ mice/condition of SK-N-AS and $n = 15$ mice/condition of SK-N-BE(2)) (Janvier Labs, Le Genest-Saint-Isle, France) in 300 μ L of PBS:Matrigel (1:1). Tumor volume was measured every 2–3 days. At the end of the experiment, the primary tumors were removed and weighted. Part of the tumors were fresh frozen and the rest fixed in 10% formalin and embedded in paraffin.

Statistical methods

Unless otherwise stated, mean \pm SEM values are representative of the average of three independent experiments. Statistical significance was determined by unpaired two-tailed Student's *t* test (GraphPad Prism Software, La Jolla, CA, USA.). * Means $p < 0.05$, ** means $p < 0.01$ and *** means $p < 0.001$.

Results

Functional high-throughput miRNA screening identified several miRNA with tumor-suppressive activity

High-throughput screening using the largest library of miRNA mimics available was performed to identify miRNA

with tumor-suppressive functions in NB. Individual miRNA mimics were transfected into the SK-N-BE(2) cells (Fig. 1a). Control miRNA (i.e., cel-miR-67 and cel-miR-239b) were used as negative controls and miR-497-5p as a positive control [7, 8] (Supplementary Fig. 1a,b). The overexpression of 52 miRNA was found to reduce ~50% cell proliferation (Z score < -2 , adjusted p value < 0.05) (Fig. 1b; Supplementary Tables 1, 2).

Since it has been suggested that miRNA with similar functions cluster together [9], we examined the genomic distribution of miRNA whose overexpression produced the highest reduction on cell proliferation. Interestingly, 7 of the 52 miRNA (13.5%) were located at 14q32 (Fig. 1c and Supplementary Table 2), a locus with high miRNA density and frequently lost or silenced in different types of tumors, including NB [10].

Restoration of miRNA located at 14q32 reduced cell viability in multiple NB cell lines

The tumor-suppressive effects of miRNA hits located at 14q32 (i.e., miR-380-5p, miR-665, miR-541-3p, miR-299-3p, miR-654-5p, miR-323a-5p and miR-342-5p) were further confirmed in an extended panel of six NB cell lines bearing genomic alterations associated with resistance to standard NB therapies and poor patient outcome (Supplementary Table 3). The overexpression of all miRNA tested reduced cell proliferation in multiple NB cell lines compared with mock- and miR-control-transfected cells being miR-323a-5p and miR-342-5p those ones with the highest therapeutic potential (Fig. 2a).

Low miR-323a-5p expression levels correlate with poor patient outcome

The expression levels of miR-323a-5p and miR-342-5p were analyzed in a large cohort of NB tissue samples and correlated with clinical parameters. Whereas lower expression levels of miR-342-5p did not correlate with the clinical parameters analyzed (Fig. 2b–c), low miR-323a-5p levels were found to correlate with MYCN genomic amplification (Fig. 2d) and shorter overall survival (Fig. 2e).

Ectopic expression of miR-323a-5p and miR-342-5p halted cell cycle progression and induced apoptosis in NB

To clarify whether the reduction in cell number upon miR-323a-5p and miR-342-5p overexpression was due to inhibition of cell proliferation and/or induction of cell death, cell cycle progression was analyzed using flow cytometry. The overexpression of miR-323a-5p induced a modest increase

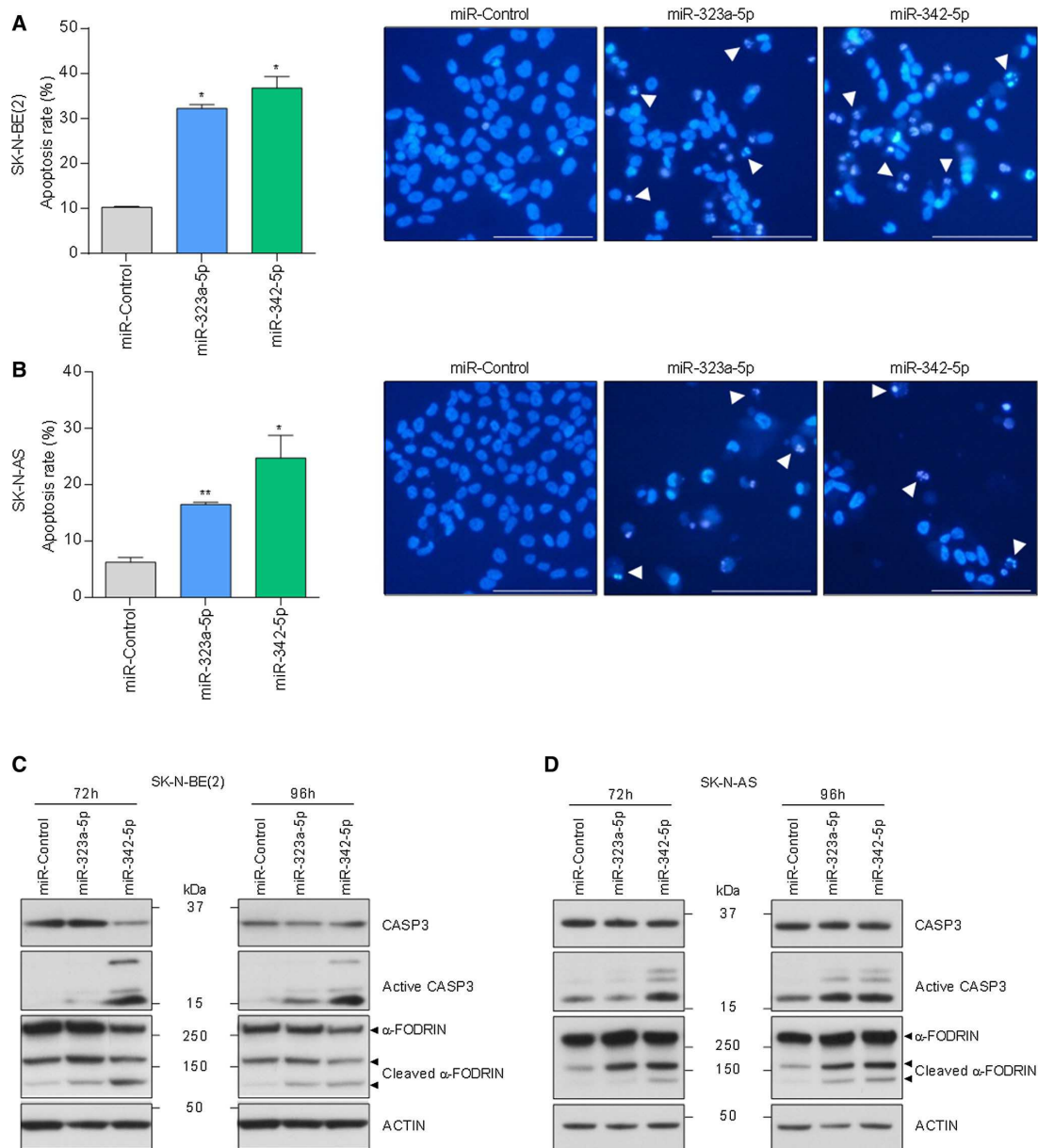


Fig. 4 MiR-323a-5p and miR-342-5p overexpression induced apoptosis in NB cells. **a, b** Analysis of chromatin fragmentation/condensation in SK-N-BE(2) (**a**) and SK-N-AS (**b**) transfected with 25 nM of miR-control, miR-323a-5p or miR-342-5p 96 h post-transfection. Images on the right show a representative field of NB cells stained with Hoechst dye. White arrowheads point to cells with condensed

and/or fragmented chromatin. Data represent mean \pm SEM of three independent experiments ($n=3$ per experiment). * $p<0.05$, ** $p<0.01$, two-tailed Student's t test. **c, d** Representative Western blot analysis of apoptosis-related proteins in SK-N-BE(2) (**c**) and SK-N-AS (**d**) transfected with miR-control, miR-323a-5p or miR-342-5p (25 nM) at 72 h and 96 h post-transfection

in the subG1 peak and an increment in G0/G1-phase population accompanied by a reduction in the S and G2/M phases. Therefore, both cell cycle arrest and increased cell death might be contributing to the miR-323a-5p overexpression phenotype (Fig. 3a–c). Concurring with these observations, a reduction in cyclins, D1, E1 and B1 was observed after miR-323a-5p overexpression at 72 h post-transfection and a consequent reduction in phospho-RB levels at later time points. Furthermore, upregulation of the cell cycle inhibitor p27 was also observed (Fig. 3d, e).

MiR-342-5p-transfected cells showed no apparent differences regarding cell cycle progression compared to miR-control cells, but did show an accumulation of cells in subG1, thereby indicating cell death induction (Fig. 3a–c). In this case, reduced levels of cyclins, D1, E1 and B1 and phospho-RB, but not increased p27 levels, were also observed (Fig. 3d, e), suggesting that cells committed to die were unable to progress through the cell cycle.

Next, we examined the chromatin status of miRNA-transfected cells by Hoechst staining. MiR-323a-5p and miR-342-5p transfected cells showed a higher percentage of cells with condensed and fragmented chromatin staining, one of the typical hallmarks of apoptosis (Fig. 4a, b). Furthermore, NB cells transfected with miR-323a-5p and miR-342-5p showed cleavage of the executor caspase-3 and one of its targets α -FODRIN, both indicative of apoptotic cell death (Fig. 4c, d).

MiR-323a-5p and miR-342-5p target cell cycle and survival genes

To find the downstream mediators of miR-323a-5p and miR-342-5p phenotypic effects in NB, a miRNA-target analysis was performed comparing five different platforms (Fig. 5a, b). For miR-323a-5p, 905 potential targets were predicted by at least four independent algorithms, whereas 1380 were predicted for miR-342-5p (Supplementary Tables 4, 5). According to the Kyoto Encyclopedia of Genes and Genomes (KEGG) pathway analysis [11], a significant number of these predicted targets were associated with cell cycle or commonly altered pathways in cancer (Fig. 5c, d, p value < 0.05). These genes were selected for validation based on their expression association with NB outcome and/or previous reported functional role in cancer (Supplementary Tables 6, 7). Transient miRNA overexpression proved to consistently reduce the mRNA levels of several miR-323a-5p (i.e., *CHAF1A*, *KIF11*, *INCENP*, *CDC25A*, *CCND1*, *FADD* and *E2F2*) and miR-342-5p (i.e., *AKT2*, *CCND1*, *MKNK2* and *BCLX*) predicted targets (Supplementary Fig. 2a–d). To confirm the reduction also in protein levels, Western blot was performed at 48 h and 72 h post-transfection of miR-323a-5p or miR-342-5p. *CHAF1A*, *KIF11*, *INCENP*, *CDC25A*, *CCND1* and *FADD* protein

levels decreased in both cell lines when cells were transfected with miR-323a-5p (Fig. 5e). On the other hand, only *CCND1* and *BCL-XL* protein levels were reduced in both cell lines when cells were transfected with miR-342-5p, whereas no differences were found in *AKT2* levels. Results for *MKNK2* were not conclusive (Fig. 5f).

To ascertain whether the potential targets were regulated directly by miR-323a-5p or miR-342-5p, we engineered luciferase-reporter vectors with the 3'UTR of genes bearing the putative miRNA-binding sites (Supplementary Fig. 3). The reporter vectors were co-transfected with a miR-control, miR-323a-5p or miR-342-5p and luciferase activity was quantified 24 h after transfection. The overexpression of miR-323a-5p caused a reduction in luciferase activity in the *CHAF1A*, *INCENP*, *CCND1* and *FADD* 3'UTR reporter vectors and no differences were observed for *KIF11* and *CDC25A*, thereby indicating that these last two genes are not direct targets (Fig. 5g). On the other hand, reduction in the luciferase activity of *CCND1* and *BCLX* 3'UTR vectors by miR-342-5p overexpression confirmed both genes as direct miR-342-5p targets (Fig. 5h).

CCND1, CHAF1A and INCENP silencing mostly reproduced miR-323a-5p overexpression effects

The contribution of each target to the miRNA overexpression phenotype was analyzed by siRNA-mediated gene silencing. Silencing of *CHAF1A*, *KIF11* and *CCND1* showed a reduction in cell proliferation similar to that induced by miR-323a-5p, while *INCENP* and *FADD* silencing only produced a moderate effect (Fig. 6a). Western blot analysis 72 h post-transfection confirmed siRNA efficacy (Fig. 6a, lower panels). Overall, *CCND1* depletion mirrored the best miR-323a-5p overexpression, not only the general effects on cell proliferation, but also on the reduction in phospho-RB levels and p27 accumulation (Fig. 6b). However, when apoptosis induction was analyzed, *CHAF1A* and *INCENP* were the direct targets that better phenocopied the effects of miR-323a-5p overexpression (Fig. 6c). These results suggest that the combination of *CCND1*, *CHAF1A* and *INCENP* inhibition is sufficient to reproduce the therapeutic effects of miR-323a-5p.

Inhibition of CCND1 and BCL-XL partially reproduces the effects of miR-342-5p

The same strategy was used to characterize the contribution of miR-342-5p targets. In this case, only the inhibition of *CCND1* showed a similar reduction in cell proliferation (Fig. 6d). In agreement with this observation, only *CCND1* silencing caused a reduction in phospho-RB levels and accumulation of the cell cycle inhibitor p27 (Fig. 6e). However, apoptosis induction was not observed with silencing

Fig. 5 MiR-323a-5p and miR-342-5p modulated the expression of multiple cancer-related genes. **a, b** Venn diagram representing the overlap of predicted target genes among five miRNA-target prediction algorithms of miR-323a-5p or miR-342-5p. **c, d** Representation of the functional annotation of predicted target genes of miR-323a-5p (**c**) or miR-342-5p (**d**) using KEGG pathways and Gene Ontology databases. Red bars indicate selected pathways to analyze potential miRNA targets. **e, f** Representative Western blot of predicted target genes in SK-N-BE(2) and SK-N-AS transfected with miR-control, miR-323a-5p (**e**) or miR-342-5p (**f**) at 48 h and 72 h post-transfection. **g, h** Luciferase 3'UTR reporter assays. Graph represents luciferase activity in HEK-293T cells co-transfected with 50 ng/well of the indicated reporter vectors and 25 nM of miR-control, miR-323a-5p (**g**) or miR-342-5p (**h**). Data represented the average \pm SEM of three independent experiments ($n=3$ per experiment). * $p<0.05$, ** $p<0.01$, *** $p<0.001$

of either CCND1 or BCL-XL (Fig. 6f) suggesting that the observed effects of miR-342-5p on cell death might require the inhibition of both or additional targets.

MiR-323a-5p and miR-342-5p overexpression reduced tumor growth in vivo

We proceeded to validate the capacity of miR-323a-5p and miR-342-5p to reduce tumor growth in vivo by subcutaneous injection of SK-N-BE(2) or SK-N-AS cells previously transfected with miR-control, miR-323a-5p or miR-342-5p into the flank of NRMI-nude mice. At the end of the experiment, all groups showed a similar percentage of tumor incidence (~80–100%, Fig. 7a, e), which suggested that miRNA overexpression did not interfere with tumor engraftment. Tumor growth was monitored every 2–3 days for 28 days for SK-N-BE(2) or 18 days for SK-N-AS. While in SK-N-AS, only the overexpression of miR-342-5p was capable of delaying cell growth in vivo, both miRNA were effective in SK-N-BE(2) cells, showing a final ~ twofold reduction in tumor growth at the end of the experiment (Fig. 7b, f). These effects were confirmed by the analysis of tumor weight (Fig. 7c, d, g, h-Supplementary Fig. 4a, b).

In summary, our results confirm miR-323a-5p and miR-342-5p as potential therapeutic tools against high-risk NB. Of note, miR-323a-5p overexpression impaired tumor growth in the MYCN-amplified cell line, but not in SK-N-AS, suggesting that higher doses of miR-323a-5p or being functional for longer periods of time may be needed to achieve a therapeutic effect. In support of this hypothesis, miRNA levels were analyzed at the beginning and at the end of experiment. Both cell lines achieved similar levels of miRNA overexpression at the time of injection (Supplementary Fig. 5a, c) ruling out the possibility of differential transfection efficiency between cell lines. However, at the end of experiment, SK-N-AS maintained much lower levels of miR-323a-5p in SK-N-AS but not in SK-N-BE(2) (Supplementary Fig. 5b, d), thus suggesting that this miRNA is processed faster in this cell line and therefore,

tumor cells overcome more easily the miR-323a-5p tumor-suppressive effects.

Discussion

Despite the emerging personalized medicine programs for pediatric tumors, which include molecular profiling of NB, the small number of recurrent somatic mutations found at diagnosis and the lack of established tumor drivers, limit the therapeutic opportunities for NB patients. On the other hand, some patients relapse and develop drug resistance when treated with anticancer drugs targeting single molecules, which might be due to the activation of alternative pathways.

MiRNA alterations have been shown to participate in the progression and outcome of NB (reviewed in [12]). We propose the use of miRNA as multi-target approach to overcome treatment resistance in NB patients, given that a single miRNA can inhibit multiple targets involved in tumorigenic processes.

Multiple pharmaceutical companies have already included miRNA in their developmental drug pipelines (e.g., miR-34 [13, 14], miR-16 [15], miR-122 [16]). The first challenge in applying this approach to the treatment of high-risk NB is to identify those miRNA with the highest therapeutic potential. Our work is the largest high-throughput functional screening performed to date to identify miRNA with tumor-suppressive functions in cancer and particularly for NB. Of the 2048 miRNA tested, we identified 52 that significantly reduced cell proliferation with a Z score lower than -2 (~50% of cell proliferation). Concurring with previous reports, multiple tumor-suppressive miRNA such as members of the let-7 miRNA tumor-suppressive family (e.g., let-7i-5p, let-7a-3p, let-7f-2-5p, let-7g-5p or let-7e-3p [17, 18]) were also identified in our screening, thereby validating our approach to identifying tumor-suppressive miRNA.

Notably, 7 of the 52 miRNA (13.5% of the total) shown to reduce cell proliferation ~50% are encoded in the 14q32 genomic region. This region is frequently altered in cancer and particularly in NB [10], which raises the possibility that this region contains tumor-suppressor genes. All 7 miRNA identified in our screening showed the capacity to reduce cell proliferation in multiple NB cell lines in vitro, with miR-323a-5p and miR-342-5p being those with the highest therapeutic potential.

In agreement with our results, miR-323a-5p has been reported to be downregulated in NB patients with MYCN amplification and associated with unfavorable outcome [19, 20]. Moreover, miR-323a-5p overexpression has been reported to reduce proliferation and promote apoptosis of human cerebral glioma cells [21]. We found that ectopic expression of miR-323a-5p suppressed cell growth through

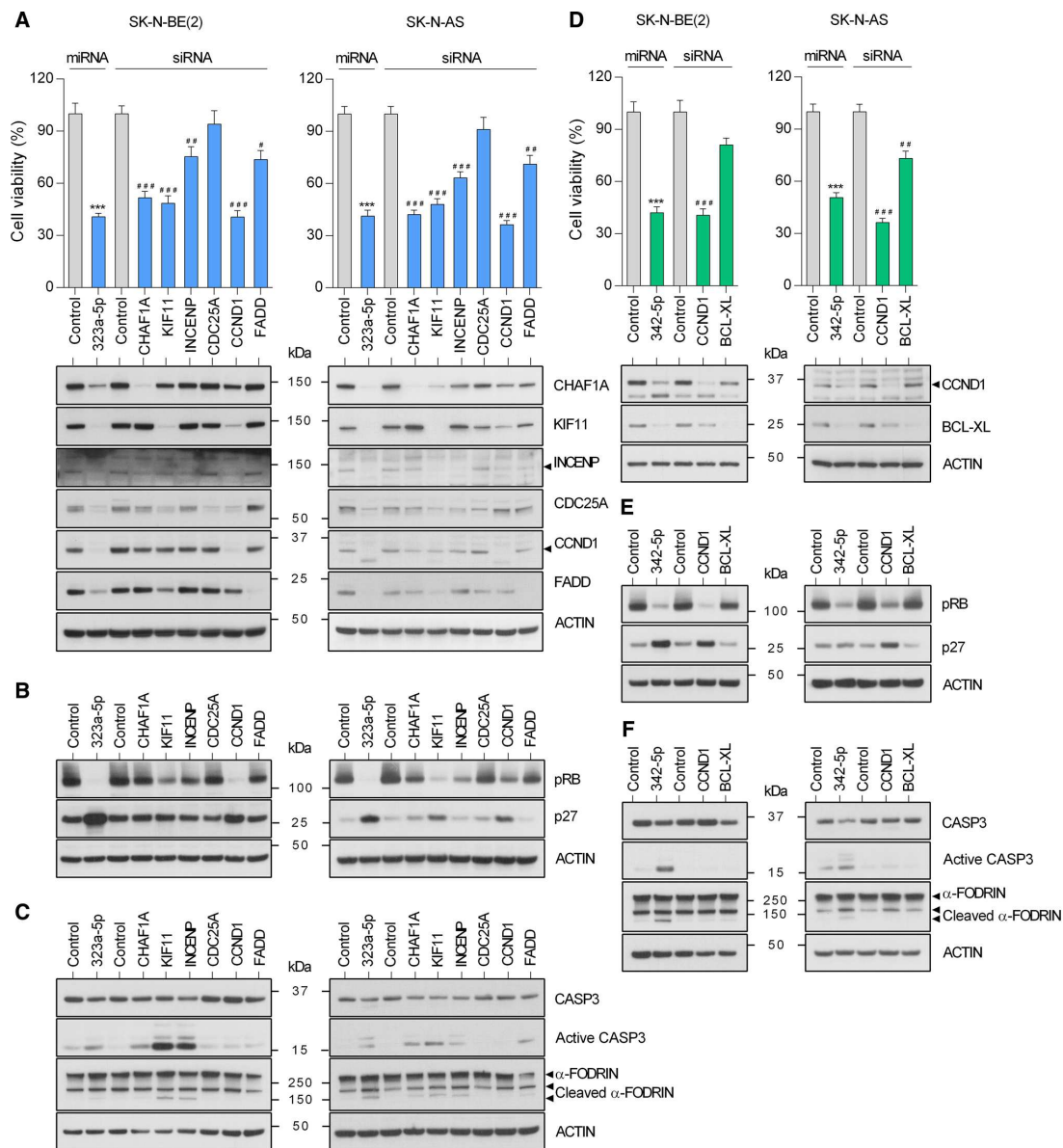


Fig. 6 MiRNA target-knockdown partially reproduced the antitumoral effects of miR-323a-5p and miR-342-5p. **a, d** Cell viability assay of SK-N-BE(2) and SK-N-AS transfected with 25 nM of miR-323a-5p, miR-342-5p or the indicated siRNA. Target protein knockdown was analyzed by Western blot at 72 h post-transfection (lower panels). **b, e** Expression of some representative cell cycle regulatory proteins in SK-N-BE(2) and SK-N-AS transfected with miR-323a-5p, miR-342-5p or the indicated siRNA (25 nM) at 96 h post-transfection.

c, f Western blot analysis of apoptosis-related proteins in SK-N-BE(2) and SK-N-AS transfected with miR-323a-5p, miR-342-5p or the indicated siRNA (25 nM) at 96 h post-transfection. Graph represents one of three independent experiments ($n=6$ per experiment). Asterisk compares miR-323a-5p or miR-342-5p versus miR-Control and hash compares each siRNA versus control siRNA. * or # $p < 0.05$, ** or ## $p < 0.01$, *** or ### $p < 0.001$, two-tailed Student's t test

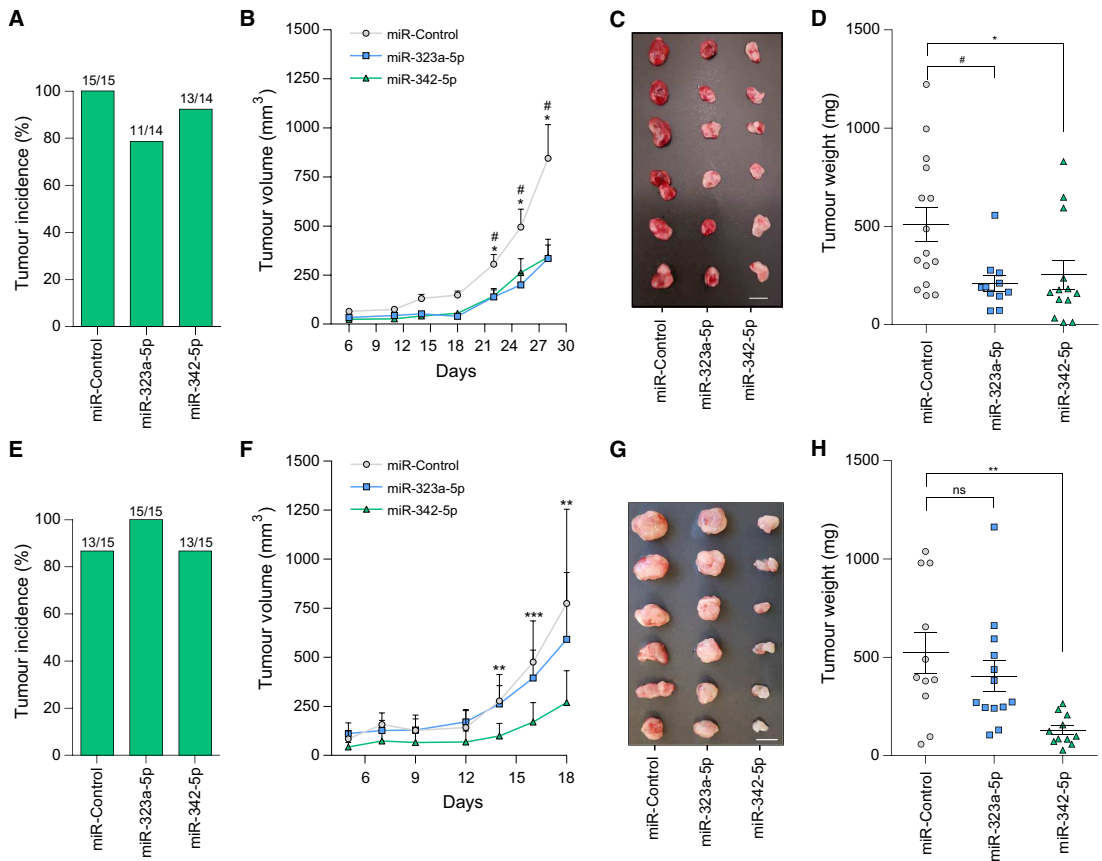


Fig. 7 MiR-323a-5p and MiR-342-5p overexpression reduced tumor growth in vivo. **a, e** Tumor formation incidence in SK-N-BE(2) (**a**) and SK-N-AS (**e**). **b, f** Tumor growth of xenografts derived from SK-N-BE(2) (**b**) SK-N-AS (**f**) cells transfected with miR-control, miR-323a-5p or miR-342-5p. Tumor measurements were taken three

times per week for ~ 3 weeks. **c, g** Representative images of dissected tumors (bar indicates 1 cm). **d, h** Tumor weight at 18 days post-injection. Hash compares miR-323a-5p versus control and asterisk compares miR-342-5p versus control. * or # $p < 0.05$, ** $p < 0.01$, *** $p < 0.001$, two-tailed Student's *t* test

the direct modulation of several cell cycle-associated genes such as *CCND1*, *CHAF1A*, *INCENP* and *FADD* and caused a G1 cell cycle arrest followed by induction of apoptosis. The silencing of the miR-323a-5p direct targets *CHAF1A*, *INCENP* and *CCND1* were those that more closely recapitulate the phenotypic effects of miR-323a-5p overexpression. *CCND1* is a well-established oncogene frequently overexpressed and associated with poor outcome in different types of tumors including NB [25]. *CCND1* interacts with *CDK4* and *CDK6* and the activation of this complex phosphorylates *RB* and other transcription factors which promote cell cycle progression [26]. To date, the best approach to targeting *CCND1* is through the use of *CDK4/6* inhibitors such as palbociclib, ribociclib and abemaciclib.

Although the best known functions of *CCND1* are related to cell cycle control, *CCND1* has CDK-independent functions. For example, *CCND1* regulates cell differentiation by binding to several transcription factors such as the estrogen receptor α (*ER* α) and the androgen receptor (*AR*) (reviewed in [27]). Therefore, a direct inhibition of *CCND1* could be therapeutically more effective than *CDK4/6* inhibition.

Another of the newly identified relevant miR-323a-5p target is *CHAF1A*, a chromatin modifier protein recently involved in maintaining the undifferentiated state of highly aggressive NB [28]. Thus, in addition to halting cell cycle progression, miR-323a-5p could also be relevant for NB therapy through repressing the expression of genes that block the differentiation of NB cells.

The silencing of *INCENP* phenocopied the apoptosis induction of miR-323a-5p overexpression. *INCENP* (inner centromere protein) is a component of the chromosomal passenger complex (CPC), a complex that regulates mitosis. *INCENP* is a scaffolding subunit for the CPC and activates Aurora B kinase [29]. Similar to *CHAF1A*, high levels of *INCENP* in primary NB tumors are associated with poor prognosis (Supplementary Table 6). In addition, silencing of *INCENP* using doxycycline-inducible shRNA led to significant decreases in growth of NB xenografts and increases mice survival (Sun et al. *Advances in Neuroblastoma Research* 2018). Therefore, targeting *INCENP* could be a novel promising therapy in NB.

Our *in vivo* studies suggested that the transient overexpression of miR-323a-5p was enough to halt the proliferation of MYCN-amplified NB cells but not in SK-N-AS xenograft models, probably due to a higher rate of miRNA processing. At that point, and owing to technical limitations, the fact that more sustained overexpression of miR-323a-5p could have a better therapeutic response cannot be ruled out.

In contrast, the transient overexpression of miR-342-5p did show faster induction of cell death *in vitro* and a clear reduction in tumor growth *in vivo* in both NB xenografts tested. In line with our observations, miR-342-5p was reported to be downregulated in breast cancer patients with early relapse [22] and was able to reduce HER2-positive breast cancer cell growth [23] and colon cancer cells [24].

Interestingly, we found that miR-342-5p is also a direct modulator of *CCND1*. *CCND1* silencing alone caused a dramatic decrease in NB cell proliferation, but was not enough to induce cell death (Fig. 6c, f). We also identified *BCL-XL* as a direct target of miR-342-5p. *BCL-XL* is an anti-apoptotic member of the B cell lymphoma 2 (*BCL-2*) protein family whose overexpression contributes to tumor progression and resistance to chemotherapeutic agents [30]. Although *BCL-XL* reduction alone only causes a minimal reduction in cell number and did not induce cell death (Fig. 6f), it may lower the threshold of apoptosis induction upon *CCND1* silencing or inhibition. Therefore, the concomitant reduction in *CCND1* and *BCL-XL* would more faithfully reproduce the overexpression effects of miR-342-5p.

Conclusions

Our strategy is confirmed as valid for the identification of novel tumor-suppressive miRNA such as miR-323a-5p and miR-342-5p in NB models, including but not limited to the ones that are resistant to conventional therapies and reveals new vulnerabilities of high-risk NB through the combined inhibition of targets such as *CCND1*, *CHAF1A*, *INCENP* and *BCL-XL*.

Acknowledgements We thank members of Laboratory Animal Service and Statistics and Bioinformatics Unit of Vall d'Hebron Research Institute and the staff of Biomolecular Screening and Protein Technologies Unit of Centre for Genomic Regulation. We thank Ms. Christine O'Hara for text correction.

Author contributions AS and MFS designed the study. MM, AS, AB, LPC, CJ and MFS performed the experiments. NM and AS collaborated in cell cycle analysis. AS, MM, OP, RLS, FW, KOH and CS analyzed the data. JST, SG provided intellectual support and expertise toward interpretation of results. MM and MFS wrote the original manuscript. All authors contributed to the edition and the critical review of the manuscript.

Funding The funding was received by Ministerio de Educación, Cultura y Deporte (Grant no. FPU16/01099), Instituto de Salud Carlos III (Grant no. CP11/00052), Instituto de Salud Carlos III (Grant no. CP16/00006), Instituto de Salud Carlos III (Grant no. P114/00561), Instituto de Salud Carlos III (Grant no. P114/00647), Instituto de Salud Carlos III (Grant no. P117/00564), Instituto de Salud Carlos III (Grant no. RD12/0036/0016), FP7 People: Marie-Curie Actions (Grant no. MIRNATHERAPYNBL_PEOPLE-2013-GIC), Fundación Científica Asociación Española Contra el Cáncer (Grant no. AECC-JB-2012-01), AGAUR (Grant no. 2014 SGR 660), Asociación Acunapatata and Asociación NEN.

Open Access This article is distributed under the terms of the Creative Commons Attribution 4.0 International License (<http://creativecommons.org/licenses/by/4.0/>), which permits unrestricted use, distribution, and reproduction in any medium, provided you give appropriate credit to the original author(s) and the source, provide a link to the Creative Commons license, and indicate if changes were made.

References

1. Maris JM, Kyemba SM, Rebbeck TR, White PS, Sulman EP, Jensen SJ, Allen C, Biegel JA, Brodeur GM (1997) Molecular genetic analysis of familial neuroblastoma. *Eur J Cancer* 33(12):1923–1928. [https://doi.org/10.1016/S0959-8049\(97\)00265-7](https://doi.org/10.1016/S0959-8049(97)00265-7)
2. Gatta G, Ferrari A, Stiller CA, Pastore G, Bisogno G, Trama A, Capocaccia R (2012) Embryonal cancers in Europe. *Eur J Cancer* 48(10):1425–1433
3. Bartel DP (2009) MicroRNAs: target recognition and regulatory functions. *Cell* 136(2):215–233
4. Peng Y, Croce CM (2016) The role of MicroRNAs in human cancer. *Signal Transduct Target Ther* 1:15004. <https://doi.org/10.1038/sigtrans.2015.4>
5. Stallings RL (2009) MicroRNA involvement in the pathogenesis of neuroblastoma: potential for microRNA mediated therapeutics. *Curr Pharm Des* 15(4):456–462
6. Lin RJ, Lin YC, Chen J, Kuo HH, Chen YY, Diccianni MB, London WB, Chang CH, Yu AL (2010) microRNA signature and expression of Dicer and Drosha can predict prognosis and delineate risk groups in neuroblastoma. *Cancer Res* 70(20):7841–7850
7. Creevey L, Ryan J, Harvey H, Bray IM, Meehan M, Khan AR, Stallings RL (2013) MicroRNA-497 increases apoptosis in MYCN amplified neuroblastoma cells by targeting the key cell cycle regulator WEE1. *Mol Cancer* 12:23
8. Soriano A, Paris-Coderch L, Jubierre L, Martinez A, Zhou X, Piskareva O, Bray I, Vidal I, Almazan-Moga A, Molist C, Roma J, Bayascas JR, Casanovas O, Stallings RL, Sanchez de Toledo J, Gallego S, Segura MF (2016) MicroRNA-497 impairs the growth

- of chemoresistant neuroblastoma cells by targeting cell cycle, survival and vascular permeability genes. *Oncotarget* 7(8):9271–9287. <https://doi.org/10.18632/oncotarget.7005>
9. Wang Y, Luo J, Zhang H, Lu J (2016) microRNAs in the same clusters evolve to coordinately regulate functionally related genes. *Mol Biol Evol* 33(9):2232–2247
 10. Hoshi M, Otagiri N, Shiwaku HO, Asakawa S, Shimizu N, Kaneko Y, Ohi R, Hayashi Y, Horii A (2000) Detailed deletion mapping of chromosome band 14q32 in human neuroblastoma defines a 1.1-Mb region of common allelic loss. *Br J Cancer* 82(11):1801–1807. <https://doi.org/10.1054/bjoc.2000.1108>
 11. Kanehisa M, Goto S (2000) KEGG: kyoto encyclopedia of genes and genomes. *Nucleic Acids Res* 28(1):27–30
 12. Boloix A, Paris-Coderch L, Soriano A, Roma J, Gallego S, Sanchez de Toledo J, Segura MF (2015) Novel micro RNA-based therapies for the treatment of neuroblastoma. *An Pediatr (Barc)*. <https://doi.org/10.1016/j.anpedi.2015.07.016>
 13. Daige CL, Wiggins JF, Priddy L, Nelligan-Davis T, Zhao J, Brown D (2014) Systemic delivery of a miR34a mimic as a potential therapeutic for liver cancer. *Mol Cancer Ther* 13(10):2352–2360. <https://doi.org/10.1158/1535-7163.mct-14-0209>
 14. Beg MS, Brenner AJ, Sachdev J, Borad M, Kang YK, Stou-demire J, Smith S, Bader AG, Kim S, Hong DS (2017) Phase I study of MRX34, a liposomal miR-34a mimic, administered twice weekly in patients with advanced solid tumors. *Investig New Drugs* 35(2):180–188. <https://doi.org/10.1007/s10637-016-0407-y>
 15. Reid G, Kao SC, Pavlakis N, Brahmabhatt H, MacDiarmid J, Clarke S, Boyer M, van Zandwijk N (2016) Clinical development of TargomiRs, a miRNA mimic-based treatment for patients with recurrent thoracic cancer. *Epigenomics* 8(8):1079–1085. <https://doi.org/10.2217/epi-2016-0035>
 16. Thakral S, Ghoshal K (2015) miR-122 is a unique molecule with great potential in diagnosis, prognosis of liver disease, and therapy both as miRNA mimic and antimir. *Curr Gene Ther* 15(2):142–150
 17. Powers JT, Tsanov KM, Pearson DS, Roels F, Spina CS, Ebright R, Seligson M, de Soysa Y, Cahan P, Theissen J, Tu HC, Han A, Kurek KC, LaPier GS, Osborne JK, Ross SJ, Cesana M, Collins JJ, Berthold F, Daley GQ (2016) Multiple mechanisms disrupt the let-7 microRNA family in neuroblastoma. *Nature* 535(7611):246–251. <https://doi.org/10.1038/nature18632>
 18. Beckers A, Van Peer G, Carter DR, Mets E, Althoff K, Cheung BB, Schulte JH, Mestdagh P, Vandesompele J, Marshall GM, De Preter K, Speleman F (2015) MYCN-targeting miRNAs are predominantly downregulated during MYCN driven neuroblastoma tumor formation. *Oncotarget* 6(7):5204–5216. <https://doi.org/10.18632/oncotarget.2477>
 19. Schulte JH, Marschall T, Martin M, Rosenstiel P, Mestdagh P, Schlierf S, Thor T, Vandesompele J, Eggert A, Schreiber S, Rahmann S, Schramm A (2010) Deep sequencing reveals differential expression of microRNAs in favorable versus unfavorable neuroblastoma. *Nucleic Acids Res* 38(17):5919–5928. <https://doi.org/10.1093/nar/gkq342>
 20. Bray I, Bryan K, Prenter S, Buckley PG, Foley NH, Murphy DM, Alcock L, Mestdagh P, Vandesompele J, Speleman F, London WB, McGrady PW, Higgins DG, O’Meara A, O’Sullivan M, Stallings RL (2009) Widespread dysregulation of MiRNAs by MYCN amplification and chromosomal imbalances in neuroblastoma: association of miRNA expression with survival. *PLoS One* 4(11):e7850
 21. Yang HA, Wang X, Ding F, Pang Q (2015) MiRNA-323-5p promotes U373 cell apoptosis by reducing IGF-1R. *Med Sci Monit Int Med J Exp Clin Res* 21:3880–3886
 22. Perez-Rivas LG, Jerez JM, Carmona R, de Luque V, Vicioso L, Claros MG, Viguera E, Pajares B, Sanchez A, Ribelles N, Alba E, Lozano J (2014) A microRNA signature associated with early recurrence in breast cancer. *PLoS One* 9(3):e91884. <https://doi.org/10.1371/journal.pone.0091884>
 23. He YJ, Wu JZ, Ji MH, Ma T, Qiao EQ, Ma R, Tang JH (2013) miR-342 is associated with estrogen receptor- α expression and response to tamoxifen in breast cancer. *Exp Ther Med* 5(3):813–818. <https://doi.org/10.3892/etm.2013.915>
 24. Yang H, Li Q, Niu J, Li B, Jiang D, Wan Z, Yang Q, Jiang F, Wei P, Bai S (2016) microRNA-342-5p and miR-608 inhibit colon cancer tumorigenesis by targeting NAA10. *Oncotarget* 7(3):2709–2720. <https://doi.org/10.18632/oncotarget.6458>
 25. Molenaar JJ, Ebus ME, Koster J, van Sluis P, van Noesel CJ, Versteeg R, Caron HN (2008) Cyclin D1 and CDK4 activity contribute to the undifferentiated phenotype in neuroblastoma. *Cancer Res* 68(8):2599–2609. <https://doi.org/10.1158/0008-5472.can-07-5032>
 26. Lukas J, Muller H, Bartkova J, Spitkovsky D, Kjerulff AA, Jansen-Durr P, Strauss M, Bartek J (1994) DNA tumor virus oncoproteins and retinoblastoma gene mutations share the ability to relieve the cell’s requirement for cyclin D1 function in G1. *J Cell Biol* 125(3):625–638
 27. Bienvenu F, Jirawatnotai S, Elias JE, Meyer CA, Mizeracka K, Marson A, Frampton GM, Cole MF, Odom DT, Odajima J, Geng Y, Zagodzoon A, Jecrois M, Young RA, Liu XS, Cepko CL, Gygi SP, Sicinski P (2010) Transcriptional role of cyclin D1 in development revealed by a genetic-proteomic screen. *Nature* 463(7279):374–378. <https://doi.org/10.1038/nature08684>
 28. Barbieri E, De Preter K, Capasso M, Chen Z, Hsu DM, Tonini GP, Lefever S, Hicks J, Versteeg R, Pession A, Speleman F, Kim ES, Shohet JM (2014) Histone chaperone CHAF1A inhibits differentiation and promotes aggressive neuroblastoma. *Cancer Res* 74(3):765–774. <https://doi.org/10.1158/0008-5472.can-13-1315>
 29. Gohard FH, St-Cyr DJ, Tyers M, Earnshaw WC (2014) Targeting the INCENP IN-box–Aurora B interaction to inhibit CPC activity in vivo. *Open Biol* 4(11):140163. <https://doi.org/10.1098/rsob.140163>
 30. Decaudin D, Geley S, Hirsch T, Castedo M, Marchetti P, Macho A, Kofler R, Kroemer G (1997) Bcl-2 and Bcl-XL antagonize the mitochondrial dysfunction preceding nuclear apoptosis induced by chemotherapeutic agents. *Cancer Res* 57(1):62–67